THE UNIVERSITY OF CHICAGO

ELUCIDATING EPIGENETIC DETERMINANTS OF DOUBLE STRAND BREAK RECOGNITION AND REPAIR

A DISSERTATION SUBMITTED TO
THE FACULTY OF THE DIVISION OF THE BIOLOGICAL SCIENCES
AND THE PRITZKER SCHOOL OF MEDICINE
IN CANDIDACY FOR THE DEGREE OF
DOCTOR OF PHILOSOPHY

COMMITTEE ON CANCER BIOLOGY

BY
JULIAN LUTZE

CHICAGO, ILLINOIS
AUGUST 2022

To my family

Thank You

TABLE OF CONTENTS

LIST OF FIGURES

LIST OF TABLES

ACKNOWLEDGMENTS

First, I would like to thank my advisor, Stephen Kron. I never felt limited or constrained working on projects in your lab. On the contrary, you have always pushed me to accomplish more and trusted me to take the project wherever it led. I have valued your emphasis on working collaboratively, and not letting the perfect be the enemy of the good. You are one of the few mentors at UChicago who is willing to put research before themselves and expect students to deliver at the bench. I appreciate your willingness to work with me though this process. My longest-term collaboration has been with my co-mentor Megan McNerney. Megan, I have appreciated your willingness to work with me on topics and techniques which were unfamiliar to you, and I hope that we have both grown and learned from one another in this process. You always challenge me to explain my reasoning and to think through eventualities of my project. It has been great working with your lab, and I am proud that by working together I have accomplished what I could not do alone.

I also want to thank my committee, both past and present: Bryan Dickinson, Jun Huang, Kay Macleod, and Jane Churpeck. Bryan has always offered insightful and challenging ideas at committee meetings that have inspired me to rethink my project. Jane, now at University of Wisconsin, was supportive in forming my initial project. I enjoyed working with you and Stephen. Jun was helpful in proving feedback on microscopy and imaging and was instrumental in writing a grant with Steve and me. Kay, you have devoted a lot to this program and every student here has been impacted by you for the better. On a personal level, you have been supportive throughout my career at UC and have always made me feel welcome and included even at recruitment.

Present and past members of the Kron and McNerney labs have been tremendously helpful and influential. Without the hard work of Amy the Kron lab could not function. I thank Don and Elena for their kindness in welcoming me to the lab and working with me throughout my tenure. Yue, my fellow grad student, has been a consistent presence in the lab to remind me that I am still grounded in some form of reality. To my undergrads Sara

and Emily, thank you for your patience in working with me and teaching me a lot about mentorship. I hope that I taught you some fraction of what I learned in mentoring you. In the McNerney lab, Saira and Dhivya have been tremendously helpful in helping me complete experiments and providing access to high-throughput sequencing. I am also thankful to Jeff both for being a great friend and for being patient enough to teach me how to analyze high-throughput sequencing data. Matt, Tanner, Raven, and others have also become more friends than colleagues. Finally, Molly was a great partner to work with while publishing our manuscript. I learned a lot working together and I appreciated your enthusiasm. I would also be remiss not to thank people in other labs to whom I have been both mentor and/or mentee: Stephen, Ben, Santiago, Yasmin. One of my proudest activities at UC has been in recruitment and committee-wide activities. I will reflect proudly on the fact that I knew and was known by most everyone in the program and had a positive impact on recruiting like-minded peers. Though I am leaving UChicago, I trust that I am leaving the department better than I found it and those I helped recruit can take it to new heights. I would also like to thank Vytas and Christine, the co-directors of the UC microscopy core, for their many days of teaching, and help they have provided me and many other students at UC. Without them my project would not have been possible.

I would also like to thank my friends I have met along the way. To Matt, Katya, Manisha, Alex, Maile, Lari, Ryan, and Dave I owe a big thank you. You have made grad school what it is and have helped form me into the person I am today. I am grateful for your friendship, you were always there to talk, listen, (especially) gossip, or reminisce. I owe a measure of my success to your patience and friendship. To my newer friends Ben, Patrick, Collin, Emma, Santiago, Rosie: one of my prouder moments of grad school was working on recruitment each year. I hope that I can make an impact on UC and CCB for many years, in part by recruiting the next generation. In the same vein, I'd also like to acknowledge the faculty members who worked above and beyond, with students, to make our program what it is today. Shannon, Alex, Marsha, Scott, Kay and others come to mind as examples of good

citizens and faculty who put students first.

Finally, I'd like to thank my family. I am sure that I could not have completed this program without the support of my parents. Dad, you have always been supportive of me in getting into grad school and in achieving my goal of graduating with a PhD. Mom, you were always available to talk or help both in good times and in bad. Especially at the end your understanding and patience was invaluable. Sylvia, thank you for always taking an interest in what I was working on. You have all been my support system through this process, and I am grateful to you all.

ABSTRACT

Radiotherapy is a ubiquitous mode of cancer treatment which is employed against an array of malignancies with diverse etiologies. The benefits of radiation, and indeed several forms of conventional cancer therapy, depend on the formation and persistence of DNA double strand breaks (DSBs) in cancer cells. Indeed, the ubiquity of radiotherapy illustrates the fundamental need for cells to maintain genome integrity and repair damaged DNA. While DSBs form in chromatin by definition, little is known about the influence of epigenetic context on DSB detection, signaling or repair.

Studies have begun to elucidate the effects of pre-existing, basal variation in chromatin on DSB repair as well as changes to the epigenome induced after DSBs are detected. Histone post-translational modifications (PTMs) may differentially impact DSB repair with varying kinetics. Further, the γH2AX mark formed upon DSB detection is considered a reliable DSB reporter, but this has not been evaluated genome wide. Indeed, tools to differentiate DSB induction from DSB repair are lacking, thus impeding efforts to understand how the epigenome differentially affects stages of the DDR. Here, we introduce new tools which can separate detection of DSBs from their induction. Using these tools in conjunction with novel genomic approaches, we uncover links between the basal epigenome and induction and/or repair of DSBs. We also elucidate mechanisms by which the epigenome is altered following DSB detection.

Initially, we probed DSB formation and detection genome-wide in the erythroleukemia cell line K562, taking advantage of ENCODE data to explore the potential influence of local epigenetic states. Our data revealed non-uniform distributions with respect to chromatin context; further, DSB induction did not overlap with, γH2AX deposition. In brief, DSBs in transcribed euchromatin were more readily detected and marked by γH2AX. Next, we turned to assessing how histone PTMs changed following IR insult. Using proteomics, we uncovered long-lasting and wide-spread epigenetic alterations. Our data pointed toward H3K27me3 as a critical regulator of DSB repair. In a third technical development, we

developed a direct DSB labeling method, TdT UdP DSB End Labeling (TUDEL) which we used to verify changes to the epigenome induced by DSBs. Finally, we uncovered two mechanisms by which the epigenome impinges upon DSB detection. First, we observed a link between transcription and DSB repair and validated this using genomic approaches as well as functional assays. Second, we confirmed previous reports linking the chromatin modifier PRC2 and its footprint H3K27me3 to the DDR. Extending previous models, we showed that PRC2 activity post IR is constrained to active euchromatin and link PRC2 and SWI/SNF activity at DSB loci. These data confirm active recruitment of PRC2 to damaged DNA and suggest a novel mechanism of action for this chromatin repressor.

Taken together, this work lays out several technical advancements and generates tools and data sets which will be useful in further analysis of epigenome-DSB interactions. We revealed novel epigenetic determinants of DSB detection and signaling that may impact DNA repair and cell survival after irradiation. Several exotic PTMs are implicated in the DDR through our work and await follow-on studies. Lastly, we refined models of DSB detection in euchromatin by suggesting that Pol II-dependent transcription mediates rapid DSB detection, rather than inducing damage. We go on to show that DSBs in repressed domains and heterochromatin may only be detected during replication. This work identifies mechanisms that may promote genomic instability and suggests new targets for sensitization to therapy. In general, we also provide new rationale for cancer-associated epigenetic changes and suggest that maintenance of genome integrity following IR may be a primary function of the epigenome and epigenetic modifiers.

CHAPTER 1

INTRODUCTION

1.1 Cancer Therapy Reveals a Gap in Our Understanding of DSB Repair

Radiotherapy (RT) is a ubiquitous treatment modality for cancer[1, 2]. The use of RT is widespread but is particularly important in treating head and neck tumors as well as breast and prostate cancer. RT works predominantly by exposing tumors to Ionizing Radiation (IR) which has pleiotropic effects including induction of ROS, disruption of the cell cycle, induction of inflammation, and direct damage to genomic DNA. Paramount among the cytotoxic effects of IR is its ability to directly or indirectly introduce DNA damage, especially double strand breaks (DSBs). Even a single unrepaired DSB can lead to cell death if not detected before replication or other processes compound the damage leading to mis-segregation of chromosomes, cell cycle arrest, and/or cell death by various pathways. Indeed, the widespread use of IR underscores the centrality of DNA repair pathways to cellular homeostasis. However, these facts belie the need for a better understanding of the cellular response to IR. Despite the potency of DSBs and much real-world evidence pointing to the efficacy of RT, radiation is not usually effective as a monotherapy[2, 3, 4, 5]. Indeed, a return to a proliferating state after chromosomal damage and cell cycle arrest is one of the hallmarks of cancer. RT is most commonly supplemented with an adjuvant such as surgical resection, chemotherapy or immunotherapy[6, 7]. Thus, a fuller understanding of cellular response to DSBs would elucidate cancer cell survival mechanisms on a fundamental level[8, 9].

Radiation acts on tumors and cells in myriad ways dependent to a degree on the dose received and the energy of radioactive particles used. Exposure to IR principally causes damage to DNA including base damage, single strand breaks and double strand breaks[10, 11, 12]. Damage can be induced by direct collisions between radioactive particles and the DNA back-

bone or, more commonly, via reaction with IR induced free radicals derived from radiolysis of water molecules[13]. In most cases, though especially with low-energy sources of IR, base damage and single strand damage far outnumbers DSBs. However, base damage or SSBs (single strand breaks) can be converted to DSBs upon further chemical reaction or by conflict with cellular processes including transcription and replication[14, 15]. Thus, while the ratio of DSBs to SSBs induced by low-energy radiation is generally low, the number of DSBs can increase over time especially in the context of inhibited or altered repair pathways[16, 12].

Low-energy radiation induces punctate foci (IR induced foci, IRIF) as particles ricochet through cells or tissues[17, 18, 19]. Collisions between low linear energy transfer (LET) IR and DNA are rare, meaning most damage is secondary, the result of attack by $\bullet$OH radicals. However, radiation with heavy ions or high-LET particles induces visible tracks of damage through cell nuclei[20, 21]. High-LET damage is associated with more direct DNA damage including DSBs, more chemical modification of histones and a higher fraction of heterochromatic damage[22, 21]. At DSB loci, DNA end chemistry induced by any type of IR can be complex, with partial oxidation or chemical modification of the sugar-phosphate backbone[23, 24, 25]. The fraction of ragged or complex ends is increased via exposure to high-LET radiation. Ragged DNA ends retard break recognition and repair as discussed below. There is also evidence for clustering of damage following exposure to high LET IR; foci from high LET treatment are more intense, suggesting grouping of breaks. Mechanisms underlying foci clustering are to be determined, though clustering of breaks call into question whether single IRIF correspond to single breaks. Perhaps several breaks can cooperate in recruitment of DDR factors, amplifying the local signal. Stepping back from DNA, RT also generates reactive oxygen species which, in turn, can react with other species including DNA, RNA and protein. The increased ROS contributes to cellular stress and triggers anti-oxidant response pathways[26, 27]. These pathways, in conjunction with direct signaling from DNA damage, attenuate the cell cycle and globally repress transcription (discussed in more detail below). If not resolved, IR insult can cause cells to permanently exit the cell cycle and

undergo senescence or programmed cell death[28, 29, 30, 31]. An understanding of DSB detection and response pathways is required to understand cell fate decisions following IR.

1.2 The Canonical Binary Model of DSB Repair Pathways

Before DSBs can be repaired, they must first be detected. Detection of DNA damage is by definition a chromatin-localized event. However, as chromatin context is ignored in traditional models of DSB detection, we will first present the traditional model of DSB recognition and repair and then consider how chromatin context changes our understanding of these processes later in this Chapter. Initial DSB detection is carried out by three (PI3K)-related kinases (PIKKs): ATR, DNA-PKcs and ATM[32]. Of the three, ATM (ataxia-telangiectasia mutated) is considered the apical kinase and is responsible for the majority of DSB recognition. ATM was first discovered by examining patients suffering from ataxia-telangiectasia (A-T) a disease which confers predisposition to malignancies and cellular sensitivity to radiation[33]. Via examination of A-T cells, it was deduced that mutations in a PIKK (ATM) ablated cell cycle stoppage following IR as well as timely repair of DSBs[34, 35]. Thus, ATM is responsible for recognition of damage as well as signaling up-stream to halt the cell cycle and induce IR response pathways (e.g. p53 and Chk2 activation)[36, 37]. Though ATM phosphorylates myriad substrates after IR insult, H2AX phosphorylation on Serine 139, to produce γH2AX, is the first, and most important step in DSB detection and repair regardless of which downstream pathway is utalized[38, 39, 40, 41]. γH2AX is a widely adopted proxy for DSBs and the modification spreads for several kilobases across the genome surrounding DSBs in a manner dependent on Mcd1 and ATM[42, 43, 44, 45]. While γH2AX is not required for IR induced checkpoint activation, it is an obligate step in recruitment of DDR proteins to DSB loci[43]. The mechanism by which ATM recognizes DSBs is discussed in more detail below[46]. ATR is a secondary kinase which is primarily responsible for initiating the replication-stress response. The third major DDR kinase, DNA-PKcs, is capable of recognizing breaks *de novo*, though it is often associated with the end-joining machinery.

Subsequent to recognition of breaks and phosphorylation of H2AX by ATM, repair proteins are recruited to breaks. Eukaryotes are thought to rely on a binary model of DSB repair which operates in a mutually-exclusive manner at DSB loci. In this model, cells utilize two main pathways to repair DSBs: Non-Homologous End Joining and Homologous Recombination (NHEJ and HR respectively), see Figure 1.1. The question of how and why cells select one pathway over another at a given loci is, despite tremendous research effort, not fully understood, though chromatin context undoubtedly plays a role[47, 48]. Canonically, NHEJ is thought to predominate over HR; it is much more rapid and predominates in G1 and early S phase. Thus, in a mixed population of cycling cells, the majority of cells will utilize NHEJ. NHEJ is perceived as error prone because it is sequence agnostic and does not require a homologous template strand. In reality however, NHEJ is responsible for the majority of DSB repair and thus must be highly accurate[49]. NHEJ is initiated when Ku70 and Ku80 bind both ends of broken DNA and form the Ku heterodimer[50, 51]. Cell-free systems indicate that the Ku complex tethers broken DNA ends and holds them in proximity for end-joining activity. Ku binding is a prerequisite for recruitment of DNA-PKcs, which phosphorylates a limited set of NHEJ proteins, most importantly itself[52]. DNA-PKcs is also required for further recruitment of DDR factors such as Artemis[32, 53, 54, 55, 56]. DNA-PKcs may also be responsible for recruitment of XRCC4 and XLF as well as LigIV which ultimately ligates the DSB. However, whether DNA-PKcs is required for DSB repair is debated. Our lab has shown that inhibition of DNA-PKcs does not attenuate end joining, but does inhibit resolution of γH2AX IRIF[57]. Indeed, some studies have suggested that DNA-PKcs is required to restrain ATM activity[58, 59].

The other core NHEJ factor is p53-binding protein 1 (53BP1)[60, 61]. Nanoscopic studies have shown that 53BP1 binds distally to free DNA ends suggesting it is not required for end joining or recruitment of other NHEJ factors to the break. Instead, 53BP1 may act as a scaffold protein– orchestrating the DSB repair domain– and has been shown to promote ubiquitination complexes such as RNF168[62]. Further, 53BP1 seems to play a

chromatin-oriented role. Recruitment of 53BP1 is dependent on PRC1 histone ubiquitination activity and also subject to regulation by histone H4 acetylation by TIP60[63, 64, 65]. More detailed examination of the chromatin-facing roles of 53BP1 await future studies linking 53BP1 binding to basal chromatin states and to changes in chromatin post IR (see below). It is well appreciated that the core function of 53BP1 is control of resection at DSB ends[66, 60]. Resection is known to be a key determinant of pathway choice; low resection is permissive for NHEJ while moderate to high resection favors HR. Exactly how 53BP1 attenuates resection to favor NHEJ is unknown but putative mechanisms include interactions with RIF1[67, 68, 69]. While 53BP1 deficient cells are radiosensitive, RIF1 loss is embryonic lethal. Loss of RIF1 results in an inability to use NHEJ and hyper-resection of DSB ends.

In addition to NHEJ, mammalian cells also possess alternative forms of end-joining, collectively termed alt-EJ[70, 71, 72]. (By contrast, NHEJ as outlined above is sometimes called classical NHEJ or c-NHEJ.) Alt-EJ is not well understood, in part due to the lack of specific alt-EJ factors. Instead, many DDR factors known to participate in NHEJ or other forms of repair including PARP1, Mre11, or CtIP also have a putative role in alt-EJ[73, 74, 75]. Thus, alt-EJ is sometimes considered a "dirty" repair pathway of last resort, invoked when NHEJ and HR fail. Alternatively, alt-EJ may represent a more ancient DDR pathway or pathways which have been subsumed by NHEJ and especially HR in higher eukaryotes. Finally, use of alt-EJ is usually associated with regions of microhomology and repair by POLQ[76, 73]. However, whether POLQ mediated repair is a subset of alt-EJ or a different pathway is not well appreciated. The identification of alt-EJ raises important questions about repair pathway choice. It seems unlikely that repair of DSBs, an activity critical for cellular survival, would be dictated by a completely stochastic choice between competing pathways. Chromatin is certainly one determinant of repair pathway choice and will be discussed below. However, other proteins have been shown to influence the propensity of cells to use NHEJ. In S/G2 cells NHEJ is actively repressed by CYREN, a protein which preserves overhangs at DSB loci creating a resection-permissive environment[77, 78]. Other

analyses including a Mass Spec based 53BP1-interactome identified the shieldin complex as an NHEJ promoting factor which both blocks end-resection and attracts 53BP1 to DSBs[79, 80, 81, 82, 83]. As discussed below, this is one of the only factors known to promote NHEJ, suggesting end-joining may be a default option at DSBs. However, given the ostensibly error-prone nature of NHEJ, much of the literature tends to downplay its importance and insists that it is not the primary repair pathway. However this model ignores the fat that NHEJ is kinetically favored and that most repair occurs very rapidly after IR especially in G1 phase cells which cannot utilize HR.

In contrast to NHEJ, homologous recombination proceeds much more slowly and is principally active in S/G2 phases of the cell cycle as it requires two copies of DNA. While ATM also promotes HR, ATM is not required for HR activity[84]. Repair pathway choice, and shunting of breaks to HR, is governed by resection of DNA ends by Exo1 and Mre11 exonucleases[85]. First, MRE11 nicks DNA 20-40 nucleotides from the beak site and resects 'backwards' toward the broken end in a 5'-3' manner. Second, more extensive 3'-5' resection is carried out by Exo1 along with BLM and DNA2[86]. Resection is a prerequisite for HR as ssDNA must be exposed to form homology with sister chromosomes; by the same token, resected DNA cannot be processed by NHEJ. Control of resection is often depicted as a battle between opposing molecular forces. Binding of Ku is known to prevent resection, while binding of CtIP promotes nicking of DNA and eventual ssDNA creation[86, 87, 88]. More well-studied is the role of BRCA1 in opposing the activity of 53BP1 at DSBs[89, 90]. In cells lacking BRCA1, loss of 53BP1 restores DDR competency and confers relative radioresistance; that loss of a negative regulator of HR restores HR function in the absence of positive regulators shows the delicate balance between these pathways[66, 89, 91]. In addition to excluding 53BP1, binding of BRCA1 promotes resection via interactions with CtIP. Further, BRCA has been proposed to act as a molecular scaffold for other HR proteins[92]. These include the BRCA-associated RING Domain protein 1 (BARD1) which is an obligate binding partner of BRCA1. BARD1 catalyzes histone H2 ubiquitination which may be important

for recruitment of the nucleosome remodeler SMARCAD1, discussed below[93, 94]. Finally, resection is also controlled at the cell cycle level via CDK dependent phosphorylation of CtIP which is required for ssDNA generation and RPA recruitment[95].

HR relies on binding of the MRN complex (NBS, MRE11, RAD50) to DSBs which promotes resection[96, 97, 98]. Following ssDNA generation, RPA binds to single stranded regions with high avidity to protect DNA and promote HR over microhomology mediated repair pathways or single strand annealing[96]. Binding of Rad51 and Rad52 competes with RPA and subsequently facilitates homology search and ultimately strand invasion of the homologous chromosome[99]. Finally, the broken section of the DNA complexes with a homologous region to form a complex DNA structure termed a Holliday junction. Once the Holliday junction has formed, DNA synthesis can begin. Much remains to be discovered about this complex process, though synthesis of the complimentary strand likely requires specialized helicases, polymerases, and, possibly, topoisomerases to relieve topological tension. Both Pol ϵ and Pol δ have been invoked as the main DNA synthesizers during HR, especially in the case of synthesis-dependent strand annealing. In rarer cases, a double Holiday junction is formed which can be resolved through the action of SLX1, SLX4 or GEN1[100, 101]. Some holiday junctions are resolved via crossing over of chromosomes while most do not require crossing over. Despite the general notion that HR is error free, crossing over can lead to loss of heterozygosity or other mutations. Thus, higher eukaryotes have evolved several pathways to limit crossover.

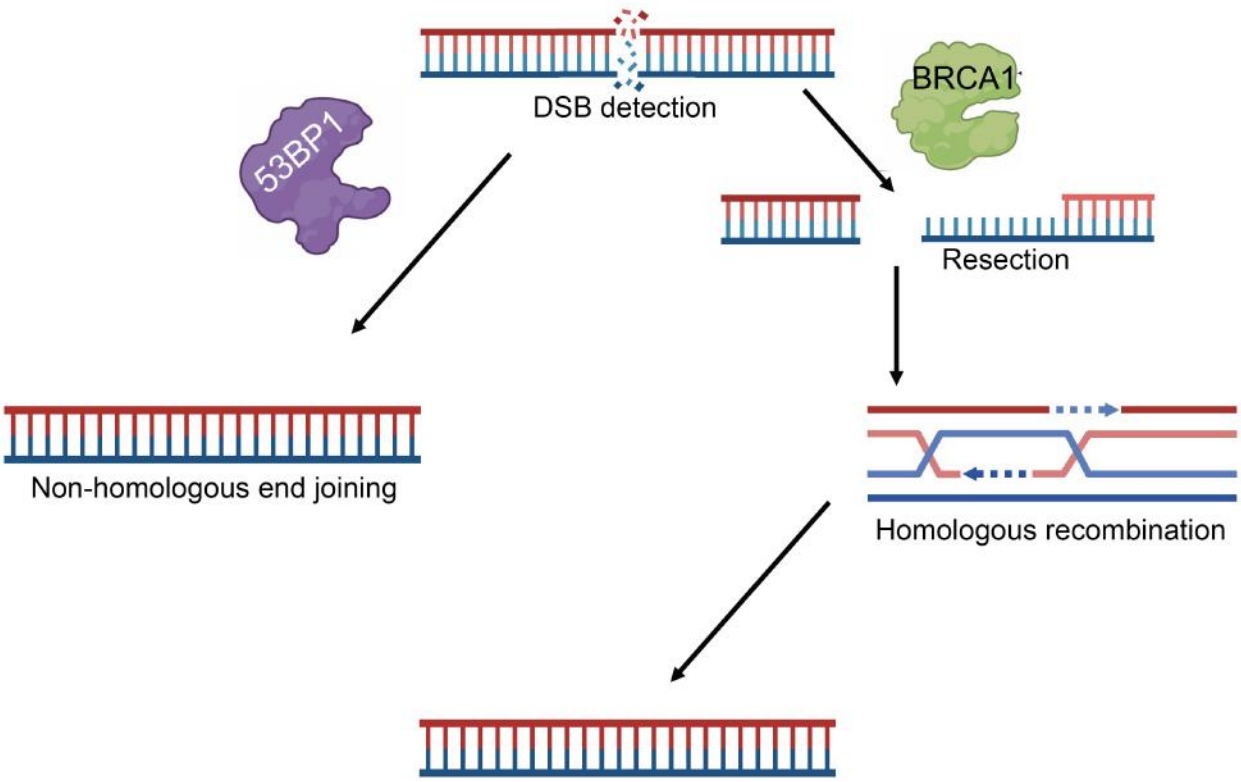

Figure 1.1: Though simplified, the binary model of DSB repair predominates in eukaryotes. AFter DSBs are detected, is is thought that NHEJ and HR compete at individual break loci. Binding of 53BP1 pushed breaks toward NHEJ and rapid repair while resection surrounding DSBs, promoted by BRCA1 among other proteins, irreversibly commits breaks to HR. HR is a more complex process, and kinetically disfavored; there may be proteins which restrain NHEJ, though end joining likely accounts for the majority of break repair. This Dissertation will largely focus on events upstream of repair pathway choice, especially in initial detection of damage.

Having described the major DSB repair pathways, we will now turn to experimental models to study DSB repair. Irradiated cells display punctate structures of DSB repair proteins, commonly seen via immunofluorescence, termed IR induced foci (IRIF)[102, 103]. γH2AX is the most ubiquitous IRIF marker; γH2AX IRIF can be seen within minutes of IR insult and reach a maximum in both size and number 1-4 h after induction of DSBs. Other DDR factors including Rad51, Ku, and 53BP1 also form IRIF. Interestingly, factors in separate DSB repair pathways colocalize at IRIF. This suggests either that competition between repair pathways occurs at individual IRIF or alternatively, that the binary model of DSB repair is over-simplified and pathways may cooperate rather than compete. While we anticipate the latter possibility is true to some extent, the binary model still provides a useful conception of DSB repair and is used throughout literature linking chromatin context to DSB repair outlined below. Some modes of competition between DDR factors such as between BRCA1 and 53BP1 have been described but more remain to be uncovered. The question remains as to why cells would desire competition at individual loci; perhaps a level of redundancy in repair pathways increases repair fidelity and robustness of the DDR. Adding complexity, nanoscopic studies have suggested that individual IRIF may contain multiple DSBs[104]. Perhaps co-localization of HR and NHEJ factors may be evidence of repair of adjacent breaks rather than competition for the same DNA ends.

Adding futher complexity, dynamics of IRIF are also not coincident with repair of DSBs, per se. IRIF form before end-joining is complete and have been shown to persist long after repair of breaks[105, 106, 107]. Residual IRIF are still visible 24 h after DSB induction, though the degree to which these IRIF map to unrepaired breaks is debated. As IRIF are not reliable indicators of DSBs, other assays have been developed to quantitate DNA damage. The comet assay, also termed single-cell electrophoresis, offers a semi-quantitive measure of DSBs[108]. Irradiated cells are embedded in an agarose matrix before electrophoresis is applied to stretch out broken DNA ends. The length and density of DNA which is pulled from the nucleus is proportional to the number of DSBs in a given cell. Other systems have been

developed to directly assay DSB repair choice. In general, these systems rely on fluorescent reporter plasmids which change color based on repair pathway outcome[109, 110, 111]. For example, the popular Traffic Light system uses a GFP reporter cassette which is cut via restriction enzyme. In the case of NHEJ, a frame shift mutation induces red fluorescent protein production, while in the case of HR, a second GFP containing donor is inserted via homology arms resulting in the reappearance of green fluorescence. These systems are facile to assay by flow cytometry, though they only give a per-cell measurement of, presumably, a single DSB. As discussed above, cells with many DSBs use HR and NHEJ concomitantly and these pathways are in competition. Further, plasmids lack chromatin context, thus obviating normal DSB detection pathways and calling into question the validity of chromatin-free repair pathway choice. As discussed below, chromatin context is a critical mediator of the DDR.

1.3 What is Epigenetics?

Epigenetics is a collective term for information encoded on or around the genome but not within the DNA sequence. First proposed by Waddington and refined over the last 30 years beginning with the work of Allis, epigenetics allows for one genotype to give rise to a plethora of phenotypes[112, 113, 114]. While there are several layers of epigenetic information spanning DNA and RNA methylation, chromatin secondary and higher-order structure, and histone modifications; this dissertation will mostly consider the latter. The human genome is highly non-uniform. At a basic level, different genomic loci vary widely in their local compliment of histone PTMs which, in turn, influence the structure and biophysical properties of chromatin[115, 116]. The vast majority (>70 percent) of the human genome is tightly packed and wound into intricate structures designed to condense DNA 10,000 fold in order to fit 3 billion bases within each cell[117]. These regions, termed heterochromatin, were first identified as darkly-staining, electron-dense regions in early EM microscopy studies. These regions do not code for proteins and are poorly understood; repetitive sequences found in these regions compound challenges of sequencing compact DNA[118]. Regions of the

genome which are expressed or participate in gene expression (e.g., promoters, enhancers) are generally uncompacted, contain fewer histones, and are decorated with Histone PTMs including H3K36Me3 and histone acetylation[119, 120, 121, 122, 123]. These regions are termed euchromatin. By contrast, some heteochromatin, called facultative heterochromatin, is actively maintained in a repressive state by histones and histone binding proteins, but may be re-formed into euchromatin during, for example, differentiation. Facultative heterochromatin is marked by the repressive PTM H3K27me3 which can be added or removed around genes to enact differential gene regulation[124, 125, 126, 127]. Modulation of these chromatin states allows one genome to give rise to highly disparate cell types. While many overlapping pathways are downstream of epigenetic modulation of phenotypes, much effort has focused on expression, or lack thereof of genes, which, in turn, is affected by chromatin accessibility at promoters or enhancers. Mechanisms by which variations within or between gnomes affect genomic integrity are only just beginning to come to light.

1.4 A Role for Epigenetics And Chromatin Context in DSB Repair

While the last 20 years have elucidated the fundamental constituents of most DSB repair pathways, studies are largely ignorant of the chromatin context in which recognition of genomic damage occurs. More recently, chromatin has been incorporated into models of the DDR starting with recognition of breaks[48, 128]. ATM precipitates several chromatin-level changes in addition to H2AX phosphorylation. These include promotion of H4 and H2 ubiquitination via the PRC1 complex; in turn H2 ubiquitination promotes NHEJ via recruitment of 53BP1[129, 130]. Indeed, recruitment of 53BP1 to DSB loci is perhaps the most completely understood epigenetic-DDR interaction. In addition to the role of ATM, 53BP1 recruitment is also promoted via methylation of the H4 tail. Tip60, a histone acetyltransferase which acetylates the H4 tail, thus serves to block recruitment of 53BP1 to chromatin

and promotes HR[131, 132, 133, 134, 135]. However it is not well understood whether marks which influence 53BP1 recruitment, like H4 acetylation, are pre-existing, basal marks or whether they are added and removed after DSB induction to facilitate repair. ATM also reinforces recruitment of CHD4 which promotes HR[136, 137, 138]. The bivalent role of ATM illustrates the lack of a cohesive understanding or model of the mechanics underlying chromatin-DDR interactions. Instead, there are few general principles.

First, there is strong evidence linking differential chromatin compaction to alterations in rates of DSB recognition and repair and indeed to repair pathway choice. Compact chromatin is thought to be resistant to DSB induction due to the radioprotective effect of histones and other proteins[139, 140, 141]. It is also true that chromatin compaction likely retards recruitment of DDR factors to DSB loci and establishment of bulky repair complexes at breaks. There is strong evidence suggesting the importance of chromatin decompaction in the DDR. PARP1 is sometimes described as a NHEJ factor but is more accurately positioned as a chromatin modifier which mediates decompaction of histones surrounding breaks[142, 143]. PARP1 is part of a larger family of PARP proteins which catalyze the deposition of poly(ADP-Ribose) (PAR) sugar chains on protein substrates[144]. While most PARP family members have mono-PAR-ylation activity, PARP1 is capable of creating large, branching PAR chains generally on glutamate or lysine residues[145, 146, 147, 148]. PAR-ylation of histones induces steric decompaction of chromatin perhaps creating a permissive environment for DSB detection[149, 150]. Indeed, PARP and PAR-ylation are accreted at DSB loci with kinetics comparable to γH2AX[151, 152, 153, 154]. Thus, PARP1 is considered to be a sensor of DNA damage. Loss of PARP1 has been shown to prevent γH2AX deposition, restrain the size of IRIF, and prevent chromatin relaxation at breaks. Chromatin relaxation proximal to DSBs is a rapid and essential element of the DDR. Many factors aside from PARP have been implicated in this process including SWI/SNF subunits, discussed below. PARP1 is further known to increase histone acetylation both by direct recruitment of HATs and/or via competition for NAD+ with SIRT1, a major

histone deacetylase[155, 156, 157, 158]. Histone acetylation may mediate DSB-proximal chromatin decompaction. Moreover, PAR-ylation affects H3K4 methylation by recruiting the histone demethylase by KDM5B to DNA lesions[159, 160]. Loss of H3K4me3 is important in recruitment of DDR factors including Ku70. Finally, PARP1 is necessary for recruitment of PRC2 to DSB loci. The observed interaction between PARP and Suz12, a PRC2 subunit, may underlie PARP dependent recruitment of PRC2. Returning briefly to repair pathway choice, PARP1 is generally considered to promote NHEJ, perhaps by attenuating resection at DNA ends[161]. It is not well understood to what extent PARP1-dependent chromatin regulation drives NHEJ, though PRC2 has been associated with NHEJ.

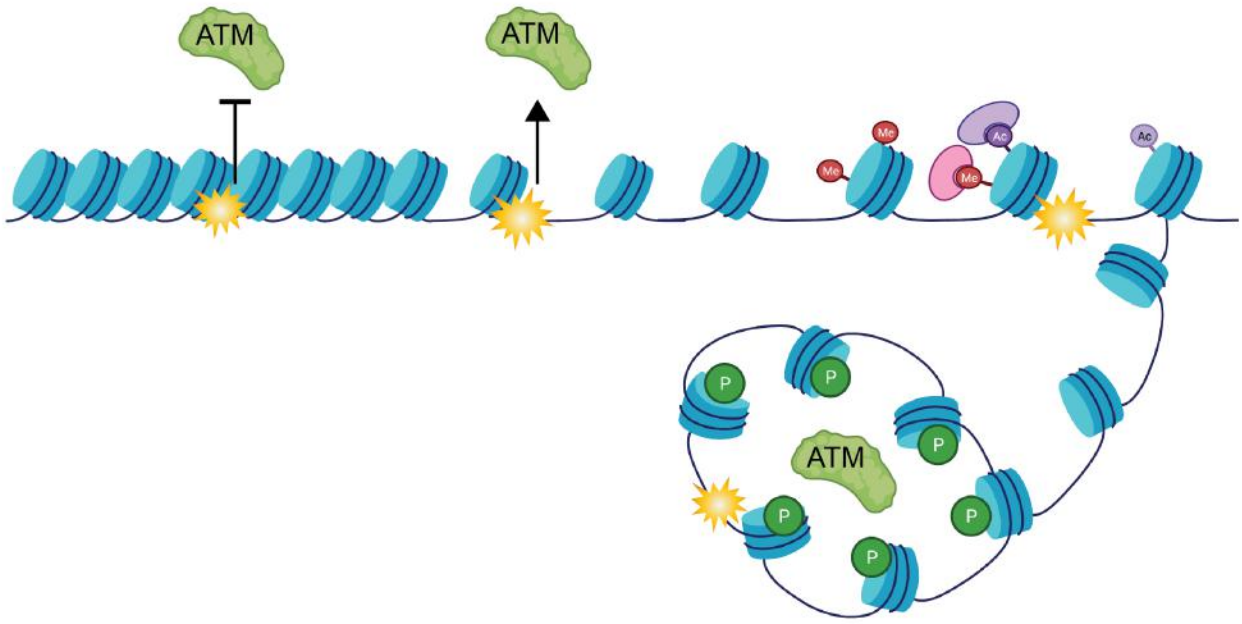

Figure 1.2: Chromatin compaction is known to mediate DSB induction, with dense chromatin shielded from break induction. Dense chromatin may also be refractory to DSB detection via steric mechanisms. Further, numerous histone modifications or modifiers are known to impact recognition of DSBs or recruitment of DDR factors. Lastly, chromatin looping or TADs demarcate the spread of γH2AX domains.

The second broad theme linking chromatin to the DDR is the effect of histone modifications on repair pathway choice. There is not a unifying theory of histone PTM:DDR cross-talk and most data comes from one-off studies linking a specific PTM to an aspect of the DDR. As a paradigmatic example, studies have evaluated the effect of H3K36me3 on repair pathway choice[123, 135]. H3K36me3 is deposited proximal to active genes where it plays a role in safeguarding transcription fidelity by restoring the basal chromatin landscape after passage of processive Pol II. H3K36me3 is thought to mediate CtIP recruitment in conjunction with H4K16Ac by Tip60. 53BP1 binds to methylated H4, though acetylation of K12/16/20 by Tip60 prevents 53BP1 binding[162, 134]. Thus, H3K36me3 indirectly promotes HR at active genes. However, H3K36me3 is also known to mediate PRC2 recruitment and is sometimes associated with H3K27me3[163]. Further, the notion that active genes are both repaired quickly and are dependent on HR is oxymoronic, suggesting more remains to be elucidated in this pathway.

Oftentimes, basal histone marks dictate repair pathway choice such as in the case of H4K20me which promotes 53BP1 recruitment. H4K20 methylation may also enforce cell-cycle dependent repair pathway preference[164]. H4K20me2 is enriched in pre-replicative chromatin and diluted out following replication; thus, NHEJ is diminished in replicating or post-replicaive cells which are competent for HR. A similar mechanism underlies the association of Dot1L and its footprint H3K79me2 in the DDR. It is thought that chromatin expansion proximal to DSBs may uncover methylated H3K79 which promotes recruitment of 53BP1[165]. At other times, histone marks are thought to be added post DSB induction. This the case for heterochromatic loci where H3K9me3 is unmasked following chromatin de-compression allowing for Tip60 dependent acetylation of H4[133]. 53BP1-dependant recognition of heterochromatic DNA damage may also be dependent on Trim28 (KAP1). ATM phosphorylates Trim28 which then promotes relaxation of heterochromatin allowing for 53BP1 binding[166]. Indeed, retention of Trim28 on heterochromatin attenuates γH2AX deposition[167].

Many of the associations between basal chromatin states and local DDR are derived from studies employing restriction enzymes (RE) to induce breaks at known genomic loci and then correlating break repair or recruitment of DDR factors with the local chromatin environment[168, 169, 170]. However, these studies contain serious methodological shortcomings. First, RE induced damage may not be recognized in the same manner as exogenously induced DSBs and these studies do not account for inherent biases in cutting efficiency of enzymes[171]. Other studies use Cas9 to induce DSBs, though these breaks have been shown to be repaired via fanconi anemia genes, a non-traditional DSB repair pathway. Cas9 or RE recognition sites are also likely not distributed evenly across the genome; studies must be careful to account for enrichment of sites in particular chromatin environments. Finally, both Cas9 and REs struggle to cut compact chromatin, thus, these studies may report on a subset of the DDR which predominates in open chromatin. There is not an obvious way to account for differential induction of DSBs in compact chromatin and open regions using RE based methods.

Related to the effect of histone modifications on local DSB repair, specialized repair pathways have been proposed for unique types of chromatin. For example, heterochromatin, especially pericentromeric heterochromatin, is refractory to DSB detection[172]. Studies in both drosophila and mammalian cells have uncovered evidence that heterochromatic breaks are recognized and immediately protected via SUMO-ylation by several SUMO-E3 ligases. Following SUMO-ylation, DSBs are relocalized to the periphery of heterochromatin domains in a process dependent on SUMO-E3 ligases including, in mammals, Nse2[173, 174, 175]. Once relocalized, heterochromatin is decompacted and HR proceeds, initiated by Ra51 binding. Similar processes are used to repair repetitive regions including telomeres or LINE elements. By contrast, centromeric breaks, which are heterochromatic, may be repaired by NHEJ or HR dependent on the cell cycle stage. This finding suggests that regulation of heterochromatin breaks is likely more complex than the above model suggests. After all, it is unlikely that heterochromatic breaks are recognized immediately, and that cells then wait

to repair breaks using HR in G2 phase. Telomeres are also imbued with specialized DDR pathways[176, 177]. TRF2, a telomere associated protein, is known to suppress NHEJ at telomeres, biasing these regions toward HR. Transcribed regions also have specialized DSB pathways, though these will be discussed in a later section.

Aside from histone PTMs, higher-order genome structures are known to play a role in DSB detection and signaling. The eukaryotic genome is folded into complex 3D topologies which influence gene activation or repression[178]. Put simply, chromatin forms loops and larger clusters which are termed topologically associated domains (TADs): DNA within loops or TADs interacts, while inter-TAD interactions are repressed. It is appreciated that TAD boundaries can delimit spreading of γH2AX. CTCF, an important element of TAD boundaries, stimulates HR and is necessary for proper γH2AX spreading[179, 180, 181]. Extrusion of DNA loops is thought to potentiate H2AX phosphorylation via interaction with CTCF[104, 182, 183]. DSBs may alter 3D genome structure as it has been shown that DSBs which disrupt a TAD boarder precipitate dissolution of that boundary and spreading of DDR factors into adjacent TADs[184]. In contrast to this process, 53BP1 may protect higher-order chromatin topology by recruiting RIF1 to TAD boundries[185].

Finally, chromatin remodeling and nucleosome addition plays an important part in the DDR. Firstly, chromatin decompaction requires the eviction of histones proximal to DSBs, especially in heterochromatin. This process is thought to be dependent on PARP1 mediated recruitment of several SMARCA family members including INO80[186]. INO80 is necessary for eviction of histone octamers containing H3.1, H2B and H2AFZ. Removal of H2AFZ by INO80 or the histone chaperone ANP32E may clear the way for γH2AX deposition proximal to breaks[186, 187, 188]. Indeed, only 10-25 percent of the genome is occupied by H2AX underscoring the need for remodeling or addition of H2AX proximal to DSBs in order to potentiate ATM dependent activities[189]. PARP1 also mediates recruitment of the FACT histone chaperone which recognizes PARylated histones and catalyzes their eviction surrounding damaged DNA[190].

Perhaps the best recognized histone remodeler is the SWItch/Sucrose Non-Fermentable (SWI/SNF) complex. The SWI/SNF family of proteins, also known as trithorax proteins in drosophila is associated with gene activation and chromatin de-repression[191, 192, 193, 194, 195, 196]. SWI/SNF complexes in humans fall into two flavors, BRG/BRM-associated factor (BAF) and polybromo-BAF (pBAF) complexes, which are comprised of slightly different subunits, but possess overlapping functions[193, 195, 196, 197, 198]. In general, SWI/SNF complexes are thought to promote gene transcription by reducing chromatin occupancy via sliding or evicting nucleosomes[199, 200, 201]. The BAF complex is built around a central ATPase, either BRG (SMARCA4) or BRM (SMARCA2) which is responsible for nucleosome remodeling and facilitating access to promoters or enhancers. Though SWI/SNF does not directly participate in histone post translational modifications, it is associated with histone acetylation and other open chromatin markers.

A role for SWI/SNF in the DDR was first discovered following the observation that mutations of SMARCA2 or SMARCA4 rendered yeast cells exquisitely sensitive to IR[202, 203]. Subsequently, several SWI/SNF subunits have been observed to localize to IRIF[204, 205, 206]. The DSB:SWI/SNF interaction is boosted via ATM-dependent phosphorylation of SMARCA4. SWI/SNF is thought to mediate enhanced access to damaged DNA by moving or ejecting histones. This process may participate in a feedback loop with ATM and be necessary for proper spreading of γH2AX. Conflicting evidence exists as to whether SWI/SNF mediates HR or NHEJ. GCN5 is known to be required for direction of SWI/SNF to HR competent breaks where SMARAC4 may mediate resection. SMARCA4 may also facilitate strand invasion via interactions with Rad51. Recruitment of SWI/SNF to NHEJ competent DSBs is mediated by p300 histone acetylation, associated with chromatin relaxation which promotes NHEJ by enabling Ku complex binding to DNA ends[207]. SWI/SNF has also been shown to repress transcription *in cis* to DSBs; this mechanism is discussed below. However, transcriptional repression is in contrast to the canonical chromatin opening role for SMARCA4.

A related chromatin modeler, though distinct from the SWI/SNF complex, is SMARCA5. Like SMARCA2/4, SMARCA5 can slide or evict nucleosomes, and is likewise implicated in the DDR[208, 209]. Specifically, SMARCA5 is known to complex with RNF168 in a PARP dependent manner whereby it promotes H2K119Ub and BRCA1 accumulation at DSBs. Loss of SMARCA5 attenuates HR via blocking Rad51 recruitment and by discouraging end resection. Indeed, both SWI/SNF and SMRCA5 have resection promoting activities, possibly via recruitment of CtIP[210, 211].

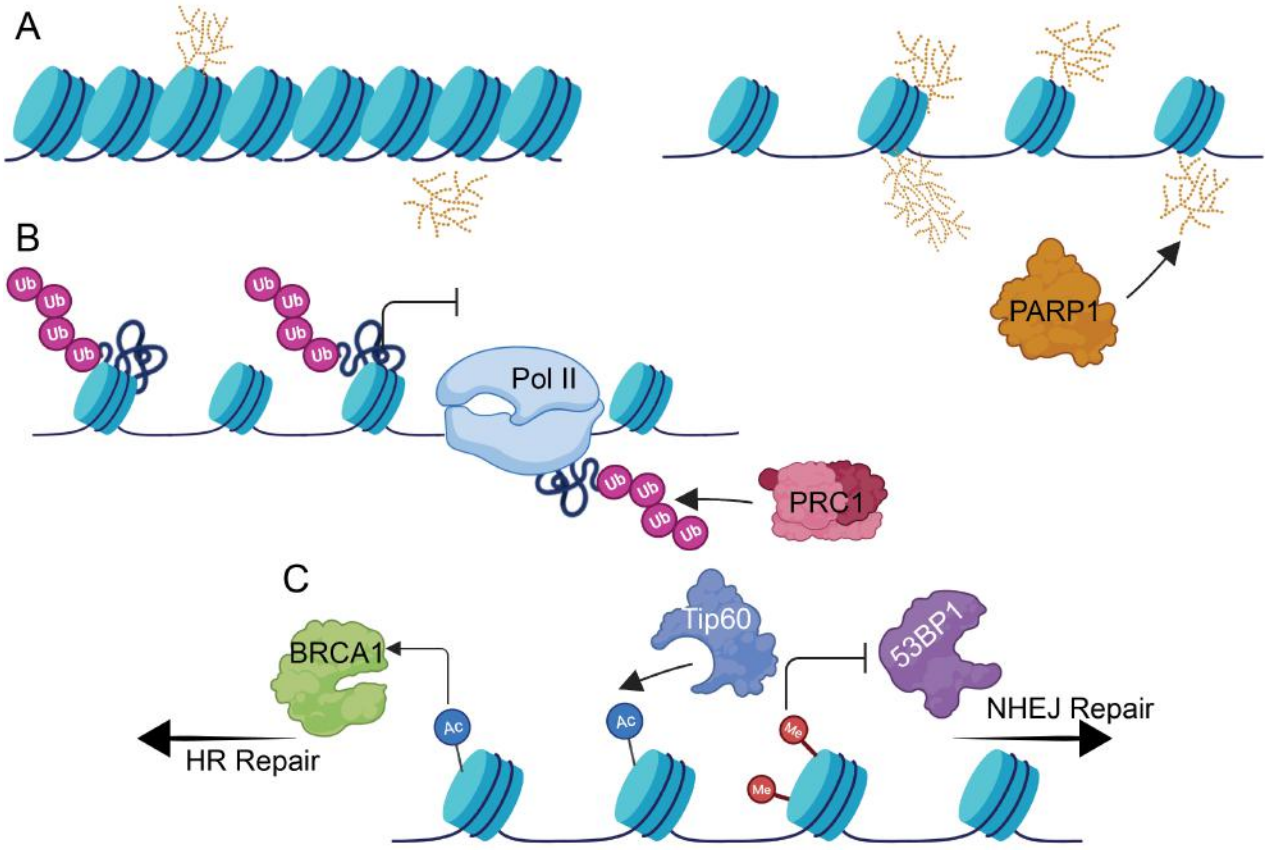

Figure 1.3: A non-exhaustive list of known chromatin:DDR interactions. **A** PARP 1 places PAR chains on histones which mediate chromatin decompaction. This may be necessary for access or recruitment of DDR factors. **B** Polycomb Repressive Complex 1 (PRC1) is responsible for histone Ubiquitination especially on H2AK119. This is necessary to represses transcription *in cis* to DSBs and prevent transcription-damage collisions. **C** Perhaps the best understood chromatin:DDR interaction involves Tip60, a histone H4 K12/16/20 acetyl-transferase. TIP60 has been shown to mediate recruitment of DDR factors and exclude binding of 53BP1 which favors NHEJ. By extension, TIP60 encourages resection and binding of BRCA1.

1.5 Epigenetics of DSB Repair and Ageing

A correlative relationship between declining epigenetic fitness and ageing is well established[212]. More recently, given the increasing connections between epigenetics and DSB repair, and long-standing associations between mutations and ageing, it has become apparent that all three processes may be different facets of the same molecular clock[213, 214]. Indeed, animal models deficient in DDR factors appear to age faster. Likewise, loss of epigenetic factors including SIRT6 accelerate the ageing process[215, 216]. SIRT6 is also a bona fide DDR factor, where it aids in recruitment of, among other factors, PARP1. PARP1 is itself affected by aging, with reduced expression in older organisms. PARP1 levels are also associated with lifespan in mammals[217].

The underlying epigenome also shifts over an organism's lifespan. Ageing is associated with loss of heterochromatin and degradation of borders demarcating active from repressed euchromatic regions[218]. In yeast, histone occupancy declines up to 50 percent with age. Perhaps aged chromatin is more susceptible to DNA damage induction owing to heterochromatin loss. Alterations in specific histone marks have also been associated with ageing, though the same mark or modifier seems to have differential effects in different organisms. Loss of the COMPASS complex extends lifespan in C. elegans but not in mammals[219]. A reduction in H3K27me3 is also associated both with ageing and with the onset of senescence in higher-eukaryotes[220]. It remains to be confirmed whether epigenetic changes mediate ageing directly, and moreover, whether they act via DNA damage-related pathways.

1.6 Outstanding Questions in Epigenetic:DDR Interplay

The above discussion of chromatin remodeling at DSBs raises several important questions. First, several of the putative DDR factors seemingly promote both HR and NHEJ. These data do not square with a mutually exclusive repair choice paradigm, or at least suggest repair choice at a given locus is highly complex, with multiple redundant inputs. Perhaps the choice

is more stochastic than most models present, and individual DSBs retain competency for both HR and NHEJ even after recruitment of some DDR factors. The question remains, then, as to what step or steps commit a given DSB to one pathway or another. While this is certainly not resolved, it would seem that resection commits a break irreversibly to HR. Secondly, the multitude of DDR factors thought to play a role in chromatin remodeling or recruitment of other DDR factors to DSBs seems to strain bio-physical constraints. Indeed, complexes such as SWI/SNF or PRC1 are large and multimeric; it is unlikely that several complexes could co-occupy a DSB locus while allowing for assembly of DDR factors at the break end. Thus, it is more likely that there is kinetic or spatial separation between factors recruited to breaks. Most models do not account for this, and kinetics of DSB detection and repair remain challenging to observe or quantitate experimentally owing to the heterogeneous nature of exogenously induced DSBs. Finally, given the extent of putative chromatin remodeling occurring at DSB loci, one must ask how, following repair, the basal chromatin landscape is re-made. Data on local chromatin restoration is light but histone chaperones including CAF1 have been shown to replace H3 variants following repair[221, 29]. It might be that restoration of damaged chromatin is dependent on orthogonal processes such as replication; indeed, histone alterations persist long after DSBs are repaired.

1.7 The Polycomb Repressive Complex 2 in DSB Repair

PRC2 is an evolutionarily conserved group of proteins first discovered in drosophila[222]. Canonically, the polycomb group of proteins is known to repress gene expression and promote the establishment or expansion of facultative hetrochromatin via deposition of the repressive mark H3K27me3[223, 224, 225, 226]. EZH2 is the core catalytic subunit of PRC2 and can deposit one or more methyl groups on H3K27, though it generally confers trimethylation[227]. EZH2 activity requires the presence of PRC2 subunits EED and Suz12 the former of which binds to H3K27me3 to initiate a positive feedback loop and increase the catalytic activity of EZH2[228]. Recruitment of PRC2 to chromatin is not well understood

through it is known that H3K27me3 increases residency of PRC2. In drosophila, polycomb is recruited via consensus polycomb Response Elements (PREs)[229, 230], though evidence for PREs in mammals is more tenuous and currently debated[231, 232, 233]. In a basal setting, PRC2 is localized to regions of heterochromatin and silenced genes especially CpG islands, though not every putative drosophila PRE contains a CpG island[234]. PRC2 has a central role in development and cell fate decisions owing to its ability to silence gene expression through deposition of the H3K27Me3 mark[235]. While there are so-called polycomb response elements at putative PRC2 target genes, recruitment of PRC2 more likely works via a threshold mechanism and levels of H3K27me3 are in competition with activating marks, thereby dynamically regulating gene expression. In accordance with this model, loss of PRC2 is not known to immediately increase transcription of PRC2 target genes. Recently, it has been suggested that PRC2 may govern placement of all forms of methylated H3K27, though mono and di-methylated forms are generally associated with gene activation as opposed to repression. Thus, it is unclear whether PRC2 controls deposition of H3K27me1 directly or whether, in the context of PRC2 ablation, other enzymes are aberrantly regulated.

The role of PRC2 in maintaining cell fate and identity is well appreciated. PRC2 loss is embryonic lethal, and deregulation of PRC2 skews cell identity, especially in stem cells. More recently, it has been appreciated that EZH2 is deregulated in cancer. Overexpression of EZH2 is associated with poor prognosis and EZH2 is oncogenic in breast and prostate cancer[236, 237]. EZH2's role in cancer has largely been explained by aberrant transcriptional modulation or on alteration of cell fate. EZH2 is also known to drive a stem like state in breast cancer and is commonly associated with a de-differentiated phenotype[125, 236, 238, 239]. As an interesting corollary, pediatric gliomas acquire mutations at H3K27 which lead to aberrant gene silencing and polycomb activity, underscoring the importance of this pathway[240, 241]. Possible oncogenic functions of PRC2 relating to maintenance of genomic integrity are understudied and will be discussed later in this Dissertation.

In addition to PRC2, the PRC1 complex also mediates transcriptional silencing though

its activities are quite different. Functionally, the PRC1 complex affects ubiquitination of histones, principally H2A at K119, through its RING-finger domains[242, 243, 244]. It has been shown that PRC1 can block transcription initiation and cause dissolution of the pre-initiation complex. PRC1 also mediates chromatin compaction, perhaps by recruitment of PRC2 and deposition of H3K27me3. Indeed, H2AUb is associated with H3K27me3 genome-wide and PRC1 is required for repression of PRC2 target genes[245, 246]. However, more recent evidence suggests PRC1 plays a role in transcriptional activation and in chromatin looping[247, 248]. Recall that 3D chromatin architecture is important for γH2AX spreading. A role for PRC1 in DSB repair is well established. A well-regulated histone ubiquitination cascade is observed at DSBs following ATM-dependent recognition. RNF8 and RNF168 are recruited to DSB loci where they mediate mono ubiquitination of H2AK13/K15[249, 250, 244]. Ubiquitination on K13/K15 then recruits 53BP1 via direct binding[251, 252]. Interestingly, H2AX is also ubiquitinated by PRC1 suggesting this modification may be important for recruitment for repair factors or perhaps for interactions with ATM. PARP1 is required for H2AUb surrounding breaks, underscoring PARP as perhaps a master regulator of chromatin organization at DSBs[253].

Our lab has recently uncovered a role for the chromatin remodeler EZH2 in DSB repair[254]. Pharmacological inhibition of EZH2 attenuated γH2AX IRIF levels shortly after IR and led to higher residual γH2AX foci 24 h after IR. Inhibition of PRC1 or EHMT2 (G9a), a mediator of H3K27me1, yielded a similar phenotype. One interpretation of these results is that regulation of H3K27 itself controls the DDR, though it is possible that inhibition of other H3K27 modifiers has second-order effects on PRC2. Indeed, PRC1 is required for PRC2 activity. Others have observed similar phenotypes and suggest a requirement for EZH2 in DSB detection, perhaps by mediating local chromatin compaction or transcriptional repression[170]. Studies seem to suggest that EZH2 is recruited to DSBs repaired by NHEJ, although an EZH2 ChIP-seq track (from ENCODE) was not a predictive marker of 53BP1 binding in a genome wide study[168, 255]. However, these studies looked at DSBs generated by restriction

enzymes, which likely do not behave analogously to IR induced DSBs[27, 171]. Direct interactions between DDR factors and PRC2 include ATM phosphorylation and PAR-ylation of histones surrounding DSBs[256, 257]. Interestingly, PAR-ylation of EZH2 is thought to reduce H3K27me3, suggesting that PARP and PRC2 may play opposing roles at DSBs. Thus, more work is needed to describe the role of EZH2 at DSB loci.

1.8 PRC2 Cofactors in the DDR

It is unknown how PRC2 localizes to sites of DSBs. However, a recent study suggested that PRC2 may make use of co-factors which co-occupy breaks with PRC2 subunits and enhance DDR activity. Specifically, the hematopoietic transcription factor Cux1 accumulates at DSBs shortly after IR insult. Cux 1 is required for normal hematopoiesis[258] and loss of Cux1 is associated with -7/del(7q) acute myeloid leukemias[259, 260]. Cux1 was also shown to play a role in DNA damage repair, specifically Base Excision Repair (BER)[261]. Cux1 has been shown to associate with OGG1 and promote BER; the absence of Cux1 delays repair of abasic sites in a variety of cells[262, 263]. Cux1 loss is also thought to cause defects in cytokinesis, a phenotype shared with other DDR factors such as PLK1 and DNAPK-cs[264, 265]. In a recent study, Cux1 was linked to the DDR through epigenetic modification[266]. Cux1 deficient cells had fewer IRIF, a phenotype which is shared with inhibition of PRC2. Further Cux1 was shown to localize to IRIF and loss of Cux1 was associated with a reduction in H3K27me2 and H3K27me3. This phenotype was ascribed to Cux1 dependent localization of EHMT2 and loss of EZH2. Taken together, these data serve to highlight the need for PRC2 at DSBs but also underscore the complex regulatory pathways at DSBs and the possible need for co-factors to recruit epigenetic modifiers to break sites. In this way, PRC2 at DSBs may operate analogously to PRC2 at promoters. Indeed, even organisms without complex gene regulation have high-fidelity DSB repair pathways. The presence of conserved transcription factors such as PRC2 at DSBs suggests that the DDR is an ancient subset of their functions. A screen identified several transcription factors recruited

to DSBs including TRIM28, ZMYND8 and p300[267]. It is possible that some of these factors are recruited in a complex as they would be to promoters; work suggesting promoter-like activity at DSB ends underscores this possibility. Additionally, ZMYND8 is thought to recruit CHD4, which in turn, prepares chromatin for recruitment of repressive proteins like EZH2. This recapitulates the activity of both proteins in basal transcription[268, 269]. Thus, basal transcription at promoters may be related to activities at DSB loci.

1.9 Outstanding Questions in EZH2 and DSB Repair

The link between EZH2 and DSB repair is well established, though no concrete mechanism has been determined. Several groups have shown that EZH2 localizes to sites of DNA damage, but it is not known if it does so as part of a larger complex[267]. Moreover, studies are conflicting as to whether H3K27me3 levels are changed at DSB sites by the presence of EZH2[270, 271]. EZH2 is a well-known repressor: its presence drives gene silencing and chromatin compaction. Its localization at DSBs, then, seems to contradict numerous reports that chromatin relaxation is a prerequisite for DSB repair[132, 272, 273]. Other efforts have shown that SWI/SNF components also localize to DSBs; the SWI/SNF complex antagonizes the actions of EZH2[205, 207, 206]. Whether or how these oppositional cofactors cooperate in the DDR is unknown. Lastly, if H3K27me3 is important for DSB repair, it follows that heterochromatic regions, replete with this mark, should be repaired more easily than other regions. This has not been demonstrated however, and contradictorily, heterochromatic regions have been shown to repair more slowly than euchromatin[172, 274].

1.10 Transcription in the DDR

Linkages between transcription and DNA damage have long been appreciated, though there is little consensus as to how these two fundamental cellular processes interact. In general, there is a correlation between transcription and DNA damage in so far as transcribed

areas accumulate relatively more DNA damage and that transcription machinery has been associated with DDR factors. Yet, whether these findings reflect transcription as a cause of DNA damage or reveal transcription machinery as promoting the DDR is debated. Indeed, the answer likely varies with respect to endogenous and exogenous sources of damage.

Eukaryotic transcription is a complex and highly regulated process. Transcription from a given gene promoter is directed by histone PTMs including acetylation of H3K27 and H3K4me3[275, 276]. H3K36me3 is thought to mark transcribed regions, especially introns[120]. By contrast, H3K27me3 is known to silence gene transcription when deposited at promoters[277]. Thus, there are inherent correlations between transcribed regions and histone PTM signatures making it challenging to differentiate between the effects of transcription or effects of transcription-associated PTMs on DSB repair. The main effector of transcription in eukaryotic cells is RNA Polymerase II (Pol II). Pol II assembles at promoters with a coterie of cofactors collectively termed the pre-initiation complex or PIC[278]. After PIC assembly, initiation of transcription is governed in large part by phosphorylation of repeated domains in the C-terminal Domain (CTD) of Pol II[279, 280, 281]. Promoter escape is governed by phosphorylation of Serine 5, while phosphorylation of Serine 2 is a prerequisite for processive elongation[282]. Antibodies specific to proteoforms of Pol II can thus be used to delineate promoter-proximal or paused Pol II from sites of processive transcription. Several interactions between PIC components and DDR factors have been identified including NELF-E, though these data may be a second order effect of an association between DSBs and transcribed chromatin[283, 284].

Transcription is a major contributor to endogenous sources of DNA damage. Indeed, the act of transcription leaves DNA in a vulnerable state; transcription requires histone removal and topological changes to the DNA which may lead to *de novo* damage or exacerbate pre-existing lesions[285, 286, 287]. Endogenous DNA damage is highly abundant and includes base modifications or removal of nucleotide bases[288]. More bulky lesions can induce Pol II pausing or backtracking and require specialized repair pathways to overcome. Damage

which impedes Pol II increases the chances for mutagenesis, slows transcription, and increases cellular stress. Replication or transcription can also convert SSBs to DSBs[288].

The most well studied causative link between transcription and DNA damage is transcription-replication conflict. The eukaryotic genome is a crowded place, leading to inevitable collisions between replication and other processes such as transcription or DNA repair. In eukaryotic cells, transcription and replication are separated either spatially or temporally to mitigate conflicts[289, 290]. However, evidence suggests that collisions, especially head-on collisions, contribute to endogenous DNA damage and can result in mutations, possibly contributing to oncogenesis[291, 292]. The incidence of collisions is increased when cells must also contend with exogenous damage, replication stressors, or oncogenic alterations to DDR or signaling pathways, all of which might perpetuate a feedback loop leading to greater damage. While the whole genome is replicated once per cell cycle, transcription only occurs in a very small portion of the genome. Thus, if transcription conflicts generate even a portion of endogenous DNA damage, the observed association between transcription and damaged DNA would appear significant on a genome-wide scale. Indeed, it has been shown that long genes (>800 kb) inevitably accumulate more transcription-replication conflicts because they are slow to transcribe and may be transcribed over more than one cell cycle[293]. Yet, these findings call into question whether transcription conflicts are an error to be avoided, or an expected feature of higher-order eukaryotes. Growing evidence suggests the involvement of DDR factors in mediation, prevention, or resolution of transcription-replication conflicts. While most challenges to the replisome only result in slowing or pausing of replication, completely stalled forks generate long stretches of ssDNA which are recognized by DDR factors[294]. Here, the replication checkpoint works to prevent fork collapse by regulating replication timing, or in some cases, dissolution of the replication complex and recruitment of DDR proteins.

Returning to the third canonical PIKK, ATR plays a role in exogenous DSB recognition, it is better understood as a replication-stress responder[32]. ATR is recruited to genomic loci where it aids in resolution of stalled replication forks[295, 296, 297, 298]. ATR is also found at

fragile promoters or very long genes which are sites of transcription-replication collisions[299]. The ATR pathway may also resolve transcription-replication conflicts by dissolving Pol II complexes proximal to stalled forks[300]. Exclusion of Pol II from breaks is likely required and additional mechanisms by which Pol II mediated break detection are discussed in Chapter 6 and 7. ATM has been shown to shut down Pol I dependent transcription of rRNA in response to damage at these highly transcribed loci[301]. Further, the direction of collisions between transcription and replication, either head-on or co-directional, activates ATR and ATM respectively. Repair pathways may also differ depending on collision orientation with only head on conflicts promoting R-Loop accumulation[302]. Perhaps R-Loops contribute to additional toxicities associated with head-on collisions. Replication timing also contributes to so-called common fragile sites (CFS), regions which are associated with frequent breakage, mutations or disruptions of oncogenes or tumor suppressors[303, 304, 305]. CFSs are known to have a dearth of replication origins and so replicate late in G2[306, 307]. CFSs are also associated with very long genes— loci in which transcription replication conflicts are common[293]. ATR, but not ATM, is required for CFS protection where it orchestrates specialized DNA synthesis and repair activities to bypass transcription-replication conflicts[295]. Fanconi Anemia genes are also involved with DNA damage processing at CFSs, though they do not traditionally participate in repair of exogenously induced damage[308, 309].

Associations between endogenous damage and transcription notwithstanding, transcribed loci are also associated with exogenous damage. Transcription-DSB collisions are potentially deleterious (Figure 1.4 B). To combat this, all three DDR-associated PIKKs have been reported to suppresses transcription proximal to DSBs[32, 130, 310]. At RNA Polymerase I dependent genes, ATM activity is required to repress transcription. DNA-PKcs inhibition has been shown to stimulate global transcription following DSB induction. DNA-PKcs is thought to mediate ejection of Pol II from chromatin in a mechanism involving proteasomal degradation of transcriptional machinery[161]. PARP1 too may mediate transcriptional repression by recruiting KAP1 and SUV39H1, the latter of which mediates deposition of

H3K9me2 and H3K9me3, both repressive marks[311, 312]. PARP1 dependent recruitment of PRC1 and PRC2 has also been shown to mediate transcriptional silencing[313]. Yet, these findings seem to be in conflict with the widely appreciated chromatin-relaxation activity of PARP1 at DSBs. Perhaps newly opened chromatin at DSBs is made available for binding of repressive complexes, though a specific signal for recruitment is not known.

In addition to transcriptional silencing at breaks, break-induced transcription has also been observed, reviewed here[314, 315, 316] (Figure 1.4 D). While the literature is inconsistent and considerable uncertainty remains, recent work has identified multiple roles for RNA polymerase II at or near DSBs, including MRN complex-dependent transcription of break-associated ncRNA[317, 318]. Small, non-coding transcripts have been associated with DSB induction even at loci which do not contain promoters. Enzymes involved in ncRNA processing including DICER and AGO2, have been shown to promote both NHEJ and HR by encouraging γH2AX IRIF formation[319, 320, 321, 322]. RNAi processing enzymes are associated with ATM autophosphorylation and recruitment to breaks. Further, DICER loss prevents chromatin compaction around breaks, suggesting that DSB induced transcription may be associated with chromatin remodeling pathways[3, 323]. Perhaps these observations shed light on an otherwise paradoxical observation: at some promoters, transcription of genes is associated with induction of DNA damage. Specifically, release of paused Pol II may be dependent on DDR factors including ATM and especially DNA-PK[285, 324]. Mechanistically, evidence is lacking, though some suggest that DDR factors are needed to resolve supercoiling or mediate R-Loop removal. However, a connection between nascent RNA transcription and these DDR associated genes has not yet been examined. Further, DSBs themselves may act as promoters. The MRN complex has been shown to recruit Pol II and promote transcription of damage-associated lncRNAs[325, 326]. ssDNA at DSBs mimics a transcription bubble and is sufficient to recruit Pol II[327]. These longer RNA species may be processed by DROSHA or DICER to generate short RNA species which promote DDR and recruitment of 53BP1[325].

Whereas historically transcription was linked to induction of DSBs, recent efforts have begun to invert the association; transcription coupled repair has emerged as a new paradigm[328, 329, 330]. Strong evidence exists linking HR to transcribed regions via a Set2-H3K36me3-CtIP axis[331]. Further, transcription linked histone acetylation of the H4 tail by the Tip60 complex impairs 53BP1 assembly[27]. Transcribed regions also contain low levels of H4K20me2, preventing binding of 53BP1[332]. Use of endonucleases to induce DSBs specifically at promoters also suggests that RAD51 is preferentially recruited to these loci over non-transcriptionally associated regions[168, 333]. These data suggest that NHEJ at transcribed regions is highly inefficient. However, a predilection towards HR seems to contradict rapid repair of transcribed regions; indeed, transcription surrounding breaks is restored after just 2 hours. One solution to this paradox is RNA-templated repair[334]. It has been proposed that RNA proximal to breaks, either produced *de novo*, or tethered to processive Pol II, can act as a scaffold[335, 336]. RNA may link DSB ends, or act as a template for HR. If HR could make use of RNA rather than waiting for availability of a sister chromatid in S/G2, HR alone could account for rapid repair at transcribed genes. Additionally, NHEJ has also been proposed to initiate via an RNA-templated mechanism.

Related to transcription-coupled repair are R-Loops, ambiguous DNA:RNA hybrid structures which seem to play both repair-promoting and repair-attenuating roles surrounding DNA damage. R-Loops arise when RNA Watson-Crick base pairs with one strand of a DNA duplex in the transcription bubble, creating a three stranded structure (Figure 1.4 C). In un-perturbed cells, R-Loops are relatively common[337, 338]. Most R-Loops are associated with transcribed regions especially bi-directional promoters[339, 340]. R-Loops are also associated with fragile promoters or CFS regions where they may contribute to endogenous DNA damage or mutagenesis at these loci. Due to their abundance, all R-Loops are likely not threats to genomic integrity, thought they have been associated with transcriptional stress, replication fork stalling, and DNA damage. Indeed, replication collisions with R-Loops can lead to DSB formation[341]. Resolution of endogenous R-Loops is generally carried out by

RNaseH, which degrades the RNA strand[335]. R-Loops can also be resolved by senataxin, which may act specifically at gene termini[342]. Lastly, Top1 may prevent R-Loop formation in the wake of processive Pol II by relieving supercoiling which contributes to DNA unwinding and complexing with RNA[343].

Outside of endogenous R-Loops, formation of DNA:RNA hybrids is associated with DSBs. Accumulation of R-Loops is dependent upon the degree of local transcription. Mechanisms of R-Loop formation include stalling, pausing or backtracking of Pol II after detection of damage. As discussed above, DSBs trigger transcriptional arrest including recruitment of NELF, a promoter-pausing regulator. R-Loops are also associated with diminished Pol II S2P and an increase in Pol II T1P which is generally deposited at the 3' termini of genes[344, 345, 346]. This shift from processive to paused Pol II may account for R-Loop formation, or may be a consequence of R-Loops: order of function is unclear. Further, H3K79 dimethylation, associated with highly transcribed chromatin, is decreased *in cis* to DSBs[170]. This finding seems to contradict a role for Dot1L which deposits H3K79me2 in DSB repair. Taken together, transcriptional shutdown near damaged DNA likely contributes to R-Loop formation. As discussed above, DSB ends may act as promoters in and of themselves, adding a new mechanism by which R-Loops may be generated[326, 347]. Importantly, this model would suggest that DSBs arising in non-transcribed regions could accrue R-Loops, though this is not observed.

Beyond correlative associations between transcribed regions and damage-promoting R-Loops, DNA:RNA hybrids may take an active role in DSB repair[348]. R-Loops may act as a kind of scaffold for assembly of DDR factors: R-Loops have been shown to stabilize BRCA1/2, Rad51 MDC1 and 53BP1 at DSBs[349, 344, 350, 351]. R-Loops act as physical roadblocks which prevent resection, thereby shunting DSBs toward NHEJ. Loss of RNaseH, which degrades R-Loops, was shown to increase resection in both yeast and mammals[352, 353]. By contrast, R-Loops have also been shown to promote Rad51 foci assembly suggesting an HR promoting role[354]. Indeed, much remains to be gleaned from

R-Loops in terms of repair promotion or pathway choice. Adding further complexity, other work has demonstrated a need to remove R-Loops, usually through the activity of DEAD Box helicases, before DSBs can be repaired[353, 355].

Summing up the work relating transcription and the DDR, several questions emerge. First, are endogenously induced breaks (arising from e.g. replication collisions or stalled Pol II) repaired analogously to exogenously induced DSBs in genic regions. Perhaps the literature has not yet clearly delineated these mechanisms. Secondly, while evidence linking transcribed regions to HR is abundant, it seems unlikely that HR alone could account for rapid repair of DSBs in transcribed regions. Finally, it is not known whether transcribed regions accumulate more DNA damage than heterochromatic regions or whether cells are merely adept at recognizing damaged in transcribed DNA.

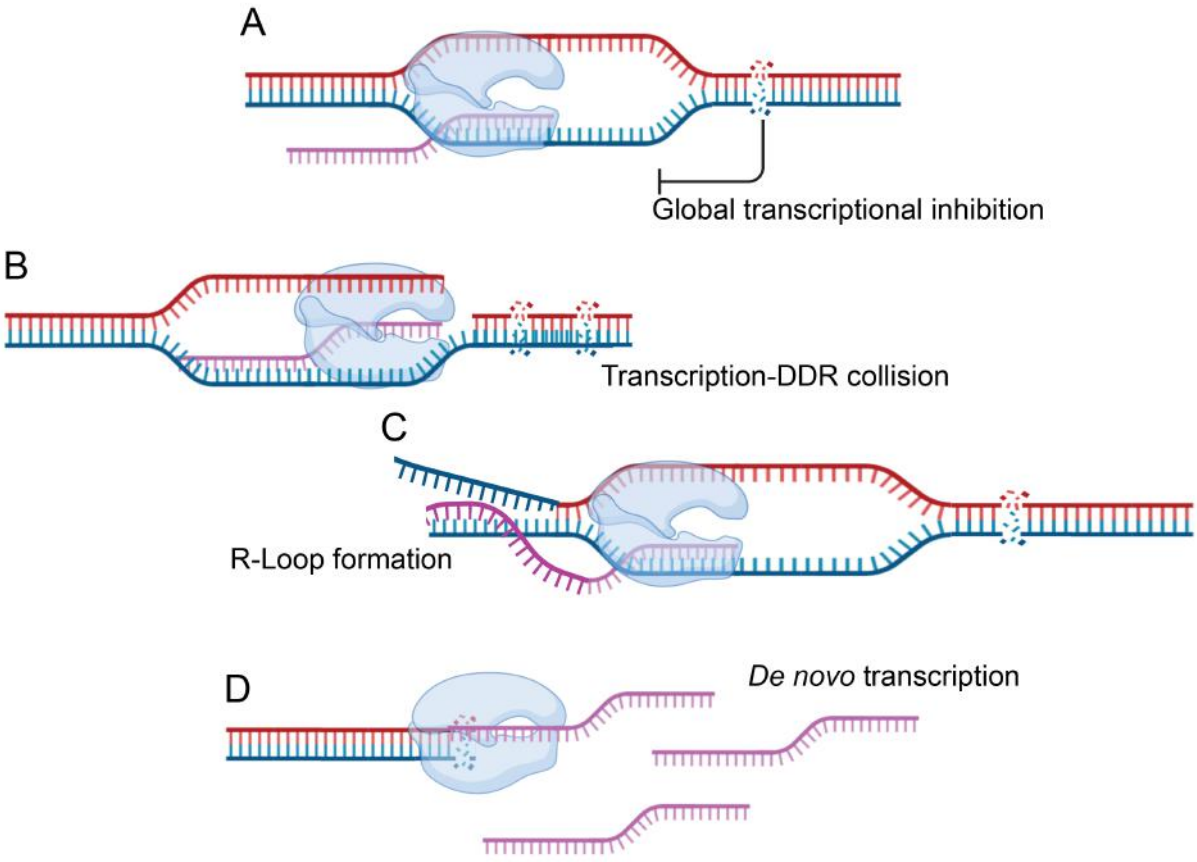

Figure 1.4: **A** It is well understood that transcription is globally attenuated after DSB induction. **B** Failure to repress transcription may lead to deleterious transcription-damage conflicts. **C** Pol II stalling or backtracking after damage is encountered may give rise to R-Loops, tri-stranded RNA:DNA hybrids which have both pro- and anti-damage activities. **D** Finally, in contrast to models which emphasize transcriptional attenuation, other work suggests *de novo* transcription occurs at DNA ends and that nascent RNA participates in the repair of DSBs.

1.11 Clinical Implications

Situating all of the above in clinical context, new opportunities for radiation therapy are apparent. Indeed, combinations of RT and epigenetic inhibitors may increase the efficacy of radiation or allow lower doses of RT to be used[356, 357, 358]. Modern RT can be precisely delivered to a tumor volume creating optimal conditions for combination therapy. Specifically, systemic administration of epigenetic inhibitors at low or moderate doses could be combined with local effects of RT while sparing most tissues including highly replicative ones.

Such a strategy looks appealing in the face of underwhelming clinical utility of epigenetic targeting drugs when used as monotherapy. Epigenetic inhibitors have pleiotropic effects and are often administered systemically for sustained dosing regimens leading to off-target toxicities. Histone modifying proteins are attractive drug targets due to their well understood binding pockets and similarity between family members[359, 360]. Extensive research has uncovered inhibitors for several classes of histone modifiers including HATs, HDACs, and HMTs (such as EZH2). At least seven agents have FDA approval in treatment of one or more malignancies. These include FK-228, an HDAC inhibitor and tazemetostat an EZH2 inhibitor[361, 362, 363]. Finally, BET bromodomain inhibitors are a well-studied class of epigenetic inhibitors now in trials for MDS, AML and solid tumors[364, 365].

There is limited evidence combining epigenetic drugs with RT in a clinical setting. HDAC inhibitors have shown promise in a radio-adjuvant setting perhaps by inducing hyper-acetylation and chromatin decondensation allowing more opportunities for IR to damage open chromatin. Though DNA methylation was not discussed herein, inhibitors of DNA methylases such as azacytidine have also shown promise in conjunction with RT[366]. However, azacytidine is also used in conjunction with chemotherapy suggesting it may directly lead to DNA damage or blunt the response to genotoxicity by downregulation of DDR genes.

Perhaps more relevant to the DDR, inhibitors of Dot1L and EZH2 have been developed. Dot1L inhibitors have had some successes in MLL-rearranged leukemias[367]. In fact, MLL

inhibitors were synergistic with chemotherapy and azacytidine[368, 369]. Perhaps this is due in part to a reduced ability of cells to recognize chemo-induced DNA damage. EZH2 inhibitors are most commonly used in patients who present with dysregulations of H3K27me3 or PRC2 mutations. Tazemetostat, an EZH2 inhibitor, and R-CHOP displayed synergy in follicular lymphoma patients leading to the approval of tazemetostat in 2020[370, 371, 372]. We cannot find major clinical trials exploring the combination of EZH2 inhibitors with radiotherapies. Further, inhibitors of SWI/SNF have not yet been developed leaving future opportunities for use of epigenetic inhibitors in a radio-adjuvant setting.

1.12 Outstanding Questions in DDR-Chromatin Interactions

Taking into account the breadth of research elucidating how epigenetics and chromatin structure influences recognition and response to DNA damage, several lines of questioning emerge. First, how are the initial parts of the DDR (PIKK recruitment, H2AX phosphorylation) able to be accomplished so quickly? Mechanisms of ATM recruitment to nascent DSBs are vague at best. While it is thought that chromatin may play a role in recruitment of ATM or detection/revelation of damage, such events would need to occur within seconds to minutes after DSB induction. Some models posit that ATM continually scans the genome for damage; however, given the size and topological constraints of the eukaryotic genome, completely stochastic models seem unlikely to account for recognition of all, or even most, DNA damage. Alternatively, chromatin itself or chromatin associated processes (transcription, replication) may be required to signal to ATM and report damage. However, this signaling pathway(s) remains unknown. Moreover, given the multiplicity of chromatin environments present in a eukaryotic genome, it is unlikely that all regions utilize the same signaling pathway. Perhaps replication signals the presence of damage via ATR while transcription makes use of DNA-PKcs or ATM. Ultimately, more studies are needed to assess the kinetics of such processes.

Relatedly, while many histone marks and histone modifiers are implicated in the DDR, we

must deconvolute the effects of basal chromatin state from marks added or removed after DSB induction. If a given mark is associated with rapid and robust DSB recognition and repair, it follows that regions replete with the mark in a basal setting should be preferentially repaired. However, this has not been shown and, in the case of repressive marks such as H3K27me3, the opposite may be true. Further, it is not known what histone marks are altered following DNA damage induction. Antibody based screening studies show that most histone marks do not change upon IR, but such efforts do not screen the full complement of histone marks and antibodies to histone marks lack specificity[373, 374]. There are several possible mechanisms by which histones may be altered following DDR activation. These include changes in gene expression, alterations to the cell cycle, and attenuation of replication. Thus, directly linking global changes in histone levels to local, DSB-proximal changes affecting end-joining is experimentally challenging. Further, while many works assay the initial response to DSBs and convincingly show alterations of the epigenome around damaged DNA, knowledge of pathways which restore basal chromatin state after repair is lacking. It is unknown how long DDR mediated changes persist. Perhaps restoring 'normal' chromatin is coupled to replication or cell division. Indeed, copying the chromatin state into two daughter cells is an important and highly effective process, and it is unlikely that both copies of the chromosome will contain DSBs at a given locus. However, epigenetic changes which are upstream of HR necessarily involve both copies of DNA adding further complexities.

The largest outstanding question in epigenetic:DDR interactions remains deducing to what extent chromosomal location affects DSB repair given that not all locations on the genome have the same compliment of histone marks. Despite much effort, only a handful of associations between epigenomic markers and DDR pathways are concretely known. Best appreciated is H3K36me3, an active transcriptional mark, which is thought to promote HR in regions where H3K36me3 is prevalent[168]. However, associations between transcribed regions and HR present a paradox which cuts to the core of DSB repair pathway choice. NHEJ is known to be much more rapid than HR; across a damaged genome or a population

of cells NHEJ accounts for the vast majority of repair[375, 376]. However, there are few pathways which seem to actively promote NHEJ. Both open chromatin (rich in H3K36me3) and heterochromatin have been linked to HR via complex and well-studied mechanisms. Yet, it seems unlikely that most chromatin regions delay repair until S/G2 phase to undergo homologous recombination. Taken together, studies suggest a mechanism where NHEJ is a default pathway which must be restrained: thus far CYREN is the most prominent candidate for inhibition of NHEJ. This model might be a legacy of older work which cast NHEJ as a dirty pathway which promotes mutagenesis, though in reality it is remarkably high-fidelity. We posit that either HR is more common and occurs quicker than most models suggest (perhaps via RNA templated repair or another mechanism) or that there are yet undiscovered pathways which promote NHEJ or retard HR in a majority of the genome. Alternatively, use of restriction enzymes or Cas9 to study DSB:chromatin interactions has given rise to false associations between open chromatin (preferentially cut by enzymes) and any DDR pathway. By extension, studies have not considered whether endogenous and exogenous DSBs may be repaired differently or which pathway is best mimicked by use of enzymes to induce DSBs.

Lastly, these studies raise several interesting implications for tumor biology and the etiology of cancers. Many cancers dysregulate epigenetic modifiers including SWI/SNF or polycomb complexes. In general, the functional significance of such changes is linked to alterations in gene expression: oncogenes are aberrantly transcribed, or tumor suppressors are themselves suppressed. However, global alterations in histone PTMs affect more than a few genes. Studies linking epigenetic alterations to maintenance of genome integrity are lacking. Given the prevalence of RT or other genotoxic therapies in management of cancer, we suggest studies be undertaken evaluating how epigenetic alterations affect therapeutic resistance irrespective of gene expression alterations. Further implications of oncogenic alterations of EZH2 and other enzymes will be discussed later in this dissertation. Along the same lines, more clinical trials combining RT with epigenetic drugs ought to be attempted, especially in the context of a fuller understanding of how histone PTMs impinge on the DDR.

By studying how transcription factors and epigenetic modifiers function in the context of the DDR, we may also glean new information on their function in basal transcription or alteration of gene expression.

CHAPTER 2

MATERIALS AND METHODS

2.1 Cell Lines and Materials

2.1.1 Cell Culture

Cell culture conditions were consistent across all experiments performed. Cells were maintained in a humidified atmosphere of 5% CO2 at 37 °C. All cells were originally obtained from the American Type Culture Collection (ATCC). All experiments were performed within 3 to 10 passages after thawing cells. Cell medium conditions varied with respect to cell type. MCF7 cells were grown in DMEM medium supplemented with 10% fetal bovine serum (Atlanta) and 4 mM L-Glutamine. K562 cells were grown in RPMI medium supplemented with 10% fetal bovine serum (Atlanta) and 4 mM L-Glutamine. HepG2 cells were grown in DMEM medium supplemented with 10% fetal bovine serum (Atlanta) and 4 mM L-Glutamine. All media was supplemented with Pen/Strep antibiotic solution. Cells were passaged via dissociation with 0.5% Trypsin-EDTA (Thermo). For all experiments, cell confluency was maintained between 20-80%.

2.1.2 Inhibitors and Drug Treatment

Small molecules used throughout this research are GSK126, an EZH2 inhibitor (Selleck Chem); GSKJ4 HCL, a JMJD2/3 inhibitor (Selleck Chem); veliparib, a PARP inhibitor (obtained from Abbvie); ACBI1, a SMARCA2/4 PROTAC (opnMe); the poly-CDK inhibitor Flavopiridol (MedChemExpress); the ATM kinase inhibitor KU-60019 (Selleck Chem); the DNA-PKcs inhibitor NU7441 (Selleck Chem); and Olaparib (obtained from Abbvie). Inhibitor stocks were diluted to 10 mM in DMSO and added to cells for the indicated length of time. Unless otherwise noted, final concentrations used were as follows. GSK126, 20 μM; GSKJ4, 10 μM; Veliparib and Olaparib 10 μM, ACBI1 (100 nM), Flavopiridol 1 μM,

KU-600019, 10 nM. DMSO was used at 1:1000 dilution for vehicle treatments.

2.1.3 DNA Damage Treatment

DNA damage was induced by exposure to a ^{60}Co γ-ray source. Cells were placed in an irradiator (MDS Nordion) and exposed to the indicated dose. Dosage rates varied between 11.7 and 8.3 cGy/s depending on the date of the experiment. Cells were placed in the irradiator for sufficient time to achieve a total dose of 6 Gy. This is sufficient to induce 30 to 80 DSBs per cell, with the wide range reflecting cell cycle and/or gene expression differences between cells. For experiments in which cells were not examined immediately after IR insult, cells were allowed to recover in a humidified incubator for the indicated time. Non-irradiated (NIR) samples were mock irradiated.

2.2 Proteomics Methods

2.2.1 Standard IP:MS Procedure

Cells were treated as desired and then lysate was prepared by addition of 500 mL of RIPA buffer to cell pellet followed by vortexting to mix. For IP, cell lysate was sonicated for 20 minutes in RIPA buffer (30 s on 15 s off) using a water emersion sonicator bath. Cell lysate was then incubated overnight at 4 °C with 10 μL of the indicated antibody to bind to target antigens. Antibody retrieval was carried out by incubating with 100 μL of Pierce protein A/G beads (Sigma) for 2 h at 4 °C followed by 5 washes with RIPA buffer and 2 washes with PBS all at RT.

30 μl eluate was in-solution digested with trypsin by first reducing in 50 mM ammonium bicarbonate with 6 μl RapiGest surfactant (Waters) and 10% 200 mM Tris(2-carboxyethyl)phosphine, alkylated with 50 mM iodoacetamide (33 μl) in the dark for 30 min at RT, and digested with 1:50 vol/vol trypsin (Promega) at 37 °C overnight. Detergent was removed with 1 μl trifluoroacetic acid at 37 °C for 45 min. Digested peptides were

cleaned up on a C18 column (Pierce), speed vacuumed, and sent to the Proteomics Core at Mayo Clinic for liquid chromatography–tandem MS (LC-MS/MS).

2.3 Histone Post-translational Modification Analysis Methods

Several methods for high-dimensional analysis of Histone PTMs via proteomics were attempted. Little concordance between methods was observed. While this may reflect biological noise or sample variability, we also contend that technical differences between methods contribute to the variability observed. Assessing the robustness or fidelity of histone PTM analysis is outside the scope of this dissertation, but is worthy of future studies.

2.3.1 Multiple Reaction Monitoring (MRM) analysis of histone PTMs

Initial histone PTM analysis was performed by the Northwestern University Proteomics Core. We used the "Epiproteomic Histone Modification Panel B" assay which is an externally-facing analysis service available on their website. Flack frozen cell pellets were shipped to Northwestern on dry ice for in-house analysis. The method, in brief, is as follows. Histones were extracted directly from flash frozen cell pellets with the addition of 5 volumes of 0.2 M H_2SO_4 for 1 h at room temperature (RT). Cellular debris was removed by centrifugation at 4,000 x g for 5 min and histones were precipitated from the supernatant with trichloroacetic acid (TCA) at a final concentration of 20% (v/v) for 1 h on ice. Precipitated histones were pelleted at 10,000 x g for 5 minutes, washed once with 0.1% HCl in acetone, then twice with 100% acetone with centrifugation at 15,000 x g for 5 minutes between washes. After the final acetone wash, histones were dried briefly and stored at -20 °C until derivatization. Histones were propionylated and digested, with the modification of a single round of propionylation for 1 h prior to and following digestion. Targeted LC-MS/MS was performed on a TSQ Quantiva (Thermo Scientific) triple quadrupole mass spectrometer and raw data were analyzed in Skyline 2 according to published methods.

2.3.2 Northwestern MRM Data Analysis

Data obtained from the Northwestern analysis were provided as a rectangular matrix with each row representing a PTM and each column containing either the raw peak area (peptide intensity value) or the residue-normalized percentage of a given PTM in a given sample. tSNE analysis was performed in R with the RtNSE package on the residue-normalized data. Default settings were used, though the perplexity was set to 1 because of the low number of datapoints. For clustering of PTMs, raw peak area data were used. The package dtwclust was utilized to perform the DTW distance calculations to obtain more accurate relationships between time-series data. The number of clusters was set at 5 after manual inspection of the elbow plot generated by dtwclust and clustering was carried out via the partitioning around medoids (PAM) algorithm. A heatmap was created using the heatmap2 package in R with a Euclidean distance metric and a Ward D2 clustering algorithm. All plots were generated using ggplot2 implemented in base R or the tidyverse packages.

2.3.3 In-house Histone Sample Preparation for LC-MS/MS

We also performed an in-house histone PTM analysis method using Epiprofile software to extract and quantitate histone PTMs from complex MS/MS spectra. The method for sample preperation is as follows. 5 x 10^6 cells were harvested, following the indicated treatment and nuclei were isolated using NEB buffer (10 mM HEPES pH 7.9, 1 mM KCl, 1.5 mM $MgCl_2$, 1mM DTT). Histones were extracted from nuclei by treatment with 0.4 N H_2SO_4 for 30 min at room temperature and then precipitated from the supernatant by dropwise addition of ice-cold trichloroacetic acid. Precipitated histone protein was spun down and washed twice with very-cold acetone. The pellet was then air dried and resuspended in ddH2O. For each sample set, 20 μg of protein was loaded and run in a gel plug for 6 minutes at 200 V. Gel sections were subjected to propionyl derivatization (at the protein level), Trypsin digestion, propionyl derivatization (at the peptide level), followed by C18 cleanup. For propionyl derivatization, propionic anhydride (Sigma) was mixed 1:3 with isopropanol pH

8.0 and reacted 37 °C for 15 min. Following protein derivatization treatment, gel sections were washed in ddH2O and de-stained using 100 mM NH_4HCO_3 pH 7.5 in 50% acetonitrile. A reduction step was performed by addition of 100 μl 50 mM NH_4HCO_3 pH 7.5 and 10 μl of 200 mM tris(2-carboxyethyl) phosphine HCl at 37 °C for 30 min. The proteins were alkylated by addition of 100 μl of 50 mM iodoacetamide prepared fresh in 50 mM NH_4HCO_3 pH 7.5 buffer and allowed to react in the dark at 20 °C for 30 minutes. Gel sections were washed in water, then acetonitrile, and vacuum dried. Trypsin digestion was carried out overnight at 37 °C with 1:50-1:100 enzyme–protein ratio of sequencing grade-modified trypsin (Promega) in 50 mM NH_4HCO_3 pH 7.5, and 20 mM $CaCl_2$. Post-digestion, peptides were derivatized with propionic anhydride:IPA 1:3 at 37 °C for 15 min and repeated for a total of two times. Peptides were then cleaned up with C18 spin columns (Pierce). Peptides were extracted with 5% formic acid and vacuum dried and sent to the Mayo Clinic Proteomics Core facility for HPLC and LC-MS/MS data acquisition.

2.3.4 LC-MS/MS and PTM Analysis via EpiProfile and MaxQuant

Once samples reached MayoClinic, samples were re-suspended in Burdick & Jackson HPLC-grade water containing 0.2% formic acid (Fluka), 0.1% TFA (Pierce), and 0.002% Zwittergent 3–16 (Calbiochem), a sulfobetaine detergent that contributes the following distinct peaks at the end of chromatograms: MH+ at 392, and in-source dimer [2 M^+ H^+] at 783, and some minor impurities of Zwittergent 3-12 seen as MH^+ at 336. The peptide samples were loaded to a 0.25 μl C8 OptiPak trapping cartridge custom-packed with Michrom Magic (Optimize Technologies) C8, washed, then switched in-line with a 20 cm by 75 μm C18 packed spray tip nano-column packed with Michrom Magic C18AQ, for a 2-step gradient. Mobile phase A was water/acetonitrile/formic acid (98/2/0.2%) and mobile phase B was acetonitrile/isopropanol/water/formic acid (80/10/10/0.2%). Using a flow rate of 350 nl/min, a 90 min, 2-step LC gradient was run from 5% B to 50% B in 60 min, followed by 50%–95% B over the next 10 min, hold 10 min at 95% B, and re-equilibrated.

Electrospray tandem mass spectrometry (LC-MS/MS) was performed at the Mayo Clinic Proteomics Core on a Thermo Q-Exactive Orbitrap mass spectrometer, using a 70,000 RP survey scan in profile mode, m/z 340–2000 Da, with lockmasses, followed by 20 MSMS HCD fragmentation scans at 17,500 resolution on doubly and triply charged precursors. Single charged ions were excluded, and ions selected for MS/MS were placed on an exclusion list for 60 seconds. An inclusion list (generated with in-house software) consisting of expected histone PTMs was used during the LC-MS/MS runs.

Sample *.raw files were extracted with pXtract ver 2.0 to obtain their MS1 and MS2 files. These along with their *.raw files were analyzed in Matlab with the Epiprofile 2.0 script. In addition to the Epiprofile modifications detected, we probed for any additional common and unique modifications, thus sample *.raw files were also searched in Maxquant version 1.5.2.8 against a histone protein fasta database downloaded 10/15/2019 from Uniprot. The PTM search was done in multiple searches at 20ppm with 1% FDR filtering using a fixed modification of Carbamiodomethyl (C), common variable modifications of Deamidation (NQ), Formyl (n-term) Oxidation (M), combined with the following additional PTMs Ac, Acetylation (K,S,T); Ar, ADP ribosylation (R,E,S); Bu Butyrylation, (K); Cit Citruillination, (R); Cr, Crontonylation (K); Fo, Formylation (K); Hib, 2-Hydroxyl-isobutyrylation (K); Ma, Malonylation (K); Me Methylation, (K,R); Me2, Di-Methylation (K,R); Me3, Tri-Methylation (K,R); Og O-glycacylation, (S,T); Oh, Hydroxylation (Y); Ph, Phosphorylation (S,T,Y); Pr, Propionylation (K); Su, Succinylation (K); and Ub, Ubituitylation aka GlyGly (K). Downstream PTM analysis was performed in Perseus version 1.6.7.0 and formatted in Perseus, Excel (Microsoft) or R.

2.4 TdT-UdP Double Strand Break End Labeling (TUDEL)

TdT-UdP Double Strand Break End Labeling, or TUDEL, is a specific and sensitive method developed for direct detection of DSBs *in situ*. Several variations of TUDEL were attempted and the method has been previously published. In brief, TUDEL involves the enzy-

matic incorporation of a functionalized nucleotide to free 3' OH DNA ends exposed at DSBs, followed by the fluorescent tagging of incorporated nucleotides. The tagged nucleotides can then be visualized by fluorescence microscopy. Additionally, exogenous nucleotides can be used as a handle for affinity purification or enrichment of DNA ends or DSB-proximal chromatin. For imaging, our best sensitivity and specificity have been achieved using TdT to incorporate ethynyl-dUTP (EdU) followed by copper-catalyzed azide-alkyne Huisgen 1,3-dipolar cycloaddition conjugation chemistry (CuAAC, a form of Click chemistry) to incorporate azide-fluorophores. The TUDEL staining protocol is as follows.

2.4.1 TUDEL Labeling

Cells are mounted on coverslips and treated as desired. When ready for staining, cells are washed 2 times in PBS. Then, coverslips are equilibrated in 1X Blunting Buffer for 10 min. Blunting buffer consists of 100 mM Tris-HCl, 50 mM NaCl, 10 mM $MgCl_2$, 0.025% Triton X-100 at pH 7.5. Following equilibration, coverslips are incubated in 100 μL of Blunting Buffer supplemented with 1 μL T4-Polymerase and T4-PNK at RT for 45 min followed by 2 washed with PBS.

Next, TUDEL labeling mix is added directly to the coverslips. Alternatively, to conserve reagents, particularly TdT, labeling mix may be spotted onto parafilm, and coverslips inverted on top of the droplets. If using this method, the parafilm is placed inside a small, humidified chamber before incubation to avoid drying of the labeling mix. Cells are then TUDEL labeled by exposure to a TdT Labeling Mix consisting of 50 μL of 5X TdT Buffer, 200 μL of 1X TBS, 5 μL of 10 mM dNTPs and 1 μL of 40 mM EdU (Sigma). 1 μL of Recombinant Roche Terminal Deoxynucleotidyl Transferase (Sigma) is added per 250 μL of buffer. TdT Buffer stock is prepared with 500 mM potassium cacodylate (pH 7.2) and 10 mM $CoCl_2$, diluted in 1X TBS. This is then aliquoted and frozen at -20 °C. Subsequently, DTT is added to a final concentration of 1 mM before use. The TdT tailing reaction is then allowed to proceed at at 37 °C for 4 h. Samples are then washed 2 times in 1X TBS. For

imaging DSBs, incorporated TdT can be labeled via "Click-chemistry" upon reaction with an azide containing fluorescent dye. Click Buffer for copper-catalyzed azide-alkyne Huisgen 1,3-dipolar cycloaddition conjugation is prepared fresh and consists of 100 μM $CuSO_4$, 500 μM THPTA (Sigma), 1 mM sodium ascorbate in 50 mM phosphate buffer, pH 7. To visualize TdT incorperated nucleotides, we use ATTO 565 Azide (ATTO-Tech, AD 565-101) in both superresolution and confocal TUDEL imaging. Dye is added to a final concentration of 1mM and the reaction is allowed to proceed for 30 min at 37 °C followed by imaging as described below.

2.4.2 TUDEL-Affinity Purification

For affinity purification of TUDEL-labeled free DSB ends, $1e^7$ cells are pelleted from culture and washed 2X in PBS before being exposed to TUDEL labeling buffer (see above) at a concentration of $1e^6$ cells per mL. TUDEL labeling is performed in a shacking heat block set to 37 °C for 6-8 h. After labeling, cells are pelleted again followed by nuclear isolation using NEB buffer (10 mM HEPES pH 7.9, 1 mM KCl, 1.5 mM $MgCl_2$, 1mM DTT). Nuclei are then fixed and sonicated according to the Standard IP:MS protocol. Nuclear lysate is then added to an azide-containing substrate for covalent capture of TUDEL-labeled DNA-chromatin complexes. Multiple azide substrates were texted including azide-functionalized agarose and azide-coupled magnetic nanobeads. Irrespective of the substrate used, lysate was incubated in click-chemistry buffer as described above. For agarose, samples were incubated overnight at 4 °C and for magnetic beads samples were incubated for 4 h at RT in accordance with the respective manufacturer's directions. Beads were then washed 5X in RIPA buffer followed by 2X washes in TBS.

2.5 Imaging and Immunostaining

2.5.1 General Immunofluorescence Imaging

For all adherent-cell imaging, 2.5 x 10^4 MCF7 or K562 cells were seeded on round 1.5 cover glass in 12 or 24 well plates and incubated until 50-80% confluency was achieved. Irradiation and/or treatment with indicated inhibitors were performed *in situ*. For slide preparation, cells were washed 2X with PBS before being fixed with 4% PFA in PBS for 10 minutes. Cells were then permeabilized in 0.1% Triton x-100 in PBS for 10 min. For basic mounting, cells were stained with 0.5 μg/mL DAPI, and mounted using ProLong Gold (Invitrogen). For immunofluorescence staining, cells were fixed as above, and blocked with 5% BSA (American Scientific) in PBS for 1 h. Then, the indicated primary antibodies were added to PBS supplemented with 5% BSA and 2% dry milk and coverslips were incubated overnight at 4 °C. All antibodies were used at 1:1000 dilution unless otherwise noted. The next day, coverslips were washed 3 X in 5% BSA and 2% dry milk in PBS supplemented with 0.1% TX-100 and 0.05% NP-40. Then, fluorescent secondary antibodies (Jackson ImmunoResearch) were applied for 1 h at RT with shaking. In general, foci images were captured on either an Olympus IX81 wide-field microscope or a Marianas spinning-disk confocal (3i Imaging) with either a 40 X or 100 X oil-immersion objective. Z-stacks were taken at 1-2 μM spacing covering 5-10 μM depending on the sample and date of the experiment. Z-stacks were deconvolved using the "no-neighbors" deconvolution module in SlideBook imaging software (3i Imaging). Deconvolved images were then used for further imaging processing. In general, the DAPI channel was not deconvolved to improve thresholding of the DAPI channel and foci counting.

2.5.2 Antibodies Used

Antibodies used for immunofluorescence in these studies are as follows: γH2AX (mouse mAb, clone JBW301, Millipore Sigma), 53BP1 (rabbit, pAB, Novus), histone H3K27me3

(rabbit, mAb, clone C36B11, CST), histone H3 (mouse, mAb, clone 6.6.2, Millipore Sigma), R-Loop (Kerafast, Rabbit mAb clone S9.6), Pol II N-Term, (CST, Rabbit mAb, D8L4Y), Pol II CTD PS2 (CST, Rabbit mAb, E1Z3G), Pol II CTD PS5 (CST, Rabbit mAb, D9N5I), ATM (CST, Rabbit mAb, D2E2). Secondary antibodies are sheep anti-mouse, Alexa Fluor 488, goat anti-rabbit, Alexa Fluor 647 and Alexa Fluor 595, all sourced from Jackson Immunoresearch. Antibodies used for CUT&RUN in these studies are as follows: γH2AX (mouse mAb, clone JBW301, Millipore Sigma), Histone H4 (ProteinTech), H2AX (ProteinTech, Rabbit pAb), H3K27me3 (CST, C36B11, Rabbit mAb).

2.5.3 IR Induced Foci Counting and Analysis

Many proteins which localize to sites of DSBs form punctate foci termed IR induced foci or IRIF. Counting of foci offers a useful proxy for DSB detection, number of DSBs, and cellular response to IR. Several automated foci counting methods were attempted, and in-house code was written in ImageJ for automated counting of foci. Briefly, nuclei were thresholded and segmented according to the DAPI channel and foci were counted within each nucleus via semi-manual thresholding and a FindMaxima routine. To analyze the amount of DSB repair proteins at IRIF, foci intensity analysis was performed by segmenting the foci as above and then measuring the mean fluorescence intensity within each focus. Foci size was determined by auto-local thresholding of the foci channel followed by segmentation and measurement of segmented foci regions. All other image analysis was carried out in ImageJ via custom macros.

2.5.4 Colocalization Analysis

Colocalization between two channels was determined by in-house code written to implement Li's ICA method73. Briefly, ROIs corresponding to individual nuclei were segmented and cropped and images were saved as intensity matrices. A custom R script was written to transform corresponding matrices into colocalization scores. Pixels were considered to

be colocalized if the intensity in a given pixel was above the mean intensity for an ROI in both channels. We reported the fraction of pixels within a given nuclear ROI which were colocalized. This method is insensitive both to the amount of staining present in an image and to variations in intensity between cells or regions of an image. As an alternative method, the γH2AX channel was thresholded in ImageJ forming a binary image matrix. The MFI of antigens thought to be enriched or depleted in γH2AX high regions was compared between the γH2AX high and γH2AX low portions of the image. Thus, the intensity of putative repair proteins could be compared within and without IR induced foci.

2.5.5 Ground State Depletion (GSD) Superresolution Imaging

For superresolution imaging, cells were seeded on 180 mm square coverslips and stained as above, but not mounted. Coverslips were washed 5X with PBS to remove non-specifically bound fluorophores, inverted over depression slides containing 50 μl of freshly prepared 300 mM MEA oxygen scavenging medium, sealed with a two-part, quick-curing epoxy, and cured 5 minutes in a 50 °C oven. For imaging, we utilized a Leica GSD 3D imaging system equipped with a 160 X/1.43 NA, 0.07 mm WD objective; Suppressed Motion (SμMo) stage; PiFoc precision focusing control system; blue (488 nm), green (532 nm) and red (642 nm) excitation lasers; fluorescein, rhodamine, and far-red emission filters and an iXon Ultra EMCCD camera. Slides were then imaged using in-house GSD imaging protocols with at least 10,000 frames captured per channel per image. GSD data analysis and processing were carried out with a series of in-house ImageJ macros. First, successive frames were aligned to compensate for sample drift. Then, consecutive frames were averaged to create a rolling-mean image. This image was then subtracted from the original image stack to so as to remove invariant image data and highlight differences between frames. This process also corrects for sample bleaching over the course of the acquisition time. Emission events were detected as bright short-lived pulses of light. Identification of emission events was performed via ImageJ plugin ThunderSTORM. Final images were then pseudo colored in ImageJ.

2.5.6 GSD Förster Resonance Energy Transfer (FRET) Imaging

To verify molecular proximity of target proteins or to verify that putative DSB repair factors did, in fact, localize to DSB loci, we exploited the power of GSD imaging to create a novel FRET imaging method. We labeled target proteins or histone PTMs with primary antibodies and utilized fluorescent secondary antibodies to introduce either a donor fluorophore (AF 594) or an acceptor fluorophore (AF 647), hereafter referred to as donor (DNR) and acceptor, (ACC) respectively. This process is also compatible with TUDEL labeled fluorophores being used as the Donor or Acceptor. To image dual-labeled samples, both DNR and ACC were imaged at their respective excitation maxima to obtain an image of DNR and ACC fluorophore locations. In the case of molecular proximity between a FRET pair, DNR energy is transferred to the ACC proportionately to the distance between DNR and ACC molecules. Bleached ACC fluorophores can no longer accept DNR energy, and more DNR energy is thus observed when exciting DNR fluorophores at DNR excitation maxima. Any increase in the DNR emission after ACC bleach is thus indicative of FRET and proportionate to the distance between ACC and DNR molecules. Thus, we bleached the Acceptor fluorophores using high intensity acceptor-wavelength laser power exposure for 60 s. Then, both DNR and ACC were reimaged at their respective excitation maxima. The post-bleach ACC image displayed negligible signal indicating efficient bleaching on ACC fluorophores. To obtain a FRET image, the DNR image before ACC bleach is subtracted from the DNR image after ACC bleach. The resultant image intensity is proportional to FRET between ACC and DNR. Thus, GSD-FRET reports both the location and the degree of FRET interactions between two labeled antigens. GSD-FRET imaging was carried out in the sequence described above. Images were pseudo-colored and manipulated in ImageJ.

2.5.7 FLIM Imaging

Fluorescence images were collected on a Leica Stellaris8 Falcon confocal microscope using a 100X NA 1.4 objective in the FLIM module of LASX software (Leica Microsystems GmbH).

Excitation by means of an extended-range white light laser was sequentially captured per fluorescent probe in by-frame mode, pulse picker 40 MHz, at intensities producing at most one photon per pulse. DAPI was excited at 440 nm for both fluorescence and lifetime data acquisition. Images were accumulated to obtain sufficient counts. DAPI was recorded on HyDX-SMD detector and other probes on HyDS or -SMD class detectors. Five fields of view were taken of each preparation. Fluorescence lifetime for DAPI was estimated using the tau-contrast module built into the Leica Stellaris FILM module. Lifetime maps were exported as .tif files and measured in FIJI. Cells were segmented by means of the 445-DAPI outlines (watershed), and then divided again with respect to γH2AX intensity. The fluorescence lifetime of DAPI molecules in γH2AX high or γH2AX regions were recorded, using custom R script.

2.5.8 Comet Single Cell Electrophoresis Assay

MCF7 cells were irradiated and/or drug-treated as indicated before collection via trypsin and embedding in low-melting agarose (Trevigen). Comet assay was performed with a Trevigen Comet Kit according to manufacturer's directions with the following modifications. Cells were electrophoresed at 23 V for 60 min and stained with SYBR Green rather than SYBR Gold. Imaging of comet slides was carried out on a wide-field microscope with a 10 X air objective. Images were analyzed using ImageJ plugin OpenComet.

2.5.9 Incucyte Analysis

For analysis of cellular growth kinetics, MCF7 cells were seeded at low density (10% confluency) in 12-well plates and then treated as indicated. Plates were incubated in the Incucyte S3 imaging system (Essen Biosciences) for 5 days and images were recorded every 4 h. Confluency was calculated automatically using Incucyte software by manually thresholding a random selection of images and applying these settings to the entire image-set. Data were then normalized to the confluency at time of treatment. Plots were generated in R.

2.5.10 SA-βGal Assay

Cells were seeded at 3×10^4 cells per well in six-well plates and treated with inhibitors for 1 h prior to irradiation. Cells were allowed to recover in a humidified incubator for 3 days before fixation and staining. Cells were then incubated in 0.5 ml of x-Gal containing staining solution per well of 6-well plate. Plate was incubated the plate 8 h or overnight at 37 °C without CO_2. Images were captured on a Zeiss Axiovert 200M microscope with a 20× Plan-NeoFluar objective and Axiocam digital camera controlled by OpenLab software. Two or more replicates were performed, and representative images are shown.

2.6 Genomic Sample Prep and Data Analysis

2.6.1 CUT&RUN Sequencing

500,000 K562 cells were pelleted and washed twice with Wash Buffer (20mM Hepes, 150mM NaCl, 0.5M Spermidine and Roche Complete Protease Inhibitor EDTA free). Washed cells were incubated with activated Concanavalin A-coated magnetic beads (Bangs Laboratories) with Dig-Wash buffer (20 mM HEPES, pH7.5, 150 mM NaCl, 0.5 mM spermidine, 0.05% Digitonin and Roche complete Protease Inhibitor tablet EDTA free) for 5-10 minutes on a rotator. 10 μl bead slurry was used per sample. The cell bound beads were incubated with indicated primary antibody (1:100) in 150 μl antibody buffer (Dig wash Buffer plus EDTA) overnight at 4 °C on a rotator.

The next day, beads were washed 3 times with 1 ml Dig Wash buffer. After washing, 150 μl of the Protein A-MNAse (CST)was added at 700 ng/mL and incubated for 1 h at 4 °C. Following incubation, the beads were washed 3 times with 1mL Dig Wash buffer before addition of 24 μl ice cold 1XpA-MNAse reaction mix (Dig Wash Buffer supplemented with 2 mM $CaCl_2$). Tubes were placed in a cold block and incubated at 0 °C for 30 minutes. Next, tubes were placed on a magnetic stand to separate beads, and the supernatant was removed. Next, of 8 μl 4X STOP Buffer (80mM EGTA, 0.05% Digitonin, 100 μg/ml RNAseA, 100

pg/mL heterologous spike-in DNA (CST)). Beads were incubated in 4X STOP Buffer at 37 °C to release CUT&RUN fragments. Tubes were returned to the magnetic stand and 30 μl of supernatent containing digested chromatin was transferred to new tubes. Immediately, library prep was commenced Ovation Ultralow Library kit (NuGEN). Illumnia NextSeq 500 paired-end 42 bp sequencing was obtained.

2.6.2 CUT&RUN Raw Data Analysis

Sequenced reads were aligned to hg19 using bwa version 0.7.12. Reads were filtered using a q10 cutoff in samtools. BAM files were generated using samtools. BAM files were used for all subsequent analysis unless otherwise indicated. For peak-based analyses, γH2AX peaks were called using MACS2 with an FDR of 0.1 and a –broad flag.

2.6.3 ENCODE Datasets

Epigenetic feature datasets were downloaded from ENCODE. Where possible, filtered aligned reds were downloaded as *.bam files. Data was then processed identically to in-house generated datasets, see above.

2.6.4 ChromHMM Intersection

ChromHMM data was obtained from UCSC genome browser. A 15 state model was used. To intersect reads with ChromHMM states, bed files containing the boundaries of each state were created. Tiles with BLISS coverage above the mean genome-wide coverage were selected and intersected with each ChromHMM state using bedtools intersect with a -wa flag and -f set to 0.5 indicating a given tile had to overlap with a ChromHMM state by at least 50% or 500 bp. Next, the proportion of enriched tiles falling into each ChromHMM state was computed and compared against the genome-wide background (the total number of base pairs occupied by each state divided by the total number of base pairs in all states).

All plotting was carried out in R. Pearson's χ^2 Goodness of Fit test was used to compare distributions between states as indicated.

2.6.5 Peak Nearest-Neighbor Analysis

The nearest neighbor to each peak in the γH2AX peak set was automatically determined using the bedtools closest function and the -each flag. Peaks which overlapped a γH2AX peak were not excluded; these distances were reported as 0 bp. Random peak sets were generated using bedtools shuffle and the -chrom flag.

2.6.6 Genomic Tiling

Bedtools makewindows was used to generate genome wide tiles of various widths. Tiles which overlapped blacklist regions were discarded. Average coverage across each tile was computed using bedtools coverage with a -mean flag. To determine optimal tile width, 10,000 1 Mbp windows were randomly generated using bedtools random and tiled at varying widths. An equal number of tiles were then randomly drawn from each dataset.

Tiles were determined to be γH2AX-High or γ-H2AX-Low depending on the coverage value with respect to the mean genome-wide γH2AX coverage value. We examined several tile widths ranging from 10 bp to 10000 bp. The distribution of γH2AX coverage values across all tile widths was comparable. We also examined the frequencies of adjacent tile pairs to select for a tile width which yielded non-random patterns of γH2AX density. Deviations from randomness were assessed by Pearson's χ^2 Goodness of Fit test. Larger tiles had strongly non-random frequencies of adjacent γH2AX-Low or γH2AX-High tiles; smaller tiles had a distribution further from the naive distribution suggesting our signal to noise ratio declined with tile width. Tiles 1 kbp in width were the smallest tile with maximal deviation from random tile-pair frequencies. Summary statistics for each tile width were computed in R. Tile pair statistics were calculated using the xtabs function. To determine whether adjacent tiles were non-randomly enriched for γH2AX, χ^2 Goodness of Fit tests were performed in

R. The expected tile pair frequencies were determined based on empirical observation that 66% of tiles were γH2AXLow and 33% γH2AX-High irrespective of the tile width.

The epigenetic feature matrix was generated by randomly sampling 250,000 1 kb tiles from across all chromosomes except ChrX, ChrY and ChrM. Average coverage across each region was computed using bedtools coverage with a -mean flag for each genomic feature. The matrix was constructed using custom R code. "High" or "Low" encoding was done by comparing the coverage in each tile with the mean genome wide coverage level for a given histone mark. Genome wide correlation was calculated using the corplot function in R. Jaccard Distances between feature a and b were determined according to standard formulae. Heatmaps were generated using the heatmap2 package. tSNE maps were generated using the Rtsne package. tSNE parameters were determined by grid sampling and visual inspection of the resultant plots. All other analyses with tiled data were performed as described in the text using custom R code.

2.6.7 ChromHMM Modeling

ChromHMM states were learned by using java ChromHMM scripts. Standard settings were used, and bin width was set to 1 kb for consistency with other data. Models which learned several numbers of states were generated. Subsequently, the 4 state model was selected based on manual inspection of the transition matrix and distribution of γH2AX coverage plots. All figures were plotted in R based on data generated by ChromHMM scripts.

2.6.8 ML Prediction of γH2AX

Machine learning models were implemented in R using in house code and the parsnip package. A random sample of genomic tiles was used to train the model. Tiles which had zero coverage across all histone marks were excluded from analysis. Only histone mark features were used as input for the model. The parsnip package was used to prepare data

for ML and implement the gradient boosted tree model. Cross validation was employed to estimate model accuracy. The ranger package was used to run the random forest model. Hyperparameter tuning was achieved by randomly sampling hyperparameters in a grid space and selecting for the highest accuracy combination of hyperparameters. Values indicated in the text reflect performance on a test set of data not used to train the model. AUC plot and summary stats are generated by the parsnip package. A gradient boosted tree model (XGboost) was also tested and gave slightly worse performance.

2.6.9 Transcription Start Site Analysis

Regions of transcription start sites were downloaded from RefTSS and converted to hg19 coordinates using liftover. To create 2 kb regions straddling each TSS, the midpoint of 20,000 randomly selected TSSs was calculated, and the resulting BED file was expanded bidirectionally using bedtools slop. Then, genomic tiles were intersected with these regions using bedtools intersect with default parameters. Genomic tiles were intersected with ChromHMM tracks as indicated. RNAseq data was previously published. The top and bottom decile of genes, ranked expression, were determined by RPKM values. The genomic loci of genes of interest were downloaded from the USSC table browser. Profile plots were generated using deeptools plot profile accessed via Galaxy. To generate TSS meta plots, TSS regions were subdivided into 50 bp windows and coverage within each window was computed via bedtools coverage. Coverage within each window was normalized to the mean coverage across the entire 2 kb TSS region. Profile plots were generated in R by fitting a generalized additive model (GAM) with the formula coverage s(position) where s(x) is a cubic spline smoothing function.

2.6.10 Common Fragile Site Analysis

CFS loci were downloaded as a BED file from HumCFS. The average coverage across each CFS was computed using bedtools coverage and a -mean flag. Random loci were determined

by shuffling the CFS BED file using bedtools shuffle and then coverage was computed across the shuffled regions.

2.7 Statistical Analysis and Plotting

All statistical analysis was performed as indicated. Test were carried out in R using the ggpubr package. In general, a Students T-test was used if n >50 per group and Wilcox test was used to analyze small sample sizes. Kruskal-Wallis and One-Way ANOVA tests were used for analyses of more than two groups, again dependent on whether n was greater or less than 50. For all plots, significance values are as follows: ns $p>0.05$; * $p<0.05$; ** $p<0.01$; *** $p<0.001$; **** $p<0.0001$. Box plots show first and third quartiles of the data as well as the median. Violin plots show the mean. In scenarios where multiple testing was considered, p-values were transformed into FDR q-values by the qvalues package in R (Storey method). All plots were generated in R using the ggplot, cowplot and ggpubr packages.

CHAPTER 3

THE DISTRIBUTIONS OF DSBS AND γH2AX FOLLOWING IR INSULT ARE NON-HOMOGENOUS AND DIRECTED BY BASAL EPIGENETIC STATES

3.1 INTRODUCTION

Histone post-translational modifications (PTMs) have been implicated in almost all aspects of chromatin biology from gene regulation to cell fate and development[113]. Information, which is not encoded in DNA but nonetheless influences phenotypic expression and cell fate, is collectively termed epigenetics. Indeed, while nearly all cells in a given organism share the same genetic information, they evince vastly different phenotypes; epigenetics, principally histone PTMs, allows for such variation to arise[377, 378, 379]. Although epigenetics encompasses several layers and types of information, from the 3D structure of the genome to DNA modification, we will focus in this Chapter on chromatin compaction and histone PTMs. While roles for histone PTMs in gene expression are well-studied, the effects of differential histone modification on genome maintenance or induction of damage are less well appreciated.

Chromatin compaction plays an important role in maintenance of genomic integrity, a process critical for cellular homeostasis. For example, it has long been appreciated that histones are themselves radio-protective and that naked DNA is highly prone to breakage[380, 381]. Ionized particles and free radicals responsible for DNA damage can instead interact with histones[382]. Thus, chromatin bound proteins act as a sort of sink, absorbing radiation or free-radicals and sparing DNA. DNA also adopts different conformations depending on the local chromatin environment; DNA conformation has been shown to influence DNA fragility[383, 384]. Given epigenetic heterogeneity, it is unlikely that all genomic regions recognize and repair DSBs in the same manner; indeed, specialized telomeric and heterochro-

matic repair pathways have been proposed[274, 385]. Changes including differential histone PTMs, and alteration of 3D genome structure may serve to hinder or promote recognition of genomic damage[386, 387].

Turning to a translational angle, cancer cells oftentimes hijack epigenetic modification pathways as a prerequisite for transformation[388, 389, 390]. It is not well understood how malignant alterations to the epigenome may enhance cancer cells' ability to tolerate genomic instability or withstand genotoxic stresses such as chemo or radiotherapy[379]. Further, several studies have identified common fragile sites (CFS) which accumulate breaks and are often the site of large-scale translocations or rearrangements which drive transformation[391, 303, 304]. Breakage at CFSs is associated with various forms of chemotherapy including cross-linking agents, suggesting that the epigenome at CFSs may be permissive to breakage under replication or genotoxic stress[305]. Controlling common fragile site breakage is crucial to maintaining genome integrity. However, CFS breakage could also be advantageous to cancer cells, which have attained resistance toward genome instability. Thus, a fuller understanding of how epigenetics directs genome maintenance, especially in response to acute exogenous DNA damage, can further inform our understanding of why epigenetic deregulation is so often observed in cancer and uncover additional avenues to enhance the efficacy of genotoxic therapies.

However, studies interrogative of the relationship between basal chromatin state and DSB repair are lacking due to technical challenges. The stochastic nature of exogenously induced DSBs represents a potential impediment to genomic localization using traditional techniques such as ChIP-seq which are dependent on averaging signal across a population of cells. Studies which have used ChIP-seq to query the genomic location of γH2AX have found an association with open, transcribed chromatin[392, 393]. This observation is consistent with the radio-protectivity conferred via heterochromatin, though γH2AX and DSB loci may not be coincident, especially if heterochromatin prevents H2AX phosphorylation but not DSB induction. It has also been shown that topologically associated domains (TADs), higher-

order genome structures including folds and loops, proscribe spreading of γH2AX away from DSB loci[182, 184]. Toward obviating technical difficulties, other studies have attempted to use model systems to simulate exogenously induced DSBs including Cas9 and endogenously expressed restriction enzymes[168, 394]. These studies have shown that the local epigenome surrounding cut sites dictates fragility. Epigenetic context also directs repair pathway utilization at restriction enzyme cut sites. However, restriction enzyme based models are likely a poor proxy for IR induced damage; restriction enzymes are biased toward open, accessible DNA whereas radiation or chemotherapy may be less so[395, 396]. Further implicating use of restriction enzymes in these studies, repair of Cas9 induced damage has been shown to rely on Fanconi Anemia genes which are not canonical DSB repair proteins[397]. Additionally, the distribution of cut sites for a given restriction enzyme may not be balanced across the genome. Overall, technical caveats contribute to a lack of studies reporting on genomic locations of exogenous DNA damage especially from a global, genome-wide perspective.

Here, we directly assay stochastic, IR-induced DNA damage and infer relationships between basal epigenetic state and cellular ability to detect DSBs. Contrary to the stochastic nature of radiation, we first show that, as expected, DSBs are excluded from compact heterochromatin. Furthermore, we show that γH2AX is not uniformly distributed genome wide. In general, transcribed euchromatin accumulates more γH2AX more quickly than repressed regions despite having equivalent average nucleosome density and DSB density. Heteochromatic regions are never marked by γH2AX and contain few DSBs. We also uncover connections between basal histone PTMs and recognition of DSBs. Finally, we suggest that the heterochromatin marker H3K27me3 plays a dual role in the DDR: basal H3K27me3 prevents DSB recognition, while we observe DDR promoting effects of H3K27me3 deposited in transcribed euchromatin after IR insult.

3.2 RESULTS

3.2.1 DNA Damage from Ionizing Radiation is Not Detected Uniformly Across the Genome

In order to assess the genome-wide distribution of DSBs following IR, we turned to BLISS, a direct assay which maps free DNA ends *in situ*[398, 399]. Using BLISS, DSBs were mapped in the human myeloid leukemia cell line K562, an ENCODE tier 1 cell line for which abundant epigenomic data are available[400]. K562 cells were exposed to 6 Gy of γ irradiation and processed for BLISS at 1 h post IR (PIR). Although DSBs which can be rejoined by direct ligation may resolve rapidly, complex DSBs— such as those produced by γ rays— require processing and persist for several hours. We mapped $5.5e^6$ BLISS reads to the genome, corresponding to $\sim$ 1 DSB end per 514 sequenceable residues. To examine if chromatin context may influence DSB formation, we adapted an approach used by the ChromHMM genome classifier[401, 402]. ChromHMM first partitions the genome into contiguous bins or tiles and subsequently determines which tiles are enriched or depleted for a variety of epigenetic features. Then, ChromHMM uses a Hidden Markov Model to partition the genome into epigenetic states (e.g., promoter regions, enhancer regions) based on histone PTM ChIP-seq data. Toward modeling the genomic distribution of DSBs, we adopted an analogous approach with BLISS data. BLISS reads were aligned to the genome before binning the genome into tiles and calculating the average BLISS coverage across each tile.

After binning BLISS reads into genomic tiles, we classified each tile as high or low with respect to the mean genome-wide BLISS coverage. Next, we intersected ChromHMM states with BLISS-high tiles to model the distribution of DSBs. We observed significant differences between the distribution of BLISS-high regions across ChromHMM states and the fraction of the K562 genome occupied by each state (Figure 3.1A). Notably, BLISS-high tiles were underrepresented in the ChromHMM state Heterochromatin (which accounts for >60% of

the K562 genome) and were proportionally enriched in other states. The Heterochromatin state represents domains largely devoid of histone marks, consistent with densely packed nucleosomes that shield the DNA from radiation damage. To examine whether chromatin accessibility might serve as a proxy for the expected distribution of DSBs, we examined the fraction of MNase-seq enriched tiles (MNase) in each ChromHMM state. The distribution of BLISS-high regions and MNase-high regions across the 15 ChromHMM states was broadly similar. A caveat is that BLISS, MNase and other seq-based methods may be similarly biased against heterochromatin which is more resistant to sonication, inaccessible to enzymes or antibodies, and characterized by repetitive sequences that frustrate alignment. To extend our analysis beyond regions of the genome classified by ChromHMM, we compared BLISS to DNAse sensitivity and MNase sensitivity across all genomic tiles (Figure 3.1B). While DNAse and MNase accessibility were highly correlated, BLISS was less so, suggesting that DSB formation and chromatin accessibility depend on distinct features.

As an intermediate approach to explore additional factors that influence the distribution of DSBs, we extended the genome-tiling approach to map the distribution of 13 well-characterized histone PTMs. The tiled genome was randomly sampled and tiles representing 0.14% of the genome were clustered using t-distributed stochastic nearest-neighbor embedding (tSNE) and plotted as a 2-dimensional projection which we have dubbed a chromatin context map, wherein each datapoint represents a single genomic tile. First, we attempted to cluster datapoints on the tSNE plot using various clustering methods including k-Means clustering, but this was largely uninformative(Figure 3.2). As an orthogonal approach, we intersected plotted tiles with ChromHMM states and color coded the chromatin context map with 3 illustrative states (Figure 3.3A). Validating this approach, color-coding tiles that intersect with the ChromHMM states Weak Transcription, Repressed, or Heterochromatin respectively decorates distinct domains on the chromatin context map. Then, labeling the map according to BLISS-high vs. -low read density reveals tiles marked as Weak Transcription or Repressed are preferentially BLISS-high ($p<2.35e^{-52}$) while those marked Heterochromatin

are primarily BLISS-low (Figure 3.3B).

Genome-wide analysis of γH2AX reveals a complex pattern distinct from DSBs and a potential role for chromatin dynamics As an independent marker of DNA damage detection, we profiled the genome-wide distribution of γH2AX, the S139-phosphorylated form of histone H2AX that accumulates adjacent to DSBs within minutes after IR. Because it reports on activation of ATM, DNA-PKcs and/or ATR upon binding at DSBs, γH2AX formation has long been used as a marker for DSB detection and initiation of the DDR[403, 404]. A caveat is that the PIKKs phosphorylate H2AX over kilobases adjacent to each DSB, making the resolution considerably lower than BLISS. Nonetheless, we examined the genomic distribution of γH2AX by CUT&RUN in duplicate on 500,000 K562 cells at 1 h and 24 h after 6 Gy irradiation. These time points were selected to examine both the initial and late phases of the DNA damage response, with the rationale of comparing "total" DSBs at 1 h to "persistent" DSBs at 24 h[405]. $7.70e^6$ γH2AX CUT&RUN reads were mapped to the genome at 1 h and $4.12e^6$ reads were mapped at 24 h, representing one read for each 36 and 68 sequenceable bases, respectively. Against expectations, mapping the 1 h and 24 h γH2AX distributions to the genomic tiles and then intersecting with ChromHMM states yielded significantly different, poorly-overlapping distributions for the two time points ($p<4.53e^{-78}$; Figure 3.1A). Whereas Weak Transcription and Repressed states displayed similar accessibility by MNAse and DSBs by BLISS, they displayed distinct patterns for γH2AX at 1 and 24 h ($p<1.04e^{-166}$; Figure 3.1A, Inset 1). γH2AX displayed a similar pattern comparing Active Promotors to Inactive Promotors (Figure 3.1A, Inset 2). Looking genome-wide, γH2AX at 1 and 24 h PIR were uncorrelated, indicating that they represent distinct genomic distributions (Figure 3.1B). Each were only weakly correlated with DNAse- or MNase-seq, suggesting that factors beyond chromatin accessibility determine PIKK activation at DSBs. In turn, γH2AX and BLISS displayed only moderate correlation, indicating that distinct epigenetic factors influence DSB formation and detection.

To explore epigenomic determinants of γH2AX formation, we relabeled the chromatin

context map to indicate regions with high γH2AX density at 1 h or 24 h PIR respectively (Figure 3.3C-D). At each time point, γH2AX high tiles were non-uniformly distributed across the map. The distribution of γH2AX at 1 and 24 h PIR differed significantly ($p<2.86e-45$), though each significantly overlapped with high BLISS tiles (1 h PIR, $p<3.93e^{-24}$; 24 h PIR, $p<5.81e^{-5}$). Toward determining epigenetic features linked to γH2AX at either timepoint, we classified the γH2AX dynamics of each 1 kb genomic region between 1 h and 24 h PIR, yielding four patterns (High to High, High to Low, Low to High, and Low to Low) which we named Persistent, Rapid, Delayed, and Refractory respectively. Next, the four γH2AX dynamic patterns were intersected with ChromHMM states. Overall, Persistent and Rapid γH2AX tiles were enriched in Weak Transcription and other expressed states while Delayed γH2AX tiles were enriched in the Repressed and Heterochromatin states[401, 406]. Refractory tiles were linked to Heterochromatin, corresponding to the protection from DSBs detected with BLISS. As expected, color coding the chromatin context map by γH2AX dynamic patterns revealed distinct distributions for each.

Given the enrichment of γH2AX at 1 h PIR in ChromHMM states associated with transcription, we labeled the chromatin context map to highlight expressed tiles using Bru-seq[407], an unbiased method to detect nascent transcripts (Figure 3.3E). High Bru-seq tiles, reflecting the genomic regions that are actively transcribed, displayed a pattern similar to ChromHMM Weak Transcription and were significantly associated with γH2AX at 1 h PIR ($p<3.29e^{-232}$). Bru-seq enriched tiles overlapped significantly with the Rapid γH2AX pattern ($p<2.09e^{-131}$). Like Bru-seq, tiles enriched in γH2AX at 1 h PIR were significantly associated with two other marks of transcribed chromatin, Pol II density and poly(A) RNA-seq (Pol II, $p<7.95e^{-158}$; RNA-seq, $p<1.25^{-164}$). Much like the ChromHMM states and other features, the chromatin context maps also displayed clustering for nearly all of the histone PTMs used to construct the maps. Surveying distributions of several candidates identified the repressive histone mark H3K27me3 as the most similar to the ChromHMM Repressed state, which displays low γH2AX at 1 h PIR, but gains γH2AX at 24 h PIR (Figure 3.3F).

In particular, the H3K27me3 high and Delayed γH2AX pattern tiles overlap significantly ($p<4.70e^{-63}$).

Plotting the read density of CUT&RUN data from γH2AX at 1 h PIR across representative genomic regions revealed a correspondence between γH2AX formation and genes (e.g. Figure 3.4A). Toward identifying genomic contexts where DSBs are more likely to arise and/or be detected, we called peaks on the 1 h PIR γH2AX data using MACS2[408] and examined the distance from γH2AX peaks to other histone PTMs. Epigenetic factor peak sets were downloaded from ENCODE and the distance between each γH2AX peak and its nearest neighbor peak was computed via bedtools[409] and compared to a random distribution. γH2AX peaks were further than would be expected from marks characteristic of repressed or inactive chromatin such as H3K27me3 but closer than expected to expressed gene marks including H3K36me3 and H3K4me3 (Figure 3.4B). That transcription is so tightly linked to rapid γH2AX formation raises the possibility that displacement of nucleosomes by polymerases may facilitate detection of DSBs.

Toward potential mechanisms underlying delayed γH2AX accumulation, the association with H3K27me3, repressed domains, and heterochromatin implicated mechanisms other than transcription. We surmised replication might serve a role much like transcription as both processes involve nucleosome remodeling and chromatin decondensation and generate ssDNA. To explore this model, we examined replication timing by Repli-seq[410]. Genomic tiles were assigned to one of 6 replication times based upon the cell cycle stage with maximum Repli-seq read density within each tile. Then, those tiles were intersected with two illustrative chromHMM states, Weak Transcription and Repressed, chosen because they had similar accessability and DSB density but significantly different kinetics of DSB detection as evidenced by γH2AX (Figure 3.5A). Tiles within each state were separated based on Repli-seq stage (Figure 3.5B). Overall, Weak Transcription domains are replicated earlier as compared to Repressed regions, potentially linking late replication to delayed H2AX accumulation. We then examined γH2AX read density across all tiles separated by their maximum

Repli-seq stage. At 1 h PIR, tiles which replicate in G1 or S1 phase had maximal γH2AX (Figure 3.6A). However, this trend was reversed by 24 h PIR, by which time late-replicating regions were maximally enriched for γH2AX (Figure 3.6B). An implication is that some DSBs that form in transcriptionally silent chromatin may only be detected during replication, concomitant with dilution of repressive marks or generation of ssDNA as a substrate for PIKKs[411, 412]. As a more direct measurement of replication timing, we mapped the distance from all genomic tiles to the nearest origin of replication and plotted this against γH2AX coverage (Figure 3.7A). A moderate trend was observed with a few tiles proximal to replication origins showing hyper H2AX phosphorylation. Finally, we turned to Hi-C data. Hi-C analysis has partitioned the genome into two flavors each found in megabase size compartments[413]. A compartments contain euchromatin and genes and are known to be early-replicating. By contrast, B compartments are hetrochromatic and replicate late; B1 compartments contain high levels of H3K27me3. Computing γH2AX coverage across the 6 compartment types revealed that, at 1 h PIR, A compartments had higher levels of γH2AX than B compartments(Figure 3.7B). By 24 h PIR, this trend was reversed; in particular B1 compartments were enriched for γH2AX at late timepoints.

3.2.2 Examining Confounding Variables as Potential Determinants of Rapid γH2AX Deposition

The genome-wide distribution of γH2AX at 1 h PIR pointed to transcription as a potential mediator of rapid DSB detection, but the same distribution could similarly be associated with other features of expressed chromatin. As CUT&RUN analysis relies upon MNase to release DNA near proteins or histone PTMs of interest, the data may be inherently biased and favor detection of any γH2AX in open chromatin, yielding a false association with expression. To confirm that γH2AX is indeed enriched in open chromatin, we performed Fluorescence Lifetime Imaging Microscopy (FLIM) with DAPI to examine DNA density. FLIM detects photon counts to infer fluorescence lifetime and, by extension, the density of fluorophores;

lower fluorophore density correlates to less dense chromatin and longer fluorescence lifetimes (Figure 3.8A). FLIM analysis of irradiated cells labeled with anti-γH2AX antibody and DAPI revealed DNA density near γH2AX foci was overall significantly lower than other regions (Figure 3.8B). To confirm an association between γH2AX and transcribed regions, we imaged irradiated cells co-stained with anti-γH2AX and anti-RNA Polymerase II (Pol II) antibodies (Figure 3.8C). Image analysis demonstrated significantly greater than random colocalization of γH2AX and Pol II at 1 h PIR (Figure 3.8D) and higher levels of Pol II near γH2AX as compared to surrounding chromatin (Figure 3.8E).These results argue against accessibility-induced bias in the γH2AX CUT&RUN sequencing data.

We then considered that DSB detection may be determined locally by availability of H2AX as a substrate for PIKKs, thus confounding patterns of γH2AX enrichment. Thus, we plotted the read counts for γH2AX against read counts of the two H2A isoforms, H2AFZ and H2AX (Figure 3.9A-B). We observed a negative correlation between H2AFZ and γH2AX, suggesting that DSBs in regions depleted of total H2AX may indeed be under-detected. However, we also observed many loci with high levels of total H2AX but low γH2AX. Toward deconvoluting DSB formation from detection, we examined how the γH2AX distribution varied with known markers of chromatin fragility, shown to predict variations in DSB density[414, 415]. Common fragile sites (CFS) are regions of the genome prone to breakage upon treatment with genotoxic agents[305]. As compared to randomly selected genomic regions, CFS identified by the HumCFS database[416] were enriched for γH2AX at 1 h PIR (Figure 3.9C). We then examined total H2AX density across the four γH2AX dynamic states (Figure 3.9D). While high total H2AX was linked to tiles scored as Persistent, this did not appear to determine tiles scored as Rapid, Delayed or Refractory. Overall, these results uncouple γH2AX formation from H2AX availability.

Next, we examined genome-wide correlation between γH2AX density and all other epigenetic features considered in this study. Pearson correlation was calculated for every pair of epigenetic features across 240,000 randomly sampled genomic tiles. Most epigenetic features

correlated with one another, consistent with the concentration of epigenetic marks in euchromatin versus the large fraction of the genome occupied by undecorated heterochromatin (Figure 3.10A)[401]. However, we observed anti-correlation between repressive and activating features, suggesting our analysis faithfully recapitulated known epigenetic relationships. We next computed the partial correlation matrix, designed to remove confounding effects of highly-correlated variables (Figure 3.10B). Hierarchical clustering revealed that repressive features like EZH2 and H3K27me3 clustered together and were anticorrelated with features of transcribed chromatin including Pol II and H3K36me3. γH2AX clustered with, and was highly correlated with, markers of transcribed chromatin. Expected correlations, such as between EZH2 and its footprint H3K27me3, and between the gene activating markers H3K9Ac and H3K4me3, were highlighted, validating this approach. Collectively, these analyses show that γH2AX is enriched in regions with features indicative of active, open chromatin and is excluded from repressed domains. This data is inconsistent with current understanding that DSB formation and detection occur in a similar pattern throughout the genome.

3.2.3 A Machine Learning Model Predicts γH2AX Distribution and Kinetics from Basal Epigenetic Marks

As an alternative strategy to identify which underlying epigenetic features might most influence DSB detection, we employed a random forest machine learning model to predict γH2AX coverage of genome tiles at 1 h PIR in K562 cells from the distribution of 13 histone PTMs drawn from ENCODE. The model accurately predicted γH2AX coverage at 1 h PIR with an AUC $>$0.9 (Figure 3.11A). The repressive mark H3K27me3 and the transcription elongation mark H3K79me2 were the strongest determinants in this model (Figure 3.11B). H3K79me2 has been implicated in the DDR. A second model trained to assign genomic tiles to the four γH2AX dynamic patterns, Persistent, Rapid, Delayed and Refractory, yeilded a balanced AUC of $>$0.8 (Figure 3.11C). Here, total H2AX was the best predictor of γH2AX dynamics, but multiple H3 methylation marks also made significant contributions (Figure

3.11D). Notably, this model failed to accurately discriminate between Persistent and Rapid tiles, suggesting their epigenetic similarity. As an alternative machine learning approach, we used ChromHMM to train a four-state epigenetic model using the same input data used to generate the chromatin context map (Figure 3.11E). The four learned states recapitulated the four patterns we manually assigned after inspecting γH2AX dynamics. State 1, high in H3K27me3, was low in γH2AX at 1 h PIR, but high at 24 h PIR, corresponding to the Delayed pattern. State 2 had low levels of all marks as found in the Refractory pattern, likely representing heterochromatin[417, 401]. States 3 and 4, with high levels of Pol II and other active marks, gained γH2AX by 1 h PIR, corresponding to the Persistent and/or Rapid patterns. That γH2AX kinetics can be readily predicted from basal epigenetic marks confirms a key role for chromatin context in DSB detection.

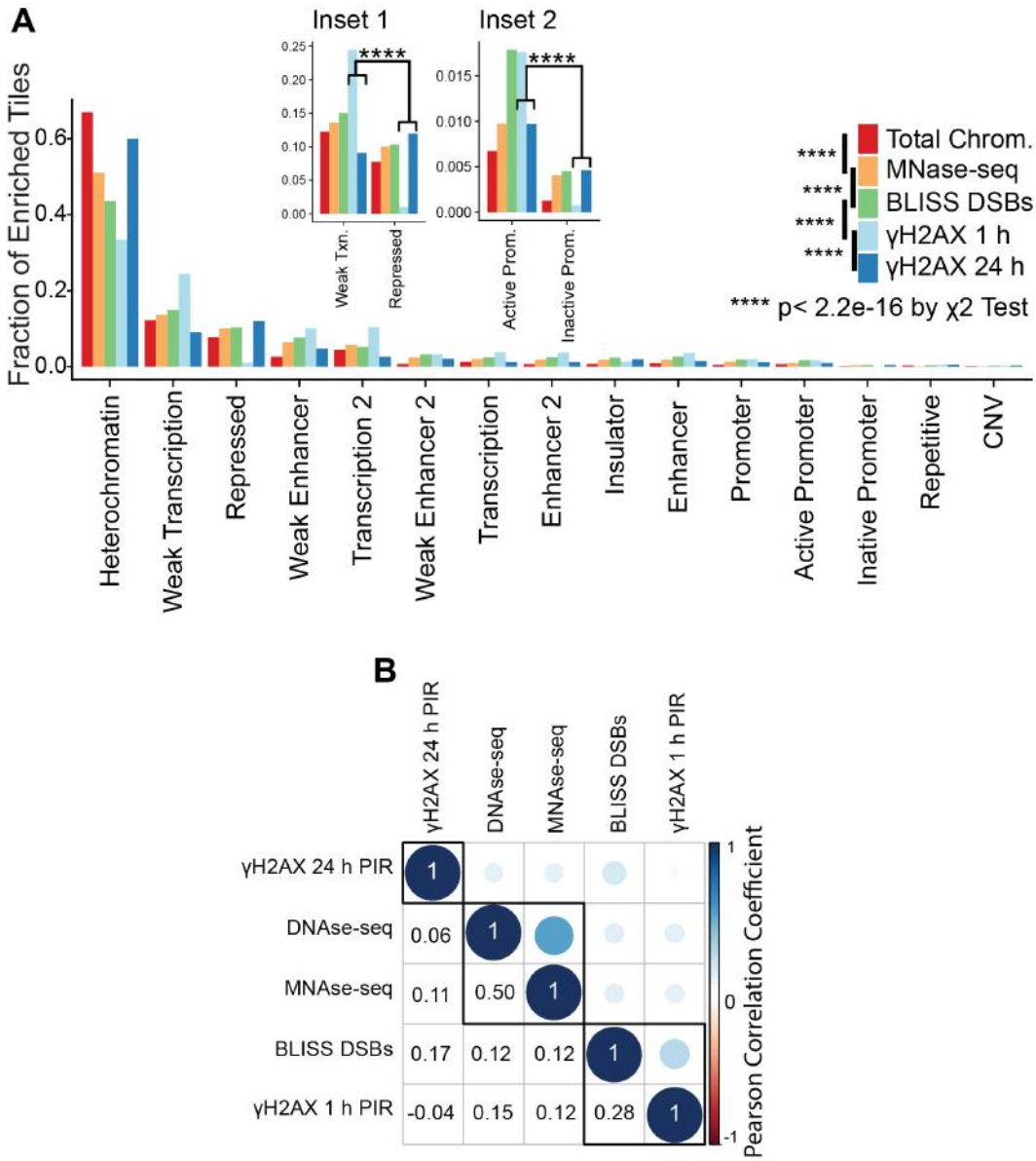

Figure 3.1: **A** Tiles enriched in the given epigenetic features were intersected with ChromHMM states. The proportion of enriched tiles in each state is plotted and compared to the fraction of the K562 genome within each state. The distribution of enriched tiles between the indicated features is compared by Pearsons's χ^2 Goodness of Fit Test. **** $p<2e^{-16}$ Inset panels show the distributions of epigenetic features between select pairs of ChromHMM states. The distribution of features between the states is compared by a X^2 Test of Association. **** $p<2e^{-16}$. **B** Correlation plot between metrics of chromatin accessibility and DSB repair as determined from 250,000 randomly sampled genomic tiles. Color and size of the circles denotes the strength of the Pearson correlation between the indicated epigenetic features. The lower triangle shows Pearson correlation coefficients. Epigenetic features are clustered according to the distance between features in the correlation matrix. Rectangles denote 3 clusters as determined by ward hierarchical clustering.

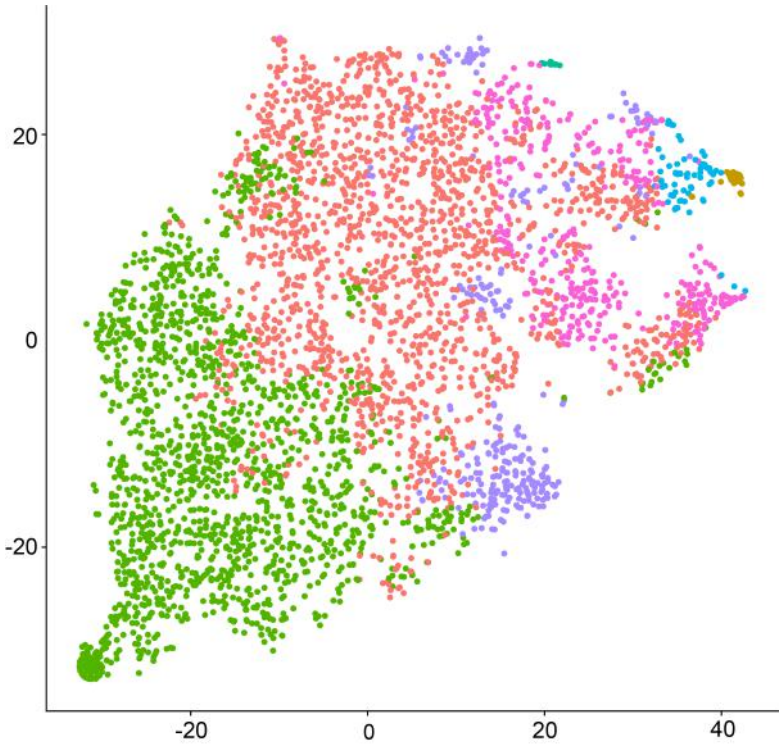

Figure 3.2: A representative tSNE plot of 2,000 randomly selected tiles which has been clustered by k-Means clustering. Here k was arbitrarily set at 7, and each color corresponds to an arbitrary cluster. Note that some very distinct clusters occupy an extremely small fraction of points.

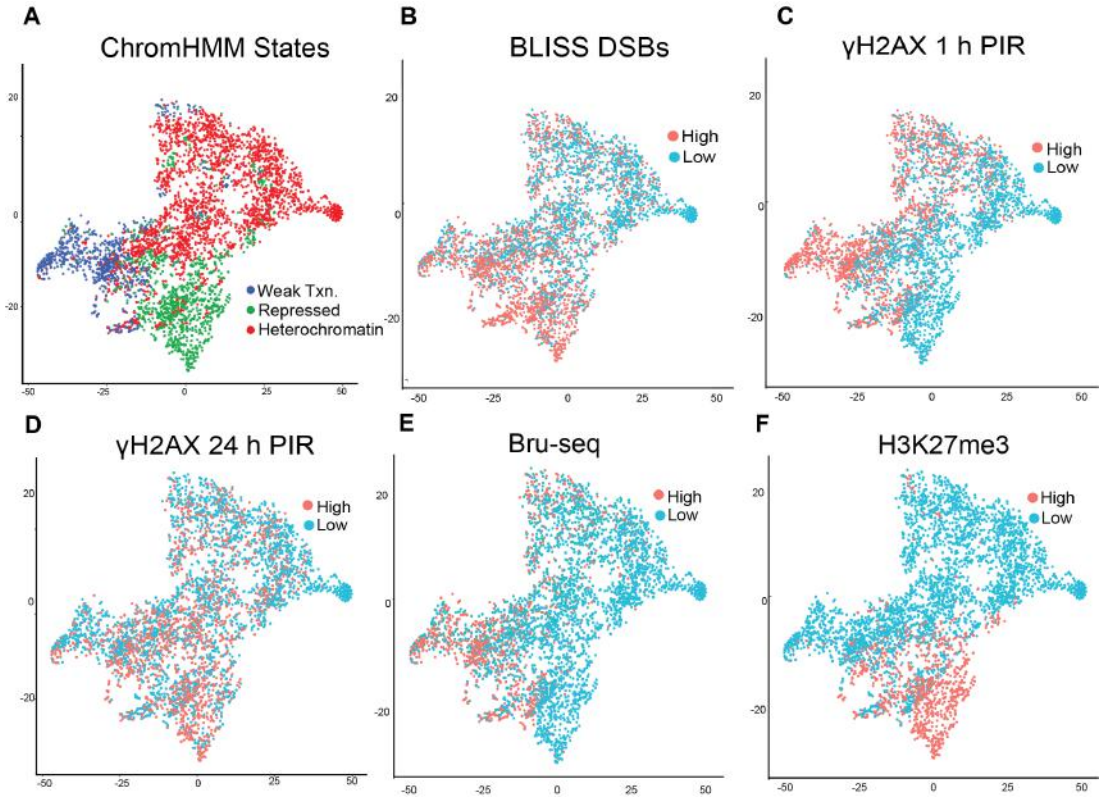

Figure 3.3: **A** tSNE plot generated from the epigenetic matrix. Each point corresponds to one 1 kb genomic tile. The plot is color coded according to one of three illustrative ChromHMM States which was maximally enriched in a given tile. 2,000 γH2AX-High and 2,000 γH2AX-Low points were randomly selected for plotting. **B** tSNE plot as in A but color coded according to the value in each tile with respect to the mean epigenome-wide coverage value of BLISS DSBs. **C** tSNE plot as in A but color coded according to γH2AX CUT&RUN coverage 1 h PIR with respect to the genome-wide mean. **D** tSNE plot as in A but color coded according to γH2AX CUT&RUN coverage 24 h PIR with respect to the genome-wide mean. **E** tSNE plot as in A but color coded according to basal Bru-seq coverage with respect to the genome-wide mean. **F** tSNE plot as in A but color coded according to basal H3K27me3 coverage with respect to the genome-wide mean.

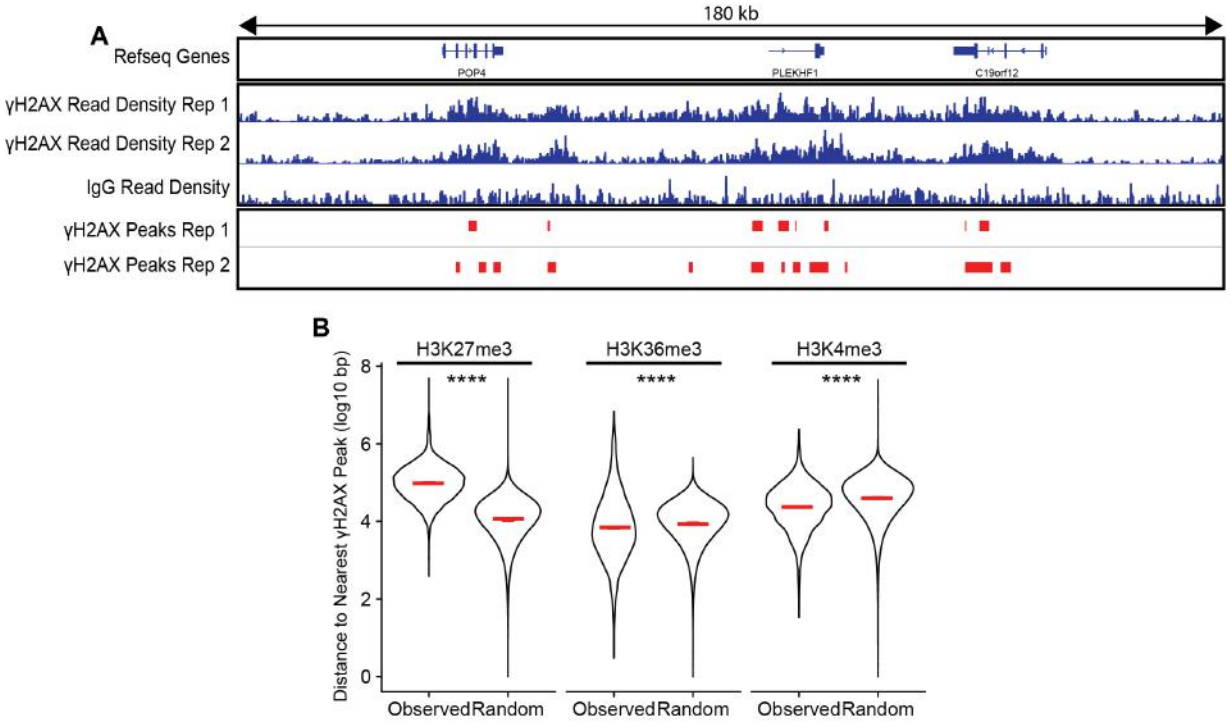

Figure 3.4: **A** Plot of γH2AX CUT&RUN coverage and peaks in a representative genomic region created by the UCSC Interactive Genomics Viewer. Two biological replicates of γH2AX CUT&RUN data are shown, along with an IgG control. Raw read density is shown in blue, and peaks called by MACS2 are shown in red. **B** Distance between γH2AX peaks and the nearest-neighbor peak for representative epigenetic features downloaded from ENCODE. Distances to the nearest neighbor peak for each γH2AX peak were calculated in bedtools. Random peaks are drawn by randomly shuffling γH2AX peaks. Data are shown as violin plots wherein red bars denote the mean. **** $p<0.0001$ by Wilcoxon rank sum test comparing observed and random distances.

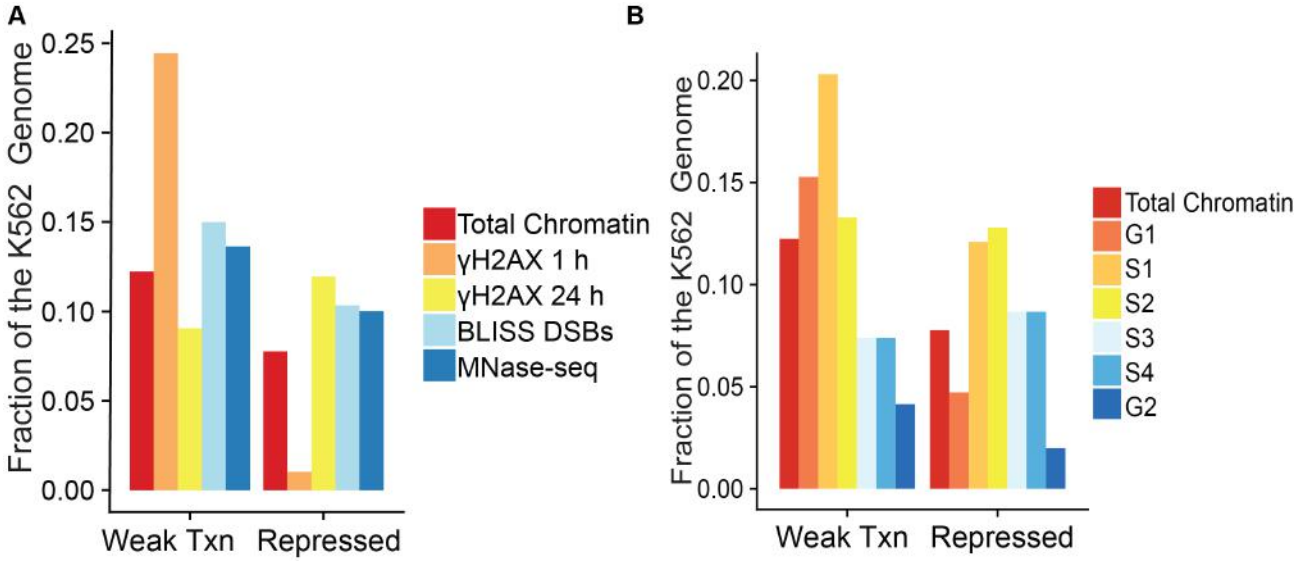

Figure 3.5: **A** Two illustrative ChromHMM regions were selected because they occupied a similar fraction of the genome, had similar MNase sensitivity, and BLISS-seq uncovered a similar number of breaks within each region. These regions differed in kinetics of γH2AX deposition. **B** Replication timing differs between these regions, suggesting one rationale by which broken DNA may be recognized late after IR insult.

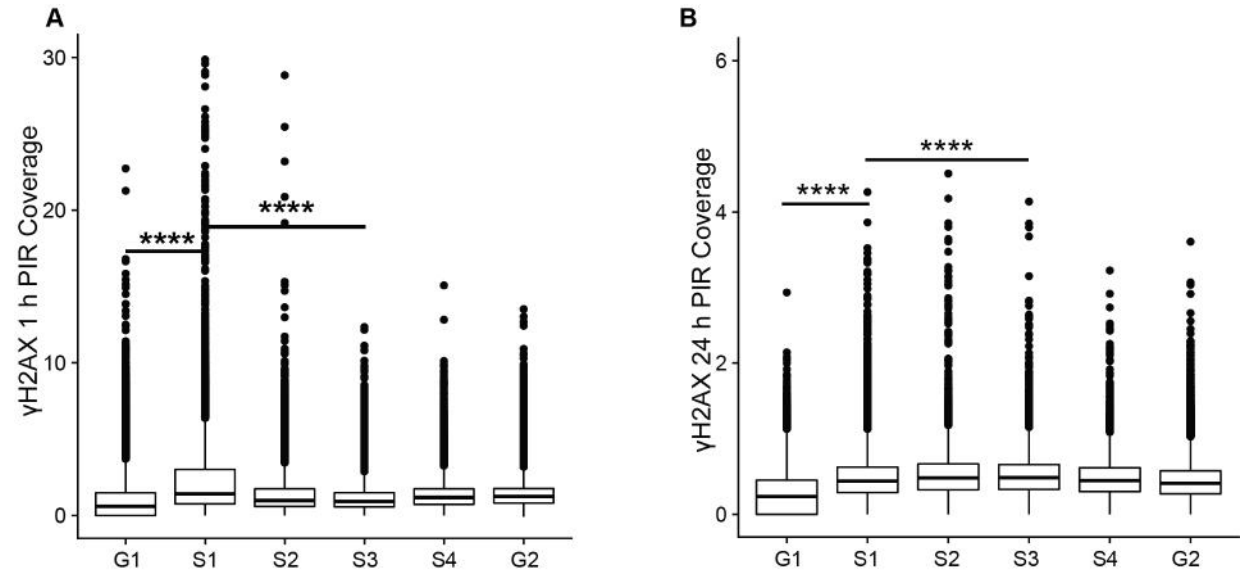

Figure 3.6: **A** Average γH2AX coverage 1 h PIR within tiles grouped by the phase of the cell cycle in which they are maximally replicated. Replication timing is assessed by measuring Repli-seq coverage within each tile across 6 cell cycle phases. **B** Plot as in A but with γH2AX coverage 24 h post IR. Coverage 24 h post IR is higher in late-replicating regions.

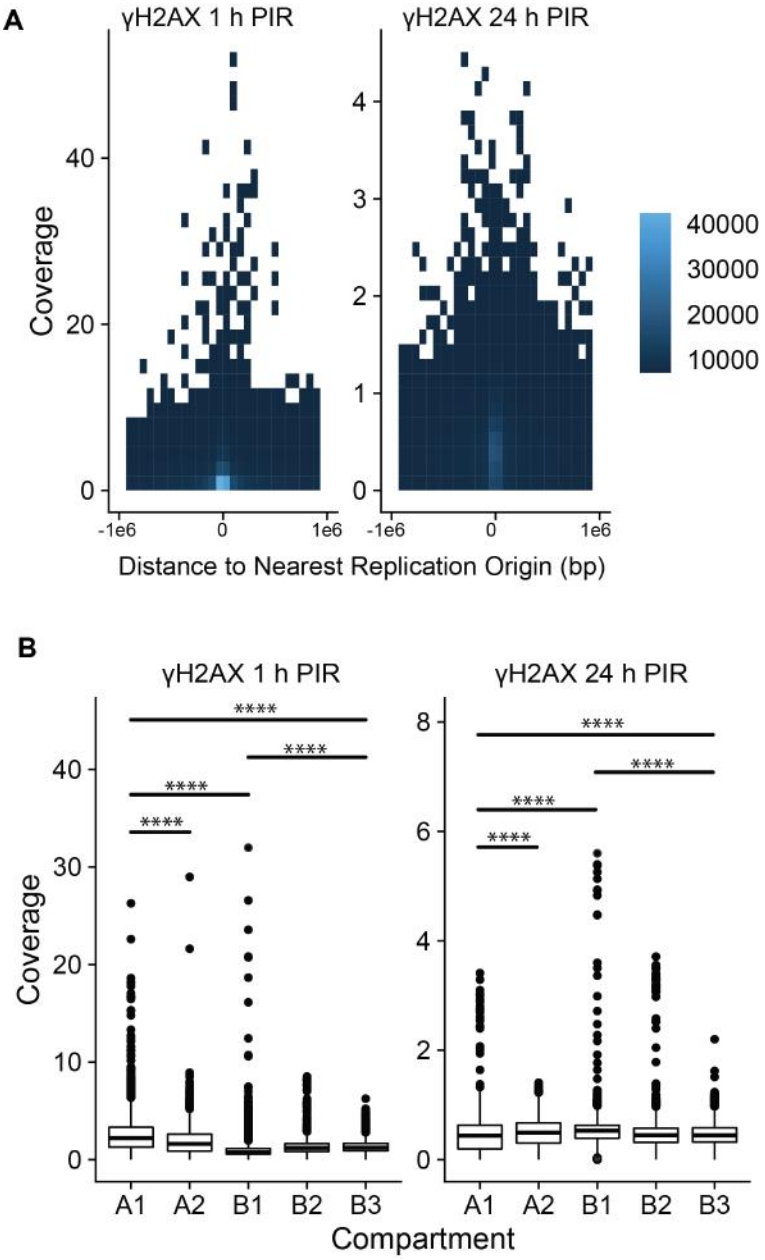

Figure 3.7: **A** Density plot showing the γH2AX coverage within each tile as compared to the distance to the nearest replication origin of that tile. Replication origins are derived from ORC1 ChIP-seq data. **B** Average γH2AX coverage at either 1 h or 24 h post-IR within tiles grouped by the HiC compartment in which they fall.

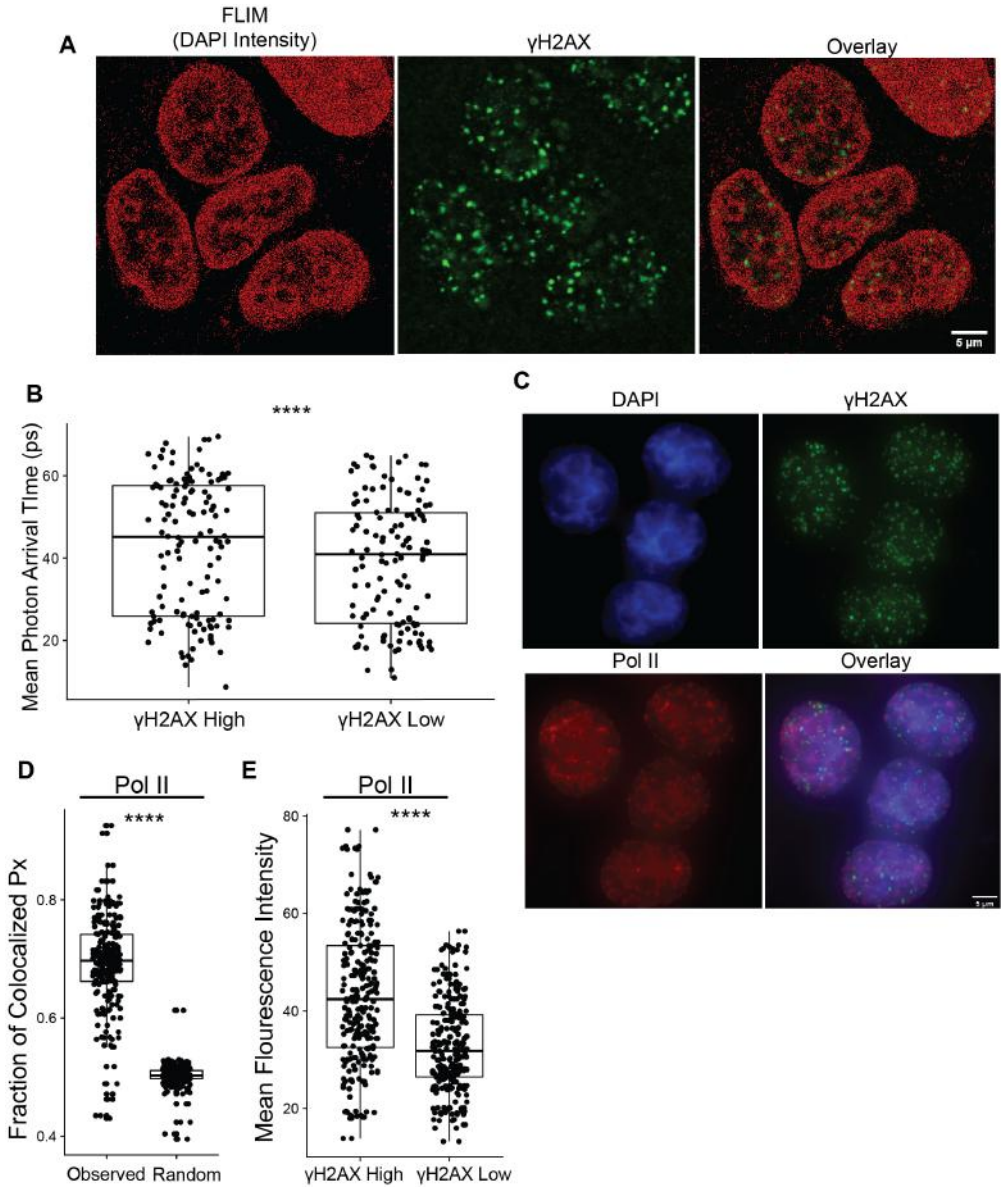

Figure 3.8: **A** FLIM imaging of γH2AX and DAPI density. A representative image is shown, depicting intensity of DAPI signal and γH2AX foci at 1 h PIR. **B** FLIM imaging of DAPI intensity in irradiated K562 Cells. Mean photon arrival time is calculated on a per pixel basis by Leica software. Nuclei are subdivided with respect to the average γH2AX fluorescence per nucleus. Longer photon arrival times indicate less dense DAPI fluorophores and more relaxed chromatin. **** $p<0.0001$ by Wilcoxon rank sum test. **C** Immunofluorescence imaging of γH2AX and Pol II 1 h PIR. A representative image is shown. **D** Immunofluorescence imaging of K562 cells 1 h PIR. Data represent colocalization between Pol II and γH2AX immunofluorescence. Colocalized pixels are defined as pixels in which γH2AX and Pol II fluorescence intensity both exceed the cellular average. Each point corresponds to one nucleus. Random colocalization is determined by shuffling the γH2AX intensity data within each nucleus. **** $p<0.0001$ by Wilcoxon rank sum test. **E** As an alternative colocalization method, the mean fluorescence intensity of Pol II was calculated within nuclei sub-divided with respect to the mean nuclear fluorescence intensity of γH2AX. **** $p<0.0001$ by Wilcoxon rank sum test.

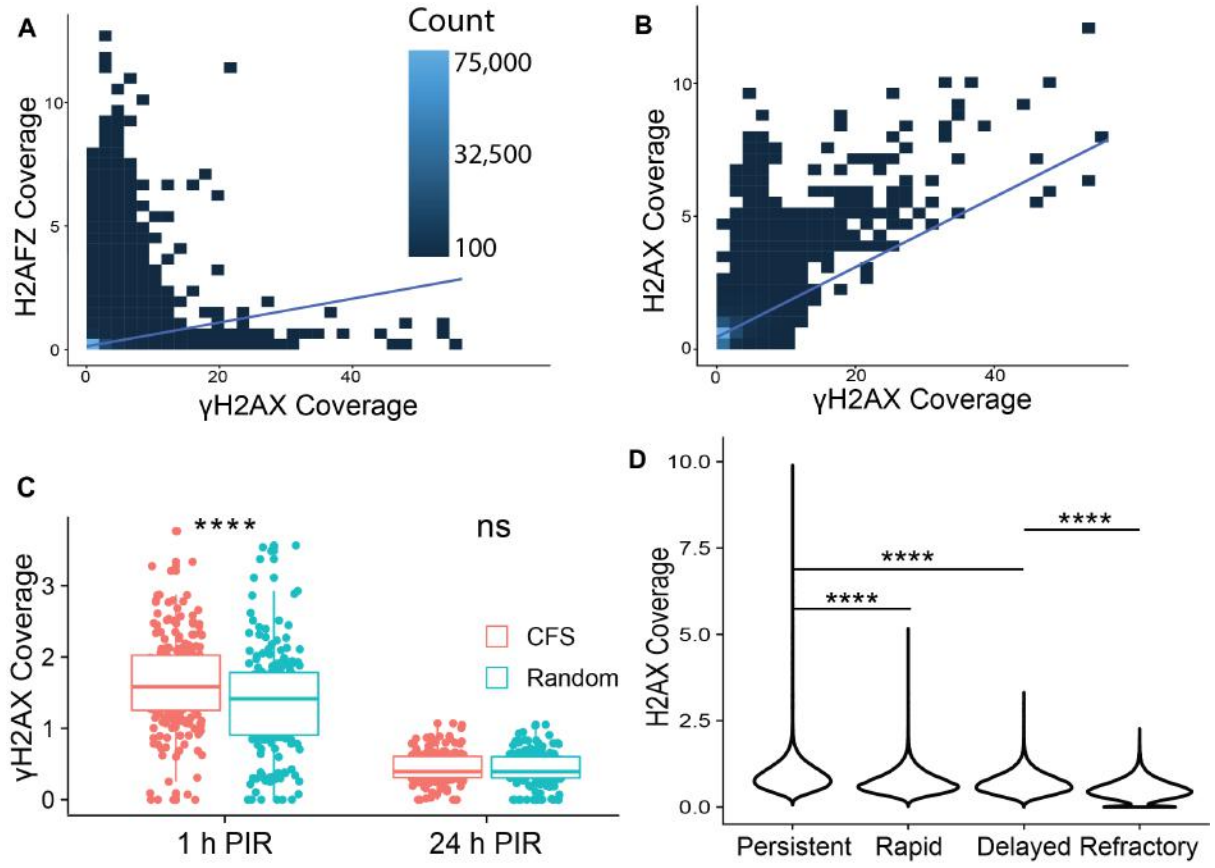

Figure 3.9: **A** Density plot of γH2AX and H2AFZ coverage. Color of each tile indicates the density of datapoints within that tile. Blue line indicates the LSRL best fit line. **B** Density plot of γH2AX and H2AX coverage. Color of each tile indicates the density of datapoints within that tile. Blue line indicates the LSRL best fit line. **C** γH2AX coverage within CFS regions as compared to randomly selected regions generated by bedtools random at the indicated timepoint PIR. **** p <0.0001 by Wilcox ranked sum test. **D** H2AX Coverage in genomic tiles grouped by γH2AX dynamic states. H2AX coverage does not meaningfully differ between regions which are uniquely occupied by γH2AX at 1 or 24 h PIR, suggesting that ATM substrate availability does not dictate kinetics of DSB detection. **** p <0.0001 by Wilcox ranked sum test.

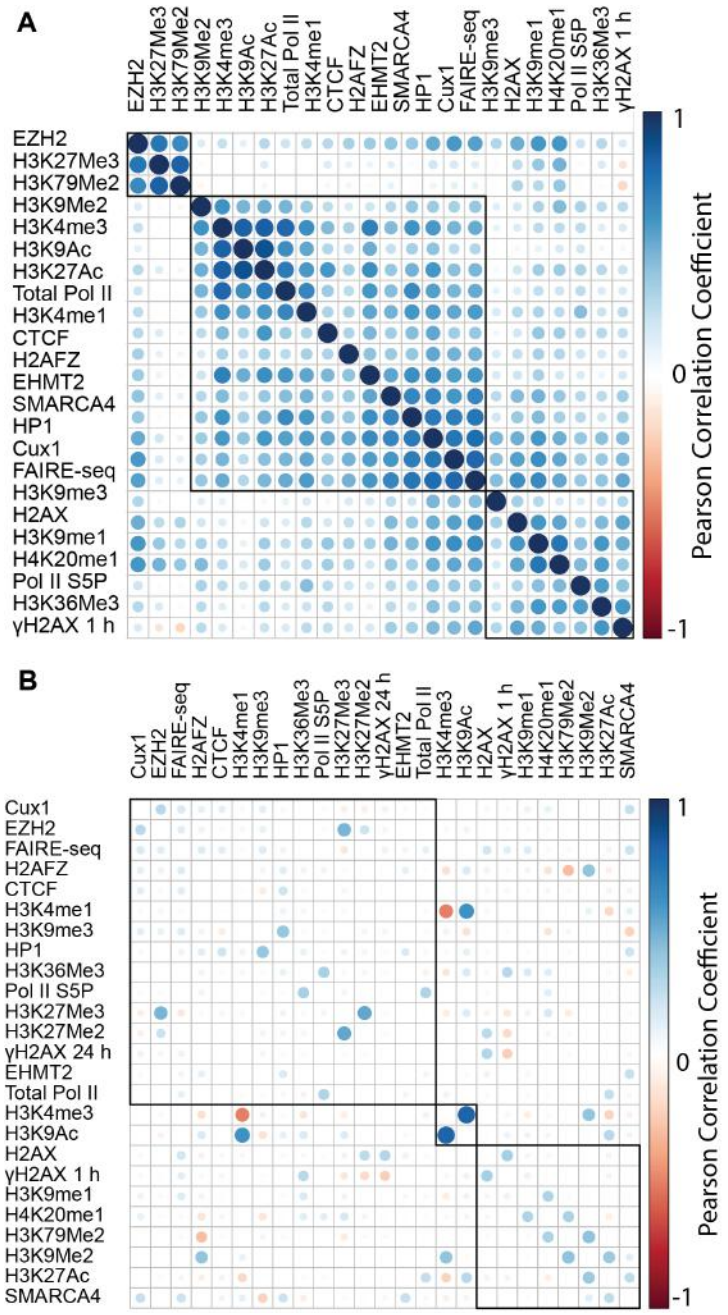

Figure 3.10: **A** Pearson's correlation matrix between epigenetic features as determined from 240,000 randomly sampled genomic tiles. Color and size of the circles denotes the strength of the Pearson correlation between the indicated epigenetic features. Epigenetic features are clustered according to the Euclidean distance between features in the correlation matrix. Rectangles denote 3 clusters as determined by ward hierarchical clustering. **B** Partial correlation matrix of the epigenetic features included in this analysis. Partial correlation accounts for confounding effects introduced by covariances between multiple variables. Color and size of the circles denotes the strength of the Pearson correlation between the indicated epigenetic features. Epigenetic features are clustered according to the Euclidean distance between features in the partial correlation matrix. Rectangles denote 3 clusters as determined by ward hierarchical clustering.

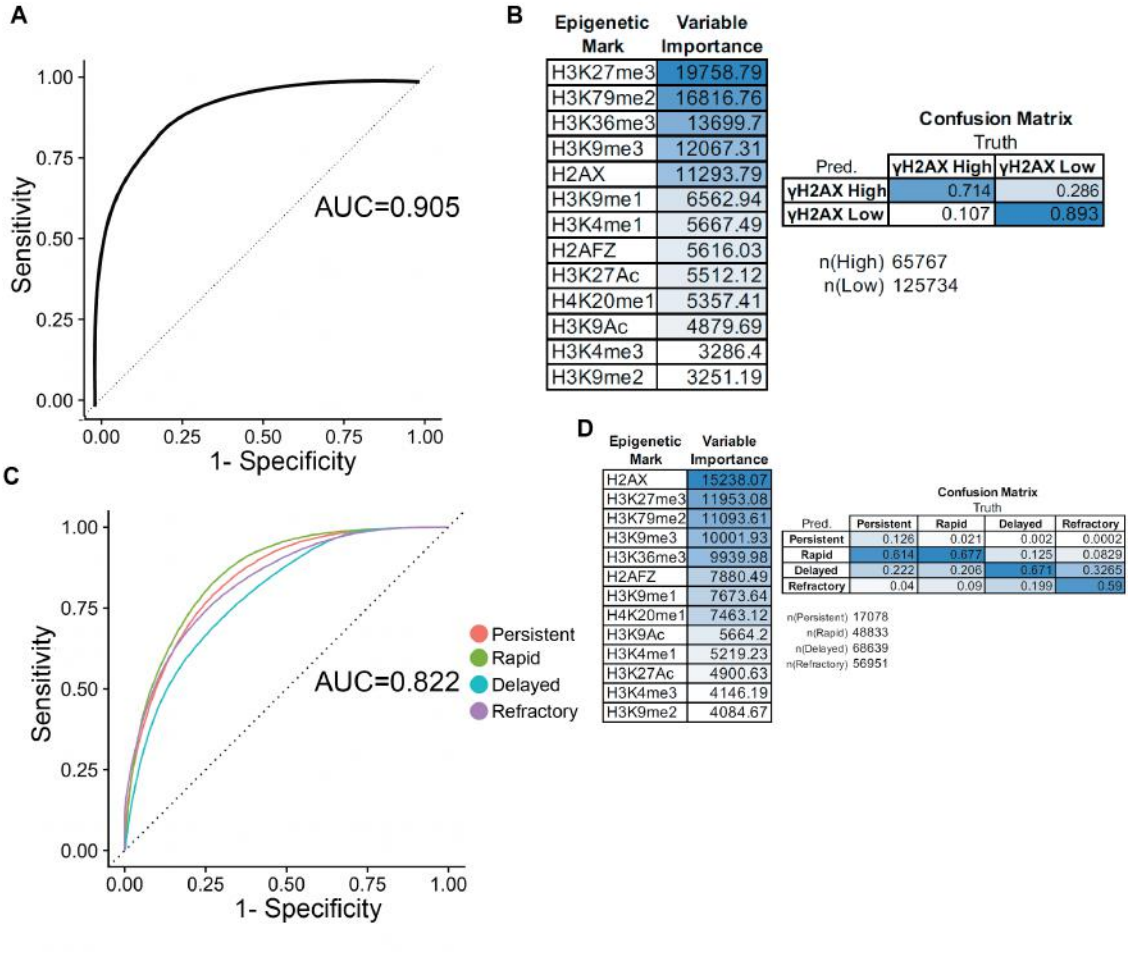

Figure 3.11: **A** Results of the Random Forest model predicting binary γH2AX coverage at 1 h PIR. AUC plot was generated by the parsnip package in R. **B** Variable importance of the Random Forrest Model. Values generated by the parsnip package in R. Higher values indicate greater contribution to the model prediction. The confusion matrix, indicating the accuracy of the model, is shown in the right panel. **C** Results of the Random Forest model predicting the four γH2AX dynamic states. Values generated by the parsnip package in R. AUC plot was generated by the parsnip package in R; lines are color coded according to the AUC for the given state. **D** Variable importance of the Random Forrest Model. Higher values indicate greater contribution to the model prediction. The confusion matrix, indicating the accuracy of the model, is shown in the right panel.

Table 3.1: Datasets used in genome-wide analyses

Epigenetic Factor	Basal or Purturbed	Cell Type	Data Source	Encode Experiment	Experiment Type
BLISS	Basal	K562	Gothe (2019).	n/a	BLISS
BrU-seq_IR	Purturbed	K562, HepG2	ENCODE	ENCSR492DKJ	BrU-seq
BrU-seq_NIR	Basal	K562, HepG2	ENCODE	ENCSR729WFH	BrU-seq
CTCF	Basal	K562	ENCODE	ENCSR000AKO	ChIP-seq
CUX1	Basal	K562	ENCODE	ENCSR000EFO	ChIP-seq
DNAse-seq	Basal	K562	ENCODE	ENCSR000EOT	DNAse-seq
EHMT2	Basal	K562	ENCODE	ENCSR175EOM	ChIP-seq
EZH2	Basal	K562	ENCODE	ENCSR000AQE	ChIP-seq
FAIRE	Basal	K562	ENCODE	ENCSR000DCM	FAIRE-seq
gH2AX_1Hr	Purturbed	K562, HepG2	In-House	n/a	CUT&RUN
gH2AX_24Hr	Purturbed	K562	In-House	n/a	CUT&RUN
H2AFZ	Basal	K562	ENCODE	ENCSR000APC	ChIP-seq
H2AX	Basal	K562, HepG2	In-House	n/a	CUT&RUN
H3K27Ac	Basal	K562	ENCODE	ENCSR000AKP	ChIP-seq
H3K27Me3_IR	Purturbed	K562	In-House	n/a	CUT&RUN
H3K27Me3_NIR	Basal	K562	ENCODE	ENCSR000AKQ	ChIP-seq
H3K36Me3	Basal	K562	ENCODE	ENCSR000AKR	ChIP-seq
H3K4Me1	Basal	K562	ENCODE	ENCSR000AKS	ChIP-seq
H3K4Me2	Basal	K562	ENCODE	ENCSR000AKT	ChIP-seq
H3K4Me3	Basal	K562	ENCODE	ENCSR668LDD	ChIP-seq
H3K79Me2	Basal	K562	ENCODE	ENCSR000APD	ChIP-seq
H3K9Ac	Basal	K562	ENCODE	ENCSR000AKV	ChIP-seq
H3K9Me1	Basal	K562	ENCODE	ENCSR000AKW	ChIP-seq
H3K9Me3	Basal	K562	ENCODE	ENCSR000APE	ChIP-seq
H4K20Me1	Basal	K562	ENCODE	ENCSR000AKX	ChIP-seq
HP1	Basal	K562	ENCODE	ENCSR000ATV	ChIP-seq
MNase-seq	Basal	K562	ENCODE	ENCSR000CXQ	Mnase-seq
Pol II PS2	Basal	K562	ENCODE	ENCSR000EGF	ChIP-seq
Pol II PS5	Basal	K562	ENCODE	ENCSR000BKR	ChIP-seq
PolyA RNAseq	Basal	K562	In-House	n/a	RNAseq
SMARCA4	Basal	K562	ENCODE	ENCSR587OQL	ChIP-seq
Total Pol II	Basal	K562	ENCODE	ENCSR031TFS	ChIP-seq

Table 3.2: Exploratory features of epigenetic datasets

Epigenetic Factor	Mean Coverage	Median Coverage	Min Coverage	Max Coverage	Prop of tiles with Zero Coverage	Prop of Tiles Encoded as "High"
BLISS	0.002	0.001	0	0.06	0.275	0.293
Bru-seq	0.741	0	0	827.529	0.688	0.226
CTCF	0.283	0.204	0	20.866	0.044	0.293
CUX1	0.323	0.288	0	11.578	0.039	0.416
DNAse	0.925	0.539	0	244.689	0.021	0.204
EHMT2	1.915	1.516	0	400.862	0.024	0.353
EZH2	0.325	0.270	0	10.096	0.039	0.390
FAIRE	0.589	0.521	0	27.220	0.019	0.398
H2AFZ	0.205	0.108	0	12.908	0.071	0.230
H2AX	0.667	0.617	0	12.280	0.023	0.439
H3K27Ac	0.090	0.036	0	25.837	0.212	0.185
H3K27Me3	0.159	0.070	0	11.076	0.113	0.275
H3K36Me3	0.152	0.104	0	7.997	0.073	0.316
H3K4Me1	0.115	0.042	0	12.812	0.174	0.190
H3K4Me3	0.141	0.028	0	39.401	0.194	0.068
H3K79Me2	0.224	0.072	0	44.325	0.083	0.131
H3K9Ac	0.172	0.062	0	22.915	0.146	0.232
H3K9Me1	0.326	0.270	0	6.834	0.030	0.401
H3K9Me2	0.094	0.034	0	14.313	0.248	0.124
H3K9Me3	0.298	0.270	0	7.891	0.021	0.427
H4K20Me1	0.131	0.090	0	6.411	0.078	0.362
H4	0.687	0.635	0	9.064	0.035	0.444
HP1	0.374	0.313	0	7.799	0.035	0.377
MNase	0.261	0.000	0	10.702	0.840	0.172
Pol II S5P	0.057	0.027	0	8.241	0.158	0.259
RNA-seq	4.170	0.000	0	2899.904	0.664	0.147
SMARCA4	1.638	1.096	0	105.592	0.026	0.287
TRIM28	1.730	1.340	0	87.215	0.014	0.333
Total Pol II	1.385	1.014	0	322.570	0.026	0.319
gH2AX 1 h PIR	1.599	1.169	0	56.448	0.027	0.343
gH2AX 24 h PIR	0.456	0.425	0	5.295	0.026	0.446

3.3 DISCUSSION

Here we undertake a genome-wide survey of the location of stochastically induced DSBs. Consistent with expectations, heteochromatin was shielded from DSBs. However, the distribution of γH2AX across the genome was highly non-uniform; disparate loci differed in their levels of γH2AX by >100 fold (Figure 3.12). Transcribed euchromatin is highly enriched for γH2AX at 1 h PIR while repressed loci only accrue γH2AX by 24 h PIR. These data stand in contrast to our traditional understanding of how radiation affects the cellular genome. We anticipate that radiotherapy produces homogenous radiation fields which affect all genomic regions equally. Further in a mixed population of cells, be they in a tumor or *in vitro*, gene expression fluctuations, cell cycle variations, and stochastic exposure to IR contribute to highly heterogeneous induction of breaks. The fact that we can observe enrichment of γH2AX in genomic loci suggests that chromatin structure or histone PTMs exert a considerable effect on recognition of DNA damage and warrants further study.

Despite robust interest in the interplay between the epigenome and DSB repair activity, few studies have assayed the genome-wide response to radiation induced DNA damage[104, 393]. We utilized CUT&RUN sequencing to assay the distribution of the core DSB marker γH2AX across the K562 genome following γ ray irradiation. Furthermore, the pattern of γH2AX coincided with variations in the underlying epigenome including chromatin accessibility and the presence or absence of various histone marks. In general, highly accessible chromatin such as in genic regions was enriched for γH2AX while repressed chromatin displayed lower levels.

The epigenome also influenced the kinetics of γH2AX deposition. At short timepoints—1 h following IR insult— γH2AX was predominantly in genic, open regions, whereas 24 h PIR, genic regions experienced a decrease in γH2AX and facultative heterochromatin, identified by H3K27me3, realized a concomitant increase. Our data also correlates with studies suggesting that transcribed areas accumulate fewer single nucleotide variations and that heterochromatic markers, including H3K27me3, are associated with higher mutation rates. Perhaps the challenge of recognizing heterochromatic damage contributes to associations between heterochromatic markers and increased mutational rates[418, 419].

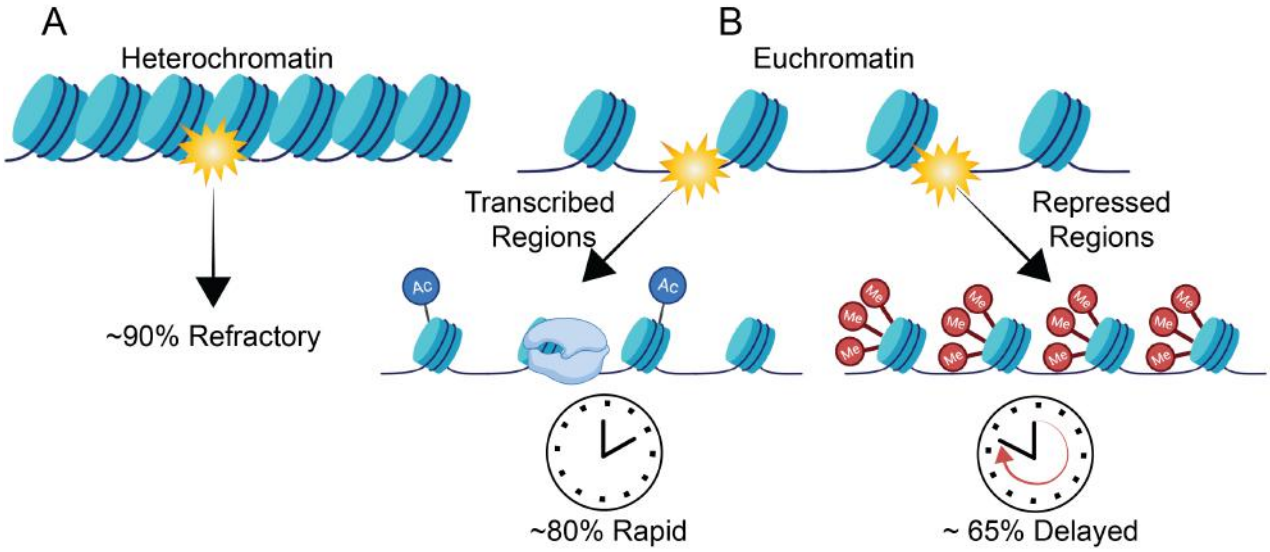

Figure 3.12: **A** In heterochromatic regions, though few breaks are induced, breaks are not recognized. **B** Euchromatin, which contains many DSBs, is repaired according to underlying chromatin states. Transcribed regions are quickly repaired, while repressed regions marked by H3K27me3 are recognized hours later.

There are two possible explanations for variations in γH2AX deposition arise. First, perhaps, DSBs are homogenously induced across the genome, and transcribed regions are more conducive to rapid recognition of DSBs because they are accessible to repair factors[420]. Secondly, DSBs are preferentially induced in euchromatin. We observe a mixture of both of these phenomena. In line with homogeneous induction of DSBs, we observe an increase of γH2AX in heterochromatin 24 h after IR insult. This suggests that there may be DSBs in dense chromatin which are recognized only long after induction of damage. We postulate

that chromatin which is refractory to recognition of breaks must rely on orthogonal processes to uncover damage, including replication. Indeed, we show that distance from replication origins as well as higher-order compartments— which vary with respect to replication timing— influence the kinetics of γH2AX introduction. While it is possible that some breaks are not yet recognized at 24 h after IR, replication sets an upper limit on DSB recognition as cells cannot replicate broken DNA without suffering loss of genomic integrity.

We also observe that DSB induction itself is affected by chromatin structure and that open chromatin may accumulates more DSBs, as condensed chromatin is radio-protective[330]. Examining BLISS data, which directly maps DSBs, we observe a non-uniform distribution which is distinct from that observed for γH2AX. Lending credence to this hypothesis, there are heterochromatic loci which never accumulate γH2AX density even 24 h after IR, suggesting that highly compact chromatin is resistant to damage induction. We concede that sequencing of compact heterochromatin is challenging and subject to technical caveats including ambiguous mappability of these regions. DSB detection is well known to induce chromatin relaxation, thus we may have detected increased signal surrounding newly relaxed heterochromatin 24 h after DSB induction. However, we do not observe this in most heterochromatic regions, suggesting they never accumulate DSBs. Future work should conduct DNAse or MNase sequencing before and after DSB induction to directly examine changes in chromatin occupancy associated with DSB repair. Histone PTMs affect both induction of breaks and recognition of damage via distinct mechanisms, though chromatin compaction seems to hinder both processes.

Further, previous associations between NHEJ or HR and open chromatin should be reevaluated in light of our findings that a substantial fraction of the genome is never enriched for γH2AX within 24 h of DSB induction[168]. These DSB-resistant regions are associated with heterochromatin markers especially H3K9me3[124, 421]. Thus associations between the DDR and euchromatic markers must take great care to account for inherent biases in the induction of DSBs. Further, much of the genome is not decorated with any

histone PTMs whatsoever[417, 401]. These regions likewise do not accumulate γH2AX read density. However, conclusions regarding undecorated heterochromatin must consider the inability of modern techniques to capture or assay compacted chromatin, especially when using enzymatically mediated techniques such as CUT&RUN. Compounding sequencing difficulties, these heterochromatic regions tend to be repetitive making unambiguous mapping of reads challenging. Thus, we used microscopy, including optical measurement of chromatin density, to validate euchromatic enrichment of γH2AX. Further, while technical challenges may contribute to an undercounting of γH2AX in heterochromatic or repetitive regions, even at 24 h after IR we did not observe γH2AX in these regions. Thus, chromatin relaxation associated with the DDR, which might ameliorate sequencing difficulties, may not occur in highly heterochromatic regions, and such loci might, in fact, be refractory to the DDR. Indeed, histones and other chromatin associated proteins are subject to radiation induced oxidative damage and are known to act as sinks which absorb charged particles and free radicals thereby sparing DNA from damage[139, 422, 423]. Other studies have also shown that repetitive, low-complexity, or LINE elements were refractory to repair[424]. Thus, we focused the bulk of our analysis on areas surrounding transcription start sites which are highly accessible and amenable to ChIP-seq or CUT&RUN assays. Even within these areas, epigenetic marks dictated the degree of H2AX phosphorylation, validating our above findings. Next, we turned to assessing the how basal epigenome is altered upon DNA damage recognition.

CHAPTER 4

USING HISTONE PTM PROTEOMICS TO PROBE IR-INDUCED CHANGES TO THE EPIGENOME

4.1 INTRODUCTION

While the previous Chapter focused on uncovering relationships between basal epigenetic states, which precede IR insult, and the location of DNA damage, we will now turn to a discussion of how histone PTMs are altered in response to DSB induction. Given that γH2AX is a chromatin-localized mark, there have been efforts to situate H2AX phosphorylation in the context of other epigenetic marks including histone modifications, histone occupancy, and higher-order genome structures[170, 386, 425, 426, 427]. Toward understanding how histones are altered following recognition of DSBs, studies have employed imaging to co-localize histone modifications with markers of DSB repair, which form punctate sub-nuclear structures termed IR induced foci (IRIF)[428]. In this way, several epigenetic modifiers including the NuRD complex, PBAF and PRC1/2 and been associated with the DDR[129, 271, 429, 430]. Further, loss of histone modifiers has been shown to blunt the DNA damage response and sensitize cells to IR insult[254, 431, 432].

Chromatin interactions at DSBs fall into three broad categories: chromatin marks can directly recruit DDR factors, they can modulate chromatin accessibility, or they can regulate up-stream events. 53BP1:chromatin interactions are among the best appreciated example of the former category. It has been shown that 53BP1 interacts with H4K20me2 in order to bind damaged DNA, though how H4K20me2 is specifically recognized at DSBs is unclear[48, 65]. The histone acetylase TIP60 has also been shown to bind H4K20 at DSBs where it precludes binding of 53BP1 by acetylating H4K8, K12, K16 and K20: all histone marks associated with open chromatin[65, 433]. Chromatin decompaction following DSB induction is thought to be an obligate step in repair of heterochromatin, and perhaps occurs in euchromatin as well[434, 435]. However, more work is needed to square such observations with the proposed role of

repressive, compaction-mediating histone marks in DSB repair[436]. It follows that TIP60 activity, and by extension, chromatin decompaction, may favor Homologous Recombination via exclusion of 53BP1, a NHEJ factor[162, 433, 437]. Thus, TIP60 activity at DSBs fulfills both the first and second categories of chromatin-DSB interactions. The H4 tail is by no means the only histone motif important in DSB repair; other histone marks linked to the DDR include H3K79me2, H3K9 methylation, and H3K36me3[374, 438, 439]. As an example of histone marks regulating cellular-level responses to DSBs, H3K27me3 has been shown to regulate senescence induction even in the absence of exogenous damage[220].

A wide range of epigenetic reader and writer enzymes previously established as transcriptional regulators have been implicated in DSB sensing, signaling and repair[272, 373, 386, 440, 441, 442, 443, 444]. However, as was observed in the last Chapter, response to DSBs is dramatically affected by chromatin state. Thus, deconvoluting stochastic associations between DSB-prone chromatin and resident histone PTMs from *de novo* epigenetic marks required for repair is challenging. For example, in Chapter 3, we observed a correlation between basal H3K79me2, catalyzed by Dot1L, and γH2AX[445]. Dot1L has been shown to accumulate at DSB loci and is necessary for DSB repair[438]. However, apparent recruitment of Dot1L to DSBs may not represent *de novo* accumulation of this protein and instead reflects basal enrichment of Dot1L near loci prone to DSB induction or detection. Further, Dot1L dependent repair may occur only in a subset of the genome already marked by Dot1L or H3K79me2. Moreover, it is important to consider the kinetics of the DDR process when attempting to link epigenetic modifications to DSB repair. As part of the response to DSBs, cell cycle checkpoints are activated, halting cell-cycle progression[446]. Transcription is also globally attenuated following IR insult[447, 448]. Both cell cycle pausing and transcriptional attenuation likely confer their own changes on the epigenome, which must be deconvoluted from epigenetic modifications proximal to DSB loci. We will return to the idea of discriminating global from local IR-induced changes in Chapter 5.

Turning to technical considerations, the large number of histone PTMs which have been

ascribed functional significance in the DDR makes global analysis of histone modifications challenging. Further, use of antibody-based methods to quantitate histone PTMs is suspect as antibodies lack specificity to delineate between single methyl groups or chemically similar substrates[449]. Mass Spec proteomics offers a potential solution to these technical limitations[450]. Indeed, proteomic techniques for analyzing histones and histone PTMs have advanced rapidly over the past decade. In general, these techniques rely upon extraction of histones from cell lysate before specialized digestion and functionalization protocols[451, 452]. Specialized software has also been developed to assist in label-free quantitation of histones and allows for normalization between samples without complex, expensive labeling experiments[451, 453]. Such methods have not yet been applied to analyze epigenetic changes following genotoxic stress. Adding further complexity, the repertoire of known histone modifications has expanded rapidly with the recent identification of metabolite-derived PTMs including Acylation, Par-ylation and o-GlcNAC-ylation[454, 455, 456, 457, 458]. Further, no epigenetic analysis of the DDR has examined modifications beyond well-understood PTMs (Ac, Me, Ph, Ub, and Sumo).

Toward elucidating PTMs which may participate in the DDR, we carried out various proteomic analyses of histone PTMs in a time course following IR insult. Using dimensionality reduction methods, we uncovered kinetic patterns of modifications which persisted up to 48 hours after DSB induction. To our knowledge this is the first large-scale survey of histone PTM regulation following radiation exposure. Results pointed to several known and novel histone modifiers which may play a role in the DDR.

4.2 RESULTS

4.2.1 Ionizing Radiation Induces Widespread and Long-Lasting Alterations to Histone Post-Translational Modifications

In order to analyze multiple Histone PTMs in a single experiment, we turned to Mass Spec proteomics. Methods for global proteomic analysis of histone post-translational modifications (PTM) have been established over the past decade[451, 452]. Such methods have not been applied to analyze epigenetic changes following genotoxic stress and no epigenetic analysis of the DDR has examined modifications beyond well-understood PTMs, despite the discovery of a wide variety of histone modifications[459]. We anticipated that changes to the epigenome may occur over different timescales. γH2AX is deposited within minutes of DSB induction; by extension, PTMs required for γH2AX deposition would be deposited on similar timescales. Further, more globally-oriented changes such as transcriptional attenuation or cell cycle pausing will induce distinct epigenetic changes, albeit more slowly. We sought to capture multiple kinetic alteration pathways in a single experiment.

Initially, we applied a multiple reaction monitoring (MRM) based targeted quantitative triple-quadrupole mass spectrometry assay, the Epiproteomic Histone Modification Panel (EHMP, Northwestern Proteomics), to analyze multiple histone PTMs over a time course following irradiation of MCF7 breast carcinoma cells using a ^{60}Co source. To sample a time course spanning DSB formation to the anticipated completion of most repair, MCF7 cells were irradiated with 6 Gy and then fixed at 1, 4, 24 and 48 h PIR[460]. Acid-extracted histones from mock irradiated and IR exposed cells were subjected to the EHMP panel to measure modifications at a per-residue level. For residues which could be in any one of several modification states such as H3K9 (which may be unmodified, acetyl, mono-, di- or tri-methylated) analysis indicated the fraction of residues in each state. Thereby, 92 histone modifications were evaluated on 30 histone residues for each sample. To assess overall changes in PTMs between time points, the data for three technical replicates for each time point were

examined by t-distributed stochastic neighbor embedding (tSNE) (Figure 4.1). Each time point after 6 Gy was distinct from the Non-IR control; 1 h and 4 h PIR samples clustered together and 24 h and 48 h PIR samples formed a separate cluster. This suggests that there are at least two kinetically separable epigenetic modification patterns following IR insult. One, which begins rapidly and concludes a few hours after IR is likely associated with recognition of damage and initial repair predominated by NHEJ. The second pattern, coincident with longer-term changes, more likely represents global epigenome alterations arising from transcriptional or changes. Alternatively, it may be associated with delayed recognition of breaks in heterochromatin likely repaired by HR.

The patterns of PTM dynamics revealed by clustering were analyzed further by dynamic-time warping (DTW) analysis to extract temporally distinct modification trajectories (Figure 4.2). The dynamic time warping algorithm allows for robust comparisons between time series data which have a similar profile, but vary with respect to rates of change. After calculating the DTW distance between PTM time-series, we performed clustering on the distance matrix. Five trajectories were selected to best represent the data. Mapping the centroids of each cluster indicated a range of histone modification dynamics in response to DNA damage. As expected, some PTMs increased rapidly after IR insult, while others peaked later, suggesting distinct functions. Dissecting the mechanism of early from late changing PTMs is beyond the scope of this dissertation but remains an area of interest. We focused herein on rapidly changing PTMs, in particular those in Cluster 2, including H3K9 methylation, H3K27 methylation, as well as H4 acetylation, known to mediate 53BP1 recruitment[427].

Toward identifying specific PTMs involved in the DNA damage response, we examined which modifications were most significantly changed over the time course. Of the 92 PTMs evaluated, 78 displayed altered abundance at one or more time points (5% FDR; Kruskal-Wallis test). Pointing to pathways that may mediate early events such as DNA damage recognition and signaling, 58 PTMs were significantly altered at 1 h PIR compared to non-

irradiated cells (5% FDR; Wilcox test) and 51 were both significantly higher at 1 h PIR and dynamic across the time course(Figure 4.3). This latter group included several PTMs previously linked to DSB repair including H3K79 methylation, catalyzed by Dot1L, and H4 methylation at K8, K12, K16 and/or K20, which mediate 53BP1 binding and NHEJ repair[427, 445]. Further validating this approach, our analysis identified H3K27 trimethylation as altered following IR. H3K27 trimethylation, catalyzed by EZH2, has been linked to DNA damage response and NHEJ,[253, 254] but mechanisms remain poorly defined.

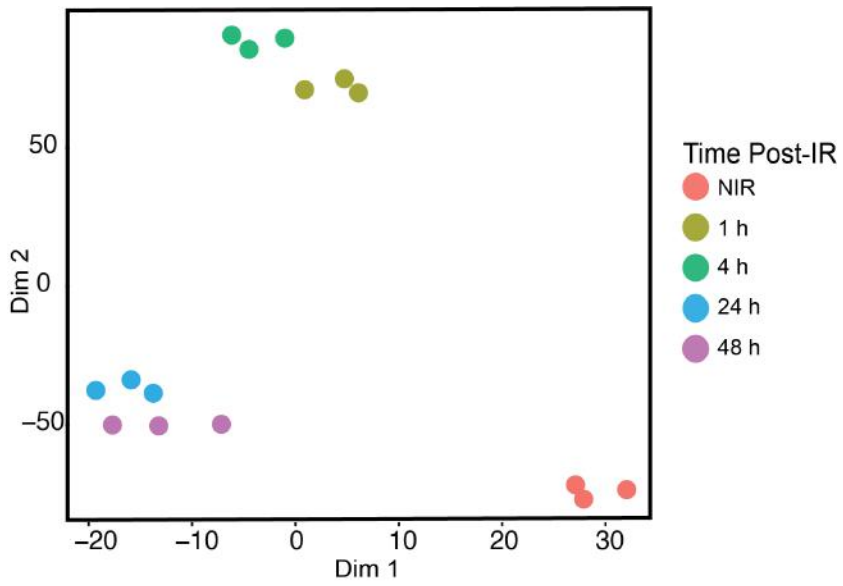

Figure 4.1: tSNE of samples from MRM histone PTM time-course analysis. Dots represent samples, color-coded to denote the timepoint after exposure to mock-irradiated (NIR) or 6 Gy (IR), using a ^{60}Co γ ray source. Data used to compute the tSNE are histone PTM per-residue percentages.

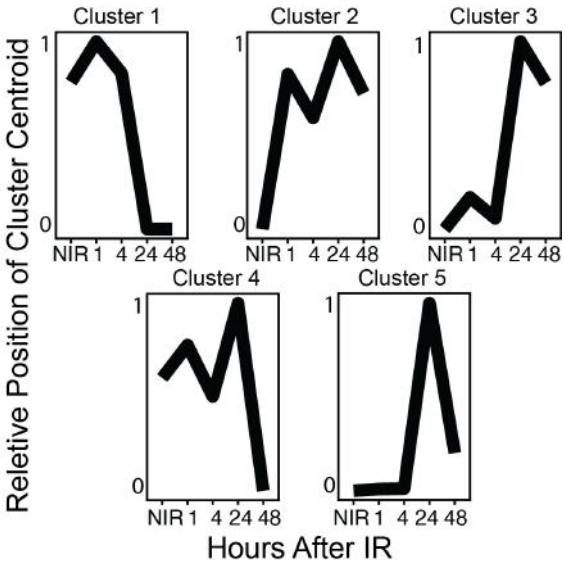

Figure 4.2: Centroid plots of histone PTM clusters. Trajectories of all PTMs were clustered according to their Dynamic Time Warping distance and then centroids were fitted and plotted by the PAM algorithm. The number of clusters was set to 5 after manual inspection of the data. The Y-axis denotes the relative average PTM density in a given cluster normalized to the NIR timepoint.

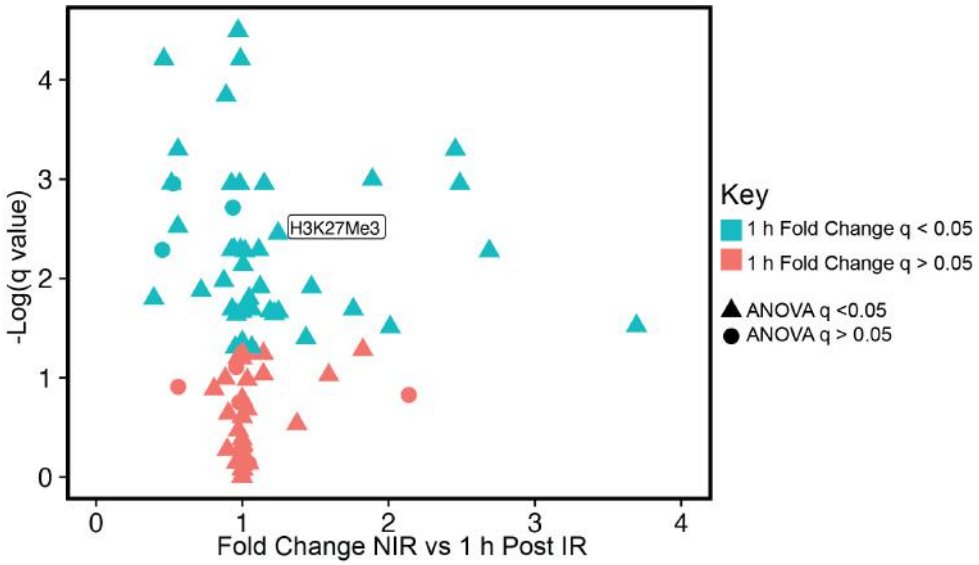

Figure 4.3: Volcano Plot of all PTMs analyzed. X-axis denotes the average fold change between the NIR and 1 h PIR timepoints. Y-axis shows the negative log of the FDR corrected P-value. Points are color-coded according to their significance at 5% FDR (comparison of NIR to 1 h PIR by Wilcox test) and their shape denotes the significance for a Kruskal-Wallis test across all timepoints, also at 5% FDR. H3K27me3 is labeled for clarity.

4.2.2 An Accurate Mass and Time Approach Confirms Global Epigenetic Changes After Irradiation

As a complementary approach, we performed an independent time-course analysis of chromatin modifications after irradiation using label-free, conventional LC-MS/MS and performed data analysis with EpiProfile 2.0, an accurate mass and time (AMT) strategy to quantify over 200 histone marks[452]. Following the EpiProfile protocol, histones from irradiated MCF7 cells were enriched by acidic extraction and then propionyl derivatized before and after trypsin digestion. The resulting peptides were subjected to Orbitrap LC-MS/MS in biological triplicate then examined with EpiProfile, manually validating spectra for PTM sites of interest. This analysis detected 204 PTM combinations, reducing to 44 single PTMs, and found dynamic changes in 38 PTMs during the time course. Among the marks which are enriched 1 h PIR are H3K56me2. Deacetylation of H3K56 by SIRT1 is associated with the DDR in S-phase[461, 462]. Other altered residues include H3K36 and the H4 tail which are both linked to DSB repair as mentioned above. Finally, we observed changes to H3K4 which has been linked to DSB repair in both yeast and humans[463, 464].

Focusing on modifications of histone H3 isoforms, we plotted relative abundances of acetylation, mono-, di-, and tri-methylation PTMs on H3 residues (Figure 4.4A). Among several notable changes, a shift from di- to tri-methyl K27 is observed at 1 h PIR. Clustering of PTM fold-changes at each of the four timepoints compared to unirradiated cells reveals distinct patterns of dynamic modification for specific residues and PTMs. Examining relative PTM changes, as compared to an unirradiated control, and grouped by modification type, reveals a trend toward increased acetylation and conversion of mono-methylation to di- and tri-methylation, particularly during the first 24 h PIR (Figure 4.4B). Separating the H3K27 modification data by H3 isoform revealed that the increase in H3K27me3 was restricted to H3.3. The H3.3 isoform is associated with transcribed regions suggesting that the epigenetic DDR may operate more rapidly in open chromatin, as suggested in Chapter 3. Thus, a potential role for increased H3K27me3, may be to suppress transcriptional conflicts[465].

4.2.3 Untargeted Analysis Reveals Additional Dynamic Histone PTMs During the DNA Damage Response

Recent work has expanded the universe of histone modifications beyond acetylation, methylation, phosphorylation and ubiquitinoylation with the discovery of novel modifications including new PTMs such as Crontonylation, Aceylation, O-glcnacylation, Propionylation, Butylation, and ADP ribosylation[459]. To extend our analysis beyond the sites identified by EHMP or EpiProfile, the *.RAW data files obtained from QE-Orbitrap LC-MS/MS of the acid extracted and propionylated histone peptides were searched with MaxQuant to detect additional dynamic histone PTMs. MaxQuant serches for pre-programmed mass shifts on all peptides in a dataset to uncover novel modifications. We queried our Epiprofile data files for 17 additional PTMs (Ac, Ar, Bu, Cit, Cr, Fo, Hib, Ma, Me1, Me2, Me3, Og, OH, Ph, Pr, Su, Ub) in a sequential searching method. This analysis detected 3076 total modifications across 5 time-points. We detected changes across several marks linked to sirtuins, a class of epigenetic modifiers which compete with PARP following IR insult[155, 466, 467, 468, 469, 470]. Although novel PTMs warrant further study, they remain challenging to assay experimentally as readers and writers are unknown. Thus, further analysis of this data remains beyond the scope of this Dissertation, yet the dataset serves as a valuable resource for future work on IR-induced changes to the epigenome or histone modifiers. Moving forward, we focused on the well characterized modification H3K27me3 which was highlighted by both EHMP and EpiProfile analyses above.

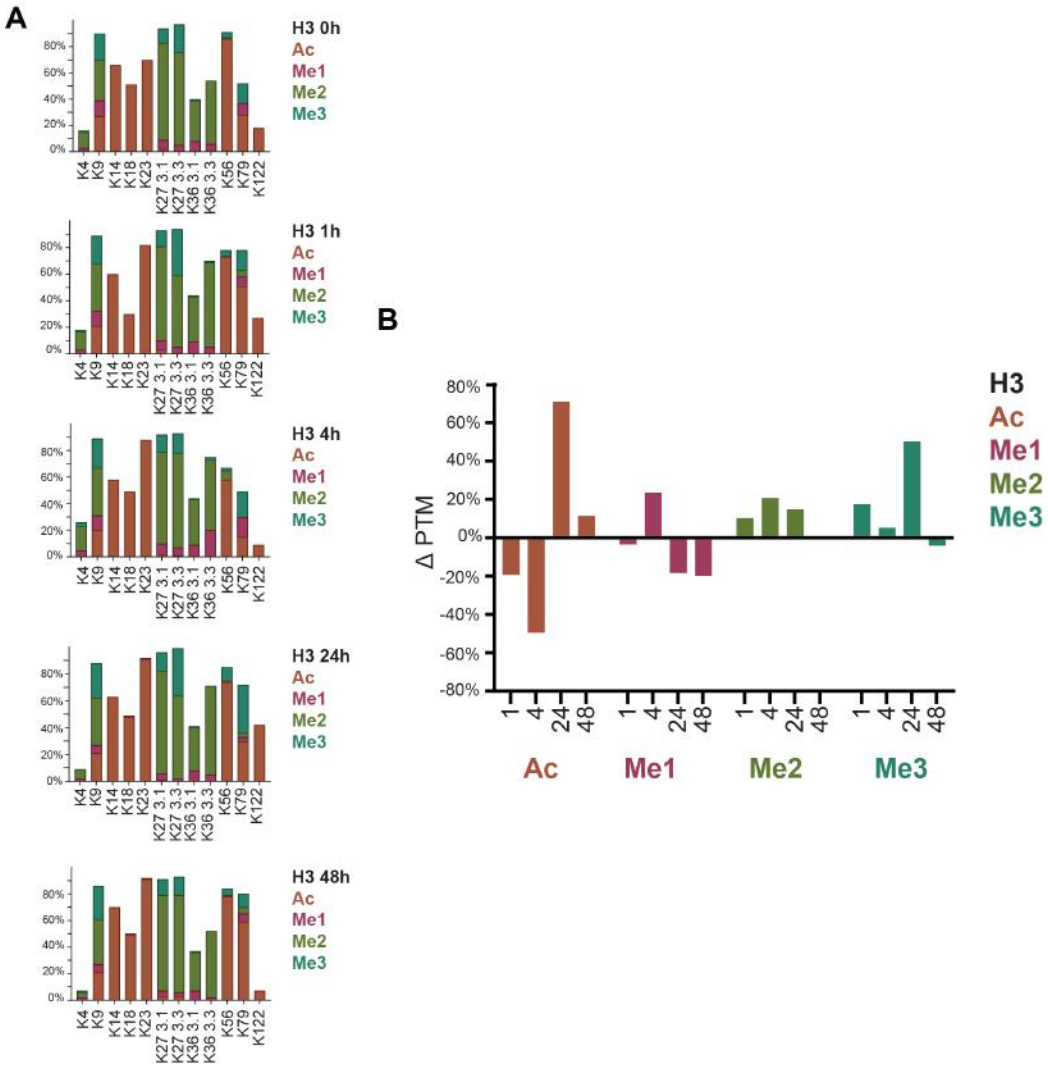

Figure 4.4: **A** Relative fraction of each residue on histone H3 in each of 4 modification states assayed. Residues between K27 and K36 are subdivided between H3.1 and H3.1. Data are mean values from 3 biological replicates. **B** Plot shows average modification changes for acetyl, mono-, di-, and tri-methylation across all residues measured for each of the timepoints relative to NIR. Three replicates are used. We observe a decrease in acetylation following IR and an increase in overall methylation specifically me1 and me3 1 h PIR. Acetylation increases after DSBs are repaired at the 24-48h PIR.

4.3 DISCUSSION

Repair of double strand breaks is a complex process which occurs at several kinetically and spatially distinct levels in the cell. Whereas much is known about the signaling-level events following DSB recognition (cell cycle arrest, transcriptional changes) and the downstream consequences of failure to repair DNA damage (apoptosis, senescence), less is known about the rapid, chromatin-level detection of DSBs. Indeed, DSBs are, by definition, a chromatin-localized event. Here, we report a global survey of changes to histone PTMs following DNA damage induced via ionizing radiation.

Analysis of histone PTMs after IR insult was carried out by AMT based MS/MS analysis and revealed widespread changes to the epigenome which persisted up to 48 h PIR (Figure 4.5). Modifications across all major histones were altered including modifications known to be key mediators of cell development such as H4 acetylation and H3K4 methylation. Clustering of PTM trajectories suggested that groups of Histone modifications were altered with distinct kinetics. Indeed, at 1 and 4 h PIR, we see a global reduction in histone lysine acetylation— an activating mark— suggesting that gene expression and chromatin accessibility are conscribed during initial stages of the DDR. It is worth noting that, even 48 h PIR, the epigenome does not resemble that of un-irradiated cells. Thus, cellular consequences of IR likely extend far beyond recognition and repair of breaks. Of the possible lingering effects of IR, changes to the cell cycle or gene expression profiles are the most likely, though we cannot disregard contributions of senescent or apoptotic cells to our histone PTM data. We also cannot delineate between effects derived from delayed repair of DSBs and effects mediated by cell-cycle or gene expression changes. While future studies could attempt to separate these possibilities by, for example, inducing cell cycle pausing or blocking transcription, these changes would likely induce epigenetic change in and of themselves while also altering the DDR directly.

We chose to focus on PTMs altered at 1 h PIR as later-occurring changes are increasingly likely to mediated by cell cycle stoppage or transcriptional alteration following IR. Our

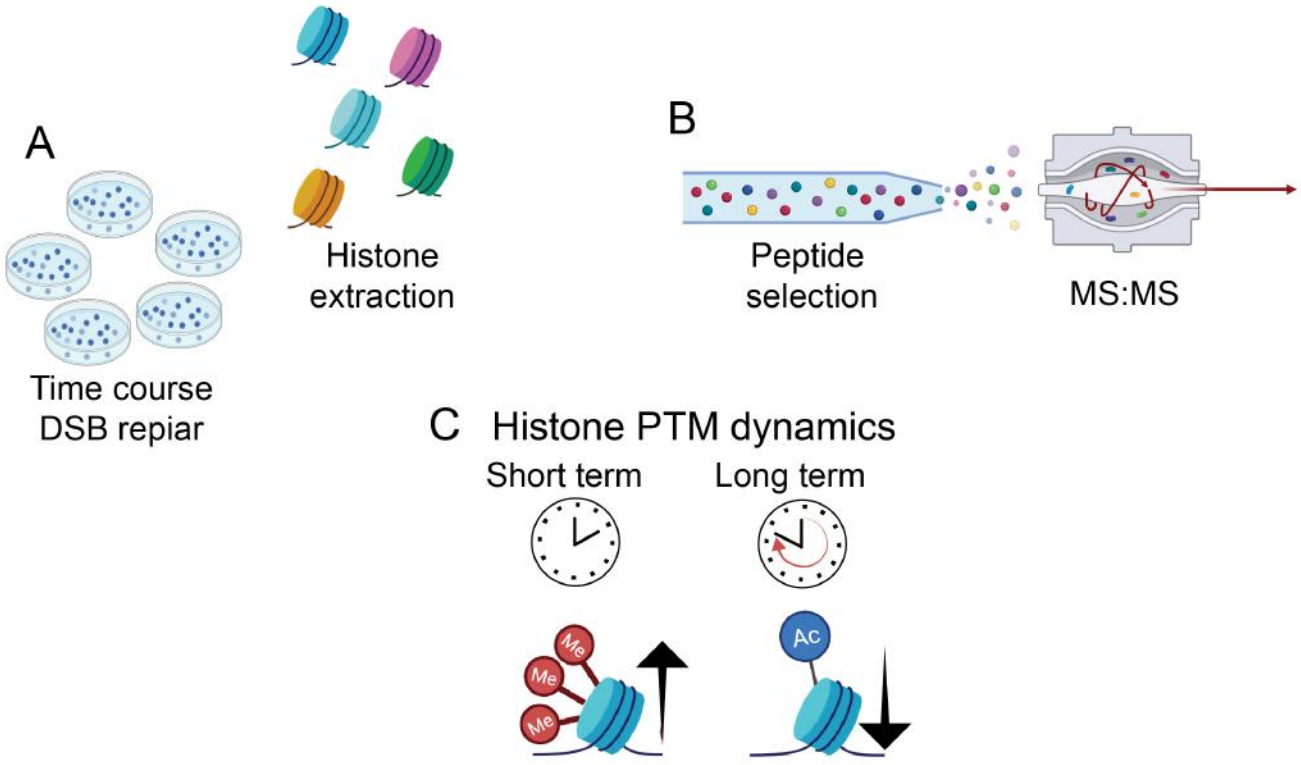

Figure 4.5: **A** We sampled a time course after IR insult spanning from 1 to 48 h PIR. **B** Histone peptides were extracted and sampled according to Epiprofiler software and sujected to MS:MS analysis. **C** While we uncovered mahy changes in individual histone PTMs, major trends included a rapid increase in histone tri-methylation (especially H3K27me3) and a delayed increase in histone Acetylation. The latter is perhaps due to chromatin decompaction.

analysis recapitulated several PTMs previously linked to DNA repair including H3K79me2, H3K27me3 and acetylation of the H4 tail. H3K79me2 is catalyzed by Dot1L which has been shown to promote recognition of breaks[445]. We also observe an increase in H3K36me3 which is associated with activity of the polycomb Repressive Complex 2 (PRC2), a putative DDR factor. By assessing non-canonical PTMs via un-biased searching for mass-shifts we expanded the repertoire of DDR associated PTMs to seventeen PTMs (at 3076 sites), including several novel PTMs. These PTMs are not yet well understood in terms of regulatory pathways or functional significance; we offer the data collected here as a resource for future investigators. Of note, we identify unusual modifications of H3K27 including butyrylation in addition to ubiquitination of H2K119 which is associated with PRC1 activity. Furthermore, though we detected small fold changes for many PTMs in our study we believe this to be reflective of larger, DSB-proximal changes diluted out by whole-chromatin analysis. Enrichment of DSB-proximal chromatin could be used to confirm our findings and definitively segregate local PTM alterations from global changes after irradiation. Such strategies will be outlined in the next Chapter.

CHAPTER 5

DEVELOPMENT OF TUDEL A SENSITIVE, SPECIFIC ASSAY FOR DSB QUANTITATION

5.1 INTRODUCTION

Taking into account the breadth of research into chromatin-DSB interactions outlined in Chapter 1, it becomes apparent that new techniques are necessary to directly assay the impact of chromatin on DSB repair. First, the kinetics of DSB recognition, IRIF formation or resolution, and DSB repair are challenging to disentangle. As discussed previously, histone PTM changes post-IR insult occur with several distinct kinetics. Perhaps some PTMs participate in recognition of damage while other epigenetic changes are required for IRIF resolution hours after damage has been repaired. Without a direct measurement of DSB repair, it is hard to accurately ascribe a mechanism to histone PTMs putatively involved in the DDR or, by extension, to discover novel radiosensitization targets. Second, while several epigenetic modifiers have been individually implicated in the DDR there have been few comprehensive surveys showing which histone binding proteins are recruited at DSBs.

Traditionally, DSBs have been assessed by counting IR induced foci (IRIF) in cells via immunofluorescent imaging of DSB markers. γH2AX, Ku70, 53BP1 and RAD51 (among numerous other proteins) have all been shown to localize to punctate foci in cells after IR or to laser micro-irradiation tracks[471, 472, 473]. The counting of foci offers a rough proxy for the extent of DSBs in cells. However, immunofluorescent labeling does not label DSBs directly and, given the multiple, non-overlapping pathways that repair DSBs, any given protein does not occupy every DSB in a cell. Further, IRIF are highly heterogeneous, differing in morphology both within and between cells[474]. Cell cycle differences as well as differential gene expression or repair pathway utilization contribute to observed heterogeneity in IRIF. Such heterogeneity poses a critical limitation affecting not only mechanistic studies of DSB repair but also limiting high content screening for repair modulating drugs[475].

As an alternative to IRIF counting, the single cell neutral gel electrophoresis (comet) assay directly measures DSBs[108]. However, it provides only an indirect, qualitative assay for DSBs and is incompatible with immunofluorescence[476, 477]. Other previously published methods provide a window into the genomic localization of DSBs via direct nucleotide labeling of free DNA ends. Break labeling, enrichment on streptavidin and next-generation sequencing (BLESS) was the first of such techniques to be developed and relies on ligation of hairpin adaptors to DSBs before purification and sequencing of DNA[478]. BLISS improved on BLESS by incorporating *in situ* ligation and an *in vitro* transcription step[479]. DSB-Capture and END-Seq are both modifications of BLESS which utilize slightly different DNA chemistries, but both rely on ligation of an adaptor to DSBs and ultimately remove DNA fragments from chromatin before purification of DSBs[255, 480]. Unfortunately, while these techniques do label DSBs directly, they preclude analysis of proteins or histones associated with damaged DNA. Thus, changes to the epigenome induced by DSBs cannot be assayed using these methods.

Attempts to identify radiosensitizers have highlighted deficiencies in the use of γH2AX or other IRIF-forming proteins as biomarkers[481, 482]. For example, our lab has shown that small molecules targeting DNA-PKcs attenuate foci resolution, but not DNA end-joining; this phenotype may be of clinical interest, though it would have been missed using only traditional DSB biomarkers[483]. Further, known radiosensitizers present different IRIF phenotypes: ATM inhibitors prevent IRIF formation, while PARP inhibitors prevent IRIF resolution. Yet, both drugs appear to confer a similar block to DSB repair when examined using the comet assay[484, 485]. Epigenetic inhibitors which have been shown to work as radiosensitizers include HDAC1 inhibitors and drugs targeting DNMT proteins[356, 486]. The mechanism of such drugs is as yet unknown. Adding further uncertainty toward interpretation of epigenetic drugs as radiosensitizers, IRIF may only reliably report damage in open chromatin. The rational development of other epigenetic drugs as radiosensitizers or radiomemetics should be undertaken in conjunction with a fuller understanding of histone-DSB

cross-talk and methods to address such interactions.

In this chapter, we detail development of TdT-UdP Double Strand Break End Labeling (TUDEL) an assay which uses Terminal Deoxynucleotidyl Transferase (TdT) to directly label DSBs *in situ*. TdT is a template independent DNA polymerase which appends nucleotides to the 3' end of free dsDNA ends. The enzymatic potential of TdT was first realized more than 50 years ago and it has since been identified as a required protein in V(D)J recombination[487, 488, 489]. TdT is commonly used in TUNEL assays to assess apoptosis wherein TdT labels DNA fragmented by apoptotic endonucleases. However, TUNEL assays give only a binary output of DNA damage by flow cytometry and do not report intra-cellular localization of breaks[490, 491, 492]. More recently, it was demonstrated that TdT can label laser micro-irradiation tracks by incorporation of a fluorescent nucleotide[493]. TdT is a flexible platform and has been shown to incorporate a wide array of modified nucleotides; this implies that our assay is flexible and adaptable to different chemistries including Copper-catalyzed click-chemistry[494]. We have extended these efforts and shown that TdT can label individual IRIF in irradiated cells via incorporation of functionalized nucleotides; this effort represents a significant improvement over previous DSB labeling efforts, as TUDEL retains DSB-associated protein information. By conjugating DSBs to a high affinity label, we can also perform affinity-purification to enrich DSB proximal chromatin. This allows for direct analysis of changes in chromatin at DSBs and binding of chromatin remodelers. In this way, we can begin to deconvolute global epigenetic changes, assayed in Chapter 4, from local changes surrounding DSB sites.

In developing TUDEL imaging, we sought to infer molecular relationships with the DDR by co-localizing proteins or histone PTMs with DSB ends. The confidence of colocalization methods is directly related to the resolution limit of the microscope used[495]. Even at the resolution limit of most confocal microscopes, one cannot discriminate between adjacent molecules and physically interacting molecular complexes with high accuracy. Recently, several microscopy methods have been developed which overcome the fundamental limitation

of visible light, which has a wavelength orders of magnitude larger than typical molecular complexes[496, 497]. Collectively termed superresolution microscopy (SR), such methods offer not only a means to distinguish objects at a resolution greater than the Rayleigh criterion but can also be used to establish colocalization beyond the Abbe diffraction limit with high precision[498, 499, 500].

Previous efforts to utilize SR imaging to determine the ultrastructure of IRIF have revealed new roles of chromatin architecture in dictating repair pathway choice at individual loci[501, 502]. Imaging studies have also revealed that while Ku directly occupies DSB ends, 53BP1 binds distally to DSB ends suggesting that concentric, spatially separated chromatin environments may exist around DSBs[428, 471, 503]. Further, nanoscopic evidence exists for multiple DSBs clustering together, possibly to increase the local concentration of repair factors[104]. Yet, none of these studies benefited from a direct DSB labeling method. Returning to the idea of deconvoluting global changes in the post-IR epigenome from local changes, we wanted to combine TUDEL with SR imaging techniques to validate observed associations between histone PTMs and DSBs.

Yet, even superresolution microscopy cannot image at sufficient resolution to discriminate molecular interactions from adjacent proteins. In practice an orthogonal measurement, such as detecting physical or chemical interactions between labeled proteins, must be employed to validate inter-molecular interactions. Förster resonance energy transfer (FRET) is an optical phenomenon wherein energy is transferred via dipole-dipole interactions between fluorophores (the Donor and Acceptor) only when the two moieties are in molecular proximity. Practically, FRET is detected as a red-shifting in emitted light when exciting the Donor fluorophore[504]. FRET efficiency declines with the 6^{th} power of distance between Donor and Acceptor, which makes FRET well suited to detecting fluorophores tethered on the same protein or two proteins in a complex. While FRET is easy to detect, and can verify proximity at higher resolution than SR imaging, quantitation of interactions is difficult, owing to inherent uncertainty in FRET measurements[505].

In this Chapter, we describe efforts to couple traditional FRET imaging with Ground State Depletion (GSD) microscopy[497, 506]. GSD imaging, a form of SR microscopy, operates by using bright illumination to transiently drive nearly all fluorophores in an imaging field to a meta-stable triplet-state, also termed a dark state. Upon returning to a visible ground state, the newly re-excited molecules produce a blink of light and then cycle back to the dark state; the total cycling time is on the order of milliseconds to seconds. Thus, for any population of fluorophores, only a tiny fraction will be emitting light at a given instance, meaning fluorophores separated by less than the diffraction limit can emit at different times and can be independently localized[507]. To construct a GSD image, $1e^3$-$1e^5$ frames are accumulated and locations of single molecules in the field of view are inferred computationally by fitting an elliptic Gaussian point-spread function[508]. Accreting the localizations derived from single molecule PSFs yields a map of the fluorophore distribution, which is equivalent to a traditional fluorescence image, albeit at higher resolution[509]. By performing multi-color GSD, molecules labeled with distinct (non-interacting) fluorophores can be depleted and imaged independently. Thereby, colocalization can be determined at nanometer precision.

Here, we describe a novel imaging modality, GSD-FRET, that leverages FRET to enable detection of molecular proximity across a distribution of molecular complexes. GSD-FRET exploits GSD to independently localize Donor and Acceptor fluorophores to enable quantitative single molecule FRET. We combine GSD-FRET with TUDEL labeling in order to validate localization of proteins and histone PTMs to DSB ends.

5.2 RESULTS

5.2.1 Development of Tdt-UDP Double Strand Break End Labeling (TUDEL)

We reasoned that technological limitations of other DSB detection or labeling methods might be overcome by using Terminal deoxynucleotide Transferase (TdT) to directly label DSBs *in situ*. TdT is a template independent polymerase which catalyzes the addition of random nucleotides to free DNA ends[494]. This technique has long been used to demarcate apoptotic cells, which have many random DNA breaks caused by caspase activated nucleases, via the TUNEL assay[492, 510, 511]. We first attempted to label irradiated cells using fluorescently labeled nucleotides. However, this yielded high, non-specific background and thus we turned to a two-part covalent labeling system. So-called click-chemistry techniques offer biocompatible strategies for covalent attachment of chemical dyes, labels, or handles[512, 513, 514]. Several click-chemistries exist and were assayed during TUDEL development as TdT has been shown to incorporate a variety of exogenous nucleotides, including those with bulky chemical moieties[494]. Finally, we arrived at using TdT to incorporate EdU followed by labeling via copper-catalyzed azide-alkyne cycloaddition (CuAAC), with an azide-functionalized fluorescent dye[515, 516]. CuACC reaction increased the observed signal-to-noise ratio, though some extra-nuclear background was still observed. To further enhance the specificity of TUDEL labeling, we adopted a pre-clearing strategy using a cytoskeletal imaging buffer and short-term incubation with RNAse-A which clears chromatin of RNA-bound proteins and cellular detritus[471]. The TUDEL protocol, in brief, is as follows. Cells are grown on untreated coverslips and exposed to γ ray IR from a ^{60}Co source. Cells are then fixed, treated with pre-clearing buffer, and permeabilized. The coverslips are then exposed to TdT containing buffer supplemented with EdU. Finally, incorporated nucleotides are labeled via Click-chemistry upon reaction with an azide containing fluorescent dye.

Following TUDEL staining, MCF7 breast carcinoma cells were imaged by a Marianas

Confocal microscope which revealed nuclear staining in the TUDEL channel. TUDEL labeling is sensitive and specific. TUDEL staining results in punctate nuclear foci reminiscent of IRIF. Cells which were not irradiated or cells which were incubated with TUDEL buffer containing no TdT have lower TUDEL staining as compared to irradiated, TdT-labeled samples 1 h PIR (Figure 5.1A). Thus, incorporation of EdU is both enzyme dependent and IR dependent, and likely reflects the presence of DSBs, as intended. Limited extra-nuclear background was observed which might be due to mitochondrial labeling. However, TUDEL often yielded pan-nuclear staining especially in samples labeled shortly after IR exposure. This observation could reflect the true nature of damaged DNA shortly after IR exposure or it could be an artifact of our labeling system and use of confocal microscopy. TdT labeled DSBs may have many fluorophores packed closely together which could lead to quenching and other artifacts. However, we note that bona fide markers of DSBs such as γH2AX also frequently appear to be pan-nuclear. Good correlation was observed between TUDEL foci and γH2AX, an early and ubiquitous marker of DSBs.

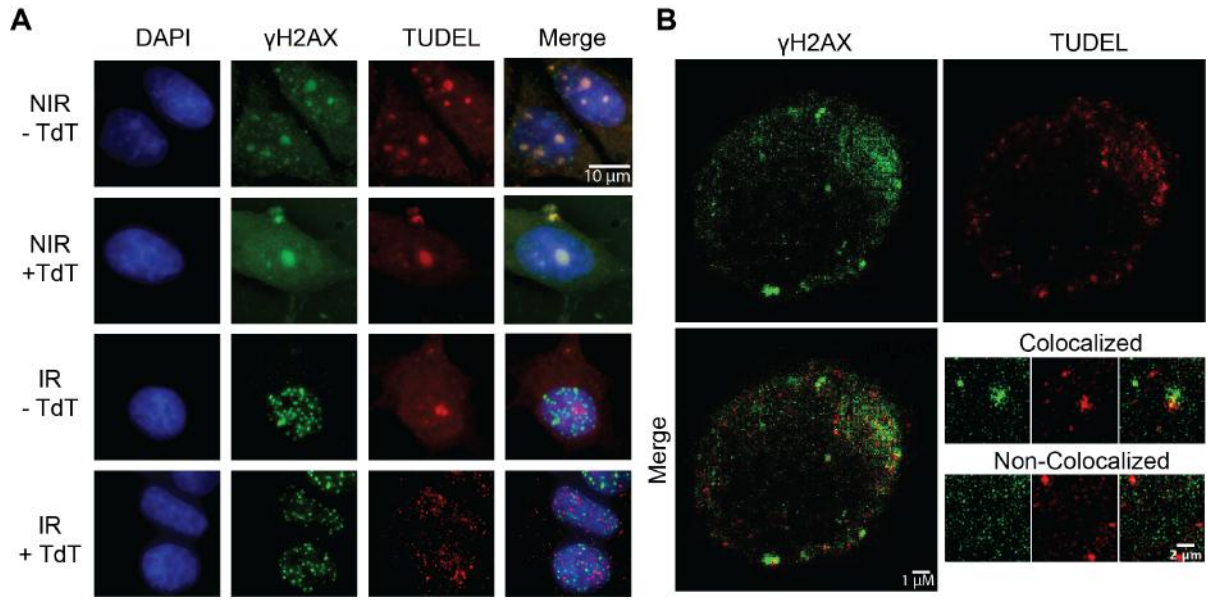

Figure 5.1: **A** MCF7 cells were exposed to 6 Gy of IR and fixed 1 h PIR followed by TUDEL staining and γH2AX immunostaining. NIR samples were mock irradiated. As a negative control, TdT was omitted from samples to verify specificity of TUDEL staining. **B** MCF7 cells were exposed to 6 Gy of IR and fixed 1 h PIR followed by TUDEL staining and γH2AX immunostaining. Images were captured on a GSD superresolution microscope. Inset images show γH2AX IRIF which colocalize with TUDEL foci. Additionally, TUDEL labels foci which are not yet marked by γH2AX, suggesting DSB recognition can be directly studied using TUDEL.

5.2.2 TUDEL as a Tool to Validate Proximity Between DSBs and Putative DDR Factors

Having developed TUDEL as a specific DSB labeling mechanism, we next sought to verify proximity between TUDEL labeled DSB ends and putative DSB repair proteins or epigenetic marks thought to be deposited proximal to DSBs. Even a single DSB can induce γH2AX spreading up to 2 Mb away from a break[404, 517, 518]. Thus, it is reasonable to assume that not all DDR factors or histone PTMs bind proximally to the break. We performed GSD superresolution imaging of TUDEL labeled MCF7 cells counterstained with γH2AX. Superresolution imaging revealed remarkable specificity of TUDEL labeling with punctate structures clearly visible in irradiated cells (Figure 5.1B). This confirmed specific labeling of DSBs by TUDEL to 50 nm resolution. GSD imaging also uncovered TUDEL positive foci which were not occupied by γH2AX, suggesting IRIF may be separable from the presence of damage using this assay (Figure 5.1B, inset). We conclude that TUDEL offers a sensitive, specific way to label single DSBs *in situ* and reveals expected, though not previously observable, variations between DSB recognition and repair.

Subsequently we utilized TUDEL in order to validate associations between histone modifications and DSB loci first uncovered from epigenomic analyses in Chapter 3. There, we observed that in regions of the genome which had high basal H3K27me3 (repressed genes or facultative heterochromatin) DSBs were slow to be recognized. DSB recognition in heterochromatin was also associated with loss of H3K27me3. However, following IR insult we observed *de novo* deposition of H3K27me3 in euchromatin which was enriched in γ H2AX. Thus we turned to imaging to verify these results. Specifically, we examined whether the repressive mark H3K27me3 was excluded from γH2AX IRIF. We examined colocalization of H3K27me3 and γH2AX 1 h PIR. Conventional immunofluorescence analysis revealed punctate domains of increased H3K27me3 immunoreactivity along with significant overlap between H3K27me3 and γH2AX (Figure 5.2A). We revealed diminished colocalization of H3K27me3 and γH2AX after treatment with an EZH2 inhibitor, as compared to vehicle

treatment, suggesting that this mark was actively deposited proximal to DSBs after damage induction.

To further examine H3K27me3 staining after DNA damage, we applied ground state depletion (GSD) superresolution immunofluorescence imaging at 1 h PIR, revealing punctate colocalization of H3K27me3 and γH2AX staining to a 50 nm resolution (Figure 5.2). In order to directly assay molecular colocalization, we adapted GSD to enable detection of molecular proximity by Forster resonance energy transfer (FRET). Here, TUDEL staining was detected with a secondary antibody labeled with the donor fluorophore (DNR) and H3K27me3 with a secondary antibody labeled with the acceptor (ACC). In areas where TUDEL labeled DSBs and H3K27me3 are in close proximity, DNR emission can be transferred to the ACC via FRET, quenching DNR fluorescence. Imaging TUDEL and H3K27me3 at 1 h PIR in the DNR and ACC channels revealed similar distributions. Upon depletion of the ACC fluorophore by intense laser power, the H3K27me3 ACC signal was lost but the TUDEL DNR signal brightened, indicating relief of FRET quenching and thus, colocalization. A pseudocolored image indicating fold increase in DNR fluorescence after ACC depletion reveals puncta of FRET signal, consistent with H3K27me3 and TUDEL forming in molecular proximity at DSBs (Figure 5.3). Taken together, these data suggest that H3K27me3 is deposited at DSB loci and histone modifications may delineate a domain surrounding DSBs to promote detection, signaling, and/or repair.

Next, we explored how TUDEL could be used in a pseudo-dosimetry model. TUDEL labeled cells were co-stained for γH2AX and the relative intensity of both TUDEL and γH2AX staining was examined at several timepoints after dosing of either low dose (2 Gy) or high dose (12 Gy) of radiation from a ^{60}Co source (Figure 5.4A-B). TUDEL labeled DSBs in irradiated cells minutes after IR insult, suggesting that TUDEL may be used to analyze initial response to radiation at very short timescales. As expected, TUDEL staining resolved within hours, concomitant with rapid DSB repair, following decoration with γH2AX. Higher doses of IR attenuated resolution of DSBs and provoked stronger and more durable γH2AX phosphorylation as expected.

Next, we treated MCF7 cells with several small molecules known to inhibit some aspect of DSB recognition or repair including inhibitors of ataxia telangiectasia mutated (ATM), DNA-dependent protein kinase, (DNA-PKcs) and p53-binding protein 1 (53BP1). We also made use of two inhibitors of poly(ADP-ribose) polymerase 1, (PARP1), Veliparib and Olaparib, which represent non-trapping and trapping inhibitors, respectively. All inhibitors were added 1 h prior to IR insult or mock-irradiation. We performed TUDEL and γH2AX immunofluorescence using the above drugs at several timepoints after IR in order to examine whether pharmacological DDR disruption affected DSB repair or recognition, a clinically relevant question (Figure 5.4C-D). As expected, inhibition of ATM resulted in blunted H2AX phosphorylation and attenuated repair of DSBs. Strikingly, we treated cells with an inhibitor of DNA-PKcs and observed a reduction in DSBs by TUDEL without concomitant reduction in γH2AX foci. This confirms our previous results using this compound[483]. Inhibition of PARP1 or 53BP1 yielded increased DSBs and IRIF to varying degrees at later timepoints. TUDEL staining was also correlated with comet tail moment, a widely used direct marker of DSBs. In summary, TUDEL shows promise as a pre-clinical method to precisely define the mechanism of action of radiosensitizers. Moreover, these results suggest that resolution of IRIF is a distinct process from DSB repair. Taken together we believe TUDEL labeling is reflective of the extent of DSBs in a given cell.

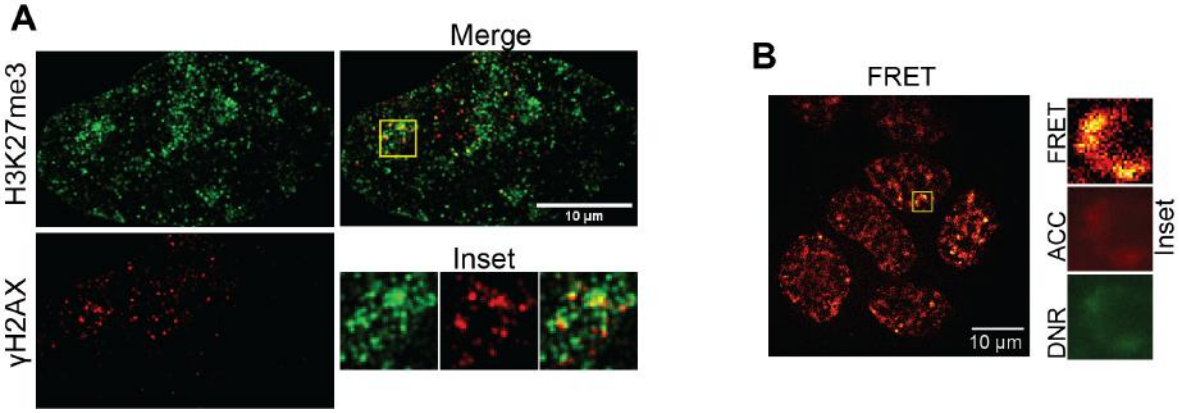

Figure 5.2: **A** Superresolution imaging of irradiated MCF7 cells. DMSO treated cells were fixed 1 h PIR and imaged on a Leica GSD imaging system. Inset shows colocalized puncta of H3K27Me3 and γH2AX. A representative image is shown from 3 replicates. **B** GSD-FRET analysis of colocalization between γH2AX and H3K27me3. MCF7 cells were fixed 1 h PIR and imaged on a Leica GSD imaging system using a 160x objective. A pseudo colored image showing the relative increase in signal in the Donor channel following Acceptor photobleach. Inset shows region with both γH2AX and H3K27me3 signal alongside the same region from the FRET image.

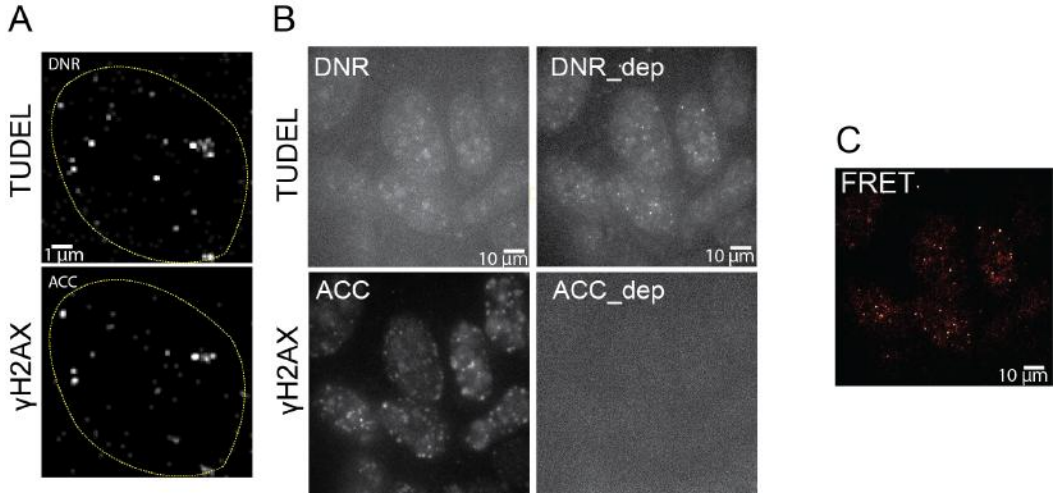

Figure 5.3: **A** Superresolution imaging of irradiated MCF7 cells. DMSO treated cells were fixed 1 h after IR and imaged on a Leica GSD imaging system. A representative image is shown from 3 replicates. **B** GSD-FRET analysis of colocalization between γH2AX and TUDEL. MCF7 cells were fixed 1 h after IR and imaged on a Leica GSD imaging system using a 160x objective. The four images show Donor and Acceptor channels before and after Acceptor photobleach. **C** A pseudo colored image showing the relative increase in signal in the Donor channel following Acceptor photobleach.

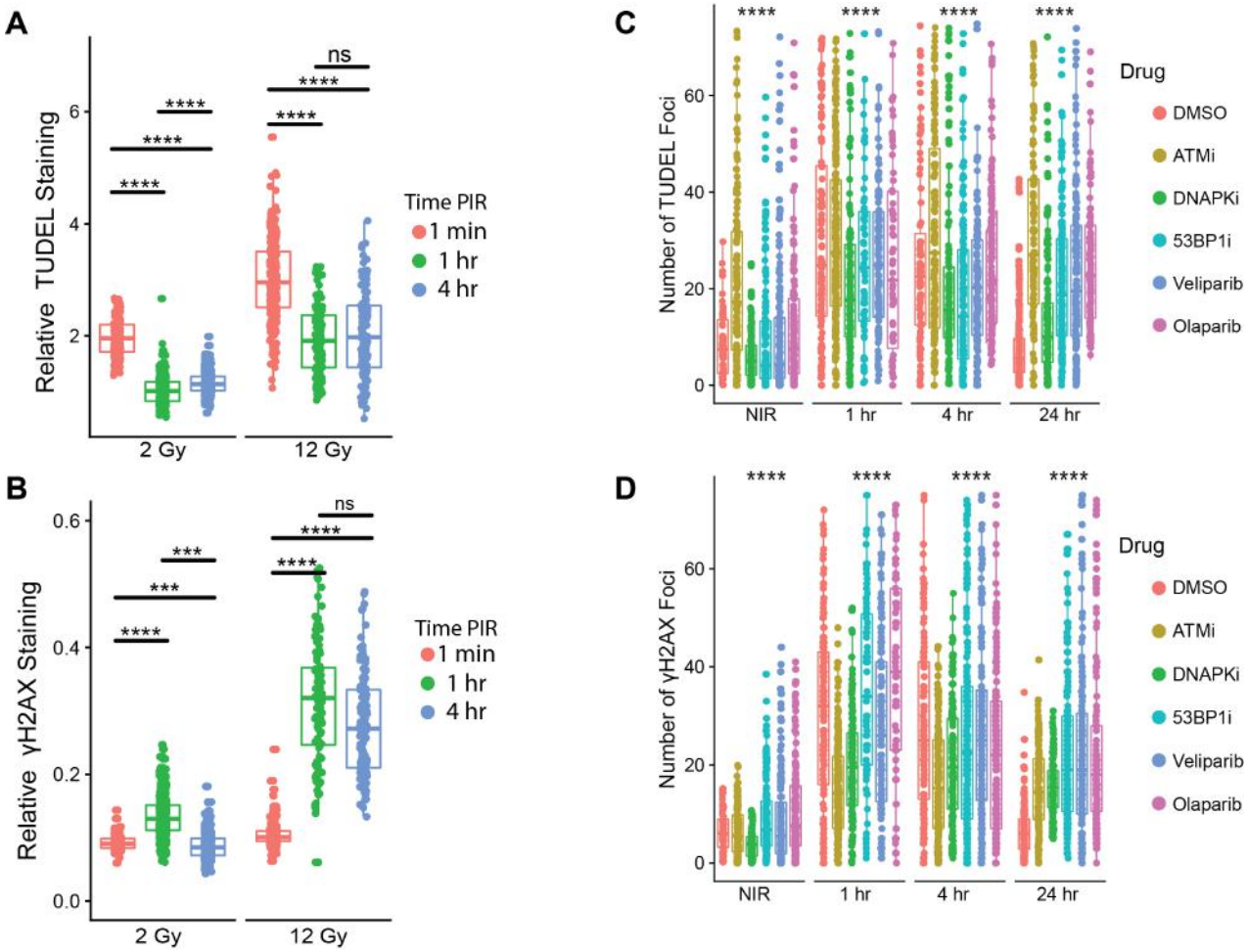

Figure 5.4: **A** MCF7 cells were exposed to the indicated dose of IR and fixed at the indicated time point. Plot shows relative TUDEL staining normalized to DAPI signal per nucleus. **B** MCF7 cells were exposed to the indicated dose of IR and fixed at the indicated time point. Plot shows relative γH2AX staining normalized to DAPI signal per nucleus. **C** MCF7 cells were exposed to 6 Gy of IR and fixed at the indicated time point. Drugs were added 1 h prior to IR insult. The number of TUDEL foci were counted using an automated foci counting macro in ImageJ. **D** MCF7 cells were exposed to 6 Gy of IR and fixed at the indicated time point. Drugs were added 1 h prior to IR insult. The number of γH2AX foci were counted using an automated foci counting macro in ImageJ.

5.2.3 Proteomic Analysis of Break-Associated Chromatin by TUDEL Affinity Purification

We wanted to extend the utility of TUDEL DSB labeling by using TdT incorporated nucleotides as a handle for enrichment of break-proximal chromatin. Specific enrichment of breaks, as opposed to immunoprecipitation of DDR factors, may yield a unique DSB proteome which is not biased to any repair pathway or process. To this end, we used $1e^7$ MCF7 breast cancer cells and exposed them to 6 Gy of IR (or mock irradiated cells) and allowed them to recover for 30 minutes. Cell nuclei were then extracted and fixed prior to TUDEL labeling for 6 hours as previously described. Cells were sonicated in RPIA buffer and lysate was incubated with azide-agarose beads in CuAAC Click buffer overnight followed by washing with RIPA buffer and extraction of affinity purified proteins.

Next, we subjected TUDEL purified chromatin from irradiated or mock-irradiated MCF7 cells to MS/MS. In total we identified 1367 proteins between the IR and NIR samples. Of these, 511 were significantly enriched in IR cells and 315 were significantly enriched in the unirradiated samples. These figures include a significant minority of proteins which were identified in only the IR or NIR conditions(Figure 5.5A). We note that proteins enriched in the NIR condition may be associated with basal DNA breaks, replicating DNA, or telomeres. Next, we performed systems level pathway analysis via Reactome and David to classify our enriched proteins. As expected, pathway analysis showed enrichment of DNA associated proteins (n=523, 38%), Chromatin associated proteins (n=173, 12%) and DNA damage or repair associated proteins (n=246, 17%) (Figure 5.5B). We are thus confident that TUDEL:AP enriches for chromatin associated with damaged DNA. Other pathways enriched in TUDEL-labeled chromatin 1 h PIR include Cell-Cycle, G2/M checkpoint and p53 related pathways. We also observed several transcriptionally associated pathways including transcription factor binding and RNA Polymerase II associated proteins. This may be reflective of transcription-associated damaged or repair (see Chapter 6) or an enrichment of DSBs in open, transcribed regions (Chapter 3).

Extensive literature has revealed that chromatin modifications and modifiers influence the DDR and are necessary for proper recognition and repair of DSBs[128, 386, 426, 519, 520]. Our TUDEL and γH2AX IPs each revealed enrichment of many chromatin modifiers (Figure 5.5C-D). We see enrichment of CHD4 and HDAC2, both previously associated with DSB repair[138, 521]. Most significantly, TUDEL:AP revealed enrichment of many components of the SWI/SNF complex. We then performed TUDEL:AP in K562 cells treated with a SMARCA2/4 degrading PROTAC ACBI1. Loss of SWI/SNF significantly affected recruitment of myriad proteins to DSBs as evidenced by TUDEL:AP. Pathway analysis revealed depletion of several chromatin modifyers as well as loss of transcription-associated proteins. This suggests a possible requirement for SWI/SNF in repairing euchromatic breaks or an association between DSBs and transcribed regions. Alternatively, SWI/SNF loss may downregulate transcriotion genome-wide as seen in Chapter 7. We then employed Epiprofiler to identify Histone PTMs enriched in our AP samples[451, 452]. Epiprofiler revealed enrichment of several Histone PTMs previously associated with DSB repair including H3K27me3 and acetylation of the H4 tail. Of note, some epigenetic features may hinder or facilitate γH2AX deposition; for example, much evidence exists for a connection between active transcription and DSB repair[330, 522, 523]. Further, open, accessible regions of the epigenome are more fragile and may inherently accumulate more DSBs. Open chromatin may also be permissive for DSB recognition, recruitment of DDR factors, and H2AX phosphorylation. It remains challenging to deconvolute enrichment of PTMs in a TUDEL:AP or γH2AX IP from expected enrichment due to the increased presence of DSBs in transcribed euchromatin.

5.3 DISCUSSION

Detection of DSBs has long relied on imaging of proxy proteins which have been shown to provide an incomplete or biased assessment of DNA damage, particularly in the context of drugs targeting repair machinery. A direct method to detect DSBs may provide insight into novel radiosensitizers or therapeutic modalities. Herein, we present a sensitive and

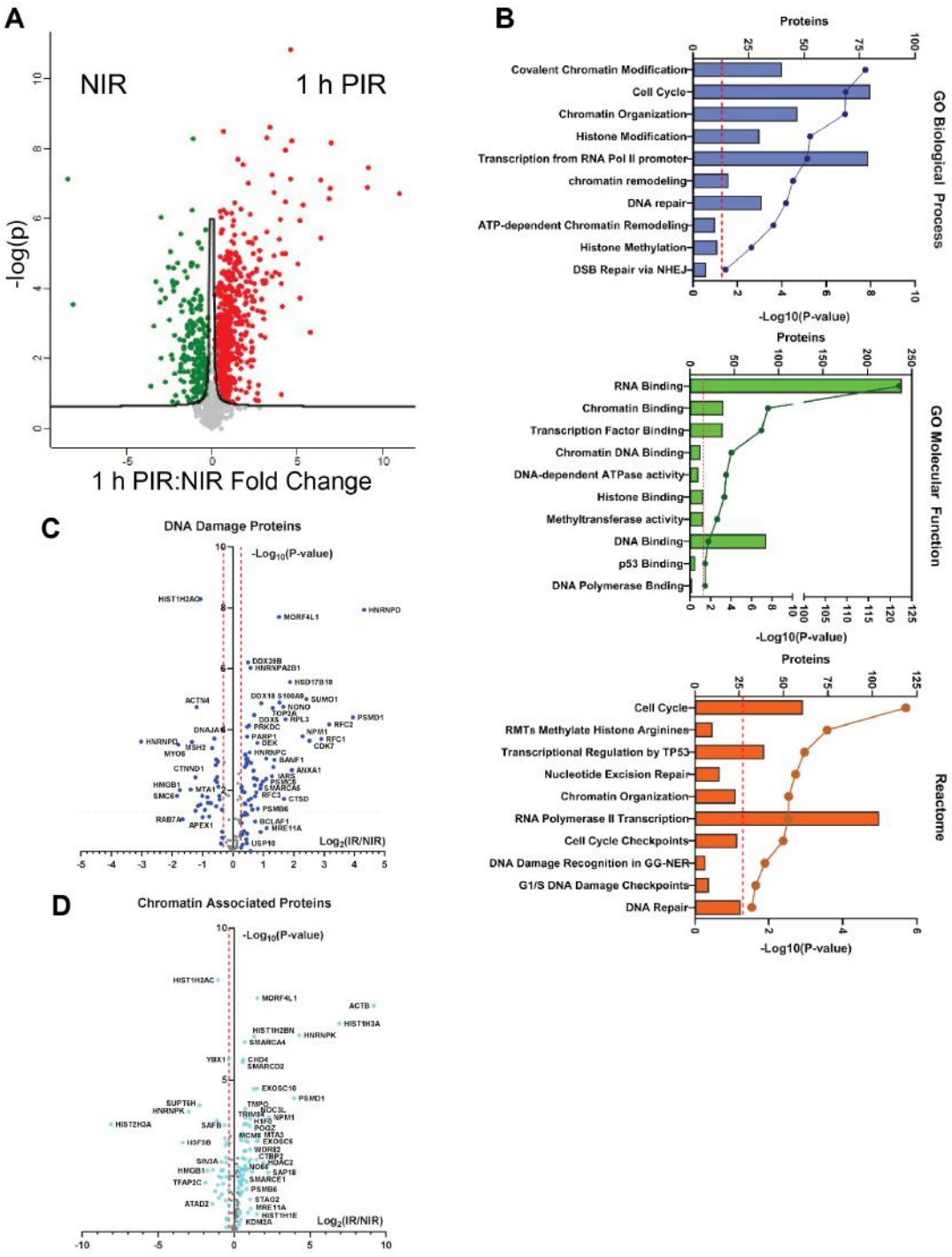

Figure 5.5: **A** TUDEL:AP enriches unique proteins in irradiated cells as compared to NIR cells. **B** Pathway analysis of proteins enriched at 1 h PIR reveal DNA damage associated proteins, chromatin modifiers, and transcriptionally associated proteins. **C** TUDEL:AP enriched DNA damage proteins may discriminate initial response to DSBs from canonical DDR proteins dependant upon PIKK activity. **D** Enrichment of DNA Damage Associated proteins in TUDEL:AP reveals known DDR-associated chromatin proteins e.g. CHD4.

specific *in situ* DSB labeling method which is capable of deconvoluting DSB recognition from presence of DSBs per se. We adapted the long-standing TUNEL assay, used to label apoptotic cells by virtue of wide-spread DNA breakage, to create TdT-UDP Dependent End Labeling (TUDEL). TUDEL uses the 3' template-independent polymerase Terminal Deoxynucleotidyl Transferase (TdT) to append labeled nucleotides to free DNA ends within damaged cells (Figure 5.6). We use TUDEL to fluorescently label DSBs in irradiated cells and confirm co-localization with common DDR markers including γH2AX. Importantly, TUDEL labels some loci which are not occupied by γH2AX suggesting that deposition of DDR factors can be separated from breaks themselves using this method. While TUDEL is sensitive and specific, we frequently observe pan-nuclear labeling of irradiated cells. Whether this is non-specific signal or reflective of heretofore unappreciated wide-spread damage remains to be determined. Unfortunately, there is not an orthogonal DSB labeling process with which to validate TUDEL, though we do note the occasional observation of pan-nuclear γH2AX signal. Combining TUDEL labeling with sequencing of damaged chromatin, especially in conjunction with other DSB sequencing methods, may offer insight into how wide-spread IR induced damage is. Direct conjugation of DNA damage has not been combined with exogenous stochastic induction of DNA damage, though results in Chapter 6 argue for the utility and importance of these experiments in future.

The utility of TUDEL was shown by validating effects of drugs on DSB recognition and repair. We confirmed previous results suggesting that catalytic inhibitors of DNA-PKcs do not attenuate DSB repair, but rather block IRIF resolution. Differential effects of trapping and non-trapping PARP inhibitors on DSB repair and IRIF persistence were also observed, highlighting the potential clinical utility of TUDEL. By understanding IRIF and DSBs as two independent, albeit linked, processes, new opportunities for radio-adjuvant therapy may be uncovered. We anticipate that epigenetic inhibitors which attenuate IRIF establishment or resolution are a rich vein to mine in conjunction with direct DSB labeling (see Chapter 7).

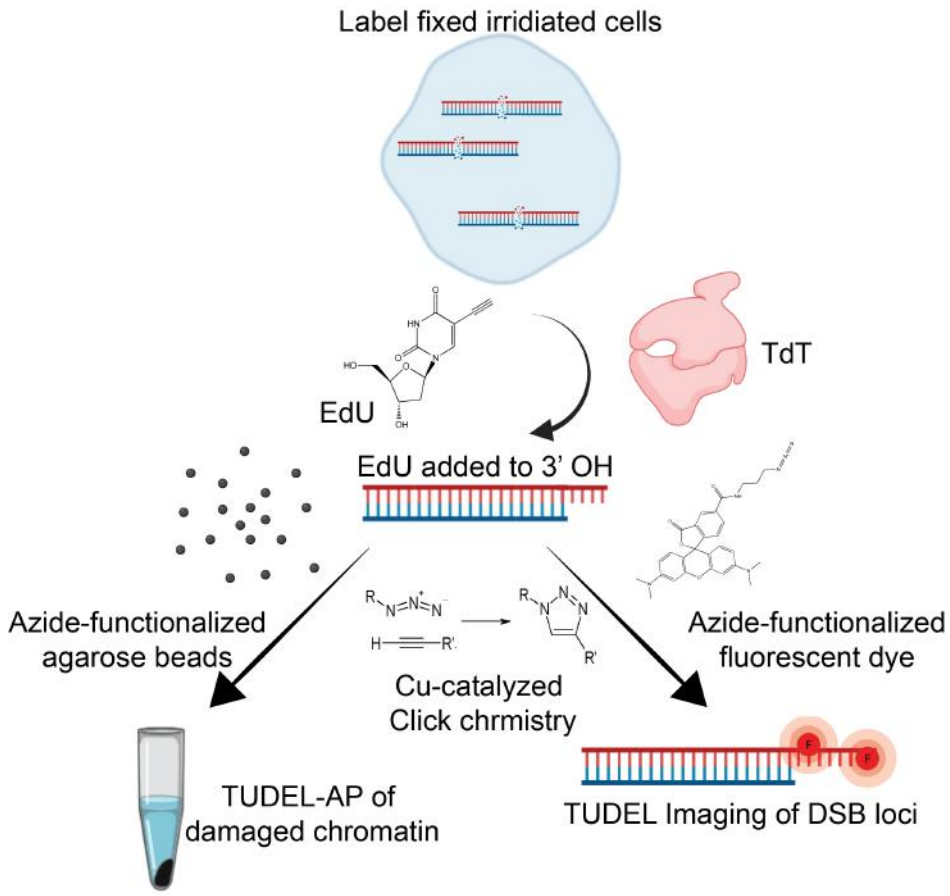

Figure 5.6: TUDEL labeling of fixed cells relies on a template independent polymerase, TdT, to append EdU to 3' OH groups at free DNA ends *in situ*. The EdU provides a handle for Click-chemistry mediated labeling using adise-functionalized dyes, or alternatively, linkage to azide-coated beads for affinity purification.

We further employed TUDEL to introduce a chemical handle at DSBs which allows for affinity purification of DSB-proximal chromatin. Using MS/MS proteomics we verified the presence of several DDR factors at TUDEL-labeled DSBs including CHD4. This further confirms the separability of DSB recognition and repair using systems such as TUDEL. Importantly, even at 1 h PIR, we observed repair of a substantial fraction of DSBs. Our TUDEL:AP samples thus likely exclude the most rapidly repaired breaks. Using TUDEL:AP, we examined epigenetic factors and histone PTMs enriched near DSBs. We noted enrichment of transcription factors and components of the RNA splicing machinery, suggesting a link between DSBs and transcription. While such links have been postulated before, we emphasize that DSBs are much more likely to arise in fragile transcribed chromatin. This was confirmed by CUT&RUN sequencing of γH2AX in Chapter 3 and will be explored in Chapter 6. Our data are consistent with enrichment of breaks in regions already decorated with transcription machinery, rather than recruitment of such factors to breaks as part of the DDR. In particular, our results confirmed enrichment of SMARAC4 at DSB loci[431]. SMARCA4 is enriched in transcribed regions, particularly at enhancers. We discuss functional roles of SMARCA4 in the DDR in Chapter 7. Chromatin enrichment also allowed us to use Epiprofiler analysis of histone PTMs to confirm local enrichment of epigenetic features in break-proximal chromatin. These results are in agreement with changes observed in whole chromatin in Chapter 4. Yet, they contrast with enrichment of breaks in areas marked by basal euchromatin as seen in Chapter 3. Taken together, the various analysis methods can delineate bona fide DDR-associated changes by comparing basal to post-IR enrichment of histone PTMs.

CHAPTER 6

TRANSCRIPTION IS A PRIMARY DRIVER OF DSB RECOGNITION AND REPAIR

6.1 INTRODUCTION

In Chapter 3, we observed an enrichment of γH2AX in open chromatin with particularly rapid deposition in transcribed regions. We postulated that enhanced accessibility of euchromatin may be permissive to DSB recognition giving rise to the observed phenotype. We also observed that DSB induction as measured by BLISS was only moderately correlated to γH2AX density. Indeed, transcribed genes contained more γH2AX than non-transcribed genes, despite an equivalent chromatin density and number of DSBs. Thus, factors beyond DSB induction rate dictate γH2AX levels; we propose both transcription and replication as key influences on γH2AX deposition. Further, using TUDEL:AP, we identified transcriptional machinery along with components of the spliceosome as enriched proximal to DSBs. Thus, we will next consider whether transcription in and of itself has any effect on DSB formation, recognition, or resolution.

Linkages between transcription and DNA damage are well appreciated, though there is little consensus as to whether transcription is damage promoting, or instead aids in repair of broken DNA[522]. In the first category, transcription is a well-known contributor to DNA fragility[399, 524, 525, 526, 527]. Several studies imply a causal link between transcription and DSB induction[285]. Inherently, transcription unwinds DNA and recruits topoisomerases leaving DNA vulnerable to damage[292, 522, 528, 529]. Transcription is also thought to give rise to DSBs via collisions between transcription machinery and other processes, principally replication[293, 530]. These replication-transcription conflicts are a driver of mutagenesis[531]. Further, previous efforts have identified so called-fragile promoters, regions which accumulate DSBs even under basal conditions, though their etiology is unclear[526]. Paradoxically, transcription at a subset of fragile promoters is downstream

from induction of DNA damage, thus suggesting one possible mechanism for the association between DSBs and transcribed regions[285, 532]. Fragile promoters are high in basal DNA breaks and enriched for TRIM28 and Top2B[525]. However, it is unclear why cells would actively generate breaks as a consequence of transcription, or whether these breaks are repaired by canonical DDR processes.

Turning to repair-promoting functions of transcription, several DDR factors have been shown to interact with members of the pre-initiation complex (PIC) and aid in attenuation of transcription-proximal damage[283]. Interactions between the canonical DSB signaling factors ATM, DNA-PKcs, and PARP1 and components of the PIC have been identified and thought to promote transcriptional attenuation at DSBs[533, 534, 535]. DNA-PKcs has been shown to promote proteosome-dependent degradation of components of the transcriptional complex[536]. Yet, order of function is unclear; it may be that transcriptional attenuation is a prerequisite for recruitment of DDR factors. Globally, while transcription of most genes is attenuated following IR, DDR genes must be upregulated, creating a challenging situation for cells[537]. It remains to be seen whether repair of breaks surrounding genes which are required following IR insult (e.g. DSB repair genes) operates via a unique mechanism. Finally, RNA may play a repair promoting role, acting as a template for repair or recruiting additional DDR factors. Lastly, components of the spliceosome have been implicated in the DDR suggesting specialized repair pathways are active at transcribed genes[322, 538].

One of the more enigmatic connections between transcription and DSBs is the formation of R-Loops. R-Loops are tri-stranded structures formed when nascent RNA intercalates into DNA and base pairs with the complimentary strand[539, 540]. Most R-Loops have been shown to be products of Pol II transcription and accumulate at transcribed promoters and 5' UTRs[541]. However, R-Loops may also be caused by *de novo* transcription from DSB ends or by stalling/backtracking of Pol II in response to detection of DSBs[326, 542]. A reduction in Pol II S2P, a processive proteofrom, is associated with R-Loop formation[543]. At first blush, R-Loops would seem to represent a threat to genome integrity as they expose

DNA and are treated as toxic byproducts of transcription by cellular machinery[544]. Indeed R-Loop formation is associated with mutations and translocations[545]. However, R-Loops have also been shown to mediate repair of DSBs via recruitment of HR factors and promotion of resection[336, 349, 546]. As with other connections between epigenetic features and DSB repair, order of function questions remain. For example, it may be that an association between R-Loops and DSBs is due to a role for R-Loops in repair or due to the inherent fragility of transcribed DNA.

Here, we examine the consequences of transcription on γH2AX deposition. Returning to the global epigenetic analyses of Chapter 3, we show that transcribed areas accrete γH2AX in proportion to the degree of transcription at a given locus. We also suggest that only active Pol II (and not paused or promoter proximal Pol II) is sufficient to direct γH2AX deposition. These results suggest a kind of transcription coupled recognition of DSBs.

6.2 RESULTS

6.2.1 Transcribed Regions Preferentially Recognize DSBs in Contrast to Theories of Transcription Associated DNA Damage

Our genomic data outlined in Chapter 3 suggested an association between transcribed regions and rapid accumulation of γH2AX coverage genome-wide. As mentioned previously, these data could be second-order associations driven by the open, accessible nature of transcribed DNA. Thus, we sought to determine the functional consequences of transcription at DSBs. We returned to ChromHMM in order to identify regions of the genome which are transcribed or associated with transcriptional activity. γH2AX coverage was calculated across promoters and transcribed regions as defined by ChromHMM. The degree of promoter activity or transcriptional output was correlated with γH2AX coverage at 1 h PIR (Figure 6.1A). An inverse relationship was observed 24 h PIR. Thus, while transcription is permissive for early DSB recognition, DSBs which are only recognized long after IR may rely on a different

process for recognition. Perhaps replication plays a role in facilitating recognition of DSBs in heterochromatin. While Pol II occupancy is known to be highest at promoters and decline across gene bodies, we note that transcribed regions contain more γH2AX than promoters, suggesting that presence of Pol II alone is not sufficient to mediate γH2AX deposition. To evaluate the effect of transcription on DNA damage recognition more directly, we analyzed poly(A) RNAseq from unperturbed K562 cells. Comparing γH2AX read density in the top and bottom decile of genes ranked by RPKM expression, we see that DSBs near highly expressed genes are preferentially marked by γH2AX at 1 h PIR (Figure 6.1B). By 24 h PIR, gene expression no longer dictates the degree of H2AX phosphorylation. Moreover, while highly expressed genes are depleted of the repressive mark H3K27me3 in a basal setting as expected, these same regions preferentially accumulate H3K27me3 following IR insult (Figure 6.1B). Thus, basal H3K27me3 likely acts differently from repressive marks added after detection of DSBs. This is in line with data from Chapter 4 suggesting that repressive marks including H3K9me3 and H3K27me3 are increased following IR. One mechanism, explored in Chapter 7, is accumulation of repressive marks which mediate transcriptional repression at broken DNA, a prerequisite for repair[129, 330]. Thus, the role of K27me3 in the DDR is particularly important in euchromatin, in contrast to its basal role in gene repression and heterochromatin establishment.

In Chapter 3, we used a genome-wide tiling approach to investigate the distribution of γH2AX following IR insult. While we uncovered strong evidence linking γH2AX deposition to euchromatin; however, these data were subject to the caveat that constitutive heterochromatin is challenging to sequence and might be under-represented in genomic analyses. Toward obviating challenges associated with global epigenetic sequencing, and in an effort to focus our efforts on transcribed regions, we repeated a similar tiling procedure in 2 kb windows centered on all known human TSSs. RPKM normalized coverage of Pol II and poly(A) RNAseq was also computed in these TSS windows. Using DeepTools, a matrix representation of Pol II and RNAseq coverage surrounding TSSs, ranked by average

coverage, was generated (Figure 6.2, left panels). We observe an expected enrichment of Pol II and poly(A) RNA-seq reads around the promoter. Further, a minority of TSSs have significant Pol II or RNAseq coverage in K562 cells. This is expected as not all genes are expressed in a given cell type. The same data was then re-ranked by γH2AX coverage values (Figure 6.2, right panels). Strikingly, the order in the left panels is largely recapitulated when re-ranking by γH2AX coverage, suggesting that γH2AX deposition is correlated with the degree of transcription surrounding TSS loci. The above analyses suggest an association between transcribed areas and γH2AX density at a low resolution.

To gain a more granular view of γH2AX density around transcription start sites, we plotted the profile of Pol II across 20,000 randomly selected transcription start sites, creating a meta-plot (Figure 6.3). Here, we made use of several proxies of transcriptional activity. Pol II occupancy was separated by proteoform: recall that the CTD of promoter proximal Pol II is phosphorylated on Serine 5 followed by subsequent phosphorylation on Serine 2 concomitant with promoter escape and processive translocation. We observed expected pileup of poised Pol II, signified by CTD S5P, at the promoter which declined across the gene body. Next, we assayed transcriptional output by examining Bru-seq; Bru-seq reports all nascent RNA, including non-coding RNA or abortive transcripts. Overlaying this transcription proxy on the TSS meta-plot, we observed a bimodal distribution for BrU-seq data. The TSS-proximal peak likely reflects abortive transcripts, while the distal increase is due to mature transcripts produced by processive Pol II[547]. Finally, we overlayed γH2AX coverage. Surprisingly, γH2AX density was not uniform across these regions; instead γH2AX saw a local minimum at the promoter and increased moving into the gene body. This contrasts with H2AX density which was maximal at promoter regions. We suggest that presence of Pol II is not sufficient to mediate DSB recognition per se, rather, only processive transcription is coupled to H2AX phosphorylation. While we had earlier shown an association between transcribed regions and γH2AX, these data imply that processive Pol II mediates DSB recognition and that active transcription is necessary for γH2AX phosphorylation. Further, our data suggest that

Pol II may be considered a DSB recognition factor, and place Pol II acts upstream of ATM, a model in contrast to previous studies[130, 548].

Several studies imply a causal link between transcription and DSB induction[285]. Mechanisms include unscheduled conflicts or collisions between cellular processes which give rise to DSBs, collisions between transcription and preexisting SSBs or base damage, and fragile promoters. Fragile promoters, regions which accumulate DSBs even under basal conditions, are associated with oncogenic genome alterations though their etiology is unclear[526]. Further, transcription of certain genes including heat shock response targets or serum-activated genes is associated with DNA damage induction; these loci may be distinct from fragile promoters. Paradoxically, it has been postulated that DSBs may drive transcription at this latter subset of genes[285]. We thus attempted to identify differences in DSB induction or detection across TSSs genome wide. First, we repeated the tSNE analysis in Chapter 3, restricting the plotted tiles to ones which overlap a known TSS[549]. Many of the genome-wide relationships between epigenetic features and γH2AX deposition held true even within TSS regions, which are relatively homogenous (Figure 6.4). For example, TSS regions which were enriched for Pol II and which did not contain H3K27me3 (i.e. actively transcribed genes) had higher levels of γH2AX 1 h PIR. γH2AX density 24 h PIR accumulated in TSSs marked by H3K27me3.

Toward a causal link between γH2AX deposition and gene expression, we exploited intra-cell type differences in gene expression. γH2AX CUT&RUN coverage was mapped in K562 myeloid leukemia and HepG2 liver carcinoma cell lines 1 h PIR. From ENCODE, we also obtained Bru-seq data from both cell lines as a metric of basal gene expression. Plotting the normalized difference in γH2AX coverage against the normalized difference in Bru-seq reads revealed a significant association between differential transcription and differential deposition of γH2AX (Figure 6.5A). Genes which were upregulated in a given cell type had correspondingly higher levels of γH2AX. Inter-cell type differences, including gene expression, thus influence the DDR; this may be an understudied way in which cell identity impinges upon response to genotoxic therapy.

Next, we re-made the tSNE chromatin context map from Chapter 3, this time restricting plotted tiles to ones which overlapped a known human TSS. Toward examining the relationship between gene function and DNA damage recognition, we designated two distinct clusters on the TSS tSNE map, both of which appeared to be high in γH2AX 1 h PIR (Figure 6.4A). TSSs in either γH2AX high cluster were linked to genes using bedtools intersect[409]. Then we performed GProfiler pathway analysis on genes mapping to either cluster[550]. Both clusters were similarly enriched in highly transcribed genes including ribosomal genes and RNA splicing factors; this association is likely not functionally significant beyond suggesting a link between transcription and γH2AX. It is widely appreciated that most transcription is attenuated following IR insult and associated cell cycle disruption[448, 551, 552]. However, DDR genes must be upregulated, raising the possibility of conflicts between transcription and damage at these loci. Thus, the TSS tSNE map was color coded to look for genes involved in the GO pathways *DNA Damage Repair* and *DNA Damage Response*[553, 554]. These genes clustered into γH2AX high clusters (Figure 6.5B). Moreover, DDR genes had higher γH2AX coverage at their TSS as compared to all other genes. This excess γH2AX was not due to high levels of basal transcription of DDR genes as measured by RNAseq. On the contrary, many DDR genes were lowly expressed but accumulated significant γH2AX.

In fact, an increase in transcription post IR at DDR or DNA Damage genes was associated with more γH2AX, in contrast to the pattern observed for all genes (Figure 6.5C-D). These observations suggest that cells preferentially recognize damage around DDR-associated genes following IR insult. Globally however, attenuation of transcription is associated with DSB recognition, suggesting that Pol II participates in DSB detection.

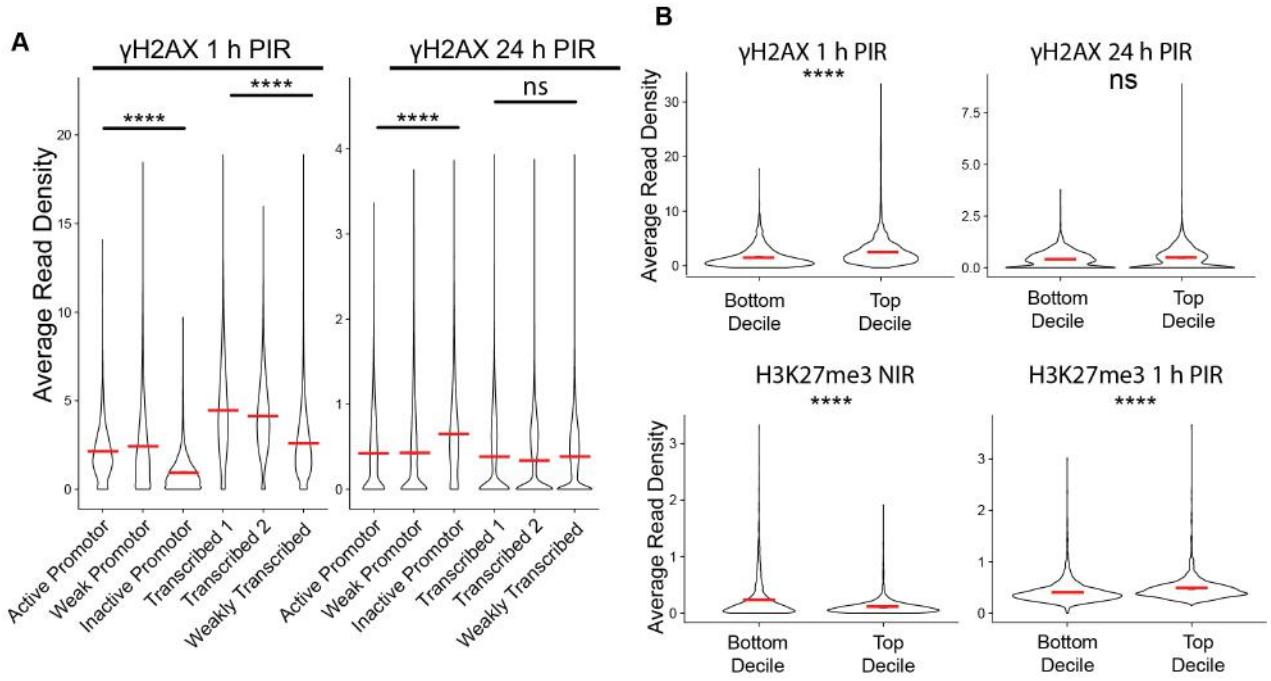

Figure 6.1: **A** γH2AX coverage across 1 kb tiles falling within the indicated ChromHMM states was calculated at 1 h and 24 h PIR. Red lines denote the mean γH2AX coverage value. **** $p < 0.0001$, ns $p > 0.05$ by Wilcoxon rank sum test comparing coverage between the indicated ChromHMM states. **B** Gene transcription was quantified by poly(A) RNAseq in K562 cells. Genes were ranked by RPKM and γH2AX coverage was calculated across the 1top or bottom decile of genes ranked by RPKM. Coverage across 2 kb regions flanking the closest TSS to the selected genes was calculated at 1 h and 24 h PIR. Red lines denote the mean coverage value. Coverage of different epigenetic features is as indicated. **** $p < 0.0001$, ns $p > 0.05$ by Wilcoxon rank sum test comparing coverage between the bottom and top decile of genes ranked by RPKM.

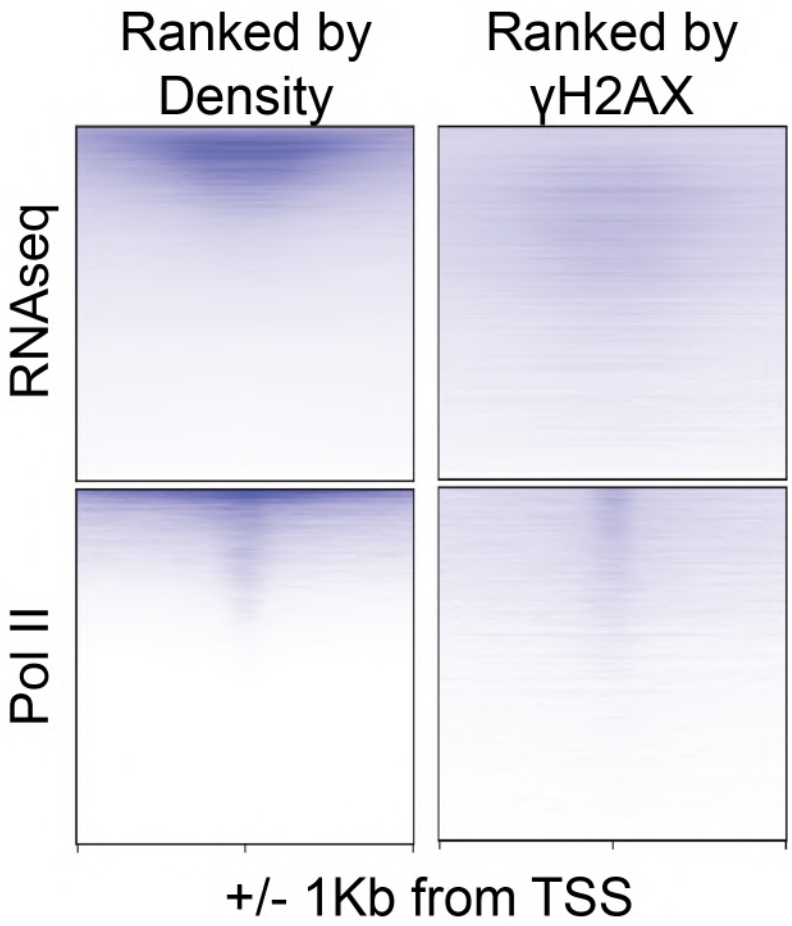

Figure 6.2: Density profile of the indicated epigenetic feature in 2 kb regions overlapping 20,000 randomly selected transcription start sites. Plots are produced by deeptools plot profile. Left panels are ranked by descending average density of the indicated feature. Right panels are ranked by descending γH2AX coverage which was calculated using bedtools coverage.

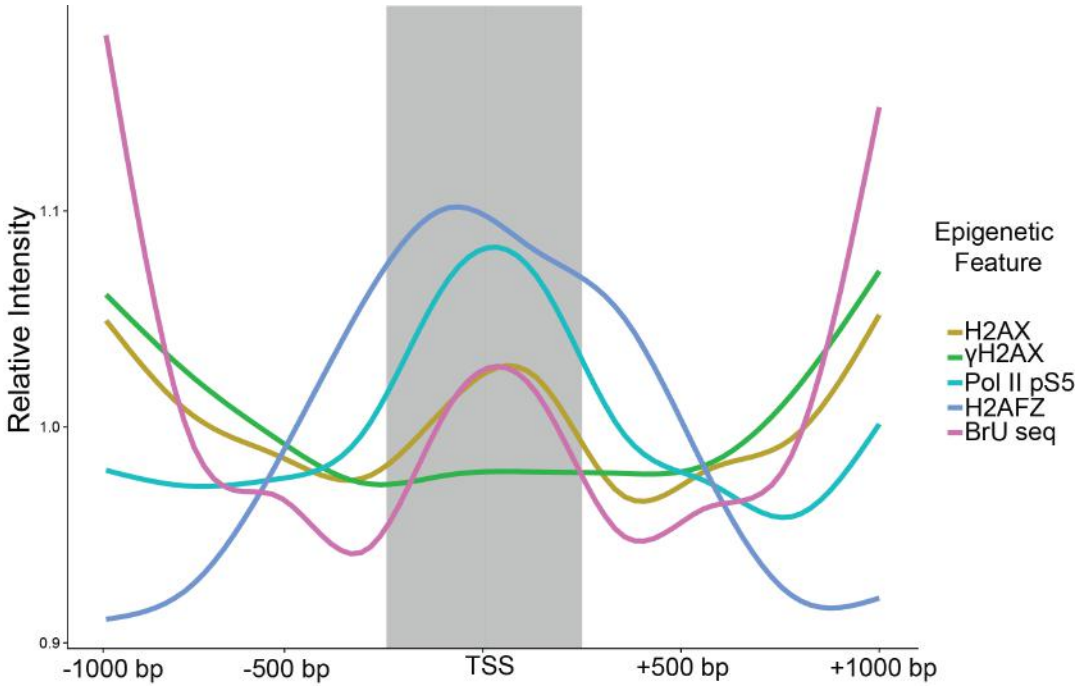

Figure 6.3: Profile plots of the relative coverage of the indicated epigenic features. Lines represent the average normalized coverage of the indicated feature across 20,000 randomly selected transcription start sites. Shaded region denotes +/- 250 bp from the TSS, or approximately 1 nucleosome. Strand information is not shown, creating a symmetric plot.

6.2.2 Transcription is a Primary Driver of DSB Recognition in Genic Regions

Returning to the link between RNA Polymerase II and γH2AX deposition, we reasoned that the two γH2AX high clusters identified in the TSS chromatin context map may differ in their transcriptional activity (Figure 6.4A). Thus, coverage data from Pol II S2P, Pol II S5P and Total Pol II was overlayed to elucidate how the mechanism of transcription may influence γH2AX repair (Figure 6.6A,B). γH2AX coverage correlated more strongly with phosphorylated forms of Pol II as compared to total Pol II, again suggesting that active transcription, but not paused Pol II, is necessary for γH2AX deposition. Next, the tSNE chromatin context map was color coded according to poly(A) RNA-seq read coverage and Bru-seq coverage from K562 cells (Figure 6.6C,D). Bru-seq detects all nascent transcripts including abortive transcripts, whereas poly(A) RNA-seq only assays completed transcrip-

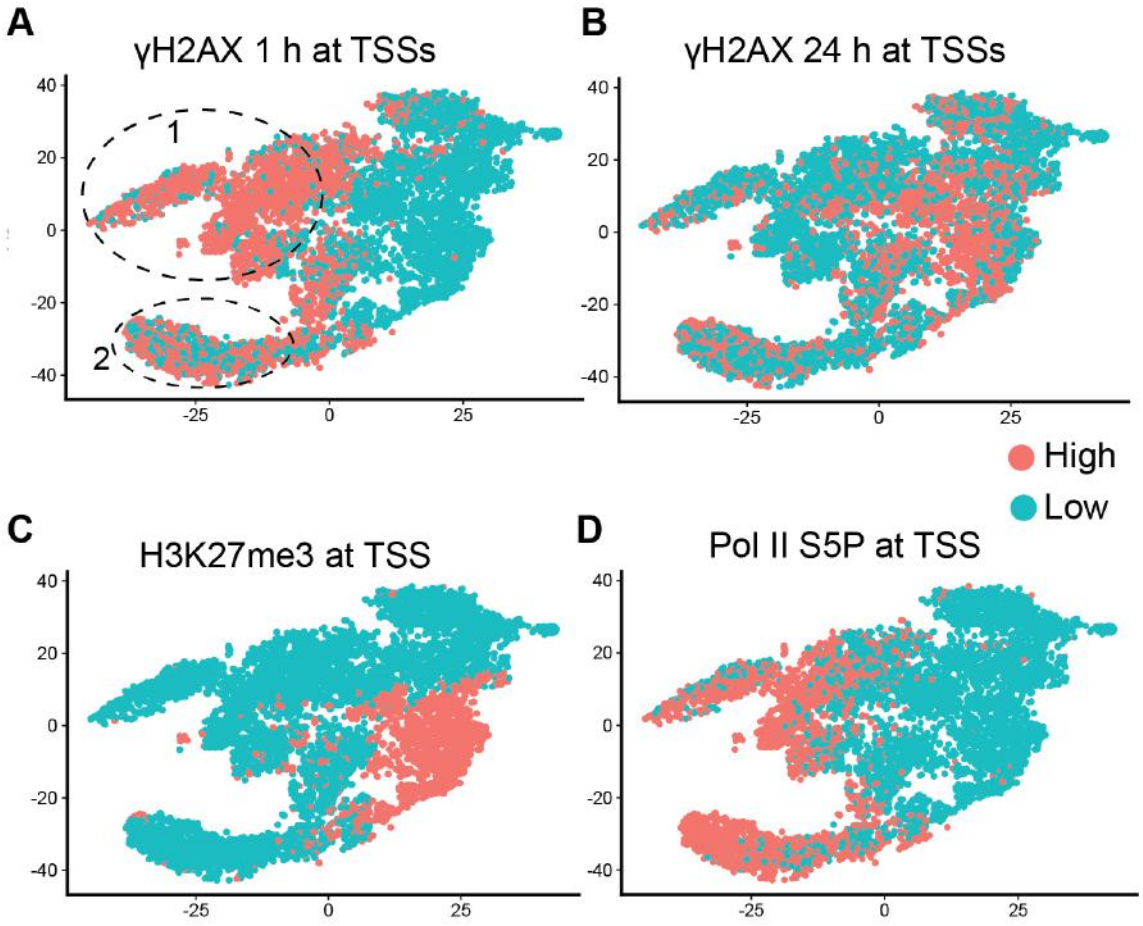

Figure 6.4: **A** tSNE plot generated from tiles spanning +/- 1 kb from 2000 γH2AX-High and 2000 γH2AX-Low TSSs. Points are color coded with respect to the mean data-set-wide γH2AX coverage value 1 h PIR. Two clusters, identified by visual inspection, are indicated with dotted lines. **B** Plot as in A, but color coded according to γH2AX coverage 24 h PIR. **C** Plot as in A, but color coded according to basal H3K27me3 coverage. **D** Plot as in A, but color coded according to basal Pol II S5P coverage.

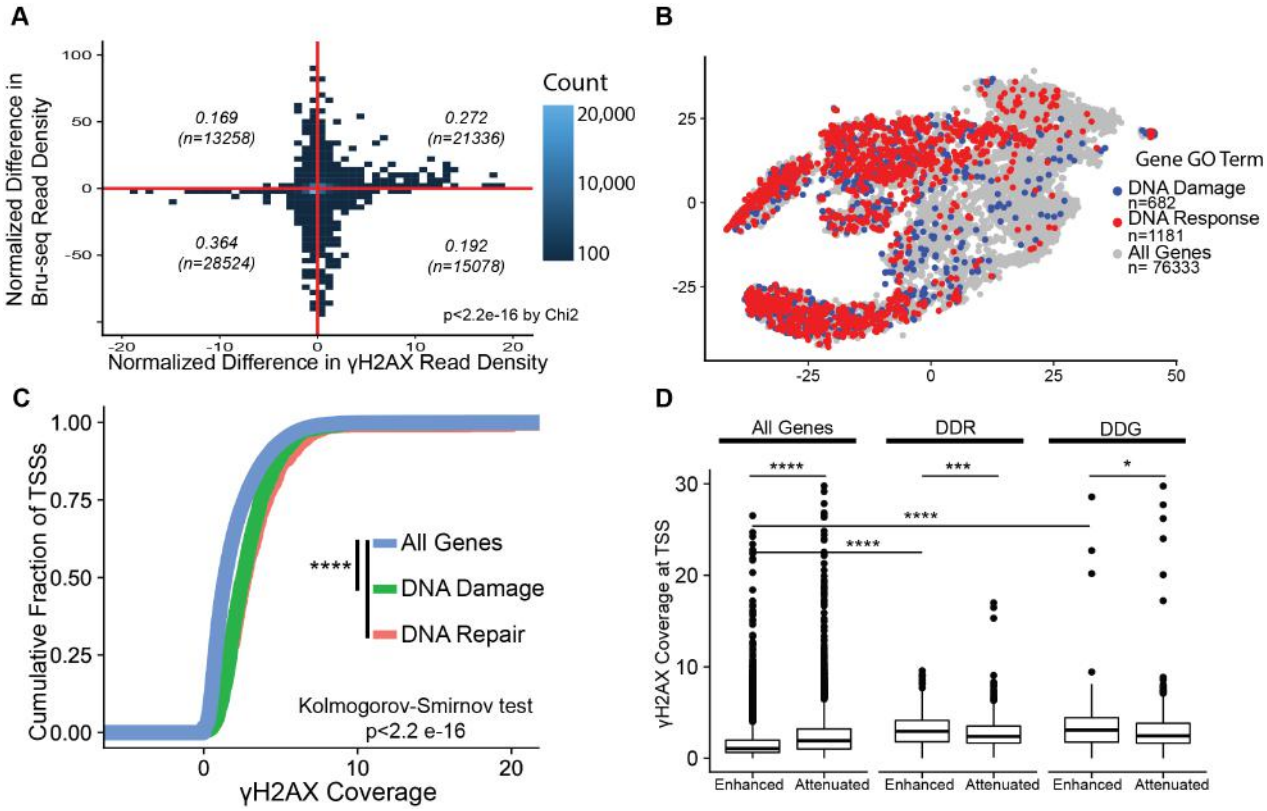

Figure 6.5: **A** Plot comparing Bru-seq and γH2AX coverage between K562 and HepG2 cell lines across 2 kb tiles spanning all human TSSs. Values indicate the proportion and number of tiles in each quadrant. Significant deviation from randomness is confirmed by Pearson's χ^2 Goodness of Fit test. **B** tSNE plot generated from tiles spanning +/- 1 kb from 20,000 randomly selected TSS regions. Points are color coded according to the gene ontology term for the closest gene to the genomic position of the TSS. 2000-γH2AX High and 2000-γH2AX Low regions are selected for plotting. **C** Cumulative distribution of γH2AX reads across 2 kb tiles spanning all human TSSs. Plot is subdivided to show TSSs mapped to DNA Damage or DNA repair genes as identified by the GO gene ontology pathways. **** p< 2.2 e-16 by Kolmogorov-Smirnov test comparing all genes to genes in DNA Damage or DNA repair pathways. **D** γH2AX coverage is calculated across 2 kb tiles spanning all human TSSs subdivided by GO gene ontology pathways as in C, and by enhanced or attenuated transcription (whether Bru-seq reads increased or decreased, respectively, between IR and NIR datasets). * p<0.05, *** p< 0.001, **** p< 0.0001, ns p>0.05 by Wilcoxon rank sum test.

tion. Cluster 1 was enriched in Bru-seq, though TSSs in this cluster did not display high levels of poly(A) RNA-seq suggesting these may be paused or poised promoters. These regions were also high in BLISS signal, DNAse-seq coverage, and were occupied by TRIM28, a marker of fragile promoters (Figure 6.6E-G).[166, 285]. Thus, fragile promoters seemed to constitute Cluster 1. By contrast, the second cluster displayed lower enrichment of fragile promoter features. Both poly(A) RNAseq and γH2AX coverage were strongly enriched in cluster 2, while Bru-seq was relatively low. Cluster 2, which was most highly enriched for γH2AX, showed high levels of Pol II S2P as compared to cluster 1, suggesting that, in this cluster, active transcription is associated with γH2AX deposition. Further, CCluster 2 was marked by low H3K4me3 and high H3K36me3 (Figure 6.6H,I). Both H3K4me3 and H3K36me3 are associated with transcribed chromatin, though H3K4me3 is enriched at the 5' end of genes and H3K36me3 accumulates distally from TSSs[120, 123, 555]. Moreover, H3K36me3 is known to direct PRC2 and mediate gene silencing; thus, H3K36me3 rich loci may rely on PRC2 to direct local DNA damage detection[556, 557]. Thus, Cluster 2 includes genes which, because they highly transcribed, or have short first exons, accumulate γH2AX quickly. By contrast, Cluster 1 includes more poised promoters which do not contribute to DSB detection, in addition to fragile promoter regions. Taken together, we suggest a role for processive Pol II in γH2AX deposition especially at regions which are not fragile promoters. Pol II can thus be reclassified as a bona fide DDR factor, rather than an upstream cause of DNA damage.

Next, to validate our genomic data, we performed immunofluorescence imaging of γH2AX in the presence of a transcription inhibitor, flavopiridol, which specifically inhibits transcription elongation[558]. Cells were acutely dosed with flavopiridol 15 min prior to IR so as to minimize confounding effects mediated by transcription of specific genes, e.g. DDR factors. Addition of flavopiridol diminished the number of γH2AX IRIF and pATM IRIF 1 h PIR, and inhibition of transcription does not induce γH2AX IRIF in the absence of exogenous damage (Figure 6.7). Thus, transcriptional activity may mediate recognition of DSBs up-

stream of ATM. Toward narrowing the effect of transcription on DSB recognition, we imaged γH2AX foci in conjunction with several proteoforms of Pol II (Figure 6.8). Significant association was observed between γH2AX and Pol II S2P but not S5P. Addition of flavopiridol specifically diminished the level and enrichment of Pol II S2P at IRIF, thus confirming the role of processive Pol II in DSB recognition. Next, we repeated the above experiments in the presence of the ATM inhibitor KU-60019. Inhibition of ATM did not prevent enrichment of Pol II S2P at IRIF, though it diminished the overall accumulation of Pol II at IRIF. Thus, ATM is not necessary for accumulation of processive Pol II at breaks sites. Accumulation of phosphorylated Pol II at DSBs in an ATM deficient setting may be driven by alternative DDR kinases such as DNA-PKcs or ATR, as previously reported[310]. More likely, these data again suggest that Pol II acts upstream of ATM in the DDR, in contrast to previous models.

Finally, we assessed epigenetic changes at IRIF toward elucidating the order of function between Pol II, H2AX phosphorylation and epigenetic modification. R-loops are RNA:DNA hybrid structures associated with transcriptional pausing proximal to damaged DNA[540, 545]. Inhibition of transcription by flavopiridol decreased H3K27me3 and R-loops at IRIF, suggesting that transcription is necessary for chromatin compaction in damaged genic regions (Figure 6.9). R-Loops are considered a consequence of paused or attenuated transcription surrounding DSB loci[541]. Addition of an ATM inhibitor also diminished H3K27me3 accumulation and R-loop formation at IRIF. However, in an ATM deficient setting, flavopiridol had no effect suggesting that while transcription is necessary for recruitment of ATM, other epigenetic changes at DSBs are downstream of ATM and H2AX phosphorylation. Thus, we propose that the role of Pol II in DSB proximal chromatin involves signaling to ATM or DNA-PKcs which, in turn, mediate chromatin compaction, R-Loop formation, and break repair. These findings are in line with our genomic data which show that transcribed regions of chromatin are proficient at recognition of DSBs and induce local H3K27me3 deposition perhaps to mediate transcriptional attenuation or DDR signaling.

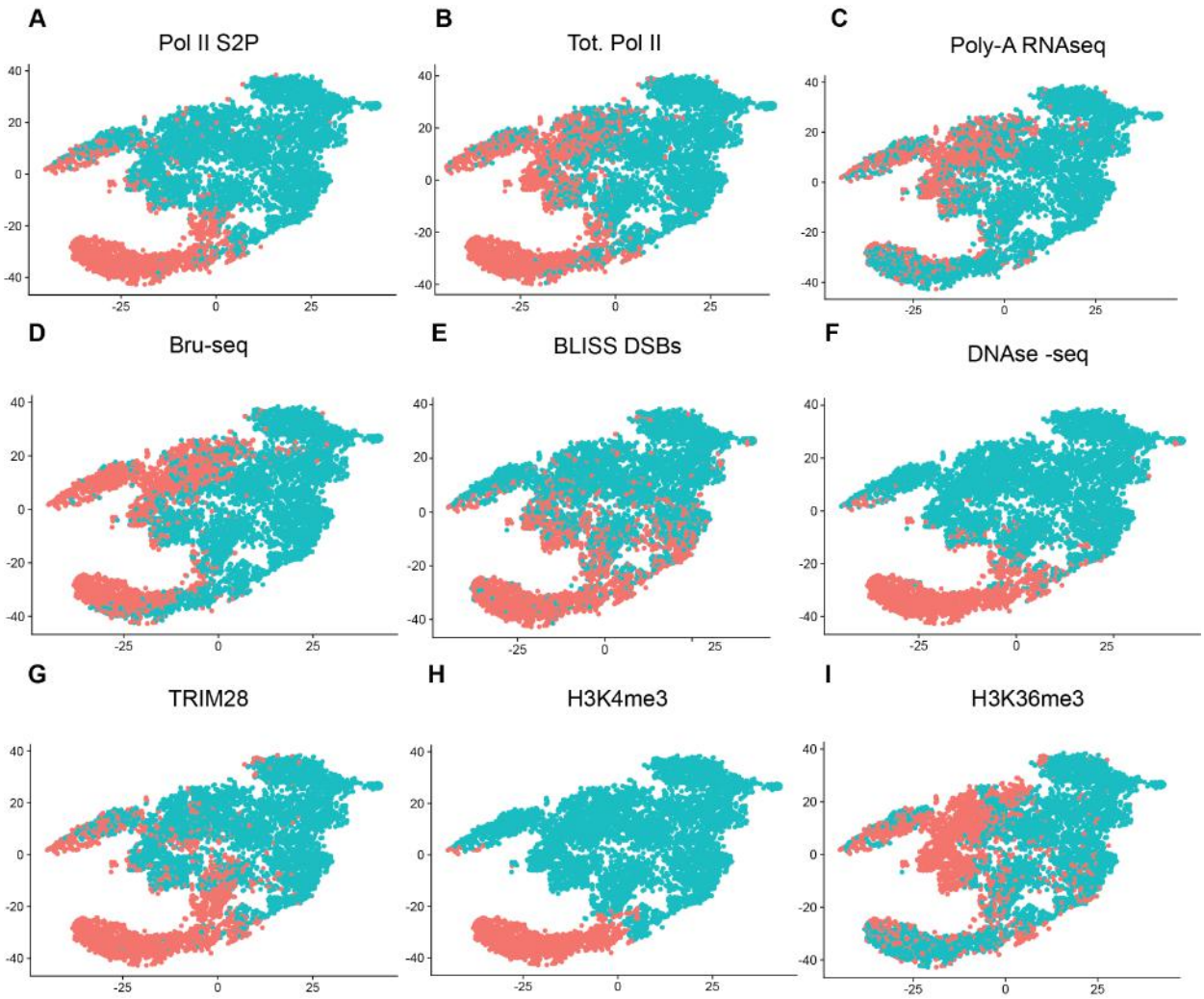

Figure 6.6: **A** 1 kb tiles spanning 5,000 randomly selected TSSs were plotted using tSNE dimensionality reduction. Points are color coded with respect to the mean sample-wide coverage of Pol II S2P. **B** tSNE plot generated from tiles spanning +/- 1 kb from 5,000 randomly selected TSS regions as in A. Points are color coded with respect to the mean sample-wide coverage of Total Pol II. **C** tSNE plot as in A. Points are color coded with respect to the mean sample-wide coverage of poly(A) RNAseq reads. **D** tSNE plot as in A. Points are color coded with respect to the mean sample-wide coverage of Bru-seq reads. **E** tSNE plot as in A. Points are color coded with respect to the mean sample-wide density of BLISS DSBs. **F** tSNE plot as in A. Points are color coded with respect to the mean sample-wide value of DNAse-seq coverage.**G** tSNE plot as in A. Points are color coded with respect to the mean sample-wide coverage of TRIM28. **H** tSNE plot as in A. Points are color coded with respect to the mean sample-wide coverage of H3K4me3. **I** tSNE plot as in A. Points are color coded with respect to the mean sample-wide coverage of H3K36me3.

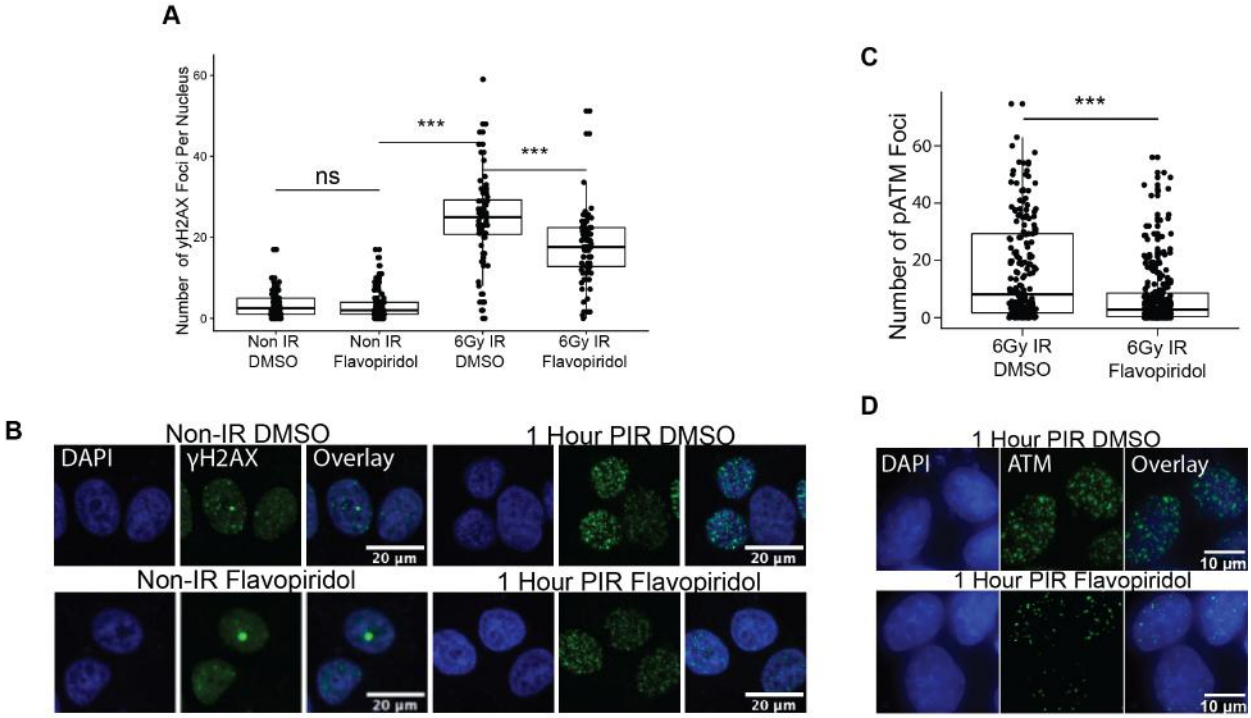

Figure 6.7: **A** Number of γH2AX foci per nucleus in the indicated conditions. Flavopiridol was added for 15 min prior to irradiation. *** $p < 0.001$, ns $p > 0.05$ by Wilcoxon rank sum test comparing the indicated conditions. **B** Representative images from immunofluorescence imaging of γH2AX IRIF 1 h PIR. Addition of the transcription inhibitor flavopiridol attenuated γH2AX foci formation. **C** Number of ATM foci per nucleus in the indicated conditions. Flavopiridol was added for 15 min prior to irradiation. *** $p < 0.001$ by Wilcoxon rank sum test comparing the indicated conditions. **D** Representative images from immunofluorescence imaging of pATM IRIF 1 h after PIR. Addition of the transcription inhibitor flavopiridol attenuated pATM foci formation.

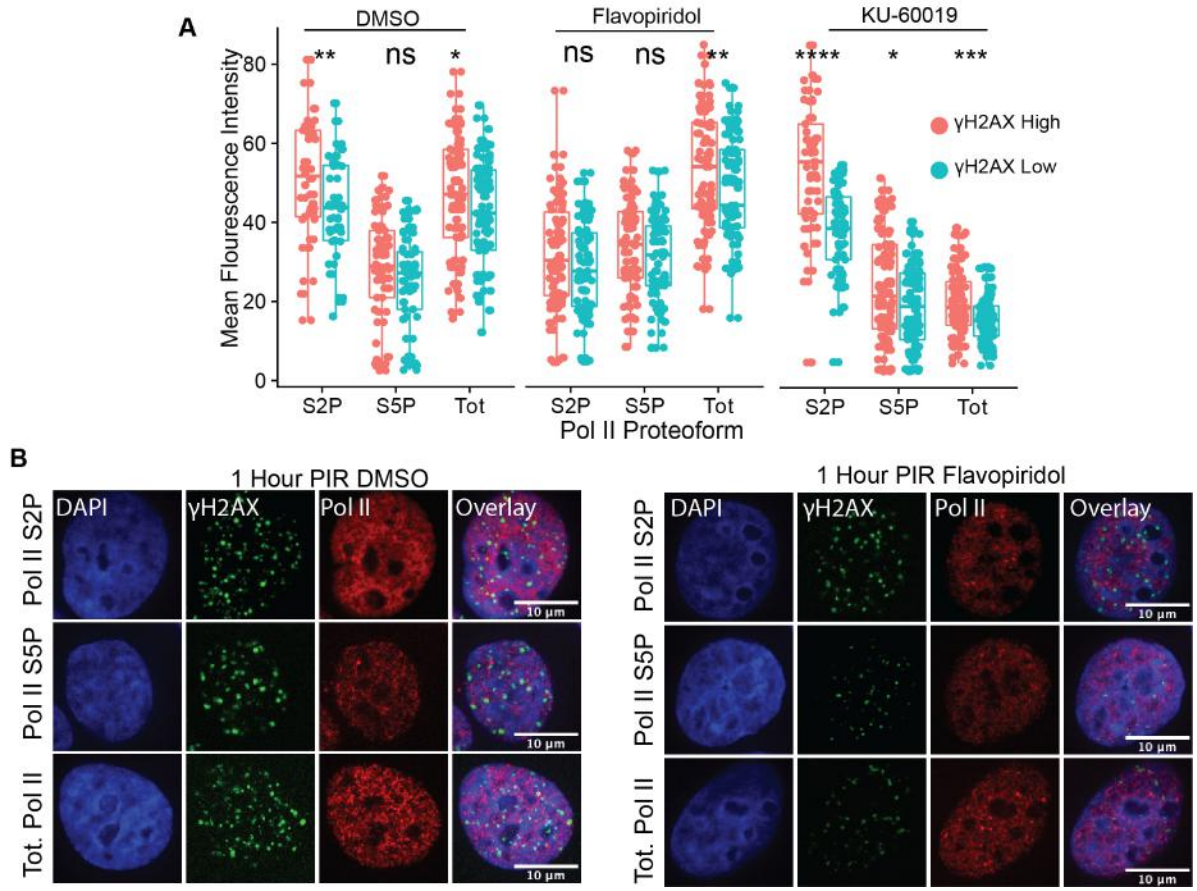

Figure 6.8: **A** Mean fluorescence intensity of the indicated Pol II proteoform within nuclei sub-divided with respect to the average nuclear fluorescence intensity of γH2AX 1 h PIR. Tot indicates an N-terminal Pol II antibody which detects total Pol II irrespective of the phosphorylation state of the CTD. KU-600019, was added overnight, and Flavopiridol was added for 15 min prior to irradiation. * $p<0.05$, ** $p< 0.01$, *** $p<0.001$, **** $p< 0.0001$, ns $p>0.05$ by Wilcoxon rank sum test comparing Pol II MFI between γH2AX-high and γH2AX-low regions. **B** Representative images from immunofluorescence imaging of γH2AX IRIF in conjunction with the indicated Pol II proteoform. Significant colocalization between processive Pol II, denoted by S2P, was observed. Addition of the transcription inhibitor flavopiridol or the ATM inhibitor KU-600019 attenuated γH2AX IRIF formation.

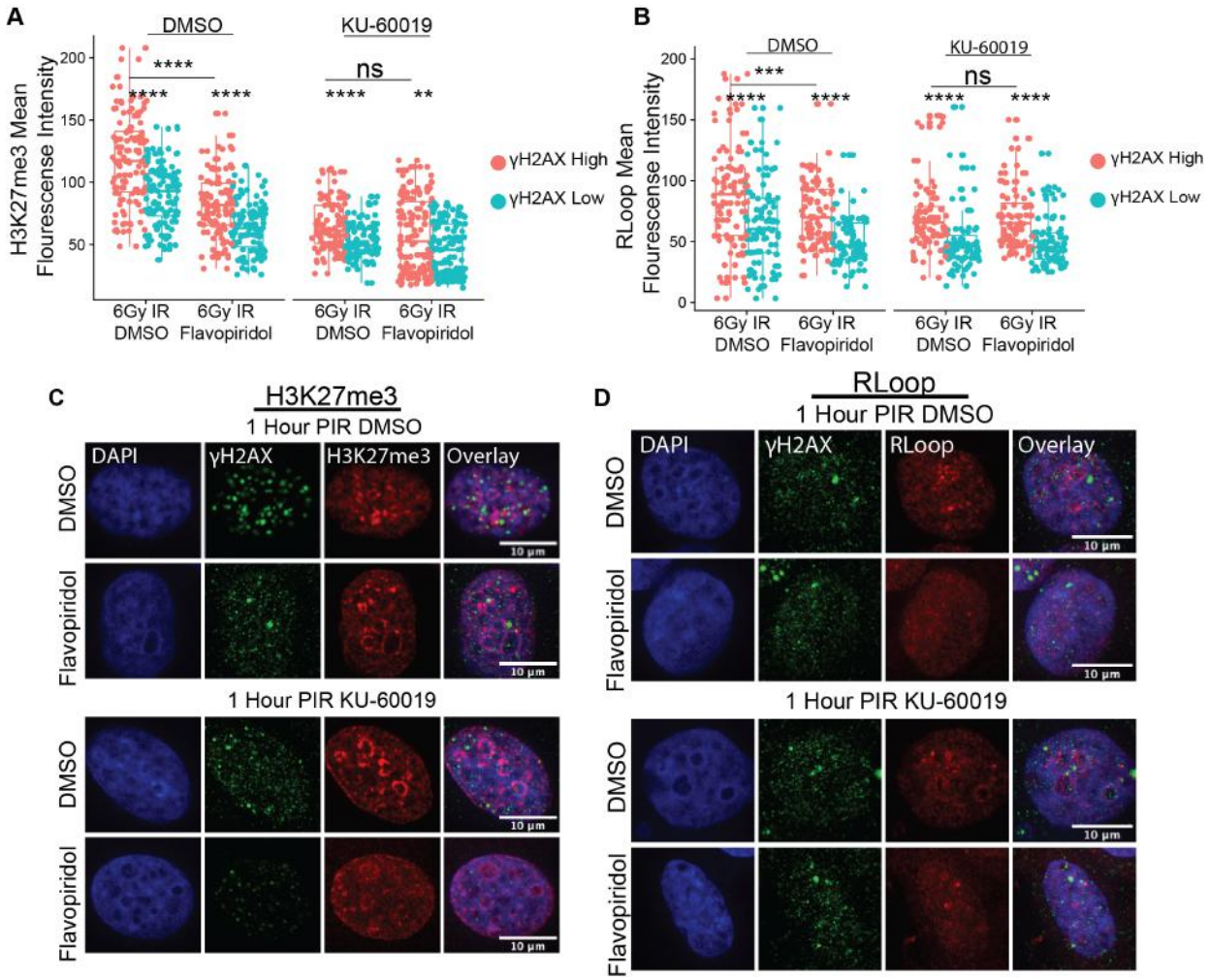

Figure 6.9: **A** Mean fluorescence intensity of H3K27me3 within nuclei sub-divided with respect to the average nuclear fluorescence intensity of γH2AX. ** p< 0.01, **** p< 0.0001, ns p>0.05 by Wilcoxon rank sum test. **B** Mean fluorescence intensity of R-Loops within nuclei sub-divided with respect to the average nuclear fluorescence intensity of γH2AX. *** p< 0.001, **** p< 0.0001, ns p>0.05 by Wilcoxon rank sum test. **C** Representative images from immunofluorescence imaging of γH2AX IRIF 1 h PIR in conjunction with H3K27Me3 +/- the ATM inhibitor KU-60019. Inhibition of transcription partially phenocopies ATM inhibition and diminishes γH2AX foci as well as H3K27me3 accumulation at foci. **D** Representative images from immunofluorescence imaging of γH2AX IRIF 1 h PIR in conjunction with R-Loops +/- the ATM inhibitor KU-60019. Inhibition of transcription partially phenocopies ATM inhibition and diminishes γH2AX foci as well as R-Loop accumulation at foci.

6.3 DISCUSSION

Transcription has long been associated with genomic damage with many models suggesting links between transcription and DSBs. Transcribed regions are among the most exposed regions of the genome and the act of transcribing DNA leaves genetic information in a physically precarious state. Many of the studies linking transcription to DSB induction have assessed damage either in a basal state or following addition of cellular stressors. In this way, induction of damage at the most vulnerable genomic regions is somewhat expected. However, this study makes use of exogenous sources of DNA damage which might induce damage irrespective of the local epigenetic milieu. Instead, we find that even with stochastic, exogenous DSBs resulting from ionizing radiation, transcribed regions are preferentially broken and breaks within these regions are preferentially recognized. Most strikingly, breaks in transcribed genes are detected more quickly than breaks in non-transcribed genes despite comparable nucelosome occupancy and DSB density (Figure 6.10). This observation is only partly influenced by fragile promoters. Indeed, of the two clusters of TSSs moderately enriched in γH2AX 1 h PIR, only one is characteristic of fragile promoter regions. These fragile regions are high in DNA breaks and enriched for TRIM28 and Top2B, as expected[525]. However, global analysis of γH2AX enrichment surrounding TSSs showed a second cluster of TSSs devoid of chromatin fragility markers, but which nonetheless had high levels of γH2AX 1 h PIR. We propose transcription coupled repair as a major driver of the DDR following IR insult at these regions.

In genic regions replete with transcribing Pol II, we show that deposition of γH2AX is associated with increased levels of transcription; highly expressed genes accumulate more γH2AX than lowly expressed genes. The profile of γH2AX surrounding transcription start sites suggests that processive Pol II, but not paused or promoter proximal polymerase, is sufficient to mediate γH2AX deposition. Transcription coupled repair regions were associated with high levels of Pol II S2P and a low pausing ratio. Pol II sheds and accumulates cofactors as it transitions from a promoter-proximal state to a processive state, raising the

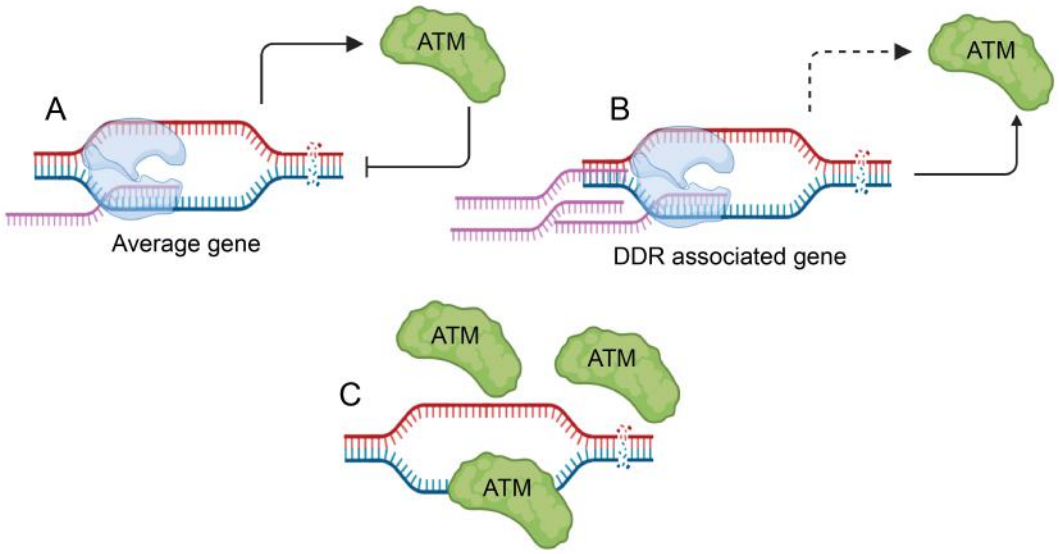

Figure 6.10: **A** Across much of the transcribed genome we propose a feedback loop between Pol II and ATM wherein transcribing Pol II detects damage and signals to the DDR machinery. ATM, in turn, attenuates transcription likely via PRC1 or other mechanisms (see Discussion). **B** By contrast, at DDR-associated genes we observe an association between increased transcription and the DDR. This may be a direct association; transcriptional machinery has been shown to associate with DDR factors. **C** Alternatively, we cannot rule out that ssDNA (i.e. at transcription bubbles) may be a preferred substrate for ATM, increasing the local concentration of DDR factors and γH2AX. Pol II is dispensable in this model and is thus not shown.

possibility that one or more co-factors mediates DSB recognition rather than Pol II itself. Disentangling the contribution of proteins associated with Pol II to the DDR warrants future exploration. In particular, past studies have implicated transcription factors such as Cux1 in the DDR[266]. Perhaps Cux1 interacts with Pol II to mediate DSB recognition.

High-γH2AX, low-fragility regions also had high H3K36me3 but low H3K4me3, indicating a possible role for PRC2 in repairing damage at these regions[557]. Alternatively, genes with shorter first exons or higher exon:intron ratios have more H3K36me3 and could be preferentially repaired[120, 559]. Imaging studies confirmed an association between γH2AX IRIF and Pol II rich chromatin. This association is stronger with Pol II S2P, a proteoform associated with active transcription, as opposed to Pol II S5P or total Pol II. Toward confirming the necessity of transcription in the DDR, addition of flaviorpiridol, a poly-CDK inhibitor which stops elongation of Pol II and, in our hands, specifically reduced Pol II S2P at γH2AX IRIF, attenuated γH2AX IRIF 1 h PIR. Loss of Pol II S2P also reduced pATM IRIF, a key signaling node in the DDR. That transcription mediates the DSB signaling cascade upstream of ATM suggests that chromatin-localized events are important in initial recognition of damage. These findings also begin to suggest new mechanisms by which ATM can rapidly recognize DSBs. Canonically, ATM activation is subject to binding of the MRN complex[560, 561]. In turn, the MRN complex is regulated by chromatin level factors including H3K36me3, associated with transcription[311, 562]. Moreover, unwound or ssDNA has been shown to stimulate ATM activation[563, 564]. Perhaps the transcription bubble presents a preferential substrate for MRN binding and subsequent attraction of ATM. As expected, Pol II S2P still accumulates at IRIF even in the presence of the ATM inhibitor KU-60019. Thus, early epigenetic changes preceding the canonical DDR may be ATM-independent. These findings reframe previous conclusions which suggested a causative link between transcription and DNA damage induction. ATM inhibition did diminish R-Loops and H3K27me3 deposition at DSB loci indicating that these factors are downstream from ATM in the DDR cascade. We explore possible mechanisms of ATM interaction with

chromatin modifiers in Chapter 7. That ATM loss reduces R-Loops is interesting and suggests that complete transcriptional attenuation may be ATM dependant. More remains to be gleaned regarding R-Loop formation and function, though our data align with studies suggesting that R-Loops are DDR promoting and possibly an integral part of DSB repair.

What is transcription coupled repair? We place Pol II upstream of ATM and suggest that transcription may act as an epigenetic searchlight which alerts the cell to local damage upon contact between processive Pol II and damaged DNA. Transcription is then attenuated, and Pol II signals to ATM which, in turn, precipitates chromatin condensation and R-Loop formation while initiating the DDR. Alternatively, IRIF observed in the absence of ATM may be mediated by DNA-PKcs[310, 533]. We further propose that fragile promoters may rely upon DNA-PKcs for local induction of DDR. Perhaps residual IRIF observed in the absence of ATM signaling reside at fragile promoters or DNA-PKcs is sufficient to mediate some transcription mediated DSB recognition.

As recognition of DSBs is tied to transcription, the DDR could be cell type specific. This observation suggests novel functions of altered gene expression between normal tissue and tumors. Indeed, we show in Chapter 3 that CFS loci, which contain oncogenes and cancer-associated breakpoints, are enriched in γH2AX 1 h PIR. Broadly, perhaps increased expression of oncogenes may induce more DNA damage in a post-therapy context. While DNA damage can be deleterious, it may also contribute to further mutations or translocations which can be cancer promoting. It is also worth noting that a hallmark of transformed cells is resistance to cell death and agnosticism to DNA damage as a consequence of altered signaling pathways (e.g., p53). In this Chapter, we show that cell-intrinsic gene expression programs influence the DDR at the gene level. Other work has suggested a link between gene length and the DDR. We observed moderate effects of gene length on γH2AX deposition, with the longest quartile of genes containing additional γH2AX at 1 h PIR. Thus, the epigenetic response to endogenous or exogenous sources of DNA damage must be considered as part of the rationale under which cancer cells modify gene expression. It should also be noted

that associations between γH2AX and transcribed regions go beyond chromatin accessibility alone. Our data suggest that chromatin fragility only partly explains variation in DSB density and DSB density incompletely explains γH2AX deposition patterns. Therefore, epigenetic marks, especially transcription, influence DSB recognition independently from DSB induction.

CHAPTER 7

THE POLYCOMB REPRESSIVE COMPLEX 2 AND THE SWI/SNF COMPLEX ARE DSB REPAIR FACTORS

7.1 INTRODUCTION

In the preceding Chapters, we outlined development of several tools with which to assess epigenetic modifications at DSBs. In conjunction, we utilized next-generation sequencing to identify genomic loci which were enriched or depleted for γH2AX, and linked patterns of γH2AX deposition to basal and IR-induced Histone PTMs. Collectively, these techniques highlighted H3K27me3 as a critical epigenetic signal controlling DSB repair. Here we will use previously outlined techniques to dissect effects of H3K27me3 and regulators thereof on DSB recognition and repair.

H3K27me3 is deposited by enhancer of zeste homologue 2 (EZH2), a catalytic subunit of the polycomb repressive complex 2 (PRC2). The polycomb complex is an ancient and highly conserved master gene regulator associated with heterochromatin[565, 566]. PRC2 plays a central role in development, gene silencing, and cell fate decisions via selective deposition of the H3K27me3 modification which induces gene silencing[235]. PRC2 and its subunits are frequently mutated or lost in cancers[567]. As polycomb controls cell fate, deregulation or deactivation of these proteins contributes to altered gene expression in cancer, inducing a loss of cell-intrinsic properties and increased cancer "stemness". It has been shown that hyperactive PRC2 may silence tumor suppressor genes including the INK4A/p16 locus[568]. Humans also express PRC1, a related protein complex that stimulates ubiquitination of H2AK119. PRC1 also binds to H3K27me3 and reinforces chromatin silencing[569, 570]. A role for PRC1 in DSB repair is well appreciated; PRC1 is thought to ubiquitinate H2AX as part of a larger ubiquitination cascade which directs repair choice and transcriptional silencing *in cis* to DSBs[571, 572, 573]. However, evidence for direct localization of PRC1 to DSBs is conflicting[574].

As was observed in Chapters 3 and 6, heterochromatin or gene silencing hinders the local DDR. Thus, by modulating heterochromatin, EZH2 and PRC2 are likely to alter radiation sensitivity. Additionally, EZH2 and other PRC2 subunits localize to DSBs[271, 313] and EZH2 may deposit H3K27me3 on DSB-proximal nucleosomes[169]. However, it is unknown whether EZH2 alone localizes to DSBs, whether additional PRC2 proteins are recruited, or what functions auxiliary PRC2 subunits may play in the DDR. It has been shown that blocking EZH2 activity immediately prior to irradiation can delay DSB repair, apparently by blocking NHEJ[575, 576]. However, other reports have ascribed the function of EZH2 to HR[577]. Indeed, H3K36me3 is associated with homologous recombination and H3K36me3 has also been shown to recruit PRC2[556]. It is not fully understood why recruitment of a repressive transcription factor to open, expressed loci would aid in repair given the apparent requirement for chromatin relaxation in the DDR, though a requirement for transcriptional silencing proximal to DSBs is one proposed rationale. Further, multiple interactions of EZH2 with PIKKs and PARPs have been described, adding additional complexity[578, 579]. For example, PARP1 directly modifies EZH2 and diminishes its methyltransferase activity[256].

The SWI/SNF complex, like PRC2, is a highly conserved master gene regulator which generally opposes action of polycomb group proteins in organisms from fly to man[235]. SWI/SNF mediates chromatin opening and gene accessibility by sliding, evicting, or altering nucleosome occupancy around promoters or enhancers[201]. Like PRC2, SWI/SNF is recurrently mutated in cancer. Mutation or loss of one or more SWI/SNF subunits is found in almost a quarter of all cancers[580]. Though a role for SWI/SNF in the DDR has been long appreciated, loss of genome integrity is not thought to be the function of SWI/SNF dysregulation in cancers[581]. However, evidence for involvement of SWI/SNF in the DDR is strong. SWI/SNF subunits localize to sites of DSBs where they are necessary to promote rapid γH2AX phosphorylation[582, 583]. SWI/SNF stimulates acetylation of H3, which, in turn, opens chromatin allowing for rapid recognition of breaks by ATM[205]. Turning to repair pathway choice, SWI/SNF promotes resection initiation via nucleosome removal

and thus stimulates HR[210, 211]. There is some evidence that SWI/SNF may be required for transcriptional silencing around breaks, activity diametric to its canonical function[129]. Interestingly, SMARCA5 may coordinate with PRC1 proteins to affect transcriptional silencing, though mechanistic details are not well understood[208, 584]. Whereas SWI/SNF and PRC proteins are in general antagonistic, with polycomb depositing heterochromatin and SWI/SNF facilitating euchromatin, there has been evidence of SWI/SNF working to repress transcription[585, 586]. Perhaps DSBs may be another situation whereby SWI/SNF and PRC2 cooperate to affect recognition and repair of DSBs.

Turning to clinical opportunities stemming from newly appreciated roles of polycomb and SWI/SNF in the DDR, we note moderate levels of success. Several EZH2 inhibitors have entered the clinic though they have limited efficacy as monotherapy and suffer from pleiotropic effects[587, 588]. Better use has been achieved through combination therapy. EZH2 inhibitors synergize with immunotherapies, and, strikingly, EZH2 inhibition has also been shown to enhance genotoxic therapy including 5-FU, though this is generally ascribed to gene expression effects such as up-regulation of p53 as opposed to direct effects of EZH2 on the DDR[589, 590]. More study is needed to understand how loss of PCR2 activity can be combined with radiotherapy or other DSB inducers. There are few inhibitors available for SWI/SNF proteins, though development of an SMARCA2 selective inhibitor showed anti-proliferative activity in SMARAC4 deficient tumors[591]. More recently, a non-specific BAF inhibitor was shown to synergize with ATR inhibition suggesting that it may work through disruption of the DDR[592]. Here we explore the mechanistic basis by which SWI/SNF and PRC2 promote DSB recognition and suggest novel cooperativity between these two complexes.

7.2 RESULTS

7.2.1 Inhibition of H3K27 tri-Methylation Attenuates DSB Recognition and Repair

Although H3K27 trimethylation is most often associated with transcriptional repression, heterochromatin formation, and maintenance of gene repression[124, 593]. Increased H3K27me3 mediated by the PRC2 catalytic subunit EZH2 has also been implicated in DSB detection and NHEJ repair[313, 430]. Demethylation of H3K27 by the jumonji-domain demethylases JMJD2 and JMJD3 (also called KDM4A and KDM6B, respectively) opposes this mechanism[594, 595]. In Chapter 6, we observed an increase in H3K27me3 coincident with loci which rapidly accrete γH2AX following IR insult. Toward establishing functional significance of H3K27 methylation in DSB recognition and repair, we acutely exposed MCF7 cells to inhibitors of EZH2 and JMJD2/3 at a concentration tenfold over IC50 to ablate enzyme activity prior to irradiation. As a control, we inhibited PARP1 with the non-trapping inhibitor veliparib, known to delay DSB repair. In our hands, veliparib is known to attenuate deposition of γH2AX producing small, diffuse IRIF which peak in number and intensity 3-6 h PIR. By contrast, under non-perturbed conditions, maximal H2AX phosphorylation is observed 30-90 min PIR with large, well-separated IRIF.

MCF7 cells were acutely treated with the EZH2 inhibitor GSK126 and/or the JMJD2/3 inhibitor GSKJ4, followed by exposure to 6 Gy of IR and allowed to recover for one hour before being fixed and immunostained for γH2AX. We confirmed the expected effects of each inhibitor on H3K27 via immunostaining with an anti-H3K27me3 antibody. Acute treatment with the inhibitors, alone or in combination, decreased γH2AX foci numbers 1 h PIR (Figure 7.1A). Additionally, we observed a reduction in fluorescence intensity of γH2AX foci in cells treated with GSK126 and/or GSKJ4, suggesting that deregulation of H3K27 methylation limits local H2AX phosphorylation (Figure 7.1B). Conversely, treatment with the PARP inhibitor veliparib somewhat increased γH2AX foci number and intensity. The short interval

(15 min or 60 min) between drug treatment and irradiation precludes effects dependent on gene repression or chromatin condensation and instead suggests that H3K27 methylation may be necessary for break recognition, as previously described. Importantly, we propose that H3K27 methylation acts upstream of H2AX phosphorylation[430]. These results are in agreement with data gleaned from whole-genome sequencing of γH2AX following IR insult which show that loci which accumulate γH2AX also increase levels of H3K27me3.

To assess effects of inhibiting EZH2 on radiation sensitivity, cells were treated with GSK126 and/or GSKJ4 for 1 h and exposed to 6 Gy IR, the media was then replaced to relieve epigenetic inhibition, and cell growth was followed for 5 days by time-lapse imaging in an IncuCyte system. Here, drug-specific phenotypes were observed, treating cells with GSKJ4 completely blocked proliferation while GSK126 attenuated recovery from IR (Figure 7.2A). Interestingly, even without IR, treatment with GSKJ4 decreased cell proliferation, possibly suggesting we used a cytotoxic dose. We explore consequences of JMJD2/3 inhibition later in this Chapter. The observed decrease in proliferation suggested that DSBs may not be repaired in the absense of EZH2 activity. Thus, single cell electrophoresis (Comet) assay was performed to assess DSB repair independently from γH2AX foci resolution. At 1 h PIR, we observed an increase in unrepaired DSBs following GSK126 treatment (Figure 7.2B). These breaks persisted 24 h PIR, indicating that EZH2 inhibition leads to unrecognized or irreparable damage and loss of genomic stability.

We next examined γH2AX foci 24 h PIR in combination with 60 min treatment with GSK126, GSKJ4 or a combination. Indeed, exposure to GSKJ4 alone or in combination with GSK126 led to increased persistent γH2AX foci indicative of a failure to wind down damage signaling following end joining (Figure 7.3A). GSK126 treatment alone did not induce persistent γH2AX foci. Persistent DSB signaling has been shown to trigger senescence, even in the absence of DSBs[106, 596]. To assay senescence induction, SA-βgal staining was conducted[596]. Cells were treated as in the IncuCyte experiment and stained for SA-βgal five days PIR. GSKJ4 treatment, alone or in combination with EZH2 inhibition, increased

cellular senescence, in contrast to GSK126 treatment (Figure 7.3B). Thus, H3K27me3 may act at multiple stages during the DDR process. As revealed in Chapter 6, H3K27me3 is deposited near active genes following IR. In order to restore transcription after repair of damage, H3K27me3 must later be removed, likely by JMJD proteins. Inhibition of JMJD proteins may thus prevent restoration of pre-IR transcription and perhaps normal cell-cycling. Both of these phenomena, along with persistent IRIF, have been associated with senescence[483, 597, 598].

Toward confirming a local effect of H3K27 methylation at DSBs, we examined colocalization of H3K27me3 and γH2AX after irradiation. Conventional immunofluorescence analysis at 1 h PIR revealed punctate domains of increased H3K27me3 immunoreactivity along with significant overlap between H3K27me3 and γH2AX (Figure 7.4). Li's ICA method[495] revealed diminished colocalization of H3K27me3 and γH2AX after treatment with GSKJ4 or GSK126, as compared to vehicle treatment, or addition of the PARP inhibitor veliparib (Figure 7.4). Taken together, these data suggest that H3K27me3 is deposited at DSB loci and histone modifications may delineate a domain surrounding DSBs to promote detection, signaling and repair. These data underscore similar observations made at the genome level in Chapter 3.

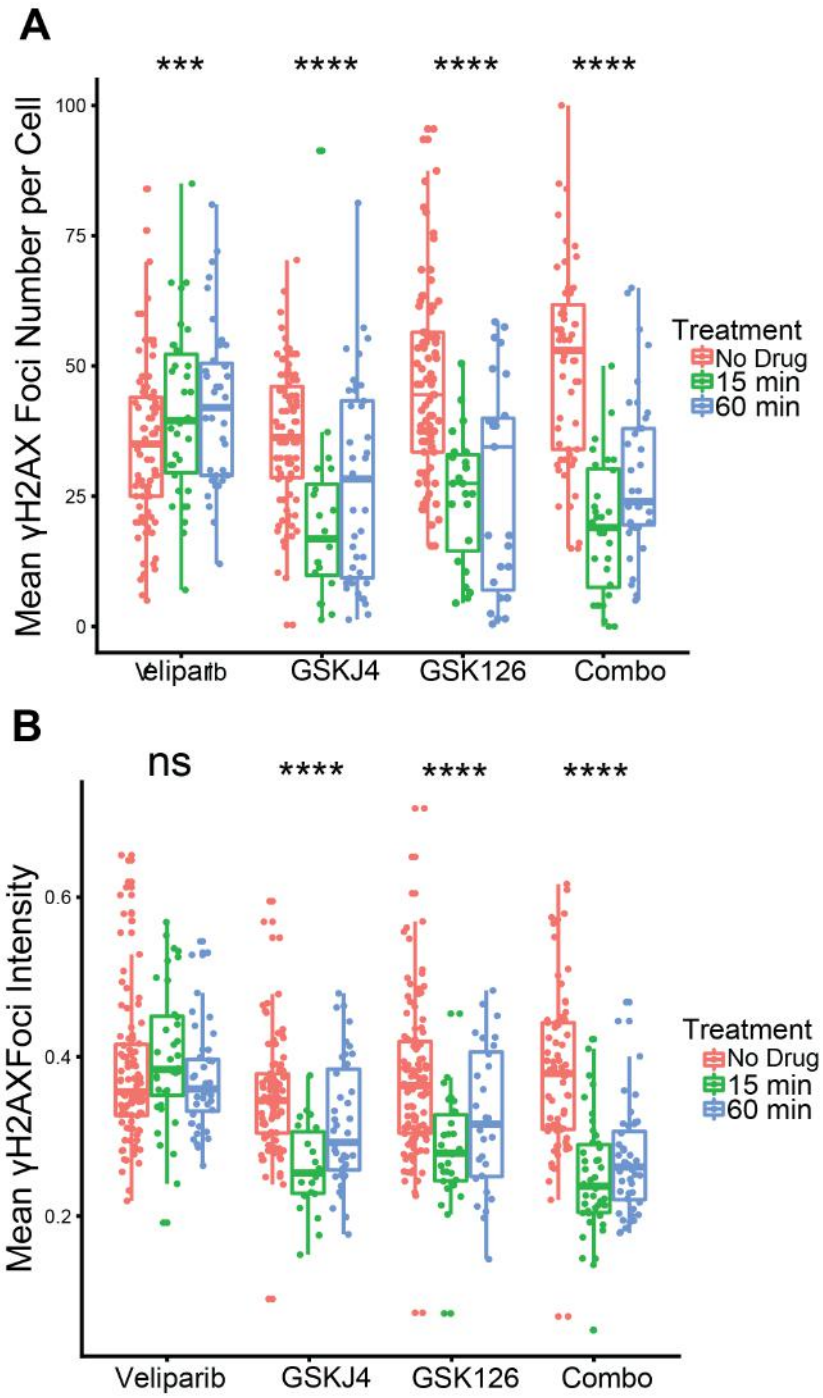

Figure 7.1: **A** Mean number of γH2AX foci after drug treatment. Foci counting was performed by a custom ImageJ macro. Drugs were added for the indicated length of time prior to dosing with 6 Gy of IR. Cells were fixed and stained 1 h PIR. Combo refers to a mixture of both GSK126 and GSKJ4 at their original concentrations. Significance was determined by a one-way Kruskall-Wallace test performed within each treatment group. Significance values are as follows: ns $p>0.05$; * $p<0.05$; ** $p<0.01$; *** $p<0.001$; **** $p<0.0001$. **B** Plot as in A but showing the mean γH2AX foci intensity. Foci intensity analysis was performed by a custom ImageJ macro. Three biological replicates were collected.

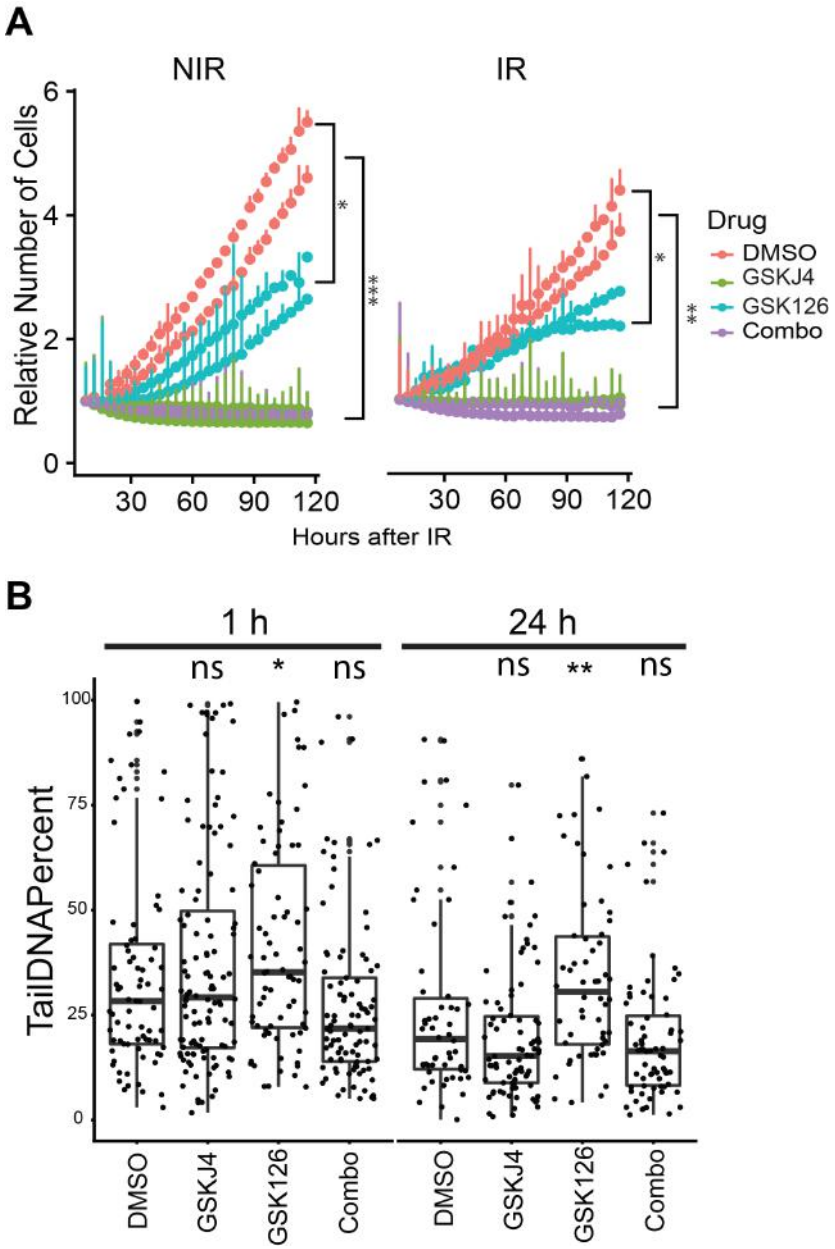

Figure 7.2: **A**Incucyte growth curves of drug treated cells. Cells were treated for 60 min with the indicated inhibitor and then exposed to IR or mock irradiated (NIR). Cell number was tracked for 120 h in an Incucyte system. The mean normalized number of cells is plotted, and error bars denote SEM for 3 replicates. Significance was determined by Dunnett's Multiple Comparisons Test against DMSO treatment. **B** Comet assay results of cells treated as in panel b and assayed either 1 or 24 h PIR. Plotted is the Tail DNA percent as reported by the ImageJ plugin OpenComet. Significance was determined by a Wilcox test against DMSO treatment. Significance values are as follows: ns $p>0.05$; * $p<0.05$; ** $p<0.01$; by Wilcox test against DMSO treatment.

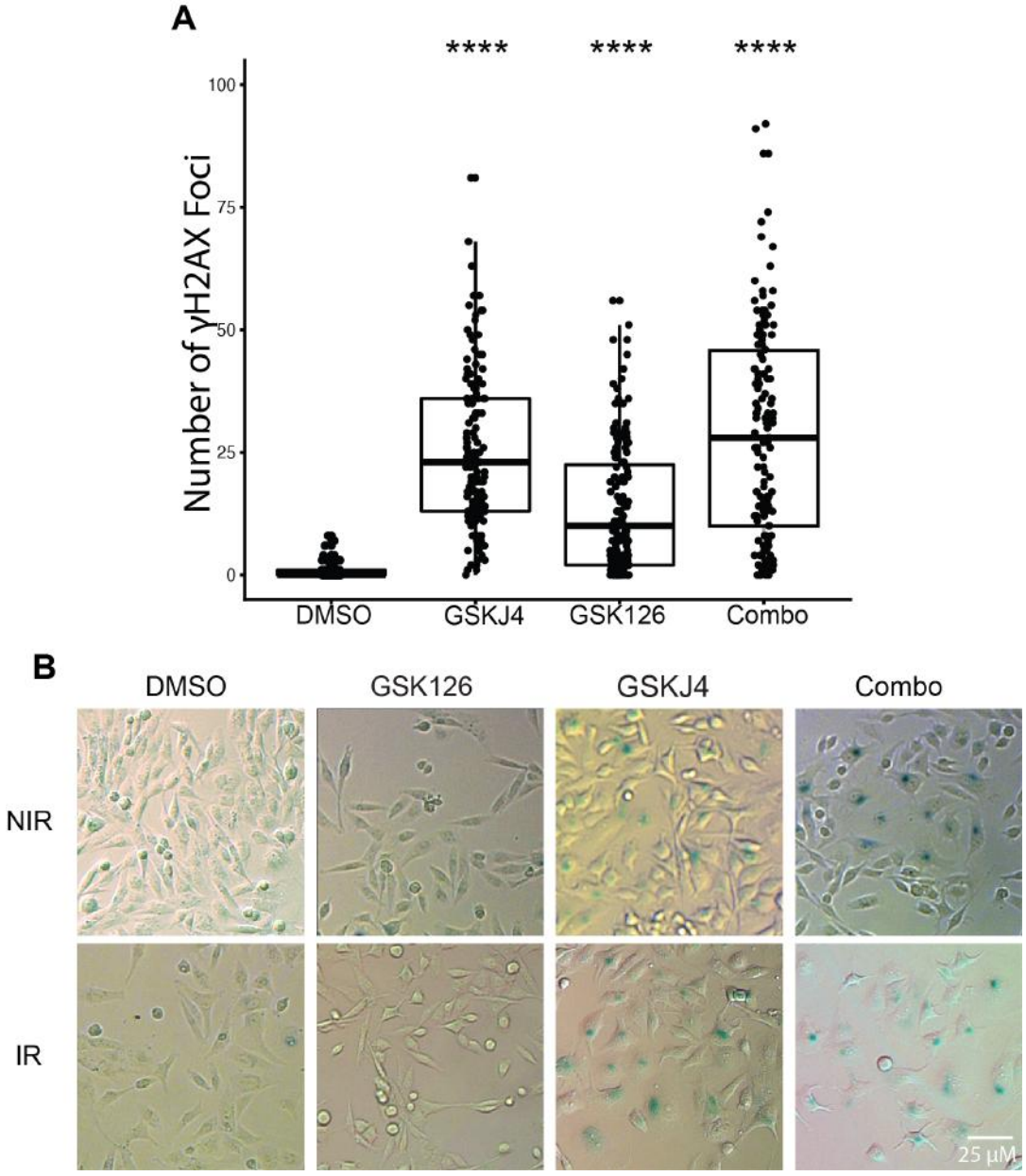

Figure 7.3: **A** Mean number of γH2AX foci 24 h PIR. Foci counting was performed by a custom ImageJ macro. Cells were fixed and stained 1 h after IR. Combo refers to a mixture of both EZH2i and JMJDi at their original concentrations. Significance was determined by a one-way Kruskall-Wallace test performed within each treatment group. **B** SA-Gal staining of cells treated for 1 h with the indicated drugs prior to IR insult and allowed to recover for 72 h before fixation and staining. A representative image, selected from three replicates, is shown for each treatment. Significance values are as follows: **** $p<0.0001$ by WIlcox test against DMSO treatment.

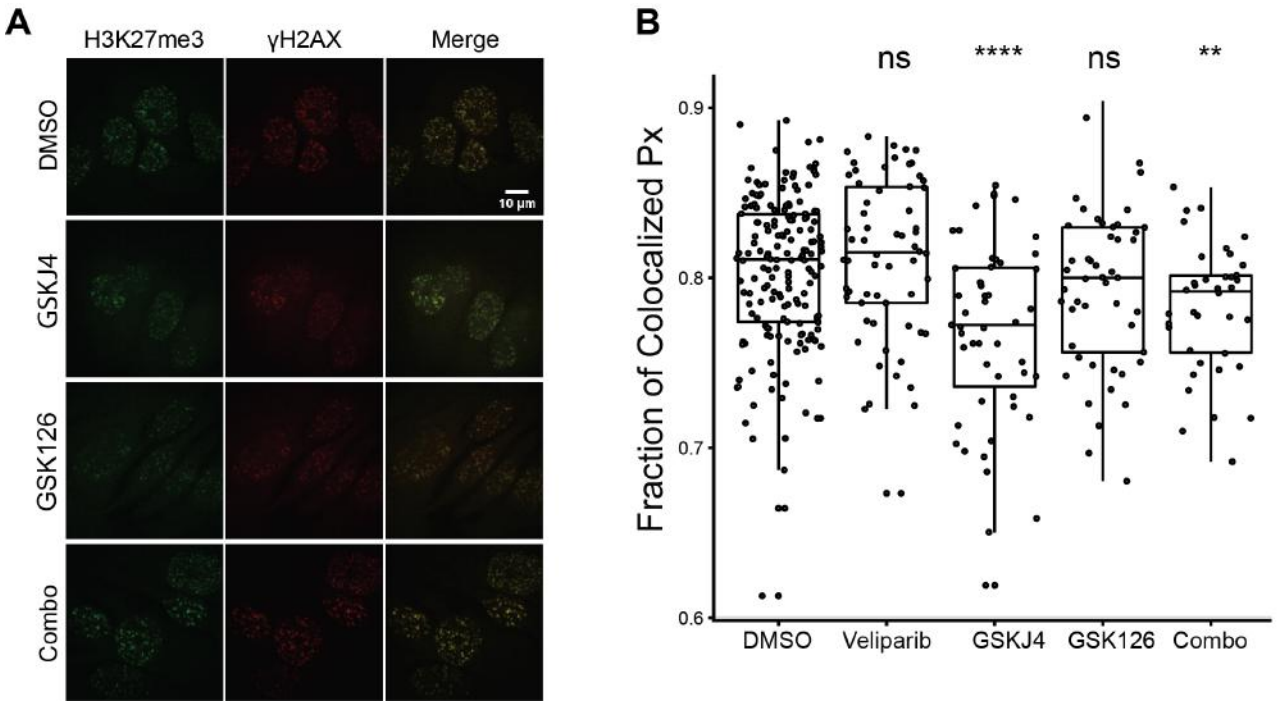

Figure 7.4: **A** Immunofluorescence images of irradiated MCF7 cells. Cells were treated with the indicated drugs for 60 min prior to dosing with 6 Gy. Cells were fixed and stained 1 h PIR. Images were acquired using a 40 X oil objective on a spinning-disk confocal microscope. A representative image is shown from 3 replicates. **B** Quantification of colocalization between γH2AX and H3K27me3 staining in the slides shown in A. The fraction of colocalized pixels was calculated per nucleus using Li's ICA method. Significance was determined by a Wilcox Test against DMSO treatment. ** $p<0.01$; *** $p<0.001$.

7.2.2 The SWI/SNF Complex is Necessary for Rapid Repair of DSBs

Having established a roll for EZH2 in the DDR, we next investigated whether SWI/SNF proteins play an analogous or an oppositional role. SWI/SNF canonically opposes the activity of polycomb group proteins and opens chromatin to mediate gene activation. Thus, we naively expected that inhibition or loss of SMARCA4 (the core subunit of SWI/SNF) might evince a pro-γH2AX phenotype similar to that seen by JMJD2/3 inhibition. Here, we made use of a PROTAC drug, ACBI1, to specifically degrade the SWI/SNF subunits SMARCA4 and SMARCA2[599]. To elucidate the mechanism by which SMARAC4 promotes the DDR we performed γH2AX and TUDEL imaging of cells exposed to 6 Gy of IR in presence or absence of ACBI1. Againnst expecttaions, we observed a decrease in γH2AX foci number in PROTAC treated cells at both 15 min and 60 min PIR (Figure 7.5A). TUDEL staining showed that PROTAC treatment attenuated rapid repair of DSBs, indicating a role for SMARCA4 in early repair of DSBs (Figure 7.5B). Notably, JMJD2/3 inhibition also conferred unrepaired DSBs, suggesting that unrestrained action of polycomb proteins at DSBs may hinder repair. In line with reduced γH2AX phosphorylation and diminished repair of DSBs, ATM foci were also decreased in SMARCA4 deficient cells (Figure 7.6A). Loss of SMARCA4 also decreased 53BP1 IRIF. 53BP1 is a canonical NHEJ factor thus these data provide a rationale for loss of rapid repair in a SMARCA4 deficient setting (Figure 7.6B). These data are consistent with proteomics data in Chapter 5 which suggest that upon ACBI1 treatment, recruitment of myriad DDR factors to DSBs is diminished.

The SWI/SNF complex is a well-established chromatin remodeler which generally removes histones to increase chromatin accessibility[201, 581]. Further, eviction of histones is thought to be necessary for resection surrounding break sites in yeast[600]. Toward a mechanistic basis by which SWI/SNF may influence recognition of DNA damage, we assessed chromatin density. Using FLIM imaging, we measured the density of DNA at DSBs (marked by TUDEL) or IRIF (marked by γH2AX) with and without ACBI1 treatment[601, 602]. FLIM imaging reports on chromatin density by measuring florescence lifetimes of DAPI

molecules— longer lifetimes equate to less dense chromatin. Nuclei were divided into 4 regions depending on the presence or absence of the two factors assessed. TUDEL-only chromatin represents unrecognized breaks, loci co-occupied by both γH2AX and TUDEL are recognized breaks, and γH2AX-only areas are locations where break repair has occurred, but IRIF have not yet resolved; the bulk of nuclear area is occupied by neither factor, and represents undamaged DNA (Figure 7.7). TUDEL-labeled chromatin was observed to be less dense than TUDEL-free DNA, suggesting either that breaks occur in less dense chromatin, seen in Chapter 3, or that breaks precipitate chromatin de-condensation, as reported[272**?** , 603]. γH2AX deposition does not significantly change the underlying chromatin density, suggesting that epigenetic changes occur upstream of ATM. In SMARCA4-deficient cells, we observed global condensation of chromatin irrespective of TUDEL or γH2AX staining. Further, TUDEL positive DNA was no longer less dense than un-broken chromatin suggesting a deficiency in the epigenetic DSB response. Thus, the DDR attenuation induced by ACBI1 may be due to both global chromatin condensation and a deficit of SWI/SNF chromatin remodelers at break loci. These data are interesting when viewed in conjunction with our observation that heterochromatin is resistant to γH2AX deposition and that transcription, frequently mediated by SWI/SNF proteins, may be necessary for DSB recognition.

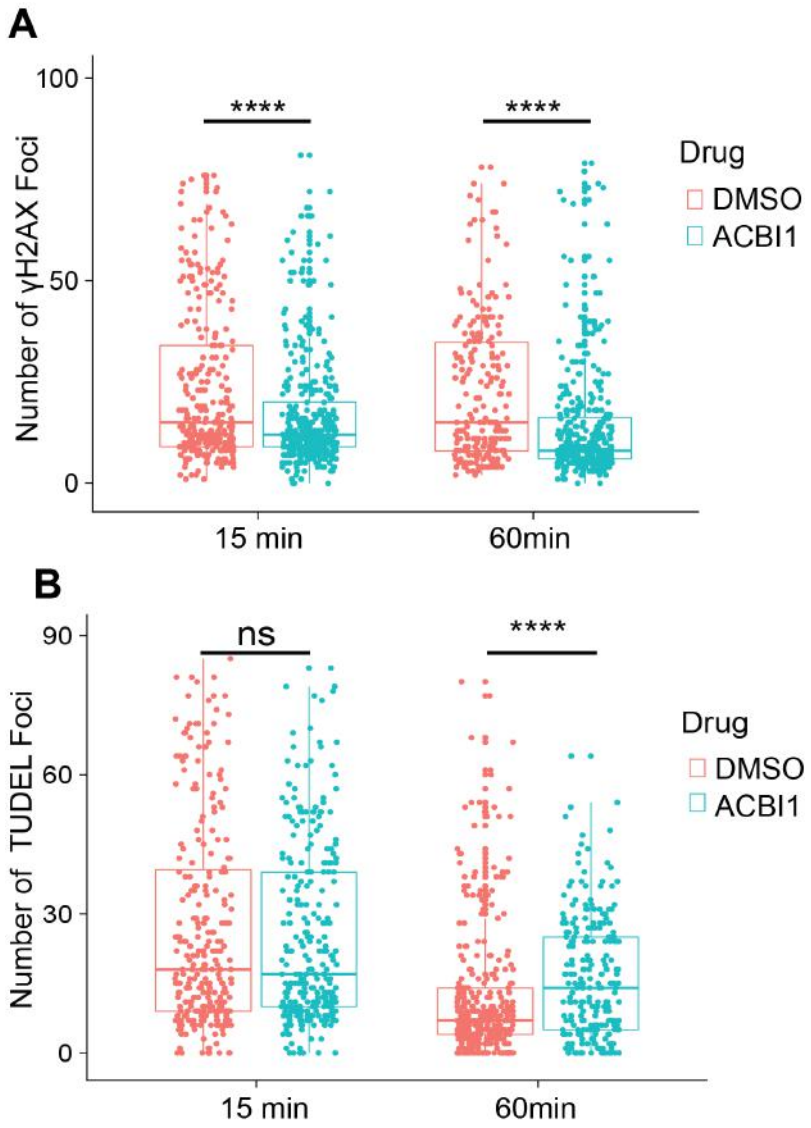

Figure 7.5: **A** Mean number of γH2AX foci after ACBI1 treatment. Foci counting was performed by a custom ImageJ macro. ACBI1 was added 18 h prior to dosing with 6 Gy of IR. Cells were fixed and stained 15 min or 60 min PIR. Significance was determined by a Wilcox test comparing DMSO to ACBI1 treatment. Significance values are as follows: ns $p>0.05$; **** $p<0.0001$. **B** Mean number of TUDEL foci after ACBI1 treatment. Foci counting was performed by a custom ImageJ macro. ACBI1 was added 18 h prior to dosing with 6Gy of IR. Cells were fixed and stained 15 min or 60 min after IR. Significance was determined by a Wilcox test comparing DMSO to ACBI1 treatment. Significance values are as follows: ns $p>0.05$; **** $p<0.0001$.

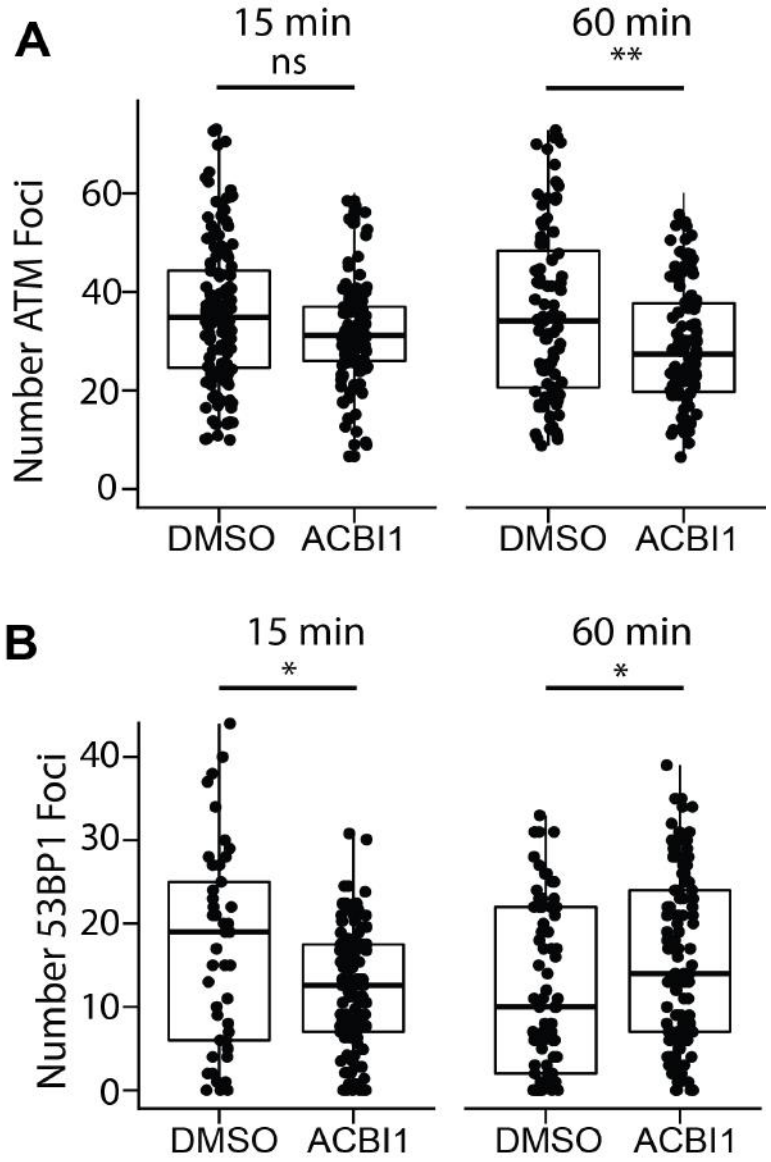

Figure 7.6: **A** Mean number of ATM foci after ACBI1 treatment. Foci counting was performed by a custom ImageJ macro. ACBI1 was added 18 h prior to dosing with 6Gy of IR. Cells were fixed and stained 15 min or 60 min PIR. Significance was determined by a Wilcox test comparing DMSO to ACBI1 treatment. Significance values are as follows: ns $p>0.05$; ** $p<0.01$. **B** Mean number of 53BP1 foci after ACBI1 treatment. Foci counting was performed by a custom ImageJ macro. ACBI1 was added 18 h prior to dosing with 6Gy of IR. Cells were fixed and stained 15 min or 60 min PIR. Significance was determined by a Wilcox test comparing DMSO to ACBI1 treatment. Significance values are as follows: ns $p>0.05$; * $p<0.05$.

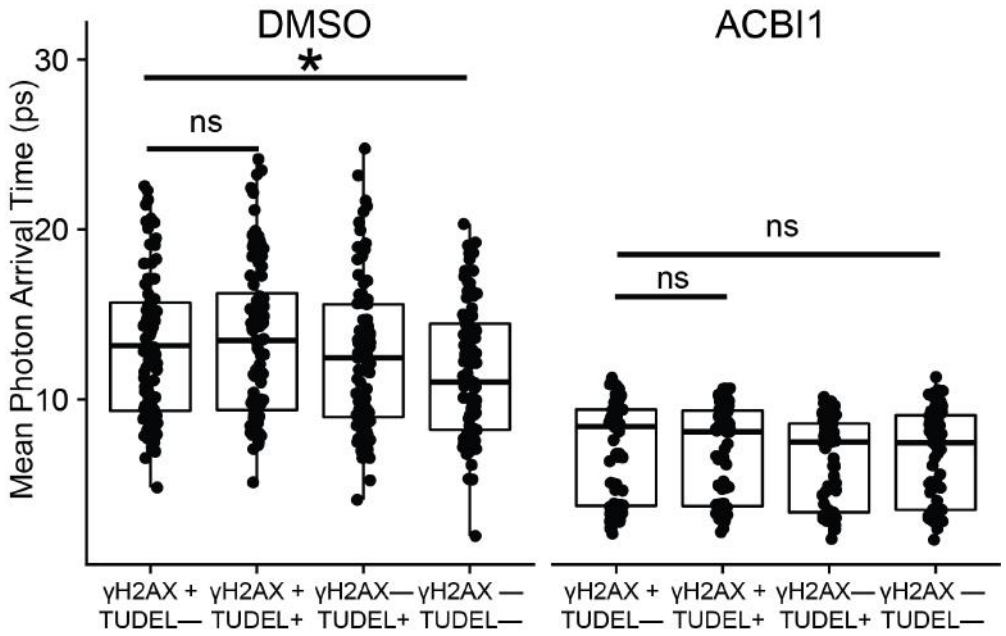

Figure 7.7: **A** FLIM density imaging of chromatin as measured by DAPI in cells treated with the SMARCA2/4 PROTAC ACBI1. Nuclei were divided into 4 regions depending on the presence or absence of the two factors assessed. TUDEL-only chromatin represents unrecognized breaks, loci co-occupied by both γH2AX and TUDEL are recognized breaks, and γH2AX only areas are locations where break repair has occurred, but IRIF have not yet resolved; the bulk of nuclear area is occupied by neither factor, and represents undamaged DNA. Significance was determined by a one-way Kruskall-Wallace test performed between the indicated groups. Significance values are as follows: ns $p>0.05$; * $p<0.05$.

7.2.3 SWI/SNF and PRC2 Cooperate to Affect DSB Transcriptional Repression Near Euchromatic DSBs

We reasoned that in addition to precipitating changes in chromatin density at damaged loci, SWI/SNF may also change the local compliment of histone isoforms to favor repair. The SWI/SNF complex is a nucleosome remodeler which can reposition or evict whole nucleosomes to affect chromatin accessibility and gene expression. Toward assaying the specific histones which may be added or removed at DSBs by SWI/SNF, we imaged γH2AX IRIF in conjunction with histone H2, Histone H3 and the repressive mark H3M27me3, a known epigenetic mediator of the DDR[313]. Addition of the SMARCA 2/4 degrading PROTAC ACBI1 attenuated Histone H2AX density at γH2AX IRIF but did not affect H3 density (Figure 7.8A). Thus, an inability to reposition H2AX containing nucleosomes proximal to DSBs represents a potential mechanism for suppression of γH2AX IRIF in a SMARCA4 deficient setting. Indeed, H2AX is not the most abundant H2 variant in eukaryotic cells suggesting that some breaks may arise in H2AX poor regions necessitating addition of H2AX before ATM can initiate DDR signaling[189].

Turning to Histone H3, we observe no differences with respect to ACBI1 treatment. In contrast to total Histone H3, H3K27me3 levels at γH2AX IRIF were depressed in a SMARCA4 deficient setting (Figure 7.8A). Thus, we examined the H3K27 tri-methylase EZH2, a component of the polycomb complex PRC2. SMARCA4 loss attenuated EZH2 levels both at γH2AX foci and in nuclei overall (Figure 7.8B). In eukaryotes, gene expression programs are in large part dictated by the opposing activities of polycomb and SWI/SNF complexes: polycomb represses genes and closes chromatin while SWI/SNF opposes these actions, decompacting chromatin to permit gene activation[235]. While SWI/SNF and polycomb are canonically in opposition, recent evidence suggests the two complexes sometimes cooperate to affect gene regulation. Moreover, while both PRC2 and SWI/SNF factors had been implicated in the DDR, no mechanism explained how these oppositional chromatin modifiers interacted at damaged loci. However, literature suggests that SMARCA4 may

be required for opening DSB proximal chromatin, creating a platform for recruitment of repressive factors including PRC2[129]. Our data suggest that the nucleosome remodeling activities of SWI/SNF are required at DSB loci and surprisingly suggest SWI/SNF activity is necessary for recruitment of the histone methyltransferase EZH2. If SWI/SNF is required to deposit H2AX, then loss of SMARCA4 may lower γH2AX breaking a feedback loop with EZH2.

The above data suggest that SMARCA4 is necessary for proper polycomb activity or localization to DSBs, and that loss of SMARCA4 prevents H3K27me3 deposition at γH2AX IRIF. However, the notion that a modification linked to heterochromatin accumulates at DSBs is difficult to reconcile with widely-reported chromatin decompaction at DSBs[272, 434, 603, 442, 604, 605]. Indeed, we hypothesized that SMARCA4 promotes chromatin relaxation at DSBs. To examine whether DSB-associated H3K27me3 induces chromatin compaction, cells were stained for H3K27me3 and total H3 at 1 h PIR. H3K27me3 foci could be clearly distinguished, most of which did not appear to be associated with structures in the H3 image (Figure 7.9A). Quantitation of the relative intensity of H3K27me3 and H3 staining indicated that H3K27me3 foci did not induce corresponding H3 foci, arguing that H3K37me3 is deposited without concomitant chromatin compaction. We thus hypothesized that nucleosomes proximal to DSBs arising in euchromatin may require H3K27 methylation, perhaps to attenuate local transcription. As a proxy for chromatin openness, the DAPI intensity at γH2AX foci was measured. Foci in areas with low DAPI had higher H3K27me3 levels as compared to foci in DAPI-high regions despite, presumably, a lower density of nucleosomes in these regions (Figure 7.9B). Thus, we concluded that deposition of repressive chromatin marks is necessary for repair of a subset of DSBs arising in euchromatin. Notably, we showed in Chapter 3 that euchromatin harbors a relatively high amount of DSBs underscoring the importance of repairing euchromatic DSBs[381, 518]. Interestingly, loss of SWI/SNF activity resulted in depression of PRC2 at DSBs. Perhaps DSBs are a rare example of cooperation between polycomb and Trithorax family members.

Building on our theory of cooperation between SMARCA4 and EZH2, we next sought to link SMARCA4 to transcriptional repression at breaks, which we have previously associated with EZH2. Recall that in Chapter 5 we observed SMARCA4 dependent enrichment of transcriptional machinery and splicing factors in damaged chromatin. Other work links SMARCA4 to transcription-coupled repair, a subset of the DDR in euchromatin which depends on RNA Polymerase II (Pol II) activity[431]. Toward establishing a role for SMARCA4 in transcriptional response to DSBs, we first examined accumulation of total Pol II at γH2AX IRIF following SMARCA4 depletion. Treatment with ACBI1 conferred an increase in total Pol II occupancy both at γH2AX foci and in the total nucleus (Figure 7.10A). We reasoned that ablation of SMARCA4 may prevent exclusion of Pol II from DSB loci, perhaps by preventing recruitment of PRC2. Indeed inhibition of EZH2 also resulted in decreased Pol II at γH2AX regions, suggesting SWI/SNF and PRC2 may cooperate to prevent transcription through DSB loci(Figure 7.10B). This could indicate that without SMARAC4, cells cannot attenuate transcription *in cis* to damaged loci and transcription-DSB conflicts might contribute to the increase in DNA damage in ACBI1 treated cells.

We then assayed R-Loop formation. R-Loops are trinary structures where newly transcribed RNA base pairs with complimentary DNA creating a DNA:RNA hybrid. While the etiology of R-Loops is unclear, studies associate them with damaged loci and Pol II stalling or backtracking when encountering damage[539]. PROTAC treatment increased R-Loops both genome wide and especially at γH2AX IRIF consistant with a failure to exclude Pol II from damaged DNA (Figure 7.10C). R-Loops are known to attenuate the DDR and must be removed to allow for repair of DSBs and resumption of transcription. In summary, treatment with the SMARCA2/4 PROTAC ACBI1 prevents attenuation of transcription at DSBs, perhaps due to an inability to recruit the repressive chromatin modifier EZH2. Relatedly, that ACBI1 treatment increased chromatin density and diminished Pol II residency globally suggests that transcription is an important element of the DDR.

Finally, we assayed the effect of chemical transcriptional inhibition prior to IR insult

toward elucidating order of function between Pol II, H2AX phosphorylation and epigenetic modification. Recall that in Chapter 6, we observed that inhibition of transcription by flavopiridol phenocopied inhibition of EZH2. Both treatments decreased H3K27me3 and R-Loops at IRIF, suggesting that transcription is necessary for recruitment of PRC2 to damaged DNA (Figure 6.8). Further, we observed that addition of an ATM inhibitor also diminished H3K27me3 accumulation and R-Loop formation at IRIF suggesting a possible feedback loop between EZH2 and ATM. Results in this Chapter suggest that SMARCA4 may also participate in this process perhaps by allowing PRC2 to access damaged DNA. Phosphorylation of H2AX by ATM spreads kilobases away from damage sites, amplifying the upstream signals required to induce the DDR even at single DSBs. To verify crosstalk between H3K27me3 and ATM activity, we assessed whether H3K27me3 might impact γH2AX spreading. Comparing the size of γH2AX foci 1 h PIR in cells treated with the EZH2 inhibitor GSK126 to vehicle treated cells revealed that deregulation of H3K27me3 impacts γH2AX spreading (Figure 7.11). Strikingly, inhibition of the repressive mark H3K27me3 appeared to reduce the spread of γH2AX, suggesting that PRC2 plays a role upstream of PIKKs in promoting signaling. We speculate that PRC2 may function to exclude Pol II from damaged chromatin or participate in degradation of PIC components. These effects may be due to diminished H3K27me3 dependent recruitment of PRC1, a known mediator of the DDR[606]. Thus, local chromatin modification may affect global DDR signaling, and ultimately, response to IR as evidenced by radiosentization induced by EZH2 inhibitors.

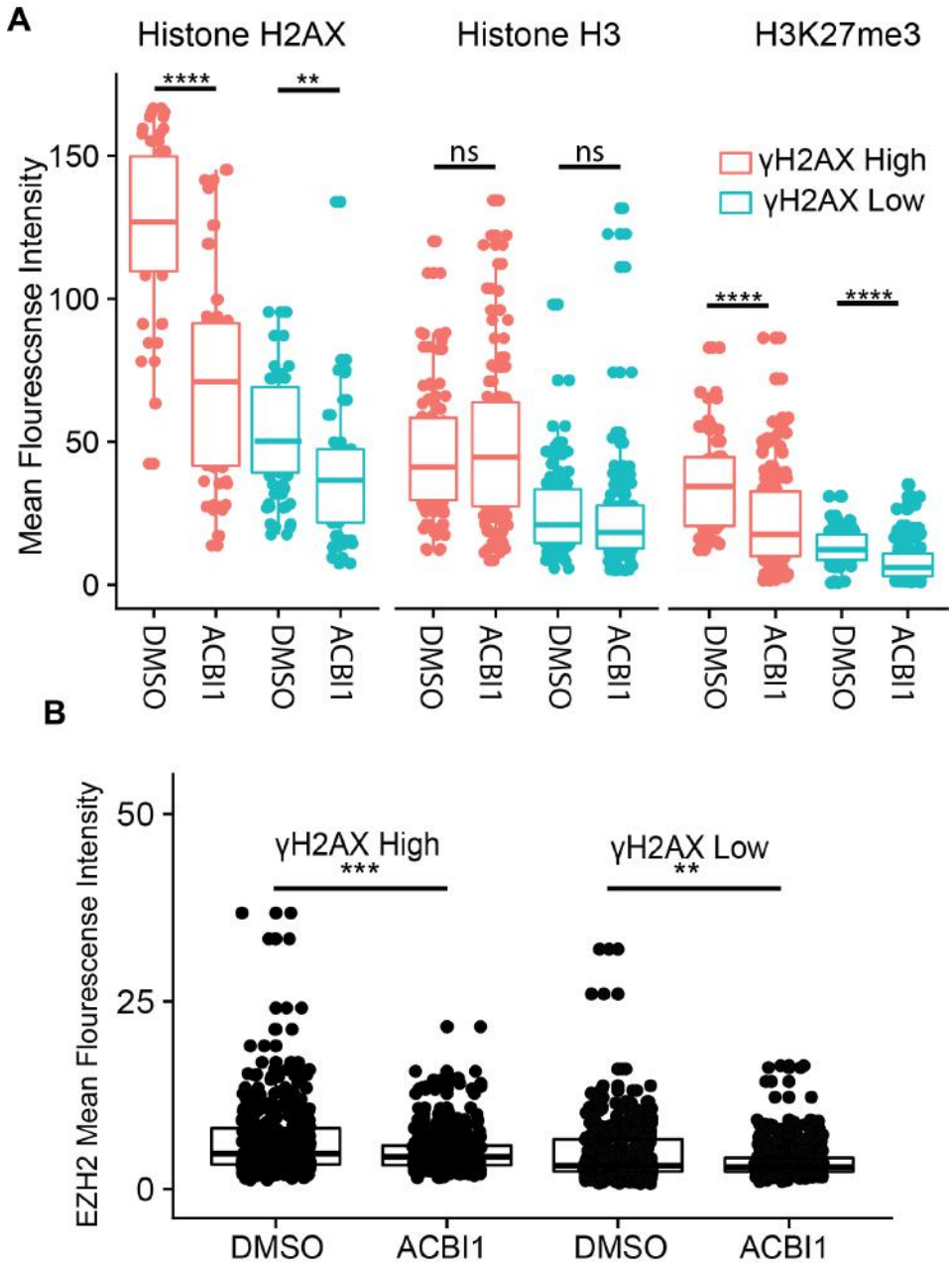

Figure 7.8: **A** Mean fluorescence intensity of the indicated histone or histone PTM within nuclei sub-divided with respect to the average nuclear fluorescence intensity of γH2AX. ACBI1 was added 18 h prior to irradiation. * $p<0.05$, ** $p< 0.01$, *** $p<0.001$, **** $p< 0.0001$, ns $p>0.05$ by Wilcoxon rank sum test comparing MFI between γH2AX high and γH2AX low regions. **B** Mean fluorescence intensity of EZH2 within nuclei sub-divided with respect to the average nuclear fluorescence intensity of γH2AX. ACBI1 was added 18 h prior to irradiation. * $p<0.05$, ** $p< 0.01$, *** $p<0.001$, **** $p< 0.0001$, ns $p>0.05$ by Wilcoxon rank sum test comparing MFI between γH2AX high and γH2AX low regions.

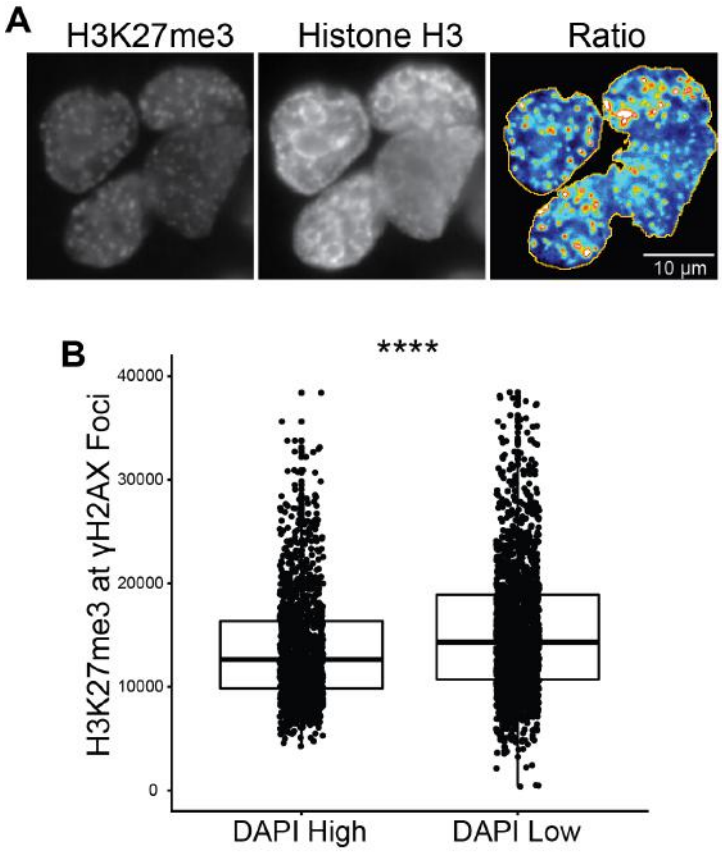

Figure 7.9: **A** Ratio-based imaging of irradiated MCF7 cells. Cells were fixed 1 h PIR and imaged using a 40 X oil objective on a spinning-disk confocal microscope. Ratios between channels were calculated in ImageJ by dividing image intensities and then the resulting image was thresholded and pseudo-colored to highlight differences in H3K27me3:H3 ratio. A representative image is shown. **B** Mean fluorescence intensity of H3K27Me3 at γH2AX foci after GSK126 treatment. Drugs were added for 1 h prior to IR. Cells were fixed and stained 1 h PIR. Foci intensity analysis was performed by a custom ImageJ macro. γH2AX foci thresholded and the MFI within foci areas in the H3K27me3 channel was recorded. Subsequently, data was divided with respect to the DAPI intensity within foci area. DAPI-High indicated foci with a DAPI intensity greater than the cell-wide mean. Significance was determined by a Wilcox Test against DMSO treatment. Significance values are as follows: ns $p>0.05$; * $p<0.05$; ** $p<0.01$; *** $p<0.001$; **** $p<0.0001$.

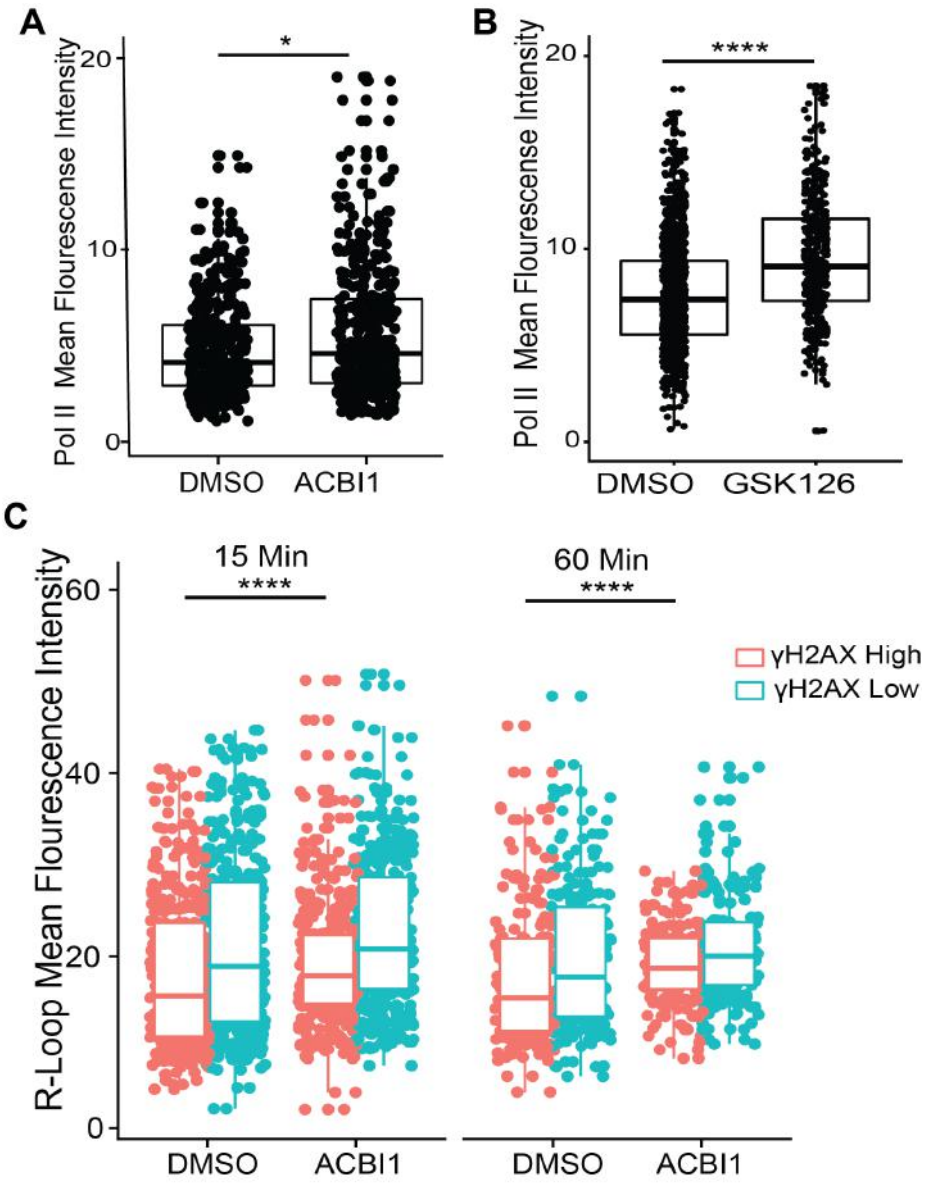

Figure 7.10: **A** Mean fluorescence intensity of total Pol II as measured by an N-terminal directed antibody within nuclei 1 h PIR. ACBI1 was added overnight prior to irradiation. **B** Mean fluorescence intensity of total Pol II as measured by an N-terminal directed antibody within nuclei 1 h PIR. GSK126 was added 1 h prior to irradiation. **C** Mean fluorescence intensity of R-Loops as measured by the S9.6 antibody within nuclei sub-divided with respect to the average nuclear fluorescence intensity of γH2AX. ACBI1 was added overnight prior to irradiation. * $p<0.05$, ** $p< 0.01$, *** $p<0.001$, **** $p< 0.0001$, ns $p>0.05$ by Wilcoxon rank sum test comparing MFI between γH2AX-high and γH2AX-low regions.

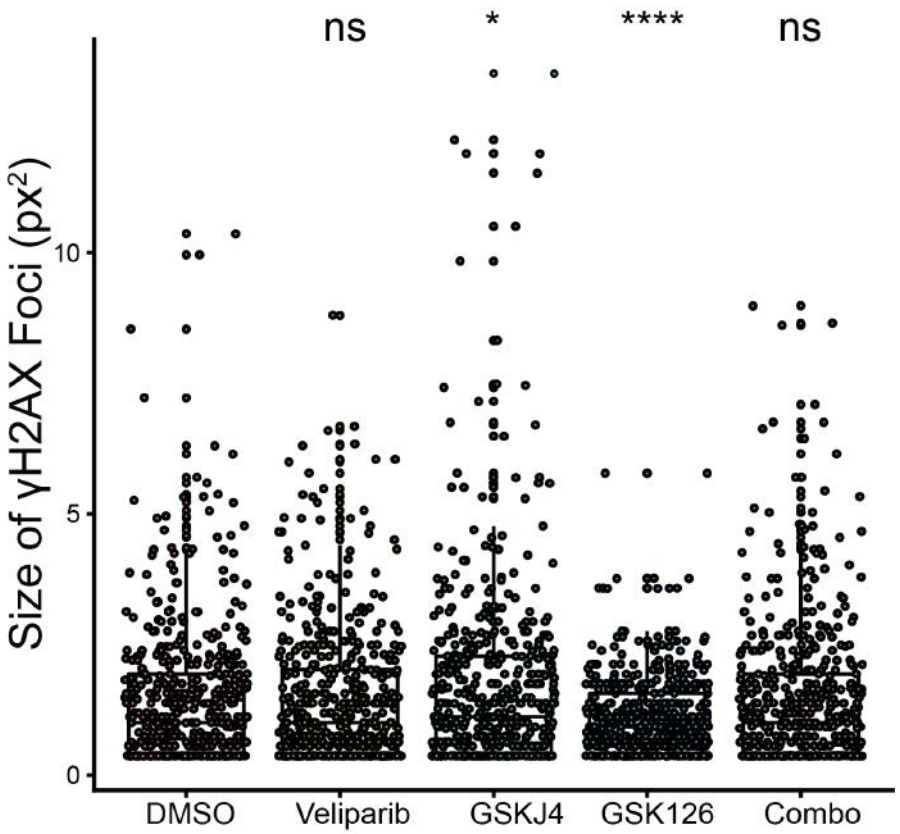

Figure 7.11: **A** Plot of the size of γH2AX foci in drug-treated MCF7 cells. Cells were treated with the indicated drugs for 60 minutes prior to dosing with 6 Gy. Cells were fixed and stained 1 h after IR. Images were acquired using a 40 X oil objective on a spinning-disk confocal microscope. Size of individual γH2AX foci were determined using a custom ImageJ macro. Significance was determined by a Wilcox Test against DMSO treatment. Significance values are as follows: ns $p>0.05$; * $p<0.05$; ** $p<0.01$; *** $p<0.001$; **** $p<0.0001$.

7.3 DISCUSSION

Here we conclude our analysis of post-IR changes in the epigenome by exploring the mechanisms behind regulation of H3K27me3 at breaks. H3K27me3 was initially observed to be depleted in regions of the genome which accumulate DNA damage, as most DNA damage is contained in euchromatin. However, we also confirmed using both MRM targeted proteomics and post-IR CUT&RUN sequencing of H3K27me3, that this mark was enriched following IR and deposition of H3K27me3 was greatest in euchromatin, coincident with γH2AX induction (Figure 7.12). We are not the first to suggest that H3K27 methylation impacts repair of DNA damage; others have presented conflicting evidence as to whether H3K27me3 or its writer, PRC2, are localized to DSBs[267, 313, 271]. In our hands, EZH2 and H3K27me3 are functional parts of the DDR. Inhibition of the methyltransferase EZH2 or the opposing demethylase, JMJD2, sensitized cells to radiation via distinct mechanisms. Blocking H3K27me3 deposition delayed break repair, while inhibiting the removal of K27 methylation precluded attenuation of DDR signaling. Thus, inhibitors of H3K27 methylation are putative radiosensitizers warranting further study, perhaps in an *in vivo* setting.

Towards a mechanism for H3K27 methylation in the DDR, we examined γH2AX foci establishment in the presence of H3K27 methylation inhibitors. Inhibition of either EZH2 or its counterpart JMJD2 attenuated γH2AX foci number and intensity shortly after IR insult. These data place histone modification upstream of DSB recognition by ATM, a key mediator of downstream DDR signaling responsible for H2AX phosphorylation. Previous work hypothesized that PRC2 may function to condense chromatin at DSB loci, in turn, inhibiting transcription across broken DNA. In our hands, we observed DSB loci with excess H3K27me3 without a concomitant increase in H3. Thus, at early time points, DSB-proximal chromatin compaction does not occur despite deposition of repressive marks. Further, we explore the relationship between EZH2 and the SWI/SNF complex and find that loss of either protein complex attenuates γH2AX. We go on to show that deposition of H3K27me3 near DSBs depends on SWI/SNF activity. This relationship goes some way to explaining

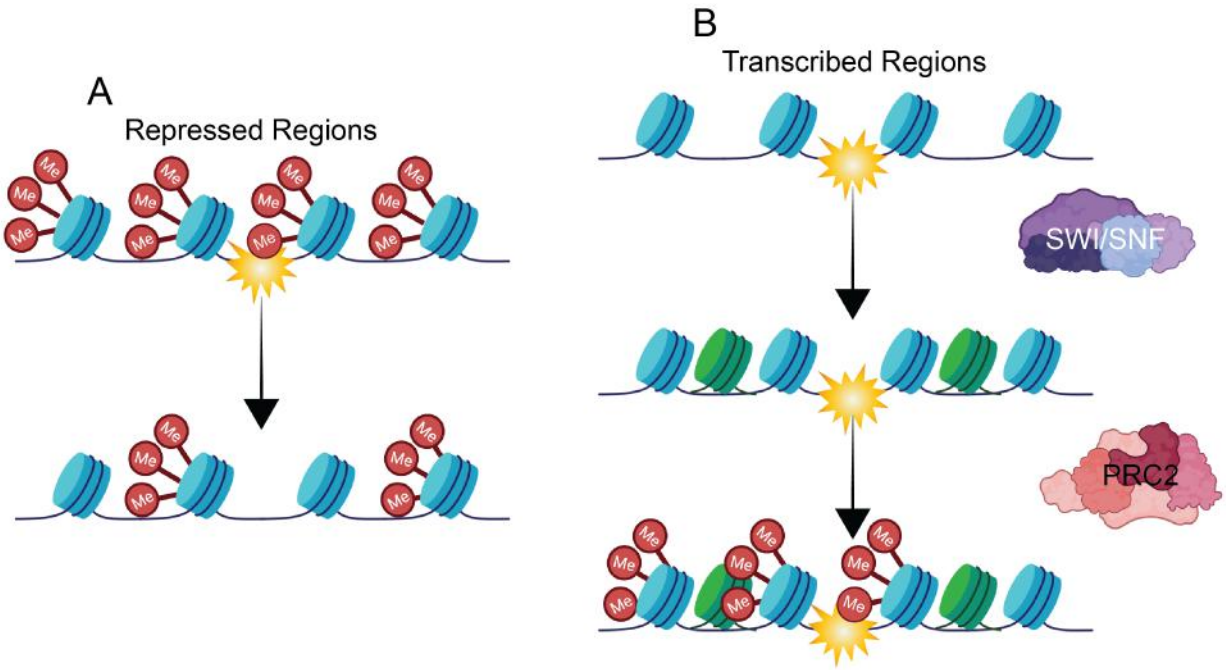

Figure 7.12: **A** Repressed regions, high in basal H3K27me3, are refractory to DSB recognition. Histones must be demethylated, perhaps by JMJD2/3 proteins, before breaks are recognized. **B** However, in transcribed regions, we invoke the SWI/SNF complex to increase the local concentration of H2AX (green) thus providing a platform for PRC2 dependent tri-methylation of H3. This cooperativity between SWI/SNF and PRC2 stands in contrast to their canonicaly opposed roles in gene regulation.

how H3K27me3 does not induce chromatin compaction at IRIF. Perhaps SWI/SNF mediates chromatin de-condensation at DSBs even in the presence of EZH2. Further, both EZH2 and SWI/SNF are linked to transcriptional repression near damaged DNA. In our model system, loss of SWI/SNF leads to global chromatin compaction and transcriptional attenuation both of which may contribute to an inability to recognize DSBs via mechanisms outlined in Chapter 6. EZH2 loss reduces R-loops at DSBs but increases Pol II suggesting an inability to attenuate transcription after break recognition. EZH2 transcriptional repression, in turn, mediates ATM recruitment and loss of EZH2 dampens a proposed feedback loop between EZH2 and ATM. Thus we propose that EZH2 functions to attenuate transcription proximal to DSBs. SWI/SNF aids in this process through nucleosome remodeling, increasing DNA accessability, recruitment of PRC2, and/or direct interaction with Pol II to affect transcriptional pausing and recognition of proximal damage.

It is interesting, and indeed apparently paradoxical, that either increased or decreased DSB proximal H3K27me3 levels are sufficient to attenuate γH2AX deposition. However, we note that inhibition of EZH2 or JMJD2 evinced different phenotypes, with only the latter accelerating cellular senescence. Additionally, we posit that our findings could be evidence of a multistep process of histone methylation at DSBs which is separated either kinetically or spatially. For example, it may be that H3K27me3 deposition is necessary for repair, but this methylation must later be removed to restore basal chromatin activity. Failure to restore the basal epigenetic state may prolong DDR signaling and contribute to senescence. Indeed, altering H3K27me3 levels has been shown to induce senescence in the absence of DNA damage[220]. Further, we observe preferential deposition of H3K27me3 in less dense chromatin consistent with our genomic data. Collectively, we posit that distal genomic regions may require distinct repair programs dependent upon their basal epigenetic state. Future studies must address the relationship between preexisting chromatin state and repair pathway. For example, many studies note special repair pathways and activities for heterochromatic regions or telomeric chromatin[385, 440].

Our findings also suggest a more fundamental purpose of highly conserved epigenetic readers and writers including the polycomb family and SWI/SNF (Trithorax). Both SWI/SNF and PRC2 were first identified in flies and are highly conserved even in organisms which lack complex gene expression control[126, 607]. Yet all eukaryotes have DNA repair systems to repair breaks and safeguard genetic information. Therefore, it is likely that the DDR activity of epigenetic modifiers including SWI/SNF and EZH2 does not represent moonlighting, but rather is an essential and ancient subset of their functions. A fuller understanding of how these enzymes function in DSB repair may, in turn, shed light on their roles in transcription. Transcription-coupled repair of DSBs has been postulated, as has transcriptional damage to DNA[330, 608]. This study reframes these concepts by suggesting transcription-independent roles for transcriptional machinery in the DDR. Lastly, we uncover new candidates for radiosensitizing drugs and suggest a general strategy of radio-adjuvant use of epigenetic inhibitors.

CHAPTER 8

CONCLUSIONS AND FUTURE DIRECTIONS

8.1 Technical Challenges and Innovations

While the DNA damage response has been extensively studied both from a basic science standpoint and translational angles (in particular cancer therapeutics), much remains unknown about the interplay between chromatin and repair of DNA damage. Repair of damaged DNA is, of course, a chromatin localized event. Given the extensive roles that histone PTMs and other chromatin marks play in regulating replication, transcription, and cell identity it stands to reason that these factors exert influence over recognition and repair of damage. However, we assert that at least three technical challenges have heretofore obviated considered analysis of epigenetic:DDR interplay. First, DNA damage induced by exogenous factors is stochastic. Second, the response to individual breaks is highly heterogeneous even within single nuclei, rendering definitive conclusions regarding the role of putative DSB repair factors challenging. And, finally, current methods are unable to deconvolute the presence of DSBs from the presence of DDR factors. The work presented in this Dissertation goes some way to ameliorating these challenges and offers novel analytical methods which can be further refined and applied in order to glean deeper mechanistic insight into the role of epigenetics in the DNA damage response.

The induction of exogenous DNA damage is stochastic. In particular, low-LET radiation sources induce localized DSBs visualized as punctate intra-nuclear foci[21]. In a mixed population of cells, each genome will receive a slightly different compliment of DSBs induced by random exposure to radioactive particles and 2^{nd} and 3^{rd} order effects such as attack by free radical species or conflicts between damage and transcription or replication. Thus, it was not known whether one could observe genome-wide trends in DSB induction and/or recognition using traditional genome profiling tools such as ChIP-seq[104, 393]. However, we have performed such an experiment and indeed shown that recognition of DNA damage, as

evidenced by γH2AX levels, differs widely across the genome. To profile γH2AX we made use of CUT&RUN sequencing which requires lower cell input than traditional ChIP-seq and also affords higher signal-to noise rations by depleting background signal[405]. Despite its advantages, we recognize that use of CUT&RUN may introduce some biases into our data, most notably a tendency to under-count signal in dense chromatin. While most ChIP-seq experiments profile chromatin elements with defined locations (transcription factors, enhancers), we attempted to profile a randomly localized element and infer relative enrichment between genomic regions. In our hands, traditional peak calling (using MACS2) did not accurately capture variations in ChIP-seq, and we thus turned to alternative analysis methods to probe patterns of γH2AX[408]. Thus, using traditional ChIP-seq to confirm our findings will be an important part of validating our conclusions herein.

We also note that correlations between any two epigenetic marks may be inflated owing confounding effects of the $\sim$66% of the genome, likely constitutive heterochromatin, which contains no histone marks. There are a few explanations for this phenomenon: first, it may be that our observation reflects biological fact and most histones are undecorated. Second, this may reflect challenges with sonicating, precipitating or sequencing dense chromatin which frustrate any sequencing method. Thus, cation should be used when drawing conclusions about genome-wide associations between any histone marks or between histone marks and DSBs and/or γH2AX. In any case, the nature of genome-wide data makes drawing definitive conclusions regarding overlap between epigenetic features challenging and susceptible to false positives. We attempted to ameliorate this by focusing on regions surrounding TSSs which are better studied and amenable to sequencing. Similar relationships between histone marks were observed at TSSs as compared to the whole genome, validating our whole-genome approach. In future examination of a subset of the genome or a particular set of well-studied loci should be used to validate genome-wide conclusions.

Nevertheless, we are confident that our overall conclusions are correct as they are corroborated by imaging studies, including direct measurement of chromatin density using FLIM

microscopy, and confirm other literature[609, 610]. Herein we also introduce new methods which are capable of deconvoluting induction of breaks from break recognition. Given that we have observed differences between induction of DSBs as measured by BLISS and induction of γH2AX measured by CUT&RUN sequencing, we anticipate such methods, principally TUDEL, to be broadly useful and to help answer questions regarding epigenetic order of function at DSBs. These observations were unexpected, and call into conclusion the validity of other work which elides DSBs and IRIF.

Finally, we note that differentiating global from local changes remains a shortcoming of the work presented herein. While we uncovered substantial and long-lasting changes to the epigenome after IR insult via proteomics, we note that many of these changes were small in magnitude. This may reflect substantial changes proximal to a small fraction of the genome which receives damage which are then diluted out by bulk chromatin. Thus we anticipate that more targeted proteomics, perhaps leveraging the TUDEL platform, will enable enrichment of DSB proximal epigenetic alterations. Concomitantly, use of microscopy, including superresolution imaging, will enable validation of DSB proximal histone modifications. While not included in this Dissertation, use of both TUDEL and γH2AX imaging to segregate histone modifications into DSB-associated or recognition-associated groups will be important in elucidating order of function. This has important implications for reevaluating previous studies, discussed below.

8.2 General Takeaways from Epigenetic:DDR Interactions

In this Dissertation, we report on the epi-genomic distribution of DSBs as well as the core DSB marker γH2AX. To our knowledge, we are among the first to employ a comprehensive, modern genomics approach to investigate DSB induction and detection. In summary, induction of DSBs, as measured by BLISS, was not uniform across the genome. Instead, DSB density was higher in open regions, especially transcribed regions or euchromatin. Interestingly, DSBs were also high in repressed regions defined by high levels of H3K27me3, despite

the general assumption that chromatin is condensed at these loci. It is well appreciated that condensed chromatin is refractory to DSBs owing to the ability of histones or other chromatin binding proteins to act as sinks which absorb radiation or free radicals, sparing DNA. Thus our results concerning BLISS were not unexpected, though we feel that the novel analytical methods employed here give new insights into genomic locations of DSBs. It was surprising that DSBs are so readily induced in repressed euchromatin. By examining MNase-seq as a proxy for chromatin density, we inferred that repressed regions have similar accessibility and chromatin density as some transcribed regions, though this was an unexpected finding. Future work should endeavor to better define these repressed regions and delineate between so called 'facultative heterochromatin,' 'constitutive heterochromatin,' and 'repressed' states. In particular, better measurements of chromatin density could be obtained to more closely link DSB induction to chromatin condensation or nucelosome occupancy.

The distribution of γH2AX was highly non-uniform, and, surprisingly, significantly distinct from the distribution of DSBs. γH2AX induction occurs much more rapidly in open, genic chromatin, while heterochromatin, by contrast, attenuates γH2AX deposition. Disparate genomic loci differ in their induction of γH2AX by as much as 100-fold. Further, we identified epigenomic features which are predictive of high γH2AX levels and show that a simple machine learning model can predict patterns of γH2AX induction with high ($\sim$90%) accuracy. In contrast to the stochastic view of DNA damage which is prevalent in the literature, we show that locations of DSB induced markers are predictable, thus confirming the strong influence of chromatin on the DDR. We uncover strong evidence that transcribed genes permit rapid detection of DSBs and γH2AX deposition. By contrast, breaks in repressed regions, sometimes termed facultative heterochromatin, are slow to be detected; γH2AX levels peak 24 h PIR. As mentioned above, approximately 66% of the K562 genome is heterochromatin, though this region accounts for, at most, 45% of DSBs and 60% of γH2AX. It is hard to draw conclusions about heterochromatic breaks from our data: the γH2AX detected in this region may correspond to breaks, though it may also be a false positive signal. More

comprehensive studies could be undertaken to validate DSBs in heterochromatin by measuring accrual of other DSB markers or changes in chromatin density after IR insult. The literature predicts chromatin decondensation is an important prerequisite for repair, though this remains to be validated via genomic approaches.

Further, more work will be required to understand the mechanistic basis of our findings. For example, does presence of a particular histone PTM directly recruit DDR factors, or are many of the observed trends attributable to biophysical factors such as chromatin packing or 3D structure? We look forward to using orthogonal data sets such as Hi-C maps, or measurements of chromatin density to answer these questions. Future efforts will also explore chromatin influences on repair pathway choice. By adding in CUT&RUN datasets which report on DDR factors such as Rad51 and 53BP1, we can examine areas which are differentially repaired, but have the same level of γH2AX. In this way we can begin to deconvolute break induction and initial response to DSBs from repair pathway choice, something lacking in previous studies. We also anticipate measuring more chromatin marks before and after IR insult to validate changes in the epigenome precipitated by the DDR.

Previous efforts which endeavored to link the genomic location of breaks to repair pathways have made use of restriction enzyme-based methods to induce DSBs[536, 611]. However, results herein call into question the appropriateness of restriction enzymes to model exogenous DNA damage. First, we showed that chromatin openness, as measured by DNAse or MNase sequencing, is predictive of γH2AX induction to some degree. Thus, restriction enzymes, which require access to the chromatin in order to cut DNA, likely report on only a subset of possible DNA repair outcomes which occur in open chromatin. Indeed, out of 1211 AsiS1 recognition sequences in the human genome, only 174 or $\sim$15 % were reported to be cut by AsiS1 using the DIVA cell system[169]. This is in contrast to our data which shows that more than 33 % of the genome was enriched for γH2AX following IR insult even at 1 h PIR. Secondly, restriction enzyme cut sites have uniform, regular end chemistries which are not indicative of breaks induced by IR or other chemical break inducers. While it is

not known how end chemistry affects repair pathway choice, we anticipate that RE cutting might skew results to a particular repair outcome. There is also evidence that cells do not recognize restriction enzyme cutting as a DSB, and instead respond using the Fanconi anemia pathway[171]. Lastly, our own analysis shows that restriction enzyme cut sites are not balanced with respect to the epigenome, and that sites reported as cut by AsiSI are biased toward open chromatin. In future, we aim to directly sequence DSB loci using TUDEL which should provide a more unbiased view of DSB induction following IR insult.

Collectively, the above factors cast doubt on one of the more well-known epiegentic:DDR interactions, the proposed influence of H4K20 methylation or acetylation on repair pathway choice[133, 162, 562]. Ostensibly, 53BP1 binds to H4K20me2 while TIP60 competes for binding and acetylates nearby residues to occlude 53BP1. Thus, H4K20 methylation ought to dictate the DDR and higher levels of the modification should correlate with use of NHEJ. Indeed, we find that H4K20 methylation was positively associated with rapid γH2AX induction These findings stand in opposition to previous studies which suggest that NHEJ in open chromatin is highly inefficient due to a low level of H4K20me2, which shunts DSBs to homologous recombination. Our finding that γH2AX is rapidly deposited in open chromatin regions suggests use of NHEJ at these loci. Indeed, most open chromatin regions had reduced their γH2AX levels by 24 h PIR. The wide-spread use of NHEJ is also in line with kinetic models of DSB repair and intuition suggesting cells ought not to delay repair of damaged loci. Our data suggest that most markers of open chromatin— indeed all histone marks aside from H3K9me3 and H3K27me3— are associated with rapid repair, and likely NHEJ. By extension, repressive marks are associated with HR, in contrast to previous models of repair. However functional studies remain to be carried out, and whether euchromatin is preferentially repaired by HR remains a paradox which is not resolved by our data. However, given that we observe changes in histone marks including changes to the H4 tail following IR insult by proteomics, it may be the case that patterns in H4 methylation or acetylation shift after IR. While we are not aware of any studies which measure changes in H4 acetyla-

tion or methylation following IR insult, we anticipate that future work assaying changes in H4 modifications will be important in establishing the link between these modifications and repair pathway choice.

In general, our data offer an important opportunity to separate bona fide DDR associated PTMs from chance correlations. In particular, associations between markers of open chromatin and DSBs may not be functionally significant, but instead are a byproduct of rapid DSB recognition in euchromatin. We anticipate that some feature of euchromatin is necessary for rapid γH2AX deposition but posit that it may be chromatin decompaction or the presence of Pol II rather than a specific histone PTM (see below). We suggest that in order to establish a PTM as associated with the DDR at least three criteria must be met. First, inhibition of the associated histone modifier must affect DSB recognition or repair. Second, levels of the histone PTM must change after IR insult. And third, changes in the histone PTM must be coincident with γH2AX peaks in sequencing data. Based on our data, we feel that only EZH2/PRC2 (H3K27Me3) meets this bar, though we anticipate assaying other putative DDR factors in a similar manner including Dot1L (H3K79me2) and Tip60 (H4K20Ac).

Another general lesson regarding DSB recognition and repair we can take from these studies is the value of kinetics data, especially short-term kinetics, in appreciating the scope of the DNA damage response. From proteomic measurements, we see fundamental alterations to the epigenome appear within 1 h after IR insult and persist beyond 48 h PIR. Thus, cellular response to IR is both more rapid and longer lasting than most appreciate. On the rapid kinetics side, which we focus on in most of the above work, we observe that inhibiting epigenetic modifiers affects γH2AX deposition which suggests that changes to the epigenome are exceptionally rapid (on the min^{-1} timescale). In terms of longer time scales, we observed epigenetic changes persisting beyond 48 h PIR and likewise detect γH2AX deposition in new regions at 24 h PIR. It is thus likely that breaks persists beyond 24 h even in normal, maximally efficient DDR. Previously, DSBs or IRIF visible at 24 h were

considered problematic or indicative of failure to recognize or repair DSBs. However, these models assumed that IRIF visible at 24 h PIR were detected rapidly and persisted. By contrast, we propose that IRIF visible at 24 h PIR may be newly formed, and thus are not necessarily indicative of a failure to repair DSBs or resolve the local DDR. The fate of these lately detected breaks is unclear and will require studies which measure γH2AX beyond 24 h PIR. We propose that resolution of these breaks may be coupled to replication which decompacts chromatin and may allow for detection of damage. Replication-DSB conflicts are well appreciated but generally considered a failure of DSB detection and repair. Our data raise the possibility that replication associated repair has a substantial role in the normal DDR, though this would seem to be a high-risk situation for cells.

On the other hand, TUDEL staining offers us a potential clue as to the rapidity of damage repair efforts. We observe loss of TUDEL signal prior to 1 h PIR, suggesting more intensive examination of early time points is needed. At short time scales, TUDEL stains nuclei intensely, yielding an almost-pan nuclear signal at times. Furthermore, extra nuclear signal, perhaps from damaged mitochondria is sometimes observed. We appreciate that such observations could represent artifacts of the TUDEL system, however we cannot rule out the possibility that TUDEL allows observation of extensive rapid DDR activity. Indeed, a reduction of TUDEL signal by 1 h PIR is repeatedly observed, suggesting a large portion of DDR activity occurs within that time frame. Rapid end-joining (NHEJ) likely accounts for this repair, in addition to repair of SSBs or other base damage which may be recognized by TUDEL. This form of rapid repair has been previously described and associated with transcribed areas as well as with the chromatin remodeler SWI/SNF[582]. Consistent with such data, loss of SWI/SNF results in increased TUDEL staining and diminished γH2AX even 20 min PIR. Perhaps this rapid repair represents a somewhat unique variant of the NHEJ pathway which can facilitate simple repair of non-damaged ends or ends held in close proximity by chromatin or other factors. We suggest that very rapid repair remains an understudied and underappreciated part of the DDR. Future efforts could concentrate on

short timescales in order to better capture the full extent of break repair; we anticipate direct labeling techniques such as TUDEL being a useful part of these efforts.

Relatedly, the literature remains divided as to how widespread end joining is. While multiple lines of evidence suggest HR promoting pathways in both euchromatin and heterochromatin, there are few pathways or factors promoting end joining. Thus, end joining may be considered the default repair pathway, consistent with it being highly utilized. Indeed, using DIVA cells Clouaire et al. showed that even cut sites which recruited Rad51, and were deemed HR-prone, still accumulated XRCC4 and Ligase 4, two key NHJE factors[169]. The binding of both NHEJ and HR factors to DSB loci is borne out by image analysis which consistently shows colocalization of factors in different repair pathways[428, 612]. Different cells within an image field or even different foci within a cell will exhibit different morphology or localization of DDR factors. Despite our extensive efforts to classify or analyze images of cells or foci, using for example neural networks or unbiased dimensionality reduction of image data (data not shown), we cannot discern features predictive of use of one pathway over another or of number of foci within a given cell. This is partly due to limitations of antibody-mediated fluorescent imaging: we were only able to profile 2 DDR markers at a time. We urge the creation of a 5+ color DDR panel comprising γH2AX along with TUDEL staining and other DDR markers from independent DDR pathways. Co-localization of multiple markers from a given pathway at a DSB loci will give more definitive results than a single marker. Further, colocalization of many markers will bolster models which suggest competition between pathways or clustering of DSBs. Thus, more work is needed to accurately assess repair pathway competition before ascribing epigenetic determinants of repair pathway choice.

As discussed above, TUDEL imaging may show evidence of rapid end joining or other DDR activities which quickly repair a major fraction of DNA damage. However, we feel that imaging analyses are likely not the most useful methods to link differential repair pathway choice to use of different drugs or other perturbations. Instead, we urge the implementation of

genomic analyses including CUT&RUN in addition to proteomic analysis to confirm histone PTM changes. Future studies mapping the genomic landscape of HR and NHEJ factors will be helpful in confirming whether these two pathways have distinct or overlapping genomic patterns. In the case that distinct patterns are observed, this would bolster the hypothesis that histone PTMs drive repair pathway choice and that repair pathways are largely mutually exclusive. However, if NHEJ and HR factors overlap, this would suggest repair pathway choice is stochastic or cell-intrinsic, adding weight to models which describe competition between individual repair factors at DSB loci[129, 613, 614].

Finally, future work should endeavor to disentangle the effects of endogenous and exogenous sources of DNA damage by treating cells with various DNA damage inducers and comparing patterns of damage induction and γH2AX signaling between them. Previous work has mapped induction of damage from replication stressors[392]. We feel that the genome tiling approach used herein might offer unique insight into differential interactions between DDR inducers and the epigenome. (Indeed, the genome tiling framework could be used to directly compare patterns of virtually any epigenomic feature, especially stochastic localization or changes in marks.) If patterns of damage are shared between damage inducers, this would suggest that a fundamental element of chromatin (i.e., fragility) determines DSB induction and response. However, we would predict that different patterns will emerge from different inducers of damage, suggesting that repair pathway choice is context dependent. For example, replication stressors would induce more transcription-replication collisions and mimic endogenous damage, while crosslinkers or direct DSB inducers may resemble exogenous induction of damage. We hope to identify locations of differential DSB or γH2AX induction using various damaging agents and leverage the unique epigenetic features to glean insight into differences between cellular response to endogenous and exogenous sources of damage.

8.3 A New Model of Chromatin-Context Aware DSB Detection

Throughout our studies, H3K27me3, the footprint of the repressive chromatin modifying complex PRC2, was consistently shown to be a key mediator of the DDR. Repressed regions, basally enriched for H3K27me3, were refractory to DSB recognition. However, we also show that, following IR insult, areas which accumulate γH2AX also increase their levels of H3K27me3. Imaging studies and use of EZH2 inhibitors confirmed H3K27me3 as necessary for γH2AX deposition. Using both γH2AX immunofluorescence and our newly developed direct DSB labeling method, TUDEL, we verified the presence of H3K27me3 at DSBs. The proximity of H3K27me3 and DSBs was further confirmed by FRET imaging suggesting that H3K27me3 decorated nucleosomes are within molecular proximity of DSB ends. Imaging also revealed post-IR enrichment of H3K27me3 in open DNA as measured by FILM lifetime imaging and by DAPI intensity. Proteomic analysis also shows an increase in H3K27me3 following IR, in particular on the H3.3 isoform associated with transcribed DNA[465, 615]. These results underscore observations from our epigenomic analysis which suggests H3K27me3 increases in euchromatic areas which also accumulate γH2AX. Further, inhibition of EZH2, which is the obligate writer of H3K27me3 attenuates γH2AX IRIF number and size.

These data suggest that fundamental changes to the epigenome surrounding DSBs precede recognition of damage by PIKKs. This finding is significant, as γH2AX IRIF appear within seconds to minutes of DSB induction. Mechanisms of ATM recruitment to damaged DNA are not yet fully understood; our data indicates epigenetic signals, including H3K27me3, potentiate ATM recruitment. Future work should attempt to identify whether γH2AX induction is completely stochastic and offer a mechanistic explanation as to how cells are able to rapidly recognize breaks anywhere on the genome. Mechanisms of ATM binding and activation are well studied but generally do not consider chromatin context or histones[616, 617, 618]. It has been shown that some histone modifiers, including Tip60, stimulate ATM binding and activity[562, 619]. While binding of the MRN complex is gen-

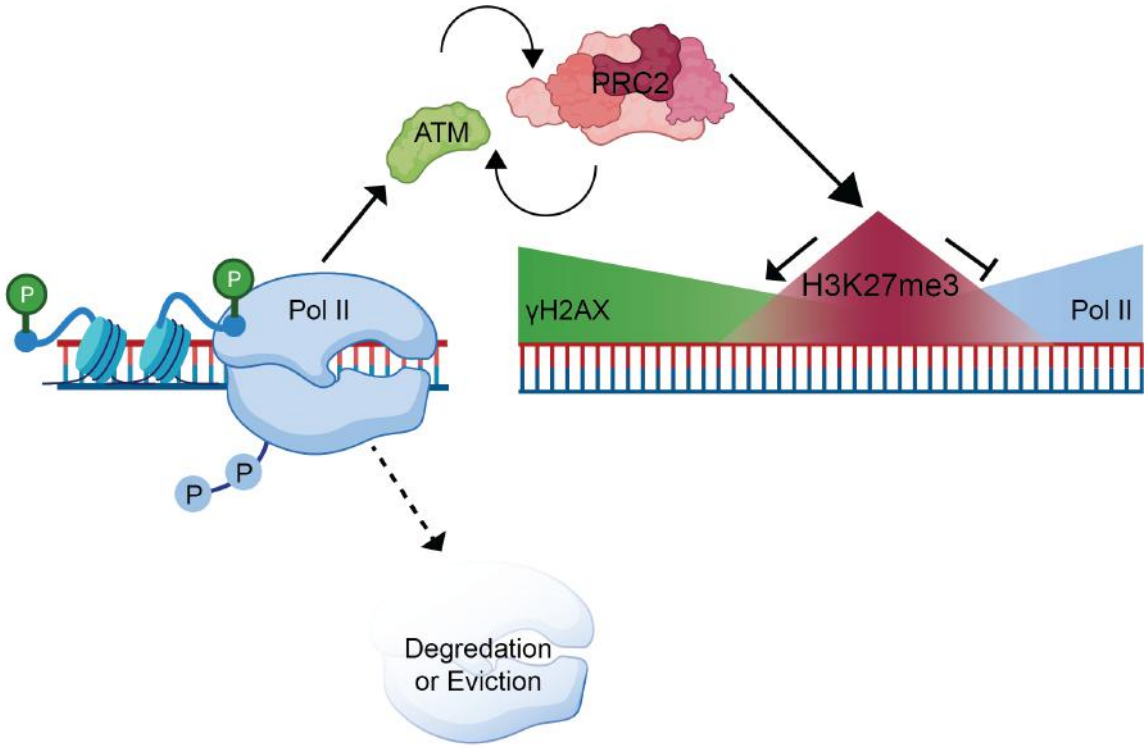

Figure 8.1: In this new model of transcription coupled repair, POL II acts as a DSB detector which then signals to ATM through an as-yet undefined mechanism. Subsequently, ATM mediates spreading of γH2AX away from the break which excludes further Pol II with the aid of PRC2 and H3K27me3. Pol II proximal to the break may be evicted or degraded by PIKK-associated processes. Subsequently, histone modifications including H2AX deposition, nucleosome eviction, or H3K27me3 deposition occur to facilitate recruitment of DDR factors.

erally considered a prerequisite for ATM activity, in the presence of exposed DNA, MRN is not required suggesting that chromatin occupancy may influence ATM binding. Little work connects H3K27me3 or EZH2 to ATM activity. However, we suggest the existance of a positive feedback mechanism. The PRC2 complex is known to bind to H3K27me3 and catalyze further trimethylation proximal to H3K27me3 rich domains[228, 620]. Perhaps PRC2 operates similarly after IR insult. Alternatively, ATM may bind one or more histone marks including H3K27me3, affecting its own positive feedback loop. As a third possibility, perhaps ATM binds directly to the PRC2 complex and is thus recruited to damage. We suggest careful structural analysis of both ATM and PRC2 subunits may uncover novel binding or interaction domains. Further, proteomics could be used to assay PRC2 phosphorylation by ATM[257]. More work is needed to study the genomic localization and histone modifying activity conferred by ATM:EZH2 interactions. This work is further complicated by the relative lack of understanding of PRC2 binding or recruitment discussed in Chapter 1. It is hard to discern whether PRC2 binding at DSBs operates via a unique mechanism or via a process analogous to binding at repressed promoters or putative PREs. While this work did not consider the impact of sequences or motifs on DSB induction or γH2AX deposition, it may be that some sequences more readily attract ATM, MRN or PRC2 allowing for rapid DSB detection.

Our observation that H3K27me3 is largely deposited in open, transcribed regions suggests that transcription may act in concert with PRC2 activity as a DSB detection mechanism. It is well appreciated that transcription must be attenuated proximal to DSBs, and that following IR insult transcription is globally attenuated[447, 621]. Thus, we propose the following mechanism for DSB detection. In euchromatin, breaks are easily induced owning to the relatively low nucleosome density. Breaks are then rapidly detected coincident with transcription. Detection may be mediated directly via Pol II or other members of the pre-initiation complex or transcription factors. In particular, transcription factors which have chromatin modifying activities (PRC2, SWI/SNF, Cux1) may play a role. Further, un-

winding of the DNA and opening of the chromatin ahead of a transcribing polymerase may uncover damage and allows for detection by, for example, topoisomerases. The mechanism or mechanisms underlying this process remains unclear. Once the break has been detected, the transcriptional machinery signals to ATM in an as-yet-unidentified manner. Perhaps unwound DNA itself signals to ATM; short tracts of naked DNA have been shown to increase ATM activity[622, 623, 624, 625]. Analogously, treatment with chromatin decondensers or even hypotonic stress induces ATM activity. Perhaps ATM samples open DNA more frequently leading to stochastic hyper-detection of breaks in genic regions. Alternatively, the transcriptional bubble may act as an ideal substrate for ATM irrespective of co-factors. An analogous mechanism may occur at replication forks, providing for recognition of breaks in non-transcribed DNA. Indeed, we observe links between late-replicating DNA and attenuated detection of DSBs.

After initial break detection, γH2AX must be spread over kilobases of DNA and transcription *in cis* to the break must be attenuated. It is tempting to connect these two processes and suggest that spreading of γH2AX may create a buffer zone which excludes polymerase. Future studies can examine spreading of DDR domains to see if the borders coincide with promoters or other transcriptional boundaries. Histone modifiers, especially PRC2, may play a role in these processes as discussed above. PRC1, a known component of the DDR machinery, dovetails nicely with such a model as PRC1/PRC2 cooperate to affect transcriptional repression and/or gene repression. It is likely that these proteins function in a similar manner at DSBs. Other known DDR factors including EHMT2 are also associated with H3K27 methylation. It is an open question whether EZH2 can catalyze tri-methylation *de novo* or whether mono- or di-methylated substrates are preferred. The involvement of EHMT2 (which catalyzes H3K27me1-2) in the DDR suggests the latter possibility may predominate at DSBs. How SWI/SNF fits into this model is unclear. SWI/SNF may evict nucleosomes around DSB ends to allow for DNA exposure, ATM binding or increased accessibility. We cannot rule out that SWI/SNF and PRC2 operate on different lesions or at

different locations (either temporal or spatial) with respect to the same lesion. Genomic data herein suggest that H3K27me3 defines the border of γH2AX domains— likely far from the broken DNA ends. Further, the epigenome must be restored after the break is repaired. SWI/SNF and JMJD proteins may play a role here too.

Our findings extend canonical models of DSB detection by showing that deposition of γH2AX around TSSs is correlated with the extent of basal transcription. A caveat is that these data could report transcription-mediated damage. However, we don't feel that this possibility is especially likely for the following reasons. First, γH2AX is not deposited homogeneously around TSSs but rather accumulates distally from promoters concomitantly with active Pol II. Second, when transcription is inhibited globally, via addition of pharmacological inhibitors of Pol II initiation or elongation, γH2AX IRIF are diminished. Further, transcriptional inhibition attenuated accumulation of H3K27me3 and R-Loops suggesting that DSB proximal attenuation of transcription is necessary for recruitment of H3K27me3. Interestingly inhibition of ATM partially phenocopies transcriptional inhibitors, as both treatments diminish H3K27me3 and R-Loops at γH2AX foci. This suggests that PRC2 and ATM may work in a feedback loop as proposed above. While mechanism remains unclear, these data go some way to resolving order of function disputes. It seems that Pol II acts upstream of ATM or PRC2 suggesting that transcription could underpin DSB recognition in euchromatin. We thus propose that Pol II actively mediates γH2AX deposition through a mechanism involving attenuation of transcription by recruiting EZH2. In this way, EZH2 activity at DSBs mirrors its traditional role in transcription. Perhaps lessons from basal transcriptional regulation may inform epigenetic:DSB interplay and vice versa. This has interesting implications for transcriptional alterations in cancer which will be discussed in greater detail below.

Central to the question of transcription coupled recognition or repair of DSBs is the role of R-Loops. Previous work has postulated that R-Loops are either DSB promoting or DSB attenuating, and consensus is lacking. While we did not directly examine R-Loops

at the sequence level, our data does uncover new mechanisms governing establishment of R-Loops. We showed that R-Loop formation is dependent both on transcription and on EZH2 activity. Thus, we propose that R-Loops form as a consequence of stalled or paused Pol II which encounters a DSB and signals to epigenetic modifiers including EZH2. The presence of R-Loops is inversely correlated with active Pol II in our data and previous studies. This mechanism suggests R-Loops are natural consequences of DSB repair, rather than deleterious factors. Future work can examine the consequences of removing R-Loops on γH2AX induction and foci persistence at a genomic level. R-Loops can be degraded globally by addition of exogenous RNaseH. We propose treating cells with RNAseH and then profiling Pol II and γH2AX following IR insult. We expect that loss of R-Loops may induce higher levels of processive Pol II and possibly diminish γH2AX in euchromatin. Alternatively, R-Loops may be downstream of transcriptional repression and H3K27me3 deposition in which case RNAseH treatment would not affect genomic localization of the above factors.

Transcription-associated repair literature is divided with respect to endogenous and exogenous sources of damage, sometimes conflating the two. In contrast, we observe differences between locations of endogenous transcriptional stress and transcription-associated DSB recognition. Multidimensional clustering revealed two types of TSSs which accumulated significant γH2AX following IR insult: one cluster bears characteristics of fragile promoters, loci of endogenous DNA damage, while the other cluster contains more active Pol II and few markers of fragile promoters. This suggests that transcription-coupled recognition, as we propose here, occurs at distinct genomic loci from transcription-associated damage. We further suggest that promoter or chromatin fragility is not the primary determinant of γH2AX induction following IR insult. Indeed, by measuring endogenous damage with BLISS-seq, we do not see strong overlap with γH2AX induction. γH2AX induction is also not strongly correlated with DNAseseq or MNase seq. We are thus confident in saying that endogenous patterns of damage have little bearing on response to exogenous damage. This is another reason why we do not feel that our data are indicative of transcription-mediated DSBs.

While it is true that transcribed regions accrue a significant amount of damage from both endogenous and exogenous sources, we feel that based on these results, and with an eye to the myriad transcription associated DDR pathways described in the literature, that endogenous and exogenous damage may be recognized via different pathways. Indeed, endogenous damage is often associated with replication of transcribed areas; we see that exogenous induction of γH2AX only moderately correlates to replication timing. Further, rapid γH2AX deposition occurs in early-replicating chromatin which is generally thought to be free of transcription-replication conflicts. Further, epigenetics might differentially impact endogenous and exogenous DDR pathways. In contrast to enrichment of H3K4 methylation and replication origins associated with replication-transcription collisions, we note that H3K9Me1, anticorrelated with H3K4 methylation, is predictive of γH2AX deposition in transcribed areas following IR insult, and distance to replication origin had little bearing on γH2AX levels[626]. If endogenous and exogenous sources of damage and repair do operate by different pathways this might go some way to explain how SWI/SNF and PRC2 are both associated with transcription coupled repair. We see evidence for both SWI/SNF and PRC2 in repair of exogenous damage, as noted here. However, others have ascribed a role for SWI/SNF principally in repair of endogenous damage[627]. Future studies could probe differential localization of endogenous and exogenous damage, as proposed above. Coupled with knockout or pharmacological inhibition of SWI/SNF or EZH2, along with ChIP-seq, these studies could uncover differential activities of these factors with respect to damage type. We further propose unraveling the signaling pathways by which endogenous sites of damage, such as collapsed forks, recruit SWI/SNF and examining whether these factors play a role in exogenous damage at transcribed loci.

In our genomic analysis of γH2AX induction, we queried whether gene function plays a role in determining the local response to DSBs. Cells face a paradox when exposed to IR or other exogenous sources of DNA damage. While they must attenuate transcription globally to prevent collisions with damaged DNA, they must concomitantly express genes needed in

the cellular DDR[621, 628]. We observed that DDR related genes accumulate more γH2AX than their counterparts, and that γH2AX is correlated with post-IR transcriptional activity rather than transcriptional attenuation. This has two broad implications. First, it suggests that there may be multiple ways in which transcription can influence the DDR as outlined above. For genes which need to be expressed following IR, transcription-associated repair may predominate, perhaps via use of RNA as a template or by using Pol II to influence recruitment of DDR factors, as has been proposed to occur at fragile promoters. Indeed, breaks may stimulate transcription of these genes after IR insult. On the other hand, at most genes transcriptional repression is an integral part of the DDR. While Pol II may serve as a break detector, it must then be degraded or excluded from DSB loci to facilitate repair and prevent further damage. Second, it suggests a new rationale for the DDR. All breaks, be they in heterochromatin or transcribed loci, are equally deleterious. Even a single break could cause mitotic catastrophe if replication forks collide with undetected damage. Thus it would seemingly behoove cells to repair all breaks rapidly. The observation that cells repair breaks in transcribed loci, and in particular at DDR genes, suggest that cells may act to preserve transcription following IR insult at the expense of rapid detection of all DSBs. Cells, and especially cancer cells, may be tolerant of breaks or loss of DNA in hetrochromatic or non-transcribed regions. Thus the DDR can be thought of not as a tool to preserve genomic integrity, but rather as a tool to maintain transcriptional homeostasis.

Future work should examine the ontology of genes with fragile promoters to see whether they occur more frequently in DDR or stress-response genes. At non-DDR genes, data suggests that PRC2 mediated transcriptional repression is a prerequisite for DSB recognition. Furthermore, that gene ontology impinges on DSB repair suggests that different cell types may possess unique patterns of DSB recognition. This is particularly interesting in a cancer setting where altered expression of oncogenes is known to drive tumors. It may be that oncogenes, which frequently accrue mutations, do so in part due to altered DSB repair activity at these loci. Indeed, oncogenes are commonly associated with fragile chromatin sites suggesting that the local chromatin environment is permissive toward mutation. In future, the epigenome at oncogene loci or CFS loci could be examined and compared with other loci which accumulate significant γH2AX following IR insult. These studies may offer an orthogonal manner by which to define oncogenes or provide another mechanism by which tumor cells are able to achieve transformation.

8.4 Translational Implications and Future Directions

While we have discussed the basic science motivations for this work above, we will now turn to the translational implications. First, this work begins to transform the way in which we think about the impact of radiotherapy on cells or tumors. While traditionally it was assumed that all cells received an equivalent dose of IR and that radiation acted homogenously on the genome, we now see this is not true. Instead, a minority of the genome, concentrated in transcribed chromatin, receives a majority of the damage and is responsible for initiating the bulk of the DDR activity. Indeed, we suggest that transcription acts as a key signaling mechanism in the DDR. This data further suggests novel radiosensitizing drugs which may bolster the activity of IR, these include EZH2 inhibitors, SWI/SNF inhibitors or degraders, and transcriptional inhibitors. The latter is likely not practical in an *in vivo* setting as transcription inhibitors require high doses and have pleiotropic effects[558, 629]. However, future work should explore use of epigenetic inhibitors in conjunction with RT in

an *in vivo* model. Our work also suggests that short, acute doses of epigenetic inhibitors preceding IR insult are effective *in vitro*, suggesting dosing and treatment regimens which may be ported to animal models. One could also exploit a therapeutic window approach whereby systemic long-term dosing with an epigenetic inhibitor at well tolerated doses can be coupled with acute IR to the tumor site thereby effecting cytotoxicity only within the tumor. Importantly, any *in vivo* study should carry through lessons of our *in vitro* work, in particular looking at the kinetics of response. While granular kinetics are challenging to measure in an animal model, one may be able to assess dosimetry via serial biopsy or examination of circulating tumor cells.

Turning to the etiology of tumors, this work suggests that genetic and epigenetic alterations may play a role beyond gene expression changes. In particular, resistance to chemotherapies or RT may be mediated by tumor-specific epigenetics. In fact, both SWI/SNF and PRC2 are associated with cancer. In the case of EZH2, either loss- or gain-of-function mutations have been observed with both types of mutations affecting H3K27 methylation[630, 631]. It is curious that either loss or gain of PRC2 components, and by extension H3K27 methylation, can affect oncogenesis. Perhaps different genotypes are cell or cancer specific. The mechanism by which PRC2 contributes to cancer is unclear but many studies point to increased "stemness" or alterations in gene expression as drivers of tumorgenesis. Genome integrity and response to damage in the context of EZH2 mutations remain understudied; it not yet understood how these alterations affect response to IR or other forms of DNA damage. Future studies could, for example, compare responses to IR between PRC2 wild-type and PRC2 mutant cells. In doing so, we could better understand how PRC2 affects the DDR. For example, does hyper trimethylation of H3K27 improve or dampen a cell's ability to recognize and/or respond to IR induced damage? SWI/SNF mutations are also associated with oncogenesis, though only loss-of-function is observed[632, 633, 634]. As SWI/SNF is more clearly linked to the DDR, this has been widely considered as a mechanism by which loss of SWI/SNF may affect tumorgenesis. However, germline SWI/SNF mutations confer

tumors with low-mutational burden, casting doubt on such a simple mechanistic link[635]. Further, reexpression of SWI/SNF in tumors with loss-of-function mutations leads to cell cycle arrest. This suggests both that novel mutations do not accrue in such cells and that SWI/SNF is linked to cell cycle progression, an important part of the DDR[636]. Instead, it is thought that transcriptional deregulation might drive SWI/SNF mutant tumors[637]. However, studies looking at response to therapy in tumors with SWI/SNF mutations are lacking. Additionally, much data comes from germline mutants, rather than acquired mutations, which might have a different phenotype.

More careful examination of the epigenomes of PRC2 or SWI/SNF mutants, especially after therapy, is warranted. Genomic analyses could link areas of, for example, differential H3K27me3 or chromatin occupancy, to differential γH2AX induction. This would not only underscore the importance of such modifications in the DDR, but also provide a mechanism by which alterations to the epigenome produce differential response to therapies. As a specific example, one could investigate DDR activity in H3K27M mutant gliomas[240, 241]. These tumors have aberrant PRC2 activity with lower levels of H3K27 methylation. From our data we hypothesize that such tumors would be radiosensitive, as H3K27me3 is a key signaling node in the DDR. Lower levels of H3K27me3 may also induce chromatin decompaction and allow for more damage to the genome. However, deconvoluting the genome integrity effects of H3K27M from alterations in gene expression would of course be important. It is not known how mutations in PRC2 or SWI/SNF may facilitate differential expression of genes involved in the DNA damage response. However, such effects could be ameliorated by focusing on short timescales perhaps in an *in vitro* model, as discussed above.

Knowledge that the underlying epigenome influences DSB induction and recognition also has bearing on the field of genomic breakpoints and recurrent translocations. It is well appreciated that cancers undergo transformation coincident with genetic mutations or rearrangements which re-occur at specific loci across tumors and even tumor types. Natural selection provides one explanation as to why a few genomic loci give rise to the preponderance

of breakpoints; cells with breaks elsewhere either die, or are not selected for. However, we assert that the underlying epigenome surrounding fragile loci may also be permissive toward rearrangements or mutations[638]. Herein, we show that CFS loci contain more γH2AX than random loci. In future, it will be interesting to correlate γH2AX distributions or markers of break induction with mutational patterns in a pan-cancer database. Perhaps regions which rapidly accumulate γH2AX are protected from mutations, alternatively this could indicate higher rates of breakage or end-joining which could be mutation promoting. Ideally, studies could examine mutational patterns in patients receiving IR or chemo separately from treatment-naïve patients. Such analyses would underscore the differential patterns of endogenous and exogenous damage, and possibly resultant mutations, as discussed above. This work could bolster studies on the etiology of tumors by suggesting specific, assay-able mechanisms by which tumor cells accumulate mutations.

Finally, these data suggest that participation in the DDR by transcription factors or epigenetic modifiers is not a coincidental or backup function, but rather is a highly conserved element of these proteins. Indeed, studies in yeast, drosophila and human cells suggest similar epigenetic pathways are utilized in the DDR and that they share overlapping functions in recognizing DSBs. Moreover, the relative lack of gene-regulatory complexity in yeast, for example, suggests that epigenetic regulators may have evolved with their DDR functions in mind, rather than the reverse. Examining repair of DSBs via the lens of gene regulation may yield new discoveries. For example, Pol II occupancy and transcription could be examined around damaged loci using assays which detect nascent transcripts or directly measure Pol II occupancy. Alternatively, nucleosome positioning assays have uncovered conserved, highly-ordered arrangements of nucleosomes surrounding promoters; such arrangements might be recapitulated at damaged loci. Though these experiments will likely have to be undertaken using restriction-enzyme mediated DSBs, they could shed light on the function of Pol II at break loci and the activity of epigenetic modifiers, in particular SWI/SNF and related nucleosome remodelers.

In summary, we explore several pathways by which the cellular epigenome influences response to external sources of DNA damage, principally ionizing radiation. We uncover influences of the basal epigenome on induction of DSBs and recognition of damage in addition to ways in which the epigenome is altered upon IR insult. At the former level, DSBs are somewhat more likely to occur in euchromatin as compared to heterochromatin while γH2AX is much more likely to be deposited in euchromatic regions. These data suggest that the basal epigenome exerts a powerful force on the DNA damage response and conscribes a cell's ability to repair its DNA. In contrast to other literature, we assert that open DNA is more rapidly repaired, and that transcription plays a primary role in this process. Rather than concentrating on transcription coupled damage, we instead posit transcription coupled repair. Indeed, we feel that many associations between transcribed DNA and damage are likely viewed backwards; transcription does not cause damage, but instead, transcribed DNA is likelier to accrue damage. Blocking transcription impaired the ability of cells to recognize damage, recruit ATM and modify chromatin surrounding breaks. Thus, transcription can be seen as a powerful director of the DDR.

We also position the long-studied chromatin modifying complexes PRC2 and SWI/SNF as important DDR factors which influence recognition of damage, especially early damage in open chromatin. PRC2 plays a repressive role, as addition of H3K27me3 occurs principally at highly transcribed regions coincident with γH2AX deposition. The function of PRC2 may be to attenuate transcription or to construct a permissive chromatin environment for the DDR. Inhibition of PRC2 attenuates γH2AX foci as well as ATM and R-Loops. SWI/SNF, while canonically opposed to PRC2, may work in concert with EZH2 at break loci. Indeed, loss of SWI/SNF subunits prevents accumulation of EZH2 and H3K27me3 at DSBs. More remains to be discovered as to the complex interplay between these two factors. Translation of this work is challenging owing to the pleiotropic effect of epigenetic inhibitors. However, through better understanding of the action of epigenetic modifiers at DSBs, synergistic effects may be achieved.

Toward such an understanding, we introduce TUDEL, a direct DSB labeling system. We show that TUDEL foci are correlated with other DSB markers though not completely, suggesting that this tool can be used to separate DSB repair from DDR factors. We anticipate using TUDEL to further dissect how epigenetic modifiers participate in the DDR. In particular we have already unvovered heretofore under-appreciated rapid repair of DSBs, likely via end-joining, which is lost when SWI/SNF is pharmacologically degraded. We also show that coupling TUDEL with other imaging techniques or proteomics can be a powerful tool for verification of epigenetic modifiers in the DDR. In future, expansion and refinement of TUDEL could be useful to unravel existing paradoxes in epiegentic:DDR interactions. For example, TUDEL imaging could confirm the persistence of breaks in heterochromatin despite these regions not accumulating γH2AX. Alternatively, TUDEL could be used as a screen for epigenetic inhibitors. Factors which attenuate γH2AX are potentially potent radiosensitizers, though they are hard to classify because lower γH2AX is generally associated with a reduction of damage and perhaps resolution of breaks. By using TUDEL to count DSBs, we can confirm the effect of epigenetic inhibitors on DSBs themselves and thus raise potential radiosensitizer candidates. In conclusion, while the work outlined in this Dissertation is largely basic science, it has important implications for how we conceptualize the effect of DNA damaging therapies and lays the ground work for *in vivo* studies using radiosensitizers uncovered herein.

REFERENCES

[1] Baumann, M. et al. Radiation oncology in the era of precision medicine. Nature Reviews Cancer 16, 234–249 (2016).

[2] Le, Q.-T., Shirato, H., Giaccia, A. J. & Koong, A. C. Emerging treatment paradigms in radiation oncology. Clinical Cancer Research 21, 3393–3401 (2015).

[3] Chen, J., Li, E. & Lai, J. The coupled effect of nucleosome organization on gene transcription level and transcriptional plasticity. Nucleus 8, 605–612 (2017).

[4] Dolgin, E. Using DNA, radiation therapy gets personal Science 353:6306, 1348-1349 (2016).

[5] Morrison, R. et al. Targeting the mechanisms of resistance to chemotherapy and radiotherapy with the cancer stem cell hypothesis. Journal of oncology (2011).

[6] Tsoutsou, P. G., Koukourakis, M. I., Azria, D. & Belkac´emi, Y. Optimal timing for adjuvant radiation therapy in breast cancer. A comprehensive review and perspectives. Critical Reviews in Oncology/Hematology 71, 102–116 (2009).

[7] Vale, C. L. et al. Adjuvant or early salvage radiotherapy for the treatment of localized and locally advanced prostate cancer: a prospectively planned systematic review and meta-analysis of aggregate data. The Lancet 396, 1422–1431 (2020).

[8] Curtin, N. J. DNA repair dysregulation from cancer driver to therapeutic target. Nature Reviews Cancer 12, 801–817 (2012).

[9] Hanahan, D. & Weinberg, R. Hallmarks of Cancer: The Next Generation. Cell 144, 646–674 (2011).

[10] Schipler, A. & Iliakis, G. DNA double-strand-break complexity levels and their possible contributions to the probability for error-prone processing and repair pathway choice. Nucleic Acids Research 41, 7589–7605 (2013).

[11] Ward, J. F. Biochemistry of DNA lesions. Radiation Research 104, S103–S111 (1985).

[12] Ward, J. F. The yield of DNA double-strand breaks produced intracellularly by ionizing radiation: a review. International journal of radiation biology 57, 1141–1150 (1990).

[13] Henner, W. D., Grunberg, S. M. & Haseltine, W. A. Sites and structure of gamma radiation-induced DNA strand breaks. Journal of Biological Chemistry 257, 11750– 11754 (1982).

[14] Sage, E. & Harrison, L. Clustered DNA lesion repair in eukaryotes: relevance to mutagenesis and cell survival. Mutation Research/Fundamental and Molecular Mechanisms of Mutagenesis 711, 123–133 (2011).

[15] Zhang, X.-P., Liu, F., Cheng, Z. & Wang, W. Cell fate decision mediated by p53 pulses. PNAS 106, 12245–12250 (2009).

[16] Eccles, L. J., O'Neill, P. & Lomax, M. E. Delayed repair of radiation induced clustered DNA damage: friend or foe? Mutation Research/Fundamental and Molecular Mechanisms of Mutagenesis 711, 134–141 (2011).

[17] Banath, J. P., Klokov, D., MacPhail, S. H., Banuelos, C. A. & Olive, P. L. Residual γH2AX foci as an indication of lethal DNA lesions. BMC cancer 10, 1–12 (2010).

[18] Belyaev, I. Y. Radiation-induced DNA repair foci: spatio-temporal aspects of formation, application for assessment of radiosensitivity and biological dosimetry. Mutation Research/Reviews in Mutation Research 704, 132–141 (2010).

[19] Bonner, W. M. et al. γH2AX and cancer. Nature Reviews Cancer 8, 957–967 (2008).

[20] Niemantsverdriet, M. et al. High and low LET radiation differentially induce normal tissue damage signals. International Journal of Radiation Oncology Biology Physics 83, 1291–1297 (2012).

[21] Roobol, S. J. et al. Comparison of high-and low-let radiation-induced DNA double strand break processing in living cells. International Journal of Molecular Sciences 21, 1–19 (2020).

[22] Pouget, J. P. et al. Formation of modified DNA bases in cells exposed either to gamma radiation or to high-LET particles. Radiation research 157, 589–595 (2002).

[23] Henner, W. D., Rodriguez, L. O., Hecht, S. M. & Haseltine, W. A. gamma Ray induced deoxyribonucleic acid strand breaks. 3'Glycolate termini. Journal of Biological Chemistry 258, 711–713 (1983).

[24] Serrano-Benitez, A., Cortes-Ledesma, F. & Ruiz, J. F. "An End to a Means": How DNA-End Structure Shapes the Double-Strand Break Repair Process. Frontiers in Molecular Biosciences 6, 1–9 (2020).

[25] Warmerdam, O., Kanaar, R. & Wyman, C. Previews From DNA End Chemistry to Cell-Cycle Response : The Importance of Structure, Even When It s Broken 1, 5–6 (2008).

[26] Kim, W. et al. Cellular Stress Responses in Radiotherapy. Cells 8, 1–18 (2019).

[27] Wang, L. et al. High-Throughput Functional Genetic and Compound Screens Identify Targets for Senescence Induction in Cancer. Cell Reports 21, 773–783 (2017).

[28] Baus, F., Gire, V., Fisher, D., Piette, J. & Dulic, V. Permanent cell cycle exit in G2 phase after DNA damage in normal human fibroblasts. The EMBO journal 22, 3992–4002 (2003).

[29] Li, Z. et al. Impaired DNA double-strand break repair contributes to the age-associated rise of genomic instability in humans. Cell Death and Differentiation 23, 1765–1777 (2016).

[30] Roos, W. P. & Kaina, B. DNA damage-induced cell death by apoptosis. Trends in molecular medicine 12, 440–450 (2006).

[31] Wyllie, A. H., Kerr, J. F. R. & Currie, A. R. Cell death: the significance of apoptosis. International review of cytology 68, 251–306 (1980).

[32] Blackford, A. N. & Jackson, S. P. Molecular Cell Review ATM, ATR, and DNA-PK: The Trinity at the Heart of the DNA Damage Response. Molecular Cell 66, 801–817 (2017).

[33] Gotoff, S. P., Amirmokri, E. & Liebner, E. J. Ataxia telangiectasia: neoplasia, untoward response to X-irradiation, and tuberous sclerosis. American journal of diseases of children 114, 617–625 (1967).

[34] Houldsworth, J. & Lavin, M. F. Effect of ionizing radiation on DNA synthesis in ataxia telangiectasia cells. Nucleic Acids Research 8, 3709–3720 (1980).

[35] Savitsky, K. et al. A single ataxia telangiectasia gene with a product similar to PI-3 kinase. Science 268, 1749–1753 (1995).

[36] Ahn, J.-Y., Schwarz, J. K., Piwnica-Worms, H. & Canman, C. E. Threonine 68 phosphorylation by ataxia telangiectasia mutated is required for efficient activation of Chk2 in response to ionizing radiation. Cancer research 60, 5934–5936 (2000).

[37] Matsuoka, S., Huang, M. & Elledge, S. J. Linkage of ATM to cell cycle regulation by the Chk2 protein kinase. Science 282, 1893–1897 (1998).

[38] Bakkenist, C. J. & Kastan, M. B. DNA damage activates ATM through intermolecular autophosphorylation and dimer dissociation. Nature 421, 499–506 (2003).

[39] Matsuoka, S. et al. ATM and ATR substrate analysis reveals extensive protein networks responsive to DNA damage. science 316, 1160–1166 (2007).

[40] Paull, T. T. et al. A critical role for histone H2AX in recruitment of repair factors to nuclear foci after DNA damage. Current Biology 10, 886–895 (2000).

[41] Rogakou, E. P., Pilch, D. R., Orr, A. H., Ivanova, V. S. & Bonner, W. M. DNA double-stranded breaks induce histone H2AX phosphorylation on serine 139. Journal of biological chemistry 273, 5858–5868 (1998).

[42] Iacovoni, J. S. et al. High-resolution profiling of γH2AX around DNA double strand breaks in the mammalian genome. The EMBO journal 29, 1446–1457 (2010).

[43] Kang, J. et al. Functional Interaction of H2AX, NBS1, and p53 in ATM-Dependent DNA Damage Responses and Tumor Suppression. Molecular and Cellular Biology 25, 661–670 (2005).

[44] Marechal, A. & Zou, L. DNA damage sensing by the ATM and ATR kinases. Cold Spring Harbor Perspectives in Biology 5, 1–18 (2013).

[45] Savic, V. et al. Formation of dynamic g-H2AX domains along broken DNA strands is distinctly regulated by ATM and MDC1 and dependent upon H2AX densities in chromatin. Molecular Cell 34, 298–310 (2009).

[46] Falck, J., Coates, J. & Jackson, S. P. Conserved modes of recruitment of ATM, ATR and DNA-PKcs to sites of DNA damage. Nature 434, 605–611 (2005).

[47] Ceccaldi, R., Rondinelli, B. & D'Andrea, A. D. Repair Pathway Choices and Consequences at the Double-Strand Break. Trends in Cell Biology 26, 52–64 (2016).

[48] Chapman, J. R., Taylor, M. R. & Boulton, S. J. Playing the End Game: DNA Double-Strand Break Repair Pathway Choice. Molecular Cell 47, 497–510 (2012).

[49] Betermier, M., Bertrand, P. & Lopez, B. S. Is Non-Homologous End-Joining Really an Inherently Error-Prone Process? PLoS Genetics 10, e1004086 (2014).

[50] Graham, T. G. W., Walter, J. C. & Loparo, J. J. Two-stage synapsis of DNA ends during non-homologous end joining. Molecular Cell 61, 850–858 (2016).

[51] Walker, J. R., Corpina, R. A. & Goldberg, J. Structure of the Ku heterodimer bound to DNA and its implications for double-strand break repair. Nature 412, 607–614 (2001).

[52] Jette, N. & Lees-Miller, S. P. The DNA-dependent protein kinase: A multifunctional protein kinase with roles in DNA double strand break repair and mitosis. Progress in biophysics and molecular biology 117, 194–205 (2015).

[53] Davis, A. J., Chen, B. P. C. & Chen, D. J. DNA-PK: a dynamic enzyme in a versatile DSB repair pathway. DNA repair 17, 21–9 (2014).

[54] Gupta, A. et al. Role of 53BP1 in the regulation of DNA double strand break repair pathway choice. Radiation research 181, 1–8 (2014).

[55] Panier, S. & Boulton, S. J. Double-strand break repair: 53BP1 comes into focus. Nature Reviews Molecular Cell Biology 15, 7–18 (2013).

[56] Ward, I. M., Minn, K., van Deursen, J. & Chen, J. p53 Binding protein 53BP1 is required for DNA damage responses and tumor suppression in mice. Molecular and cellular biology 23, 2556–63 (2003).

[57] Liu, Y., Efimova, E. V., Ramamurthy, A. & Kron, S. J. Repair-independent functions of DNA-PKcs protect irradiated cells from mitotic slippage and accelerated senescence. Journal of Cell Science 132, (2019).

[58] Finzel, A., Grybowski, A., Strasen, J., Cristiano, E. & Loewer, A. Hyperactivation of ATM upon DNA-PKcs inhibition modulates p53 dynamics and cell fate in response to DNA damage. Molecular Biology of the Cell 27, 2360–2367 (2016).

[59] Zhou, Y. et al. Regulation of the DNA Damage Response by DNA-PKcs Inhibitory Phosphorylation of ATM. Molecular Cell 65, 91–104 (2017).

[60] Escribano-Diaz, C. et al. A cell cycle-dependent regulatory circuit composed of 53BP1-RIF1 and BRCA1-CtIP controls DNA repair pathway choice. Molecular Cell 49, 872–883 (2013).

[61] Iwabuchi, K., Bartel, P. L., Li, B., Marraccino, R. & Fields, S. Two cellular proteins that bind to wild-type but not mutant p53. PNAS 91, 6098–6102 (1994).

[62] Doil, C. et al. RNF168 binds and amplifies ubiquitin conjugates on damaged chromosomes to allow accumulation of repair proteins. Cell 136, 435–446 (2009).

[63] Hsiao, K.-Y. & Mizzen, C. A. Histone H4 deacetylation facilitates 53BP1 DNA damage signaling and double-strand break repair. Journal of molecular cell biology 5, 157–165 (2013).

[64] Pei, H. et al. MMSET regulates histone H4K20 methylation and 53BP1 accumulation at DNA damage sites. Nature 470, 124–128 (2011).

[65] Tang, J. et al. Acetylation limits 53BP1 association with damaged chromatin to promote homologous recombination. Nature Structural & Molecular Biology 20, 317–325 (2013).

[66] Bunting, S. F. et al. 53BP1 inhibits homologous recombination in Brca1-deficient cells by blocking resection of DNA breaks. Cell 141, 243–254 (2010).

[67] Chapman, J. R. et al. RIF1 is essential for 53BP1-dependent nonhomologous end joining and suppression of DNA double-strand break resection. Molecular Cell 49, 858–871 (2013).

[68] Feng, L., Fong, K.-W., Wang, J., Wang, W. & Chen, J. RIF1 counteracts BRCA1- mediated end resection during DNA repair. Journal of Biological Chemistry 288, 11135–11143 (2013).

[69] Silverman, J., Takai, H., Buonomo, S. B. C., Eisenhaber, F. & de Lange, T. Human Rif1, ortholog of a yeast telomeric protein, is regulated by ATM and 53BP1 and functions in the S-phase checkpoint. Genes & Development 18, 2108–2119 (2004).

[70] Corneo, B. et al. Rag mutations reveal robust alternative end joining. Nature 449, 483–486 (2007).

[71] Oh, S. et al. DNA ligase III and DNA ligase IV carry out genetically distinct forms of end joining in human somatic cells. DNA Repair 21, 97–110 (2014).

[72] Wang, H. et al. Biochemical evidence for Ku-independent backup pathways of NHEJ. Nucleic Acids Research 31, 5377–5388 (2003).

[73] Mansour, W. Y., Rhein, T. & Dahm-Daphi, J. The alternative end-joining pathway for repair of DNA double-strand breaks requires PARP1 but is not dependent upon microhomologies. Nucleic Acids Research 38, 6065–6077 (2010).

[74] Xie, A., Kwok, A. & Scully, R. Role of mammalian Mre11 in classical and alternative nonhomologous end joining. Nature Structural and Molecular Biology 16, 814–818 (2009).

[75] Zhang, Y. & Jasin, M. An essential role for CtIP in chromosomal translocation formation through an alternative end-joining pathway. Nature Structural and Molecular Biology 18, 80–85 (2011).

[76] Kent, T., Chandramouly, G., Mcdevitt, S. M., Ozdemir, A. Y. & Pomerantz, R. T. Mechanism of microhomology-mediated end-joining promoted by human DNA polymerase. Nature Structural and Molecular Biology 22, 230–237 (2015).

[77] Arnoult, N. et al. Regulation of DNA repair pathway choice in S and G2 phases by the NHEJ inhibitor CYREN. Nature 549, 7673, 548-52 (2017).

[78] Slavoff, S. A., Heo, J., Budnik, B. A., Hanakahi, L. A. & Saghatelian, A. A human short open reading frame (sORF)-Encoded polypeptide that stimulates DNA end joining. Journal of Biological Chemistry 289, 10950–10957 (2014).

[79] Liang, L. et al. Molecular basis for assembly of the shieldin complex and its implications for NHEJ. Nature Communications 11, 1–15 (2020).

[80] Mirman, Z. et al. 53BP1–RIF1–shieldin counteracts DSB resection through CST-and Polg-dependent fill-in. Nature 560, 112–116 (2018).

[81] Noordermeer, S. M. et al. The shieldin complex mediates 53BP1-dependent DNA repair. Nature 560, 117–121 (2018).

[82] Gupta R. et al. DNA Repair Network Analysis Reveals Shieldin as a Key Regulator of NHEJ and PARP Inhibitor Sensitivity. Cell 173, 972–974 (2018).

[83] Xu, G. et al. REV7 counteracts DNA double-strand break resection and affects PARP inhibition. Nature 521, 541–544 (2015).

[84] Takata, M. et al. Homologous recombination and non-homologous end-joining pathways of DNA double-strand break repair have overlapping roles in the maintenance of chromosomal integrity in vertebrate cells. EMBO Journal 17, 5497–5508 (1998).

[85] Garcia, V., Phelps, S. E., Gray, S. & Neale, M. J. Bidirectional resection of DNA double-strand breaks by Mre11 and Exo1. Nature 479, 241–244 (2011).

[86] Daley, J. M. et al. Enhancement of BLM-DNA2-Mediated Long-Range DNA End Resection by CtIP. Cell Reports 21, 324–332 (2017).

[87] Limbo, O. et al. Ctp1 Is a Cell-Cycle-Regulated Protein that Functions with Mre11 Complex to Control Double-Strand Break Repair by Homologous Recombination. Molecular Cell 28, 134–146 (2007).

[88] Sartori, A. A. et al. Human CtIP promotes DNA end resection. Nature 450, 509–514 (2007).

[89] Bouwman, P. et al. 53BP1 loss rescues BRCA1 deficiency and is associated with triple-negative and BRCA-mutated breast cancers. Nature Structural & Molecular Biology 17, 688–695 (2010).

[90] Chapman, J. R., Sossick, A. J., Boulton, S. J. & Jackson, S. P. BRCA1-associated exclusion of 53BP1 from DNA damage sites underlies temporal control of DNA repair. Journal of cell science 125, 3529–3534 (2012).

[91] Cao, L. et al. A Selective Requirement for 53BP1 in the BiologicalResponse to Genomic Instability Induced by Brca1 Deficiency. Molecular Cell 35, 534–541 (2009).

[92] Huen, M. S., Sy, S. M. & Chen, J. BRCA1 and its toolbox for the maintenance of genome integrity. Nature Reviews Molecular Cell Biology 11, 138–148 (2010).

[93] Densham, R. M. & Morris, J. R. Moving Mountains—The BRCA1 Promotion of DNA. Resection. Frontiers in Molecular Biosciences 6 (2019).

[94] Zhou, W. et al. Spatiotemporal Control of CRISPR/Cas9 Function in Cells and Zebrafish using Light-Activated Guide RNA. Angewandte Chemie - International Edition 59, 8998–9003 (2020).

[95] Huertas, P. & Jackason, S. P. Human CtIP mediates cell cycle control of DNA end resection and double strand break repair. Journal of Biological Chemistry 284, 9558– 9565 (2009).

[96] Krogh, B. O. & Symington, L. S. Recombination proteins in yeast. Annual Review Genetics 38, 233–271 (2004).

[97] Lee, N. K. et al. Accurate FRET Measurements within Single Diffusing Biomolecules Using Alternating-Laser Excitation. Biophysical Journal 88, 2939–2953 (2005).

[98] Williams, G. J., Lees-Miller, S. P. & Tainer, J. A. Mre11–Rad50–Nbs1 conformations and the control of sensing, signaling, and effector responses at DNA double-strand breaks. DNA repair 9, 1299–1306 (2010).

[99] Jensen, R. B., Carreira, A. & Kowalczykowski, S. C. Purified human BRCA2 stimulates RAD51-mediated recombination. Nature 467, 678–683 (2010).

[100] Shah Punatar, R., Martin, M. J., Wyatt, H. D. M., Chan, Y. W. & West, S. C. Resolution of single and double Holliday junction recombination intermediates by GEN1. PNAS 114, 443–450 (2017).

[101] Wyatt, H., Sarbajna, S., Matos, J. & West, S. Coordinated Actions of SLX1-SLX4 and MUS81-EME1 for Holliday Junction Resolution in Human Cells. Molecular Cell 52, 234–247 (2013).

[102] Kinner, A., Wu, W., Staudt, C. & Iliakis, G. Gamma-H2AX in recognition and signaling of DNA double-strand breaks in the context of chromatin. Nucleic Acids Research 36, 5678–5694 (2008).

[103] Lobrich, M. et al. γH2AX foci analysis for monitoring DNA double-strand break repair: strengths, limitations and optimization. Cell Cycle 9, 662–669 (2010).

[104] Natale, F. et al. Identification of the elementary structural units of the DNA damage response. Nature Communications 8 (2017).

[105] Fumagalli, M. et al. Telomeric DNA damage is irreparable and causes persistent DNA-damage-response activation. Nature Cell Biology 14, 355–65 (2012).

[106] Labay, E. et al. Ionizing radiation-induced foci persistence screen to discover enhancers of accelerated senescence. International journal of high throughput screening 2, 1 (2011).

[107] Markova, E., Torudd, J. & Belyaev, I. Long time persistence of residual 53BP1/g- H2AX foci in human lymphocytes in relationship to apoptosis, chromatin condensation and biological dosimetry. International journal of radiation biology 87, 736–745 (2011).

[108] Olive, P. L., Wlodek, D. & Ban´ath, J. P. DNA double-strand breaks measured in individual cells subjected to gel electrophoresis. Cancer research 51, 4671–6 (1991).

[109] Certo, M. T. et al. Tracking genome engineering outcome at individual DNA breakpoints. Nature Methods 8, 671–676 (2011).

[110] Gunn, A. & Stark, J. M. I-SceI-Based Assays to Examine Distinct Repair Outcomes of Mammalian Chromosomal Double Strand Breaks. DNA Repair Protocols, 379–391

[111] Kuhar, R. et al. Novel fluorescent genome editing reporters for monitoring DNA repair pathway utilization at endonuclease-induced breaks. Nucleic Acids Research 42, e4 (2016).

[112] Allis, C. D. & Jenuwein, T. The molecular hallmarks of epigenetic control. Nature Reviews Genetics 17, 487–500 (2016).

[113] Waddington, C. H. The epigenotype. Endeavour 1, 18–20 (1942).

[114] Waddington, C. H. Canalization of development and the inheritance of acquired characters. Nature 150, 563–565 (1942).

[115] Bannister, A. J. & Kouzarides, T. Regulation of chromatin by histone modifications. Cell Research 21, 381–395 (2011).

[116] Campos, E. I. & Reinberg, D. Histones: Annotating chromatin. Annual Review of Genetics 43, 559–599 (2009).

[117] Trojer, P. & Reinberg, D. Facultative heterochromatin: is there a distinctive molecular signature? Molecular Cell 28, 1–13 (2007).

[118] Amemiya, H. M., Kundaje, A. & Boyle, A. P. The ENCODE Blacklist: Identification of Problematic Regions of the Genome. Scientific Reports 9, 1–5 (2019).

[119] Bannister, A. J. et al. Spatial distribution of di-and tri-methyl lysine 36 of histone H3 at active genes. Journal of Biological Chemistry 280, 17732–17736 (2005).

[120] Kolasinska-Zwierz, P. et al. Differential chromatin marking of introns and expressed exons by H3K36me3. Nature Genetics 41, 376 (2009).

[121] Lavarone, E., Barbieri, C. M. & Pasini, D. Dissecting the role of H3K27 acetylation and methylation in PRC2 mediated control of cellular identity. Nature Communications 10, 1–16 (2019).

[122] Schneider, R. et al. Histone H3 lysine 4 methylation patterns in higher eukaryotic genes. Nature Cell Biology 6, 73–77 (2004).

[123] Sims, R. J. & Reinberg, D. Processing the H3K36me3 signature. Nature Genetics 41, 270–271 (2009).

[124] Boros, J., Arnoult, N., Stroobant, V., Collet, J.-F. & Decottignies, A. Polycomb repressive complex 2 and H3K27me3 cooperate with H3K9 methylation to maintain heterochromatin protein 1 at chromatin. Molecular and cellular biology 34, 3662–74 (2014).

[125] Sparmann, A. & Van Lohuizen, M. Polycomb silencers control cell fate, development and cancer (2006).

[126] Margueron, R. & Reinberg, D. The Polycomb complex PRC2 and its mark in life. Nature 469, 343–349 (2011).

[127] Van Kruijsbergen, I., Hontelez, S. & Veenstra, G. J. C. Recruiting polycomb to chromatin. International Journal of Biochemistry and Cell Biology 67, 177–187 (2015).

[128] Clouaire, T. & Legube, G. DNA double strand break repair pathway choice: a chromatin based decision? Nucleus 6, 107–113 (2015).

[129] Kakarougkas, A. & Jeggo, P. A. DNA DSB repair pathway choice: An orchestrated handover mechanism. British Journal of Radiology 87 (2014).

[130] Shanbhag, N. M., Rafalska-Metcalf, I. U., Balane-Bolivar, C., Janicki, S. M. & Greenberg, R. A. ATM-Dependent chromatin changes silence transcription in cis to dna double-strand breaks. Cell 141, 970–981 (2010).

[131] Shogren-Knaak M, et al. Histone H4-K16 acetylation controls chromatin structure and protein interactions. Science. 311, 5762, 844-847 (2006).

[132] Murr, R. et al. Histone acetylation by Trrap–Tip60 modulates loading of repair proteins and repair of DNA double-strand breaks. Nature Cell Biology 8 (2006).

[133] Renaud, E., Barascu, A. & Rosselli, F. Impaired TIP60-mediated H4K16 acetylation accounts for the aberrant chromatin accumulation of 53BP1 and RAP80 in Fanconi anemia pathway-deficient cells. Nucleic Acids Research 44, 648–656 (2015).

[134] Li ML, et al Phosphorylation of TIP60 suppresses 53BP1 localization at DNA damage sites. Molecular and cellular biology.39, 1, 209-218 (2019).

[135] Sun, Y. et al. Histone H3 methylation links DNA damage detection to activation of the tumour suppressor Tip60. Nature Cell Biology 11 (2009).

[136] Polo, S. E., Kaidi, A., Baskcomb, L., Galanty, Y. & Jackson, S. P. Regulation of DNA-damage responses and cell-cycle progression by the chromatin remodeling factor CHD4. EMBO Journal 29, 3130–3139 (2010).

[137] Stanley, F. K., Moore, S. & Goodarzi, A. A. CHD chromatin remodeling enzymes and the DNA damage response. Mutation Research – Fundamental and Molecular Mechanisms of Mutagenesis 750, 31–44 (2013).

[138] Urquhart, A. J., Gatei, M., Richard, D. J. & Khanna, K. K. ATM mediated phosphorylation of CHD4 contributes to genome maintenance. Genome Integrity 2, 1–12 (2011).

[139] Chiu, S.-m. & Oleinick, N. L. Radioprotection against the formation of DNA double strand breaks in cellular DNA but not native cellular chromatin by the polyamine spermine. Radiation research 148, 188–192 (1997).

[140] Newton, G. L., Aguilera, J. A., Ward, J. F. & Fahey, R. C. Polyamine-induced compaction and aggregation of DNA: a major factor in radioprotection of chromatin under physiological conditions. Radiation research 145, 776–780 (1996).

[141] Xue, L.-Y., Friedman, L. R., Oleinick, N. L. & Chiu, S.-M. Induction of DNA Damage in γ-irradiated Nuclei Stripped of Nuclear Protein Classes: Differential Modulation of Double strand Break and DNA—protein Crosslink Formation. International journal of radiation biology 66, 11–21 (1994).

[142] Ciccarone, F., Zampieri, M. & Caiafa, P. PARP1 orchestrates epigenetic events setting up chromatin domains. Seminars in Cell and Developmental Biology 63, 123–134 (2017).

[143] Ray Chaudhuri, A. & Nussenzweig, A. The multifaceted roles of PARP1 in DNA repair and chromatin remodeling. Nature Reviews Molecular Cell Biology 18, 610– 621 (2017).

[144] Ame, J. C., Spenlehauer, C. & De Murcia, G. The PARP superfamily. BioEssays 26, 882–893 (2004).

[145] d'amours, D., Desnoyers, S., d'silva, I. & Poirier, G. G. Poly(ADPribosyl)-ation reactions in the regulation of nuclear functions. Biochemical Journal 342, 249–268 (1999).

[146] Isabelle, M. et al. Investigation of PARP-1, PARP-2, and PARG interactomes by affinity-purification mass spectrometry. Proteome Science 8, 1–11 (2010).

[147] Jungmichel, S. et al. Proteome-wide identification of poly(ADP-Ribosyl)ation targets in different genotoxic stress responses. Molecular Cell 52, 272–285 (2013).

[148] Huambachano, O., Herrera, F., Rancourt, A. & Satoh, M. S. Double-stranded DNA binding domain of poly(ADP-ribose) polymerase-1 and molecular insight into the regulation of its activity. Journal of Biological Chemistry 286, 7149–7160 (2011).

[149] Messner, S. et al. PARP1 ADP-ribosylates lysine residues of the core histone tails. Nucleic Acids Research 38, 6350–6362 (2010).

[150] Poirier, G. G., Murciat, G. D. E., Jongstra-bilent, J. & Niedergangt, C. Poly(ADPribosyl)-ation of polynucleosomes causes relaxation of chromatin structure 79, 3423–3427 (1982).

[151] Aguilar-Quesada, R. et al. Interaction between ATM and PARP-1 in response to DNA damage and sensitization of ATM deficient cells through PARP inhibition. BMC Molecular Biology 8, 1–8 (2007).

[152] Ali, A. A. et al. The zinc-finger domains of PARP1 cooperate to recognize DNA strand breaks. Nature Structural and Molecular Biology 19, 685–692 (2012).

[153] Haince, J. F. et al. Ataxia telangiectasia mutated (ATM) signaling network is modulated by a novel poly(ADP-ribose)-dependent pathway in the early response to DNA damaging agents. Journal of Biological Chemistry 282, 16441–16453 (2007).

[154] Langelier, M. F. & Pascal, J. M. PARP-1 mechanism for coupling DNA damage detection to poly(ADP-ribose) synthesis. Current Opinion in Structural Biology 23, 134–143 (2013).

[155] Canto, C., Sauve, A. A. & Bai, P. Crosstalk between poly(ADP-ribose) polymerase and sirtuin enzymes. Molecular Aspects of Medicine 34, 1168–1201 (2013).

[156] Liu, T., Liu, P. Y. &Marshall, G.M. The critical role of the class III histone deacetylase SIRT1 in cancer. Cancer Research 69, 1702–1705 (2009).

[157] Malik, N. & Smulson, M. A Relationship between Nuclear Poly(adenosine diphosphate ribosylation) and Acetylation Posttranslational Modifications. 1. Nucleosome Studies. Biochemistry 23, 3721–3725 (1984).

[158] Verdone, L. et al. Poly(ADP-ribosyl)ation affects histone acetylation and transcription. PLoS ONE 10, 1–14 (2015).

[159] Krishnakumar, R. & Kraus, W. L. PARP-1 Regulates Chromatin Structure and Transcription through a KDM5B-Dependent Pathway. Molecular Cell 39, 736–749 (2010).

[160] Xi, L. & Cech, T. R. Inventory of telomerase components in human cells reveals multiple subpopulations of hTR and hTERT. Nucleic Acids Research 42, 8565–8577 (2014).

[161] Caron, P. et al. WWP2 ubiquitylates RNA polymerase II for DNA-PK-dependent transcription arrest and repair at DNA breaks. Genes & Development 33, 684–704 (2019).

[162] Fischle, W. Tip60-ing the balance in dSB repair. Nature Cell Biology 11 (2009).

[163] Ballare, C. et al. Phf19 links methylated Lys36 of histone H3 to regulation of Polycomb activity. Nature Structural & Molecular Biology 19, 1257–1265 (2012).

[164] Pellegrino, S., Michelena, J., Teloni, F., Imhof, R. & Altmeyer, M. Replication-Coupled Dilution of H4K20me2 Guides 53BP1 to Pre-replicative Chromatin. Cell Reports 19, 1819–1831 (2017).

[165] Huyen, Y. et al. Methylated lysine 79 of histone H3 targets 53BP1 to DNA doubles trand breaks. Nature 432, 406–411 (2004).

[166] Noon, A. T. et al. 53BP1-dependent robust localized KAP-1 phosphorylation is essential for heterochromatic DNA double-strand break repair. Nature Cell Biology 12, 177–184 (2010).

[167] Kalousi, A. et al. The nuclear oncogene SET controls DNA repair by KAP1 and HP1 retention to chromatin. Cell Reports 11, 149–163 (2015).

[168] Aymard, F. et al. Transcriptionally active chromatin recruits homologous recombination at DNA double-strand breaks. Nature Structural and Molecular Biology 21, 366–374 (2014).

[169] Clouaire, T. et al. Comprehensive Mapping of Histone Modifications at DNA Double- Strand Breaks Deciphers Repair Pathway Chromatin Signatures. Molecular Cell 72, 250–262 (2018).

[170] Mourad, R., Ginalski, K., Legube, G. & Cuvier, O. Predicting double-strand DNA breaks using epigenome marks or DNA at kilobase resolution. Genome Biology 19, 34 (2018).

[171] Richardson, C. D., Kazane, K. R., Feng, S. J. & Bray, N. L. CRISPR-Cas9 Genome Editing in Human Cells Works Via The Fanconi Anemia Pathway. bioRxiv (2017).

[172] Janssen, A., Colmenares, S. U., Lee, T. & Karpen, G. H. Timely double-strand break repair and pathway choice in pericentromeric heterochromatin depend on the histone demethylase dKDM4A. bioRxiv 295220 (2018).

[173] Churikov, D. et al. SUMO-Dependent Relocalization of Eroded Telomeres to Nuclear Pore Complexes Controls Telomere Recombination. Cell Reports 15, 1242–1253 (2016).

[174] Oza, P., Jaspersen, S. L., Miele, A., Dekker, J. & Peterson, C. L. Mechanisms that regulate localization of a DNA double-strand break to the nuclear periphery. Genes and Development 23, 912–927 (2009).

[175] Ryu, T. et al. Heterochromatic breaks move to the nuclear periphery to continue recombinational repair. Nature Cell Biology 17, 1401–1411 (2015).

[176] Mattarocci, S. et al. Rif1 maintains telomeres and mediates DNA repair by encasing DNA ends. Nature Structural & Molecular Biology 24, 588–595 (2017).

[177] Ribes-Zamora, A., Indiviglio, S. M., Mihalek, I., Williams, C. L. & Bertuch, A. A. TRF2 Interaction with Ku Heterotetramerization Interface Gives Insight into c- NHEJ Prevention at Human Telomeres. Cell Reports 5, 194–206 (2013).

[178] Rowley, M. J. & Corces, V. G. Organizational principles of 3D genome architecture. Nature Reviews Genetics 19, 789–800 (2018).

[179] Gelot, C. et al. The Cohesin Complex Prevents the End Joining of Distant DNA Double-Strand Ends. Molecular Cell 61, 15–26 (2016).

[180] Lang, F. et al. CTCF prevents genomic instability by promoting homologous recombination-directed DNA double-strand break repair. PNAS 114, 10912–10917 (2017).

[181] Strom, L., Lindroos, H. B., Shirahige, K. & Sjogren, C. Postreplicative recruitment of cohesin to double-strand breaks is required for DNA repair. Molecular Cell 16, 1003–1015 (2004).

[182] Arnould, C. et al. Loop extrusion as a mechanism for formation of DNA damage repair foci. Nature 590, 660–665 (2021).

[183] Davidson, I. F. et al. DNA loop extrusion by human cohesin. Science 366, 1338–1345 (2019).

[184] Collins, P. L. et al. DNA double-strand breaks induce H2Ax phosphorylation domains in a contact-dependent manner. Nature Communications 11 (2020).

[185] Ochs, F. et al. Stabilization of chromatin topology safeguards genome integrity. Nature 574, 571–574 (2019).

[186] Alatwi, H. E. & Downs, J. A. Removal of H2A.Z by INO 80 promotes homologous recombination. EMBO reports 16, 986–994 (2015).

[187] Gursoy-Yuzugullu, O., Ayrapetov, M. K. & Price, B. D. Correction for Histone chaperone Anp32e removes H2A.Z from DNA double-strand breaks and promotes nucleosome reorganization and DNA repair. PNAS 112, E3750 (2015).

[188] Xu, Y. et al. Histone H2A.Z Controls a Critical Chromatin Remodeling Step Required for DNA Double-Strand Break Repair. Molecular Cell 48, 723–733 (2012).

[189] Georgoulis, A., Vorgias, C. E., Chrousos, G. P. & Rogakou, E. P. Genome instability and γH2AX. International Journal of Molecular Sciences 18, 1–10 (2017).

[190] Gao, S.-B. et al. Enhancing chemotherapy sensitivity by targeting PcG via the ATM/p53 pathway. American journal of cancer research 7, 1874 (2017).

[191] Alver, B. H. et al. The SWI/SNF chromatin remodeling complex is required for maintenance of lineage specific enhancers. Nature communications 8, 1–10 (2017).

[192] Mittal P, Roberts CW. The SWI/SNF complex in cancer—biology, biomarkers and therapy. Nature Reviews Clinical Oncology.17, 7, 435-448(2020).

[193] Hodges, C., Kirkland, J. G. & Crabtree, G. R. The many roles of BAF (mSWI/SNF) and PBAF complexes in cancer. Cold Spring Harbor Perspectives in Medicine 6, 1–25(2016).

[194] Kassis, J. A., Kennison, J. A. & Tamkun, J. W. Polycomb and trithorax group genes in drosophila. Genetics 206, 1699–1725 (2017).

[195] Raab, J. R., Resnick, S. & Magnuson, T. Genome-wide transcriptional regulation mediated by biochemically distinct SWI/SNF complexes. PLoS genetics 11, (2015).

[196] Wang, W. et al. Purification and biochemical heterogeneity of the mammalian SWISNF complex. EMBO Journal 15, 5370–5382 (1996).

[197] Kaeser, M. D., Aslanian, A., Dong, M. Q., Yates, J. R. & Emerson, B. M. BRD7, a novel PBAF-specific SWI/SNF subunit, is required for target gene activation and repression in embryonic stem cells. Journal of Biological Chemistry 283, 32254–32263 (2008).

[198] Middeljans, E. et al. SS18 together with animal-specific factors defines human BAFtype SWI/SNF complexes. PLoS ONE 7 (2012).

[199] Jaskelioff, M., M. Gavin, I., Peterson, C. L. & Logie, C. SWI-SNF-Mediated Nucleosome Remodeling: Role of Histone Octamer Mobility in the

Persistence of the Remodeled State. Molecular and Cellular Biology 20, 3058–3068 (2000).

[200] Cote, J., Peterson, C. L. & Workman, J. L. Perturbation of nucleosome core structure by the SWI/SNF complex persists after its detachment, enhancing subsequent transcription factor binding. PNAS 95, 4947–4952 (1998).

[201] Kassabov, S. R., Zhang, B., Persinger, J. & Bartholomew, B. SWI/SNF unwraps, slides, and rewraps the nucleosome. Molecular Cell 11, 391–403 (2003).

[202] Koyama, H., Itoh, M., Miyahara, K. & Tsuchiya, E. Abundance of the RSC nucleosome-remodeling complex is important for the cells to tolerate DNA damage in Saccharomyces cerevisiae. FEBS Letters 531, 215–221 (2002).

[203] Shim, E. Y., Ma, J.-l., Oum, J.-h., Yanez, Y. & Lee, S. E. The Yeast Chromatin Remodeler RSC Complex Facilitates End Joining Repair of DNA Double-Strand Breaks Molecular and Cellular Biology 25, 3934–3944 (2005).

[204] Kakarougkas, A. et al. Requirement for PBAF in transcriptional repression and repair at DNA breaks in actively transcribed regions of chromatin. Molecular Cell 55, 723–732 (2014).

[205] Lee, J. et al. Supplementary to Single-molecule four-color FRET. Angewandte Chemie - International Edition 49, 9922–9925 (2010).

[206] Park, J.-H. et al. Mammalian SWI/SNF complexes facilitate DNA double-strand break repair by promoting c-H2AX induction. The EMBO Journal 25, 3986–3997 (2006).

[207] Ogiwara, H. et al. Histone acetylation by CBP and p300 at double-strand break sites facilitates SWI/SNF chromatin remodeling and the recruitment of non-homologous end joining factors. Oncogene 30, 2135–2146 (2011).

[208] Smeenk, G. et al. Poly (ADP-ribosyl) ation links the chromatin remodeler SMARCA5/SNF2H to RNF168-dependent DNA damage signaling. Journal of cell science 126, 889–903 (2013).

[209] Toiber, D. et al. SIRT6 recruits SNF2H to DNA break sites, preventing genomic instability through chromatin remodeling. Molecular Cell 51, 454–468 (2013).

[210] Hays, E. et al. The SWI/SNF ATPase BRG1 stimulates DNA end resection and homologous recombination by reducing nucleosome density at DNA double strand breaks and by promoting the recruitment of the CtIP nuclease. Cell Cycle 19, 3096– 3114 (2020).

[211] Wiest, N. E., Houghtaling, S., Sanchez, J. C., Tomkinson, A. E. & Osley, M. A. The SWI/SNF ATP-dependent nucleosome remodeler promotes resection initiation at a DNA double-strand break in yeast. Nucleic Acids Research 45, 5887–5900 (2017).

[212] Zhang, W., Qu, J., Liu, G. H. & Belmonte, J. C. I. The ageing epigenome and its rejuvenation. Nature Reviews Molecular Cell Biology 21, 137–150 (2020).

[213] Benayoun, B. A., Pollina, E. A. & Brunet, A. Epigenetic regulation of ageing: Linking environmental inputs to genomic stability. Nature Reviews Molecular Cell Biology 16, 593–610 (2015).

[214] Sen, P., Shah, P. P., Nativio, R. & Berger, S. L. Epigenetic mechanisms of longevity and aging. Cell 166, 822–839 (2016).

[215] O'hagan, H. M. et al. Oxidative Damage Targets Complexes Containing DNA Methyltransferases, SIRT1, and Polycomb Members to Promoter CpG Islands. Cancer Cell 20, 606–619 (2011).

[216] Paredes, S. et al. The epigenetic regulator SIRT7 guards against mammalian cellular senescence induced by ribosomal DNA instability. Journal of Biological Chemistry 293, 11242–11250 (2018).

[217] Grube, K. & Burkle, A. Poly(ADP-ribose) polymerase activity in mononuclear leukocytes of 13 mammalian species correlates with species-specific life span. PNAS 89, 11759–11763 (1992).

[218] Lee, J.-H., Kim, E. W., Croteau, D. L. & Bohr, V. A. Heterochromatin: an epigenetic point of view in aging. Experimental & Molecular Medicine 52, 1466–1474 (2020).

[219] Greer, E. L. et al. Members of the H3K4 trimethylation complex regulate lifespan in a germline-dependent manner in C. elegans. Nature 466, 383–387 (2010).

[220] Ito, T. et al. Regulation of Cellular Senescence by Polycomb Chromatin Modifiers through Distinct DNA Damage- and Histone Methylation-Dependent Pathways. Cell Reports 22, 3480–3492 (2018).

[221] Kim, J. A. & Haber, J. E. Chromatin assembly factors Asf1 and CAF-1 have overlapping roles in deactivating the DNA damage checkpoint when DNA repair is complete. PNAS 106, 1151–1156 (2009).

[222] Lewis, E. B. & Mislove, R. F. New mutants report. Drosoph. Inf. Serv 21, 69 (1947).

[223] Beisel, C. et al. Comparing active and repressed expression states of genes controlled by the Polycomb/Trithorax group proteins. PNAS 104, 16615–16620 (2007).

[224] Fischle, W. et al. Molecular basis for the discrimination of repressive methyl lysine marks in histone H3 by Polycomb and HP1 chromodomains. Genes & Development 17, 1870–1881 (2003).

[225] Schwartz, Y. B. et al. Genome-wide analysis of Polycomb targets in Drosophila melanogaster. Nature Genetics 38, 700–705 (2006).

[226] Simon, J., Chiang, A., Bender, W., Shimell, M. J. & O'Connor, M. Elements of the Drosophila bithorax complex that mediate repression by Polycomb group products. Developmental Biology 158, 131–144 (1993).

[227] Ferrari, K. J. et al. Polycomb-dependent H3K27me1 and H3K27me2 regulate active transcription and enhancer fidelity. Molecular Cell 53, 49–62 (2014).

[228] Margueron, R. et al. Role of the polycomb protein EED in the propagation of repressive histone marks. Nature 461, 762–767 (2009).

[229] Kassis, J. A. & Brown, J. L. Polycomb group response elements in Drosophila and vertebrates. Advances in genetics 81, 83–118 (2013).

[230] Steffen, P. A. & Ringrose, L. What are memories made of? How Polycomb and Trithorax proteins mediate epigenetic memory. Nature Reviews Molecular Cell Biology 15, 340–356 (2014).

[231] Chan, C.-S., Rastelli, L. & Pirrotta, V. A Polycomb response element in the Ubx gene that determines an epigenetically inherited state of repression. The EMBO journal 13, 2553–2564 (1994).

[232] Woo, C. J., Kharchenko, P. V., Daheron, L., Park, P. J. & Kingston, R. E. A region of the human HOXD cluster that confers polycomb-group responsiveness. Cell 140, 99–110 (2010).

[233] Sing, A. et al. A vertebrate Polycomb response element governs segmentation of the posterior hindbrain. Cell 138, 885–897 (2009).

[234] Mendenhall, E. M. et al. GC-rich sequence elements recruit PRC2 in mammalian ES cells. PLoS Genetics 6, e1001244 (2010).

[235] Schuettengruber, B., Bourbon, H.-M., Croce, L. D. & Cavalli, G. Leading Edge Review Genome Regulation by Polycomb and Trithorax: 70 Years and Counting. Cell 171, 34–57 (2017).

[236] Kleer CG, et al. EZH2 is a marker of aggressive breast cancer and promotes neoplastic transformation of breast epithelial cells. PNAS, 100, 20,11606-11611 (2003).

[237] Kim, K. H. & Roberts, C. W. M. Targeting EZH2 in cancer. Nature medicine 22, 128–134 (2016).

[238] Gonzalez, M. E. et al. EZH2 expands breast stem cells through activation of NOTCH1 signaling. PNAS 111, 3098–3103 (2014).

[239] Wen, Y., Cai, J., Hou, Y., Huang, Z. & Wang, Z. Role of EZH2 in cancer stem cells: from biological insight to a therapeutic target. Oncotarget 8, 37974–37990 (2017).

[240] Harutyunyan, A. S. et al. H3K27M induces defective chromatin spread of PRC2- mediated repressive H3K27me2/me3 and is essential for glioma tumorigenesis. Nature Communications 10 (2019).

[241] Harutyunyan, A. S. et al. H3K27M in Gliomas Causes a One-Step Decrease in H3K27 Methylation and Reduced Spreading within the Constraints of H3K36 Methylation. Cell Reports 33, 108390 (2020).

[242] de Napoles, M. et al. Polycomb group proteins ring1A/B link ubiquitylation of histone H2A to heritable gene silencing and X inactivation. Developmental Cell 7, 663–676 (2004).

[243] Endoh, M. et al. Histone H2A mono-ubiquitination is a crucial step to mediate PRC1- dependent repression of developmental genes to maintain ES cell identity. PLoS Genetics 8 (2012).

[244] Stock, J. K. et al. Ring1-mediated ubiquitination of H2A restrains poised RNA polymerase II at bivalent genes in mouse ES cells. Nature Cell Biology 9, 1428–1435 (2007).

[245] Loubiere, V. et al. Coordinate redeployment of PRC1 proteins suppresses tumor formation during Drosophila development. Nature Genetics 48, 1436–1442 (2016).

[246] Tolhuis, B. et al. Genome-wide profiling of PRC1 and PRC2 Polycomb chromatin binding in Drosophila melanogaster. Nature Genetics 38, 694–699 (2006).

[247] Eagen, K. P., Aiden, E. L. & Kornberg, R. D. Polycomb-mediated chromatin loops revealed by a subkilobase-resolution chromatin interaction map. PNAS 114, 8764–8769 (2017).

[248] Kondo, T. et al. Polycomb Potentiates Meis2 Activation in Midbrain by Mediating Interaction of the Promoter with a Tissue-Specific Enhancer. Developmental Cell 28, 94–101 (2014).

[249] Fradet-Turcotte, A. et al. 53BP1 is a reader of the DNA-damage-induced H2A Lys 15 ubiquitin mark. Nature 499, 50–54 (2013).

[250] Mattiroli, F. et al. RNF168 ubiquitinates K13-15 on H2A/H2AX to drive DNA damage signaling. Cell 150, 1182–1195 (2012).

[251] Mattiroli, F. & Penengo, L. Histone Ubiquitination: An Integrative Signaling Platform in Genome Stability. Trends in Genetics 37, 566–581 (2021).

[252] Uckelmann, M. & Sixma, T. K. Histone ubiquitination in the DNA damage response. DNA Repair 56, 92–101 (2017).

[253] Chou, D. M. et al. A chromatin localization screen reveals poly (ADP ribose)-regulated recruitment of the repressive polycomb and NuRD complexes to sites of DNA damage. PNAS 107, 18475–18480 (2010).

[254] Efimova, E. V. et al. DNA Damage and Repair Linking Cancer Metabolism to DNA Repair and Accelerated Senescence. Molecular Cancer Research 14, 2, 173-184 (2016).

[255] Lensing, S. V. et al. DSBCapture: in situ capture and sequencing of DNA breaks. Nature Methods 13, 855–857 (2016).

[256] Caruso, L. B. et al. Poly(ADP-ribose) Polymerase 1, PARP1, modifies EZH2 and inhibits EZH2 histone methyltransferase activity after DNA damage. Oncotarget 9, 10585–10605 (2018).

[257] Li, J. et al. EZH2-mediated H3K27 trimethylation mediates neurodegeneration in ataxia-telangiectasia. Nature neuroscience. 16, 12 1745-1753 (2013)

[258] Sinclair, A. M. et al. Lymphoid apoptosis and myeloid hyperplasia in CCAAT displacement protein mutant mice. Blood 98, 3658–67 (2001).

[259] An, N. et al. Gene dosage effect of CUX1 in a murine model disrupts HSC homeostasis and controls the severity and mortality of MDS. Blood 131, 2682–2697 (2018).

[260] McNerney, M. E. et al. CUX1 is a haploinsufficient tumor suppressor gene on chromosome 7 frequently inactivated in acute myeloid leukemia. Blood 121, 975–983 (2013).

[261] Arthur, R. K., An, N., Kahn, S. & McNerney, M. E. Enhancer-Promoter Looping Deciphers Dosage of the Haploinsufficient Transcription Factor, CUX1. Blood 128 (2016).

[262] Kaur, S. et al. CUX1 stimulates APE1 enzymatic activity and increases the resistance of glioblastoma cells to the mono-alkylating agent temozolomide. Neuro-Oncology 20, 484–493 (2018).

[263] Ramdzan, Z. M. et al. RAS Transformation Requires CUX1-Dependent Repair of Oxidative DNA Damage. PLoS Biology 12 (2014).

[264] Huang, B. et al. DNA-PKcs Associates With PLK1 and Is Involved in Proper Chromosome Segregation and Cytokinesis. Journal of Cellular Biochemistry 115, 1077–1088 (2014).

[265] Sansregret, L. et al. Cut homeobox 1 causes chromosomal instability by promoting bipolar division after cytokinesis failure. PNAS 108, 1949–1954 (2011).

[266] Imgruet, M. K. et al. Loss of a 7q gene, CUX1, disrupts epigenetic-driven DNA repair and drives therapy-related myeloid neoplasms. Blood (2021).

[267] Gong, F. et al. Screen identifies bromodomain protein ZMYND8 in chromatin recognition of transcription-associated DNA damage that promotes homologous recombination. Genes and Development 29, 197–211 (2015).

[268] Arends, T. et al. CHD4 is essential for transcriptional repression and lineage progression in B lymphopoiesis. PNAS 166, 10927–10936 (2019).

[269] Xia, L. et al. CHD4 Has Oncogenic Functions in Initiating and Maintaining Epigenetic Suppression of Multiple Tumor Suppressor Genes. Cancer Cell 31, 653–668 (2017).

[270] Campbell, S., Ismail, I. H., Young, L. C., Poirier, G. G. & Hendzel, M. J. Polycomb repressive complex 2 contributes to DNA double strand break repair. Cell Cycle 12, 2675–2683 (2013).

[271] Chou, D. M. et al. A chromatin localization screen reveals poly (ADP ribose)-regulated recruitment of the repressive polycomb and NuRD complexes to sites of DNA damage. PNAS 107, 18475–18480 (2010).

[272] Burgess, R. C., Burman, B., Kruhlak, M. J. & Misteli, T. Activation of DNA Damage Response Signaling by Condensed Chromatin. Cell Reports 9, 1703–1718 (2014).

[273] Floyd, S. R. et al. The bromodomain protein Brd4 insulates chromatin from DNA damage signaling. Nature 498, 246–250 (2013).

[274] Chiolo, I. et al. Double-Strand Breaks in Heterochromatin Move Outside of a Dynamic HP1a Domain to Complete Recombinational Repair. Cell 144, 732–744 (2011).

[275] Barski, A. et al. High-resolution profiling of histone methylations in the human genome. Cell 129, 823–837 (2007).

[276] Jin, C. et al. H3. 3/H2A. Z double variant–containing nucleosomes mark nucleosome free regions of active promoters and other regulatory regions. Nature Genetics 41, 941–945 (2009).

[277] Guo, Y., Zhao, S. & Wang, G. G. Polycomb Gene Silencing Mechanisms: PRC2 Chromatin Targeting, H3K27me3'Readout', and Phase Separation-Based Compaction. Trends in Genetics (2021).

[278] Sainsbury, S., Bernecky, C. & Cramer, P. Structural basis of transcription initiation by RNA polymerase II. Nature reviews Molecular Cell Biology 16, 129–143 (2015).

[279] Eick, D. & Geyer, M. The RNA Polymerase II Carboxy-Terminal Domain (CTD) Code Chemical reviews. 113, 11, 8456-8490. (2013).

[280] Harlen, K. M. et al. Comprehensive RNA Polymerase II Interactomes Reveal Distinct and Varied Roles for Each Phospho-CTD Residue. Cell Reports 15, 2147–2158 (2016).

[281] Milligan, L. et al. Strand-specific, high-resolution mapping of modified RNA polymerase II. Molecular Systems Biology 12, 874 (2016).

[282] Zaborowska, J., Egloff, S. & Murphy, S. The pol II CTD: New twists in the tail. Nature Structural and Molecular Biology 23, 771–777 (2016).

[283] Awwad, S. W., Abu-Zhayia, E. R., Guttmann-Raviv, N. & Ayoub, N. NELF-E is recruited to DNA double-strand break sites to promote transcriptional repression and repair. EMBO reports 18, 745–764 (2017).

[284] Pessina, F. et al. Functional transcription promoters at DNA double-strand breaks mediate RNA-driven phase separation of damage-response factors. Nature Cell Biology 21, 1286–1299 (2019).

[285] Bunch, H. et al. Transcriptional elongation requires DNA break-induced signaling. Nature Communications 6 (2015).

[286] De Bont, R. & van Larebeke, N. Endogenous DNA damage in humans: A review of quantitative data. Mutagenesis 19, 169–185 (2004).

[287] Haradhvala, N. J. et al. Mutational Strand Asymmetries in Cancer Genomes Reveal Mechanisms of DNA Damage and Repair. Cell 164, 538–549 (2016).

[288] Tubbs, A. & Nussenzweig, A. Endogenous DNA Damage as a Source of Genomic Instability in Cancer. Cell 168, 644–656 (2017).

[289] Smirnov, E. et al. Separation of replication and transcription domains in nucleoli. Journal of Structural Biology 188, 259–266 (2014).

[290] Srivatsan, A., Tehranchi, A., MacAlpine, D. M. & Wang, J. D. Co-orientation of replication and transcription preserves genome integrity. PLoS Genetics 6 (2010).

[291] Brambati, A., Colosio, A., Zardoni, L., Galanti, L. & Liberi, G. Replication and transcription on a collision course: Eukaryotic regulation mechanisms and implications for DNA stability. Frontiers in Genetics 6, 1–8 (2015).

[292] Garcia-Muse, T. & Aguilera, A. Transcription-replication conflicts: How they occur and how they are resolved. Nature Reviews Molecular Cell Biology 17, 553–563 (2016).

[293] Helmrich, A., Ballarino, M. & Tora, L. Collisions between replication and transcription complexes cause common fragile site instability at the longest human genes. Molecular Cell 44, 966–977 (2011).

[294] Zou, L. & Elledge, S. J. Sensing DNA damage through ATRIP recognition of RPAssDNA complexes. Science 300, 1542–1548 (2003).

[295] Casper, A. M., Nghiem, P., Arlt, M. F. & Glover, T. W. ATR regulates fragile site stability. Cell 111, 779–789 (2002).

[296] Couch, F. B. et al. ATR phosphorylates SMARCAL1 to prevent replication fork collapse. Genes and Development 27, 1610–1623 (2013).

[297] Im, J. S. et al. ATR checkpoint kinase and CRL1TRCP collaborate to degrade ASF1 and thus repress genes overlapping with clusters of stalled replication forks. Genes and Development 28, 875–887 (2014).

[298] Koundrioukoff, S. et al. Stepwise Activation of the ATR Signaling Pathway upon Increasing Replication Stress Impacts Fragile Site Integrity. PLoS Genetics 9 (2013).

[299] Barlow, J. H. et al. Identification of early replicating fragile sites that contribute to genome instability. Cell 152, 620–632 (2013).

[300] Costanzo, V. et al. An ATR- and Cdc7-dependent DNA damage checkpoint that inhibits initiation of DNA replication. Molecular Cell 11, 203–213 (2003).

[301] Kruhlak, M. et al. The ATM repair pathway inhibits RNA polymerase I transcription in response to chromosome breaks. Nature 447, 730–734 (2007).

[302] Hamperl, S., Bocek, M. J., Saldivar, J. C., Swigut, T. & Cimprich, K. A. Transcription-Replication Conflict Orientation Modulates R-Loop Levels and Activates Distinct DNA Damage Responses. Cell 170, 774–786 (2017).

[303] Franchitto, A. Genome instability at common fragile sites: searching for the cause of their instability. BioMed research international (2013).

[304] Gumucs, G., Sungurouglu, A., Tukun, A., Sayin, D. B. & Bokesoy, I. Common fragile sites associated with the breakpoints of chromosomal aberrations in hematologic neoplasms. Cancer genetics and cytogenetics 133, 168–171 (2002).

[305] Ma, K. et al. Common fragile sites: genomic hotspots of DNA damage and carcinogenesis. International journal of molecular sciences 13, 11974–11999 (2012).

[306] Le Beau, M. M. et al. Replication of a common fragile site, FRA3B, occurs late in S phase and is delayed further upon induction: Implications for the mechanism of fragile site induction. Human Molecular Genetics 7, 755–761 (1998).

[307] Wang, L. et al. Allele-specific late replication and fragility of the most active common fragile site, FRA3B. Human Molecular Genetics 8, 431–437 (1999).

[308] Howlett, N. G., Taniguchi, T., Durkin, S. G., D'Andrea, A. D. & Glover, T. W. The Fanconi anemia pathway is required for the DNA replication stress response and for the regulation of common fragile site stability. Human Molecular Genetics 14, 693–701(2005).

[309] Madireddy, A. et al. FANCD2 Facilitates Replication through Common Fragile Sites. Molecular Cell 64, 388–404 (2016).

[310] Pankotai, T., Bonhomme, C., Chen, D. & Soutoglou, E. DNAPKcs-dependent arrest of RNA polymerase II transcription in the presence of DNA breaks. Nature Structural and Molecular Biology 19, 276–282 (2012).

[311] Ayrapetov, M. K., Gursoy-Yuzugullu, O., Xu, C., Xu, Y. & Price, B. D. DNA double strand breaks promote methylation of histone H3 on lysine 9 and transient formation of repressive chromatin. PNAS 111, 9169–9174 (2014).

[312] Young, L. C., McDonald, D. W. & Hendzel, M. J. Kdm4b histone demethylase is a DNA damage response protein and confers a survival advantage following γ-irradiation. Journal of Biological Chemistry 288, 21376–21388 (2013).

[313] Campbell, S., Ismail, I. H., Young, L. C., Poirier, G. G. & Hendzel, M. J. Polycomb repressive complex 2 contributes to DNA double-strand break repair. Cell Cycle 12, 2675–2683 (2013).

[314] Long Q, Liu Z, Gullerova M. Sweet Melody or Jazz? Transcription Around DNA Double-Strand Breaks. Frontiers in Molecular Biosciences 8:1–14 (2021).

[315] Vitelli V, Galbiati A, Iannelli F, Pessina F, Sharma S, D'Adda di Fagagna F. Recent Advancements in DNA Damage-Transcription Crosstalk and High-Resolution Mapping of DNA Breaks. Annual Review of Genomics and Human Genetics 18:87–113 (2017).

[316] D'Alessandro G, di Fagagna F d'Adda. Transcription and DNA damage: holding hands or crossing swords? Journal of molecular biology. Journal of Molecular Biology 429:3215–29 (2017).

[317] Sharma S, Anand R, Zhang X, Francia S, Michelini F, Galbiati A, Williams H, Ronato DA, Masson JY, Rothenberg E, Cejka P. MRE11-RAD50-NBS1 complex is sufficient to promote transcription by RNA polymerase II at double-strand breaks by melting DNA ends. Cell Reports 5;34(1):108565 (2021).

[318] Michelini, F., Pitchiaya, S., Vitelli, V., Sharma, S., Gioia, U., Pessina, F., Cabrini, M., Wang, Y., Capozzo, I., Iannelli, F. and Matti, V.Damage-induced lncRNAs control the DNA damage response through interaction with DDRNAs at individual double-strand breaks. Nature Cell Biology 19:1400–11 (2017).

[319] Francia, S. et al. Site-specific DICER and DROSHA RNA products control the DNA damage response. Nature 488, 231–235 (2012).

[320] Lu, W.-T. et al. Drosha drives the formation of DNA: RNA hybrids around DNA break sites to facilitate DNA repair. Nature communications 9, 1–13 (2018).

[321] Michalik, K. M., Bottcher, R. & Forstemann, K. A small RNA response at DNA ends in Drosophila. Nucleic Acids Research 40, 9596–9603 (2012).

[322] Wei, W. et al. A role for small RNAs in DNA double-strand break repair. Cell 149, 101–112 (2012).

[323] Chitale, S. & Richly, H. DICER and ZRF1 contribute to chromatin decondensation during nucleotide excision repair. Nucleic Acids Research 45, 5901–5912 (2017).

[324] Rouquette, J. et al. Double-strand break-induced transcriptional silencing is associated with loss of tri-methylation at H3K4. Chromosome Research 19, 883–899 (2011).

[325] Michelini, F. et al. Damage-induced lncRNAs control the DNA damage response through interaction with DDRNAs at individual double strand breaks. Nature Cell Biology 19, 1400–1411 (2017).

[326] Sharma, S. et al. MRE11-RAD50-NBS1 Complex Is Sufficient to Promote Transcription by RNA Polymerase II at Double-Strand Breaks by Melting DNA Ends. Cell Reports 34, 108565 (2021).

[327] Cramer, P. Structure and function of RNA polymerase II. Advances in protein chemistry 67, 1–42 (2004).

[328] Hanawalt, P. C. & Spivak, G. Transcription-coupled DNA repair: Two decades of progress and surprises. Nature Reviews Molecular Cell Biology 9, 958–970 (2008).

[329] Lesage, E., Clouaire, T. & Legube, G. Repair of DNA double-strand breaks in RNAPI- and RNAPII-transcribed loci. DNA Repair 104, 103139 (2021).

[330] Marnef, A. & Legube, G. Organizing DNA repair in the nucleus: DSBs hit the road. Current Opinion in Cell Biology 46, 1–8 (2017).

[331] Pfister, S. X. et al. SETD2-Dependent Histone H3K36 Trimethylation Is Required for Homologous Recombination Repair and Genome Stability. Cell Reports 7, 2006–2018 (2014).

[332] Paquin, K. L. & Howlett, N. G. Understanding the histone DNA repair code: H4K20me2 makes its mark. Molecular Cancer Research 16, 1335–1345 (2018).

[333] Ouyang, J. et al. RNA transcripts stimulate homologous recombination by forming DR-loops. Nature 594, 283–288 (2021).

[334] Keskin, H. et al. Transcript-RNA-templated DNA recombination and repair. Nature 515, 436–439 (2014).

[335] D'Alessandro, G. et al. BRCA2 controls DNA:RNA hybrid level at DSBs by mediating RNase H2 recruitment. Nature Communications 9 (2018).

[336] Ohle, C. et al. Transient RNA-DNA Hybrids Are Required for Efficient Double-Strand Break Repair. Cell 167, 1001–1013 (2016).

[337] Ginno, P. A., Lott, P. L., Christensen, H. C., Korf, I. & Ch´edin, F. R-Loop Formation Is a Distinctive Characteristic of Unmethylated Human CpG Island Promoters. Molecular Cell 45, 814–825 (2012).

[338] Sanz, L. A. et al. Prevalent, Dynamic, and Conserved R-Loop Structures Associate with Specific Epigenomic Signatures in Mammals. Molecular Cell 63, 167–178 (2016).

[339] Tan-Wong, S. M., Dhir, S. & Proudfoot, N. J. R-Loops Promote Antisense Transcription across the Mammalian Genome. Molecular Cell 76, 600–616 (2019).

[340] Uesaka, M. et al. Bidirectional promoters are the major source of gene activation-associated non-coding RNAs in mammals. BMC Genomics 15 (2014).

[341] Gan, W. et al. R-loop-mediated genomic instability is caused by impairment of replication fork progression. Genes and Development 25, 2041–2056 (2011).

[342] Cohen, S. et al. Senataxin resolves RNA:DNA hybrids forming at DNA double strand breaks to prevent translocations. Nature Communications 9 (2018).

[343] Promonet, A. et al. Topoisomerase 1 prevents replication stress at R-loop-enriched transcription termination sites. Nature Communications 11, 1–12 (2020).

[344] Shivji, M. K., Renaudin, X., Williams, H. & Venkitaraman, A. R. BRCA2 Regulates Transcription Elongation by RNA Polymerase II to Prevent R-Loop Accumulation. Cell Reports 22, 1031–1039 (2018).

[345] Zatreanu, D. et al. Elongation Factor TFIIS Prevents Transcription Stress and R-Loop Accumulation to Maintain Genome Stability. Molecular Cell 76, 57–69 (2019).

[346] Zhang, X. et al. Attenuation of RNA polymerase II pausing mitigates BRCA1- associated R-loop accumulation and tumorigenesis. Nature Communications 8, 1–11 (2017).

[347] Vitor, A. C. et al. Single-molecule imaging of transcription at damaged chromatin. Science Advances 5 (2019).

[348] Meers, C. et al. Genetic Characterization of Three Distinct Mechanisms Supporting RNA-Driven DNA Repair and Modification Reveals Major Role of DNA Polymerase. Molecular Cell 79, 1037–1050 (2020).

[349] Hatchi, E. et al. BRCA1 recruitment to transcriptional pause sites is required for R-loop-driven DNA damage repair. Molecular Cell 57, 636–647 (2015).

[350] Skourti-Stathaki, K. et al. R-Loops Enhance Polycomb Repression at a Subset of Developmental Regulator Genes. Molecular Cell 73, 930–945 (2019).

[351] Yasuhara, T. et al. Human Rad52 Promotes XPG-Mediated R-loop Processing to Initiate Transcription-Associated Homologous Recombination Repair. Cell 175, 558– 570 (2018).

[352] Alfano, L. et al. Depletion of the RNA binding protein HNRNPD impairs homologous recombination by inhibiting DNA-end resection and inducing R-loop accumulation. Nucleic Acids Research 47, 4068–4085 (2019).

[353] Matsui, M. et al. USP42 enhances homologous recombination repair by promoting R-loop resolution with a DNA–RNA helicase DHX9. Oncogenesis 9 (2020).

[354] Teng, Y. et al. ROS-induced R loops trigger a transcription-coupled but BRCA1/2-independent homologous recombination pathway through CSB. Nature Communications 9 (2018).

[355] Yu, Z. et al. DDX5 resolves R-loops at DNA double-strand breaks to promote DNA repair and avoid chromosomal deletions. NAR Cancer 2, 1–19 (2020).

[356] De Schutter, H. & Nuyts, S. Radiosensitizing potential of epigenetic anticancer drugs. Anti-cancer agents in medicinal chemistry 9, 99–108 (2009).

[357] Peng, Q. et al. A Perspective of Epigenetic Regulation in Radiotherapy. Frontiers in Cell and Developmental Biology 9, 1–15 (2021).

[358] Smits, K. M. et al. Epigenetics in radiotherapy: Where are we heading? Radiotherapy and Oncology 111, 168–177 (2014).

[359] Ganesan, A., Arimondo, P. B., Rots, M. G., Jeronimo, C. & Berdasco, M. The timeline of epigenetic drug discovery: From reality to dreams. Clinical Epigenetics 11, 1–17 (2019).

[360] Morel, D., Jeffery, D., Aspeslagh, S., Almouzni, G. & Postel-Vinay, S. Combining epigenetic drugs with other therapies for solid tumours — past lessons and future promise. Nature Reviews Clinical Oncology 17, 91–107 (2020).

[361] Gulati, N., Beguelin, W. & Giulino-Roth, L. Enhancer of zeste homolog 2 (EZH2) inhibitors. Leukemia & lymphoma 59, 1574–1585 (2018).

[362] Kuntz, K. W. et al. The importance of being me: magic methyls, methyltransferase inhibitors, and the discovery of tazemetostat. Journal of medicinal chemistry 59, 1556–1564 (2016).

[363] Kwon, H. J., Kim, M. S., Kim, M. J., Nakajima, H. & Kim, K. W. Histone deacetylase inhibitor FK228 inhibits tumor angiogenesis. International Journal of Cancer 97, 290–296 (2002).

[364] Shapiro, G. I. et al. A Phase 1 study of RO6870810, a novel bromodomain and extraterminal protein inhibitor, in patients with NUT carcinoma, other solid tumours, or diffuse large B-cell lymphoma. British Journal of Cancer 124, 744–753 (2021).

[365] Shorstova, T., Foulkes, W. D. & Witcher, M. Achieving clinical success with BET inhibitors as anti-cancer agents. British Journal of Cancer 124, 1478–1490 (2021).

[366] Serrao, A. et al. Azacitidine followed by radiotherapy as effective treatment for chronic myelomonocytic leukemia with extramedullary localization. Leukemia and Lymphoma 54, 411–412 (2013).

[367] Daigle, S. R. et al. Potent inhibition of DOT1L as treatment of MLL-fusion leukemia. Blood, The Journal of the American Society of Hematology 122, 1017–1025 (2013).

[368] Emran, A. A. et al. Targeting DNA Methylation and EZH2 Activity to Overcome Melanoma Resistance to Immunotherapy. Trends in Immunology 40, 328–344 (2019).

[369] Klaus, C. R. et al. DOT1L inhibitor EPZ-5676 displays synergistic antiproliferative activity in combination with standard of care drugs and hypomethylating agents in MLL-rearranged leukemia cells. Journal of Pharmacology and Experimental Therapeutics 350, 646–656 (2014).

[370] Gounder, M. M. et al. Phase 2 multicenter study of the EZH2 inhibitor tazemetostat in adults with INI1 negative epithelioid sarcoma (NCT02601950) Journal of clinical oncology 35, 15, 11058-11058 (2017).

[371] Italiano, A. et al. Tazemetostat, an EZH2 inhibitor, in relapsed or refractory B-cell non-Hodgkin lymphoma and advanced solid tumours: a first-in-human, open-label, phase 1 study. The Lancet Oncology 19, 649–659 (2018).

[372] Sarkozy, C. et al. A LYSA phase Ib study of tazemetostat (EPZ-6438) plus R-CHOP in patients with newly diagnosed diffuse large B-cell lymphoma (DLBCL) with poor prognosis features. Clinical Cancer Research 26, 3145–3153 (2020).

[373] Hunt, C. R. et al. Histone Modifications and DNA Double-Strand Break Repair after Exposure to Ionizing Radiations. Radiation Research 179, 383–392 (2013).

[374] Tjeertes, J. V., Miller, K. M. & Jackson, S. P. Screen for DNAdamage-responsive histone modifications identifies H3K9Ac and H3K56Ac in human cells. The EMBO Journal 28, 1878–1889 (2009).

[375] Mao, Z., Bozzella, M., Seluanov, A. & Gorbunova, V. Comparison of nonhomologous end joining and homologous recombination in human cells. DNA repair 7, 1765–1771 (2008).

[376] Shibata, A. et al. Factors determining DNA double-strand break repair pathway choice in G2 phase. The EMBO journal 30, 1079–1092 (2011).

[377] Jenuwein, T. & Allis, C. D. Translating the histone code. Science 293, 1074–1080 (2001).

[378] Kouzarides, T. Chromatin modifications and their function. Cell 128, 693–705 (2007).

[379] Wang, G. G., Allis, C. D. & Chi, P. Chromatin remodeling and cancer, part I: covalent histone modifications. Trends in Molecular Medicine 13, 363–372 (2007).

[380] Spotheim-Maurizot, M., Ruiz, S., Sabattier, R. & Charlier, M. Radioprotection of DNA by Polyamines. International Journal of Radiation Biology 68, 571–577 (1995).

[381] Barone, F., Belli, M., Pazzaglia, S., Sapora, O. & Tabocchini, M. A. Radiation damage and chromatin structure. Annali dell'Istituto superiore di sanita 25, 59—67 (1989).

[382] Reisz, J. A., Bansal, N., Qian, J., Zhao, W. & Furdui, C. M. Effects of ionizing radiation on biological molecules—mechanisms of damage and emerging methods of detection. Antioxidants & redox signaling 21, 260–292 (2014).

[383] Bernal, M. A. et al. The influence of DNA configuration on the direct strand break yield. Computational and Mathematical Methods in Medicine (2015).

[384] Semsarha, F., Goliaei, B., Raisali, G., Khalafi, H. & Mirzakhanian, L. An investigation on the radiation sensitivity of DNA conformations to ^{60}Co gamma rays by using Geant4 toolkit. Nuclear Instruments and Methods in Physics Research, 323, 75–81 (2014).

[385] Webb, C. J., Wu, Y. & Zakian, V. A. DNA Repair at Telomeres: Keeping the Ends Intact. Cold Spring Harbor Perspectives in Biology 5, a012666–a012666 (2013).

[386] Jeggo, P. A., Downs, J. A. & Gasser, S. M. Chromatin modifiers and remodelers in DNA repair and signaling. Philosophical Transactions of the Royal Society B: Biological Sciences 372, (2017).

[387] Wilson, M. D. & Durocher, D. Reading chromatin signatures after DNA double strand breaks. Philosophical transactions of the Royal Society of London. Series B, Biological sciences 372 (2017)

[388] Cheng, Y. et al. Targeting epigenetic regulators for cancer therapy: Mechanisms and advances in clinical trials. Signal Transduction and Targeted Therapy 4 (2019).

[389] Kurdistani, S. K. Histone modifications as markers of cancer prognosis: A cellular view. British Journal of Cancer 97, 1–5 (2007).

[390] Zhao, Z. & Shilatifard, A. Epigenetic modifications of histones in cancer. Genome Biology 20, 1–16 (2019).

[391] Burrow, A. A., Williams, L. E., Pierce, L. C. T. &Wang, Y.-H. Over half of breakpoints in gene pairs involved in cancer-specific recurrent translocations are mapped to human chromosomal fragile sites. BMC Genomics 10, 1–11 (2009).

[392] Lyu, X., Chastain, M. & Chai, W. Genome-wide mapping and profiling of γH2AX binding hotspots in response to different replication stress inducers. BMC Genomics 20, 1–13 (2019).

[393] Seo, J. et al. Genome-wide profiles of H2AX and γH2AX differentiate endogenous and exogenous DNA damage hotspots in human cells. Nucleic Acids Research 40, 5965–5974 (2012).

[394] Schep, R. et al. Impact of chromatin context on Cas9-induced DNA double-strand break repair pathway balance. Molecular Cell 1–15 (2021).

[395] Daer, R. M., Cutts, J. P., Brafman, D. A. & Haynes, K. A. The Impact of Chromatin Dynamics on Cas9-Mediated Genome Editing in Human Cells. ACS Synthetic Biology 6, 428–438 (2017).

[396] Jain, S. et al. TALEN outperforms Cas9 in editing heterochromatin target sites. Nature Communications 12, 4–13 (2021).

[397] Richardson, C. D. et al. CRISPR–Cas9 genome editing in human cells occurs via the Fanconi anemia pathway. Nature Genetics 50, 1132–1139 (2018).

[398] Bouwman, B. A. et al. Genome-wide detection of DNA double-strand breaks by in-suspension BLISS. Nature Protocols 15, 3894–3941 (2020).

[399] Gothe, H. J. et al. Spatial Chromosome Folding and Active Transcription Drive DNA Fragility and Formation of Oncogenic MLL Translocations. Molecular Cell 75, (2019).

[400] Birney, E. et al. Identification and analysis of functional elements in 1% of the human genome by the ENCODE pilot project. Nature 447, 799–816 (2007).

[401] Ernst, J. & Kellis, M. ChromHMM: Automating chromatin-state discovery and characterization. Nature Methods 9, 215–216 (2012).

[402] Ernst, J. & Kellis, M. Chromatin-state discovery and genome annotation with ChromHMM. Nature Protocols 12, 2478–2492 (2017).

[403] Burma, S., Chen, B. P., Murphy, M., Kurimasa, A. & Chen, D. J. ATM Phosphorylates Histone H2AX in Response to DNA Double-strand Breaks. Journal of Biological Chemistry 276, 42462–42467 (2001)

[404] Rogakou, E. P., Pilch, D. R., Orr, A. H., Ivanova, V. S. & Bonner, W. M. DNA double-stranded breaks induce histone H2AX phosphorylation on serine 139. Journal of Biological Chemistry 273, 5858–5868 (1998).

[405] Skene, P. J. & Henikoff, S. An efficient targeted nuclease strategy for high-resolution mapping of DNA binding sites. Elife 6, e21856 (2017).

[406] Trojer, P. & Reinberg, D. Facultative Heterochromatin: Is There a Distinctive Molecular Signature? Molecular Cell 28, 1–13 (2007).

[407] Paulsen, M. T. et al. Use of Bru-Seq and BruChase-Seq for genome-wide assessment of the synthesis and stability of RNA. Methods 67, 45–54 (2014).

[408] Gaspar, J. M. Improved peak-calling with MACS2. bioRxiv 496521 (2018).

[409] Quinlan, A. R. & Hall, I. M. BEDTools: A flexible suite of utilities for comparing genomic features. Bioinformatics 26, 841–842 (2010).

[410] Marchal, C. et al. Genome-wide analysis of replication timing by next-generation sequencing with E/L Repli-seq. Nature Protocols 13, 819–839 (2018).

[411] Jadhav, U. et al. Replicational Dilution of H3K27me3 in Mammalian Cells and the Role of Poised Promoters. Molecular Cell 78, 141–151 (2020).

[412] Petruk, S. et al. Delayed Accumulation of H3K27me3 on Nascent DNA Is Essential for Recruitment of Transcription Factors at Early Stages of Stem Cell Differentiation. Molecular Cell 66, 247–257 (2017).

[413] Rao, S. S. et al. A 3D map of the human genome at kilobase resolution reveals principles of chromatin looping. Cell 159, 1665–1680 (2014).

[414] Biernacka, A. et al. i-BLESS is an ultra-sensitive method for detection of DNA double-strand breaks. Communications Biology 1 (2018).

[415] Mieczkowski, J. et al. MNase titration reveals differences between nucleosome occupancy and chromatin accessibility. Nature Communications 7 (2016).

[416] Kumar, R. et al. HumCFS: a database of fragile sites in human chromosomes. BMC Genomics 19, 1–8 (2019).

[417] Ernst, J. et al. Mapping and analysis of chromatin state dynamics in nine human cell types. Nature 473, 43–49 (2011).

[418] Hodgkinson, A. & Eyre-Walker, A. Variation in the mutation rate across mammalian genomes. Nature Reviews Genetics 12, 756–766 (2011).

[419] Schuster-Bockler, B. & Lehner, B. Chromatin organization is a major influence on regional mutation rates in human cancer cells. Nature 488, 504–507 (2012).

[420] Murga, M. et al. Global chromatin compaction limits the strength of the DNA damage response. Journal of Cell Biology 178, 1101–1108 (2007).

[421] Svobodova Kovarikova, A., Legartova, S., Krejci, J. & Bartova, E. H3K9me3 and H4K20me3 represent the epigenetic landscape for 53BP1 binding to DNA lesions. Aging 10, 2585–2605 (2018).

[422] Ljungman, M. & Hanawalt, P. C. Efficient protection against oxidative DNA damage in chromatin. Molecular carcinogenesis 5, 264–269 (1992).

[423] Miller, A. C., Cohen, S., Stewart, M., Rivas, R. & Lison, P. Radioprotection by the histone deacetylase inhibitor phenylbutyrate. Radiation and Environmental Biophysics 50, 585–596 (2011).

[424] Natale, F. et al. DNA replication and repair kinetics of Alu, LINE-1 and satellite III genomic repetitive elements. Epigenetics & Chromatin 11, 61 (2018).

[425] Chiu, L.-Y., Gong, F. & Miller, K. M. Bromodomain proteins: repairing DNA damage within chromatin. Philosophical Transactions of the Royal Society B: Biological Sciences 372, 20160286 (2017).

[426] Clouaire, T. & Legube, G. A Snapshot on the Cis Chromatin Response to DNA Double-Strand Breaks. Trends in Genetics 35, 330–345 (2019).

[427] Dhar, S., Gursoy-yuzugullu, O., Parasuram, R., Price, B. D. & Price, B. D. The tale of a tail: histone H4 acetylation and the repair of DNA breaks. Philosophical Transactions of the Royal Society B: Biological Sciences 372 (2017).

[428] Reindl, J. et al. Chromatin organization revealed by nanostructure of irradiation induced γH2AX, 53BP1 and Rad51 foci. Scientific Reports 7, 1–11 (2017).

[429] Cai, Y. et al. The NuRD complex cooperates with DNMTs to maintain silencing of key colorectal tumor suppressor genes. Oncogene 33, 2157–2168 (2013).

[430] Izhar, L. et al. A Systematic Analysis of Factors Localized to Damaged Chromatin Reveals PARP-Dependent Recruitment of Transcription Factors. Cell Reports 11, 1486– 1500 (2015).

[431] Rother, M. B. & Attikum, H. V. DNA repair goes hip-hop: SMARCA and CHD chromatin remodelers join the break dance. Philosophical Transactions of the Royal Society B: Biological Sciences 372 (2017).

[432] Wu, Z. et al. Polycomb protein EZH2 regulates cancer cell fate decision in response to DNA damage. Cell Death and Differentiation 18, 1771–1779 (2011).

[433] Jacquet, K. et al. The TIP60 Complex Regulates Bivalent Chromatin Recognition by 53BP1 through Direct H4K20me Binding and H2AK15 Acetylation. Molecular Cell 62, 409–421 (2016).

[434] Kruhlak, M. J. et al. Changes in chromatin structure and mobility in living cells at sites of DNA double-strand breaks. The Journal of Cell Biology (2006).

[435] Tsouroula, K. et al. Temporal and Spatial Uncoupling of DNA Double Strand Break Repair Pathways within Mammalian Heterochromatin. Molecular Cell 63, 293–305 (2016).

[436] Kuser-Abali, G. et al. An EZH2-mediated epigenetic mechanism behind p53-dependent tissue sensitivity to DNA damage. PNAS (2018).

[437] Murr, R. et al. Histone acetylation by Trrap-Tip60 modulates loading of repair proteins and repair of DNA double-strand breaks. Nature Cell Biology 8, 91–99 (2006).

[438] Ljungman, M., Parks, L., Hulbatte, R. & Bedi, K. The role of H3K79 methylation in transcription and the DNA damage response, Mutation Research/Reviews in Mutation Research. 780, 48-54 (2017).

[439] Pai, C.-C. et al. A histone H3K36 chromatin switch coordinates DNA double strand break repair pathway choice. Nature Communications 5, 4091 (2014).

[440] Chiolo, I., Caridi, P. C., Delabaere, L. & Zapotoczny, G. And yet, it moves: nuclear and chromatin dynamics of a heterochromatic double- strand break. Philosophical transactions of the Royal Society of London. Series B, Biological sciences 372 (2017).

[441] Delgoffe, G. M. et al. The kinase mTOR regulates the differentiation of helper T cells through the selective activation of signaling by mTORC1 and mTORC2. Nature immunology 12, 295–303 (2011).

[442] Dellaire, G., Kepkay, R. & Bazett-Jones, D. P. High resolution imaging of changes in the structure and spatial organization of chromatin, γH2AX and the MRN complex within etoposide-induced DNA repair foci. Cell Cycle 8, 3750–3769 (2009).

[443] Lavelle, C. & Foray, N. Chromatin structure and radiation-induced DNA damage: From structural biology to radiobiology. International Journal of Biochemistry and Cell Biology 49, 84–97 (2014).

[444] Segurel, L. & Bon, C. Recent Advancements in DNA Damage–Transcription Crosstalk and High-Resolution Mapping of DNA Breaks. Annual Review Genomics Human Genetics 18, 87–113 (2017).

[445] Nguyen, A. T. & Zhang, Y. The diverse functions of Dot1 and H3K79 methylation. Genes & Development 25, 1345–58 (2011).

[446] Shaltiel, I. A., Krenning, L., Bruinsma, W. & Medema, R. H. The same, only different DNA damage checkpoints and their reversal throughout the cell cycle. Journal of Cell Science 128, 607–620 (2015).

[447] Heine, G. F., Horwitz, A. A. & Parvin, J. D. Multiple mechanisms contribute to inhibit transcription in response to DNA damage. Journal of Biological Chemistry 283, 9555–9561 (2008).

[448] Zhai, W. & Comai, L. Repression of RNA Polymerase I Transcription by the Tumor Suppressor p53. Molecular and Cellular Biology 20, 5930–5938 (2000).

[449] Shah, R. N. et al. Examining the Roles of H3K4 Methylation States with Systematically Characterized Antibodies. Molecular Cell 72, 162–177 (2018).

[450] Karch, K., Sidoli, S. & Garcia, B. Chapter One – Identification and Quantification of Histone PTMs Using High-Resolution Mass Spectrometry. In Methods in Enzymology, vol. 574, 3–29 (2016).

[451] Yuan, Z.-F. et al. EpiProfile Quantifies Histone Peptides With Modifications by Extracting Retention Time and Intensity in High-resolution Mass Spectra. Molecular & Cellular Proteomics 14, 1696– 1707 (2015).

[452] Yuan, Z.-F. et al. EpiProfile 2.0: A Computational Platform for Processing Epi- Proteomics Mass Spectrometry Data. Journal of Proteome Research 17, 2533–2541 (2018).

[453] Rauniyar, N. Parallel reaction monitoring: A targeted experiment performed using high resolution and high mass accuracy mass spectrometry International journal of molecular sciences (2015).

[454] Arnaudo, A. M. & Garcia, B. A. Proteomic characterization of novel histone posttranslational modifications. Epigenetics and Chromatin 6, 1–7 (2013).

[455] Dehennaut, V., Leprince, D. & Lefebvre, T. O-GlcNAcylation, an epigenetic mark. Focus on the histone code, TET family proteins, and polycomb group proteins. Frontiers in Endocrinology 5, 1–7 (2014).

[456] Huang, H., Lin, S., Garcia, B. A. & Zhao, Y. Quantitative proteomic analysis of histone modifications. Chemical Reviews 115, 2376–2418 (2015).

[457] Sabari, B. R., Zhang, D., Allis, C. D. & Zhao, Y. Metabolic regulation of gene expression through histone acylations. Nature Reviews Molecular Cell Biology 18, 90–101 (2017).

[458] Yang, G. et al. Poly(ADP-ribosyl)ation mediates early phase histone eviction at DNA lesions. Nucleic Acids Research 48, 3001–3013 (2020).

[459] Huang, H., Lin, S., Garcia, B. A. & Zhao, Y. Quantitative proteomic analysis of histone modifications Chemical reviews. 225, 115, 2376-2418. (2015).

[460] Banath, J. P., MacPhail, S. H. & Olive, P. L. Radiation sensitivity, H2AX phosphorylation, and kinetics of repair of DNA strand breaks in irradiated cervical cancer cell lines. Cancer Research 64, 7144–7149 (2004).

[461] Michishita, E. et al. Cell cycle-dependent deacetylation of telomeric histone H3 lysine K56 by human SIRT6. Cell Cycle 8, 2664–2666 (2009).

[462] Yuan, J., Pu, M., Zhang, Z. & Lou, Z. Histone H3-K56 acetylation is important for genomic stability in mammals. Cell Cycle 8, 1747–1753 (2009).

[463] Faucher, D. & Wellinger, R. J. Methylated H3K4, a transcription-associated histone modification, is involved in the DNA damage response pathway. PLoS Genetics 6 (2010).

[464] Li, X. et al. Histone demethylase KDM5B is a key regulator of genome stability. PNAS 111, 7096–7101 (2014).

[465] Goldberg, A. D. et al. Distinct Factors Control Histone Variant H3.3 Localization at Specific Genomic Regions. Cell 140, 678–691 (2010).

[466] Bosch-Presegue, L. & Vaquero, A. Sirtuin-dependent epigenetic regulation in the maintenance of genome integrity. FEBS Journal 282, 1745–1767 (2015).

[467] Fan, J., Krautkramer, K. A., Feldman, J. L. & Denu, J. M. Metabolic regulation of histone post-translational modifications. ACS Chemical Biology 10, 95–108 (2015).

[468] Martinez-Redondo, P. & Vaquero, A. The Diversity of Histone Versus Nonhistone Sirtuin Substrates. Genes and Cancer 4, 148–163 (2013).

[469] Zhang, M., Li, M., Zhang, W., Han, Y. & Zhang, Y. H. Simple and efficient delivery of cell-impermeable organic fluorescent probes into live cells for live cell superresolution imaging. Light: Science and Applications 8 (2019).

[470] Bao, X. et al. Identification of 'erasers' for lysine crotonylated histone marks using a chemical proteomics approach. eLife 3, e02999 (2014).

[471] Britton, S., Coates, J. & Jackson, S. P. A new method for high-resolution imaging of Ku foci to decipher mechanisms of DNA double strand break repair. Journal of Cell Biology 202, 579–595 (2013).

[472] Kochan, J. A. et al. Meta-analysis of DNA double-strand break response kinetics. Nucleic Acids Research 45, 12625–12637 (2017).

[473] Riballo, E. et al. A Pathway of Double-Strand Break Rejoining Dependent upon ATM, Artemis, and Proteins Locating to γH2AX Foci 16, 715–724 (2004).

[474] Rothkamm K, et al. DNA damage foci: Meaning and significance. Environmental and molecular mutagenesis. 56, 6, 491-504 (2015).

[475] Fu, S. et al. γH2AX kinetics as a novel approach to high content screening for small molecule radiosensitizers. PLoS ONE 7 (2012).

[476] Gyori, B. M., Venkatachalam, G., Thiagarajan, P. S., Hsu, D. & Clement, M. V. OpenComet: An automated tool for comet assay image analysis. Redox Biology 2, 457–465 (2014).

[477] Liu, S. K., Olive, P. L. & Bristow, R. G. Biomarkers for DNA DSB inhibitors and radiotherapy clinical trials. Cancer and Metastasis Reviews 27, 445–458 (2008).

[478] Crosetto, N. et al. Nucleotide-resolution DNA double-strand break mapping by next-generation sequencing. Nature Methods 10, 361–365 (2013).

[479] Yan, W. X. et al. BLISS is a versatile and quantitative method for genome-wide profiling of DNA double-strand breaks. Nature Communications 8, 15058 (2017).

[480] Canela, A. et al. DNA Breaks and End Resection Measured Genome wide by End Sequencing. Molecular Cell 63, 898–911 (2016).

[481] [476] Rothkamm, K. & Horn, S. gamma-H2AX as protein biomarker for radiation exposure. Ann Ist Super Sanita 45, 265–271 (2009).

[482] Rybak, P. et al. Low level phosphorylation of histone H2AX on serine 139 (γH2AX) is not associated with DNA double-strand breaks. Oncotarget 7, 49574 (2016).

[483] Liu, J., Francois, J. M. & Capp, J. P. Gene expression noise produces cell-to-cell heterogeneity in eukaryotic homologous recombination rate. Frontiers in Genetics 10, 1–12 (2019).

[484] E., L. et al. Repurposing cephalosporin antibiotics as pro-senescent radiosensitizers. Oncotarget 7, 33919–33933 (2016).

[485] Kron, S. Ionizing radiation-induced foci persistence screen to discover enhancers of accelerated senescence. International Journal of High Throughput Screening 2, 1 (2011).

[486] Kim, H. J. et al. DNMT (DNA methyltransferase) inhibitors radiosensitize human cancer cells by suppressing DNA repair activity. Radiation Oncology 7, 39 (2012).

[487] Bollum, F. J. Calf Thymus Polymerase*. Tech. Rep. 8 (1960).

[488] Gilfillan, S., Dierich, A., Lemeur, M., Benoist, C. & Mathis, D. Mice lacking TdT: mature animals with an immature lymphocyte repertoire. Science (New York, N.Y.) 261, 1175–8 (1993).

[489] Motea, E. A. & Berdis, A. J. Terminal deoxynucleotidyl transferase: the story of a misguided DNA polymerase. Biochimica et biophysica acta 1804, 1151–66 (2010).

[490] Gavrieli, Y., Sherman, Y. & Ben-Sasson, S. A. Identification of programmed cell death in situ via specific labeling of nuclear DNA fragmentation. The Journal of cell biology 119, 493–501 (1992).

[491] Gorczyca, W., Gong, J. & Darzynkiewicz2, Z. Detection of DNA Strand Breaks in Individual Apoptotic Cells by the in Situ Terminal Deoxynucleotidyl Transferase and Nick Translation Assays. Cancer Research 53 (1945)

[492] Loo DT. TUNEL assay. In Situ Detection of DNA Damage. (2002).

[493] Bradshaw, P. S., Stavropoulos, D. J. & Meyn, M. S. Human telomeric protein TRF2 associates with genomic double-strand breaks as an early response to DNA damage. Nature Genetics 37, 193–197 (2005).

[494] Winz, M. L., Linder, E. C., Andr, T., Becker, J. & Jschke, A. Nucleotidyl transferase assisted DNA labeling with different click chemistries. Nucleic Acids Research 43 (2015).

[495] Bolte, S. & Cordelieres, F. P. A guided tour into subcellular colocalization analysis in light microscopy. Journal of Microscopy 224, 213–232 (2006).

[496] Verdaasdonk, J. S., Stephens, A. D., Haase, J. & Bloom, K. B ending the Rules: Widefield Microscopy and the Abbe Limit of Resolution. Journal of cellular physiology 229, 132–138 (2014).

[497] Weiss, S. Shattering the diffraction limit of light: A revolution in fluorescence microscopy? 97, 8747–8749 (2000).

[498] Henriques, R., Griffiths, C., Hesper Rego, E. & Mhlanga, M. M. PALM and STORM: Unlocking live-cell super-resolution. Biopolymers 95, 322–331 (2011).

[499] Huang, B., Wang, W., Bates, M. & Zhuang, X. Three-Dimensional Super-Resolution Imaging by Stochastic Optical Reconstruction Microscopy. Science 319, 810–813 (2008).

[500] Tam, J. & Merino, D. Stochastic optical reconstruction microscopy (STORM) in comparison with stimulated emission depletion (STED) and other imaging methods. Journal of Neurochemistry 135, 643–658 (2015).

[501] Falk, M. et al. Heterochromatinization associated with cell differentiation as a model to study DNA double strand break induction and repair in the context of higher-order chromatin structure. Applied Radiation and Isotopes 83, 177–185 (2014).

[502] Falk, M. & Hausmann, M. A paradigm revolution or just better resolution—will newly emerging superresolution techniques identify chromatin architecture as a key factor in radiation-induced DNA damage and repair regulation? Cancers 13, 1–30 (2021).

[503] Sednev, V. et al. Nanoscopic exclusion between Rad51 and 53BP1 after ion irradiation in human HeLa cells. Physical Biol 12, 66005 (2015).

[504] Clegg, R.M. Fluorescence resonance energy transfer. Current Opinion in Biotechnology 6, 103–110 (1995).

[505] Gopich, I. V. & Szabo, A. Theory of the energy transfer efficiency and fluorescence lifetime distribution in single-molecule FRET. PNAS 109, 7747–7752 (2012).

[506] Hell, S. W. & Kroug, M. Ground-state-depletion fluorescence microscopy: A concept for breaking the diffraction resolution limit. Applied Physics B 60, 495–497 (1995).

[507] Heilemann, M. et al. Sub-diffraction-Resolution Fluorescence Imaging with Conventional Fluorescent Probes. Angewandte Chemie International Edition 47, 6172–6176 (2008).

[508] Dixon, R. E., Vivas, O., Hannigan, K. I. & Dickson, E. J. Ground state depletion superresolution imaging in mammalian cells. JoVE (2017).

[509] Sage, D. et al. Super-resolution fight club: assessment of 2D and 3D single molecule localization microscopy software. Nature Methods 16, 387–395 (2019).

[510] Didenko, V. V. In Situ Detection of DNA Damage, vol. 203 (2002).

[511] Hornsby, P. J. & Didenko, V. V. In situ ligation: A decade and a half of experience. Methods in Molecular Biology 682, 49–63 (2011).

[512] Fantoni, N. Z., El-Sagheer, A. H. & Brown, T. A Hitchhiker's Guide to Click-Chemistry with Nucleic Acids. Chemical Reviews (2021).

[513] Horisawa, K. Specific and quantitative labeling of biomolecules using click chemistry. Frontiers in Physiology 5, 1–6 (2014).

[514] Yuan, Y. & Liang, G. A biocompatible, highly efficient click reaction and its applications. Organic and Biomolecular Chemistry 12, 865–871 (2014).

[515] Kolb, H. C., Finn, M. G. & Sharpless, K. B. Click chemistry: diverse chemical function from a few good reactions. Angewandte Chemie International Edition 40, 2004–2021 (2001).

[516] Rostovtsev, V. V., Green, L. G., Fokin, V. V. & Sharpless, K. B. A stepwise huisgen cycloaddition process: copper (I)-catalyzed regioselective "ligation" of azides and terminal alkynes. Angewandte Chemie 114, 2708–2711 (2002).

[517] Iacovoni, J. S. et al. High-resolution profiling of γH2AX around DNA double strand breaks in the mammalian genome. EMBO Journal 29, 1446–1457 (2010).

[518] Kim, J. A., Kruhlak, M., Dotiwala, F., Nussenzweig, A. & Haber, J. E. Heterochromatin is refractory to γH2AX modification in yeast and mammals. Journal of Cell Biology 178, 209–218 (2007).

[519] Rossetto, D., Truman, A. W., Kron, S. J. & Cote, J. Epigenetic modifications in double-strand break DNA damage signaling and repair. Clinical Cancer Research 16, 4543–4552 (2010).

[520] Wilson, B. G. et al. Epigenetic antagonism between polycomb and SWI/SNF complexes during oncogenic transformation. Cancer Cell 18, 316–328 (2010).

[521] Hou, T. et al. SIRT6 coordinates with CHD4 to promote chromatin relaxation and DNA repair. Nucleic Acids Research 48, 2982–3000 (2020).

[522] Sebastian, R. & Oberdoerffer, P. Transcription-associated events affecting genomic integrity. Philosophical Transactions of the Royal Society B: Biological Sciences 372(2017).

[523] Watanabe, R., Kanno, S.-I., Mohammadi Roushandeh, A., Ui, A. & Yasui, A. Nucleosome remodeling, DNA repair and transcriptional regulation build negative feedback loops in cancer and cellular ageing. Philosophical Transactions of the Royal Society B: Biological Sciences 372, 20160473 (2017).

[524] Bouwman, B. A. & Crosetto, N. Endogenous DNA double-strand breaks during DNA transactions: Emerging insights and methods for genome-wide profiling. Genes 9 (2018).

[525] Ju, B.-G. et al. A topoisomerase IIß-mediated dsDNA break required for regulated transcription. Science 312, 1798–1802 (2006).

[526] Madabhushi, R. et al. Activity-induced DNA breaks govern the expression of neuronal early-response genes. Cell 161, 1592–1605 (2015).

[527] Yang, F., Kemp, C. J. & Henikoff, S. Anthracyclines induce double-strand DNA breaks at active gene promoters. Mutation Research/Fundamental and Molecular Mechanisms of Mutagenesis 773, 9–15 (2015).

[528] Kuzminov, A. Single-strand interruptions in replicating chromosomes cause double strand breaks. PNAS 98, 8241–8246 (2001).

[529] Ma, J. & Wang, M. D. DNA supercoiling during transcription. Biophysical Reviews 8, 75–87 (2016).

[530] Wilson, T. E. et al. Large transcription units unify copy number variants and common fragile sites arising under replication stress. Genome research 25, 189–200 (2015).

[531] Schroeder, J. W., Sankar, T. S., Wang, J. D. & Simmons, L. A. The roles of replication-transcription conflict in mutagenesis and evolution of genome organization. PLoS Genetics 16, e1008987 (2020).

[532] Dellino, G. I. et al. Release of paused RNA polymerase II at specific loci favors DNA double-strand-break formation and promotes cancer translocations. Nature Genetics 51, 1011–1023 (2019).

[533] Caron, M. C. et al. Poly(ADP-ribose) polymerase-1 antagonizes DNA resection at double-strand breaks. Nature Communications 10 (2019).

[534] Pan, M.-R. et al. Chromodomain helicase DNA-binding protein 4 (CHD4) regulates homologous recombination DNA repair, and its deficiency sensitizes cells to poly (ADPribose) polymerase (PARP) inhibitor treatment. Journal of Biological Chemistry 287, 6764–6772 (2012).

[535] Ui, A., Nagaura, Y. & Yasui, A. Transcriptional elongation factor ENL phosphorylated by ATM recruits polycomb and switches off transcription for DSB repair. Molecular Cell 58, 468–482 (2015).

[536] Caron, P. et al. Non-redundant Functions of ATM and DNA-PKcs in Response to DNA Double-Strand Breaks. Cell Reports 13, 1598–1609 (2015).

[537] Capozzo, I., Iannelli, F., Francia, S. & d'Adda di Fagagna, F. Express or repress? The transcriptional dilemma of damaged chromatin. FEBS Journal 284, 2133–2147 (2017).

[538] Pederiva, C., Bohm, S., Julner, A. & Farnebo, M. Splicing controls the ubiquitin response during DNA double-strand break repair. Cell Death and Differentiation 23, 1648–1657 (2016).

[539] Marnef, A. & Legube, G. R-loops as Janus-faced modulators of DNA repair. Nature Cell Biology 23, 305–313 (2021).

[540] Sollier, J. & Cimprich, K. A. Breaking bad: R-loops and genome integrity. Trends in Cell Biology 25, 514–522 (2015).

[541] Sanz, L. A. & Chedin, F. High-resolution, strand-specific R-loop mapping via S9.6-based DNA–RNA immunoprecipitation and high throughput sequencing. Nature Protocols 14, 1734–1755 (2019).

[542] Jonkers, I. & Lis, J. T. Getting up to speed with transcription elongation by RNA polymerase II. Nature reviews Molecular Cell Biology 16, 167–177 (2015).

[543] Iannelli, F. et al. A damaged genome's transcriptional landscape through multilayered expression profiling around in situ-mapped DNA double-strand breaks. Nature Communications 8 (2017).

[544] Brambati, A., Zardoni, L., Nardini, E., Pellicioli, A. & Liberi, G. The dark side of RNA: DNA hybrids. Mutation Research/Reviews in Mutation Research 784, 108300 (2020).

[545] Aguilera, A. & Garcia-Muse, T. R loops: from transcription byproducts to threats to genome stability. Molecular Cell 46, 115–124 (2012).

[546] Welty, S. et al. RAD52 is required for RNA-templated recombination repair in postmitotic neurons. Journal of Biological Chemistry 293, 1353–1362 (2018).

[547] Paulsen, M. T. et al. Use of Bru-Seq and BruChase-Seq for genome-wide assessment of the synthesis and stability of RNA. Methods 67, 45–54 (2014).

[548] Berger, N. D., Stanley, F. K., Moore, S. & Goodarzi, A. A. ATM-dependent pathways of chromatin remodeling and oxidative DNA damage responses. Philosophical Transactions of the Royal Society B: Biological Sciences 372 (2017).

[549] Abugessaisa, I. et al. refTSS: A Reference Data Set for Human and Mouse Transcription Start Sites. Journal of Molecular Biology 431, 2407–2422 (2019).

[550] Raudvere, U. et al. g: Profiler: a web server for functional enrichment analysis and conversions of gene lists (2019 update). Nucleic Acids Research 47, W191–W198 (2019).

[551] Adam, S. & Polo, S. E. Blurring the line between the DNA damage response and transcription: The importance of chromatin dynamics. Experimental Cell Research 329, 148–153 (2014).

[552] Heine, G. F., Horwitz, A. A. & Parvin, J. D. Multiple mechanisms contribute to inhibit transcription in response to DNA damage. Journal of Biological Chemistry 283, 9555–9561 (2008).

[553] Carbon, S. et al. The Gene Ontology resource: Enriching a GOld mine. Nucleic Acids Research 49, D325–D334 (2021).

[554] Gene Ontology Consortium. Gene Ontology: tool for the unification of biology Gene Expression 25, 25–29 (2000).

[555] Murray, S. C. et al. H3K4me3 is neither instructive for, nor informed by, transcription. bioRxiv 709014 (2019).

[556] Abed, J. A. & Jones, R. S. H3K36me3 key to Polycomb-mediated gene silencing in lineage specification. Nature Structural and Molecular Biology 19, 1214–1215 (2012).

[557] Sun, Z. et al. H3K36me3, message from chromatin to DNA damage repair. Cell and Bioscience 10, 1–9 (2020).

[558] Bensaude, O. Inhibiting eukaryotic transcription. Which compound to choose? How to evaluate its activity? Transcription 2, 103–108 (2011).

[559] Dhami, P. et al. Complex exon-intron marking by histone modifications is not determined solely by nucleosome distribution. PLoS ONE 5 (2010).

[560] Lee, J.-H. & Paull, T. T. ATM activation by DNA double-strand breaks through the Mre11-Rad50-Nbs1 complex. Science 308, 551–554 (2005).

[561] Paull, T. T. Mechanisms of ATM activation. Annual Review of Biochemistry 84, 711–738 (2015).

[562] Sun, Y., Jiang, X., Chen, S., Fernandes, N. & Price, B. D. A role for the Tip60 histone acetyltransferase in the acetylation and activation of ATM. PNAS 102, 13182–13187 (2005).

[563] Cannon, B. et al. Visualization of local DNA unwinding by Mre11/Rad50/Nbs1 using single-molecule FRET. PNAS 110, 18868–18873 (2013).

[564] Shiotani, B. & Zou, L. Single-stranded DNA orchestrates an ATM-to-ATR switch at DNA breaks. Molecular Cell 33, 547–558 (2009).

[565] Aranda, S., Mas, G. & Di Croce, L. Regulation of gene transcription by Polycomb proteins. Science Advances 1, 1–16 (2015).

[566] Di Croce, L. & Helin, K. Transcriptional regulation by Polycomb group proteins. Nature Structural and Molecular Biology 20, 1147–1155 (2013).

[567] Vallot, C., Herault, A., Boyle, S., Bickmore, W. A. & Radvanyi, F. PRC2-independent chromatin compaction and transcriptional repression in cancer. Oncogene 34, 741–751 (2015).

[568] Bracken, A. P. et al. The Polycomb group proteins bind throughout the INK4A-ARF locus and are disassociated in senescent cells. Genes and Development 21, 525–530 (2007).

[569] Blackledge, N. P. et al. Variant PRC1 complex-dependent H2A ubiquitylation drives PRC2 recruitment and polycomb domain formation. Cell 157, 1445–1459 (2014).

[570] Wang, L. et al. Hierarchical recruitment of polycomb group silencing complexes. Molecular Cell 14, 637–646 (2004).

[571] Barbour, H., Daou, S., Hendzel, M. & Affar, E. B. Polycomb group mediated histone H2A mono-ubiquitination in epigenome regulation and nuclear processes. Nature Communications 11, 1–16 (2020).

[572] Ismail, I. H., Andrin, C., McDonald, D. & Hendzel, M. J. BMI1-mediated histone ubiquitylation promotes DNA double-strand break repair. Journal of Cell Biology 191, 45–60 (2010).

[573] Schwertman, P., Bekker-Jensen, S. & Mailand, N. Regulation of DNA double-strand break repair by ubiquitin and ubiquitin-like modifiers. Nature Reviews Molecular Cell Biology 17, 379–394 (2016).

[574] Chandler, H. et al. Role of polycomb group proteins in the DNA damage response-A reassessment. PLoS ONE 9 (2014).

[575] Veneti, Z., Gkouskou, K. K. & Eliopoulos, A. G. Molecular Sciences Polycomb Repressor Complex 2 in Genomic Instability and Cancer (2017).

[576] Zhang, Y. et al. Histone H3K27 methylation is required for NHEJ and genome stability by modulating the dynamics of FANCD2 on chromatin. Journal of cell science 1-15(2018).

[577] Karakashev, S. et al. EZH2 Inhibition Sensitizes CARM1-High, Homologous Recombination Proficient Ovarian Cancers to PARP Inhibition. Cancer Cell 37, 157–167 (2020).

[578] Li, J. et al. EZH2-mediated H3K27 trimethylation mediates neurodegeneration in ataxia-telangiectasia. Nature Neuroscience 16, 1745–1753 (2013).

[579] Wang, Y. et al. DNA-PK-mediated phosphorylation of EZH2 regulates the DNA damage-induced apoptosis to maintain T-cell genomic integrity. Cell Death and Disease 7, 1–10 (2016).

[580] Kadoch, C. et al. Proteomic and bioinformatic analysis of mammalian SWI/SNF complexes identifies extensive roles in human malignancy. Nature Genetics 45, 592– 601 (2013).

[581] Mittal, P. & Roberts, C. W. The SWI/SNF complex in cancer — biology, biomarkers and therapy. Nature Reviews Clinical Oncology 17, 435–448 (2020).

[582] Kakarougkas, A., Downs, J. A. & Jeggo, P. A. The PBAF chromatin remodeling complex represses transcription and promotes rapid repair at DNA double-strand breaks. Molecular and Cellular Oncology 2 (2015).

[583] Park, J. H. et al. Mammalian SWI/SNF complexes facilitate DNA double-strand break repair by promoting γH2AX induction. EMBO Journal 25, 3986–3997 (2006).

[584] Schaaf, C. A. et al. Cohesin and polycomb proteins functionally interact to control transcription at silenced and active genes. PLoS Genet 9, e1003560 (2013).

[585] Martens, J. A. & Winston, F. Recent advances in understanding chromatin remodeling by Swi/Snf complexes. Current opinion in genetics & development 13, 136-142 (2003).

[586] Pal, S., Vishwanath, S. N., Erdjument-Bromage, H., Tempst, P. & Sif, S. Human SWI/SNF-Associated PRMT5 Methylates Histone H3 Arginine 8 and Negatively Regulates Expression of ST7 and NM23 Tumor Suppressor Genes. Molecular and Cellular Biology 24, 9630–9645 (2004).

[587] Li, C. et al. Finding an easy way to harmonize: a review of advances in clinical research and combination strategies of EZH2 inhibitors. Clinical Epigenetics 13, 1–12 (2021).

[588] Yap, T. A. et al. Phase I study of the novel enhancer of zeste homolog 2 (EZH2) inhibitor GSK2816126 in patients with advanced hematologic and solid tumors. Clinical Cancer Research 25, 7331–7339 (2019).

[589] Gao, Y. et al. SSRP1 cooperates with PARP and XRCC1 to facilitate single-strand DNA break repair by chromatin priming. Cancer Research 77, 2674–2685 (2017).

[590] Tan, X. et al. Inhibition of EZH2 enhances the therapeutic effect of 5-FU via PUMA upregulation in colorectal cancer. Cell Death and Disease 11 (2020).

[591] Papillon, J. P. et al. Discovery of Orally Active Inhibitors of Brahma Homolog (BRM)/SMARCA2 ATPase Activity for the Treatment of BRG1/SMARCA4-Mutant Cancers. Journal of Medicinal Chemistry 61, 10155–10172 (2018).

[592] Chory, E. J. et al. Chemical Inhibitors of a Selective SWI/SNF Function Synergize with ATR Inhibition in Cancer Cell Killing. ACS Chemical Biology 15, 1685–1696 (2020).

[593] Wiles, E. T. & Selker, E. U. H3K27 methylation: a promiscuous repressive chromatin mark. Current Opinion in Genetics and Development 43, 31–37 (2017).

[594] Agger, K. et al. UTX and JMJD3 are histone H3K27 demethylases involved in HOX gene regulation and development. Nature 449, 731–734 (2007).

[595] Nichol, J. N., Dupere-Richer, D., Ezponda, T., Licht, J. D. & Miller, W. H. H3K27 Methylation: A Focal Point of Epigenetic Deregulation in Cancer. Advances in Cancer Research 131, 59–95 (2016).

[596] Feringa, F. M. et al. Persistent repair intermediates induce senescence. Nature Communications 9 (2018).

[597] Fumagalli, M. et al. Telomeric DNA damage is irreparable and causes persistent DNA-damage-response activation. Nature Cell Biology 14, 355–365 (2012).

[598] Fumagalli, M., Rossiello, F., Mondello, C. & D'Adda Di Fagagna, F. Stable cellular senescence is associated with persistent DDR activation. PLoS ONE 9, 44–46 (2014).

[599] Farnaby, W. et al. BAF complex vulnerabilities in cancer demonstrated via structure-based PROTAC design. Nature Chemical Biology 15, 672–680 (2019).

[600] Hauer, M. H. et al. Histone degradation in response to DNA damage enhances chromatin dynamics and recombination rates. Nature Structural and Molecular Biology 24, 99–107 (2017).

[601] Lou, J. et al. Phasor histone FLIM-FRET microscopy quantifies spatiotemporal rearrangement of chromatin architecture during the DNA damage response. PNAS 116, 7323–7332 (2019).

[602] Sherrard, A. et al. Streamlined histone-based fluorescence lifetime imaging microscopy (FLIM) for studying chromatin organization. Biology Open 7 (2018).

[603] Ziv, Y. et al. Chromatin relaxation in response to DNA double-strand breaks is modulated by a novel ATM-and KAP-1 dependent pathway. Nature Cell Biology 8, 870–876 (2006).

[604] Ogiwara, H. et al. Histone acetylation by CBP and p300 at double-strand break sites facilitates SWI/SNF chromatin remodeling and the recruitment of non-homologous end joining factors. Oncogene 30, 2135–2146 (2011).

[605] Sellou, H. et al. The poly(ADP-ribose)-dependent chromatin remodeler Alc1 induces local chromatin relaxation upon DNA damage. Molecular Biology of the Cell 27, 3791–3799 (2016).

[606] Vissers, J. H., Van Lohuizen, M. & Citterio, E. The emerging role of Polycomb repressors in the response to DNA damage. Journal of Cell Science 125, 3939–3948 (2012).

[607] Lewis, E. B. A gene complex controlling segmentation in Drosophila. Nature 276, 565–570 (1978).

[608] Gregersen, L. H. & Svejstrup, J. Q. The Cellular Response to Transcription- Blocking DNA Damage. Trends in Biochemical Sciences 43, 327–341 (2018).

[609] Cowell, I. G. et al. γH2AX foci form preferentially in euchromatin after ionizing radiation. PLoS ONE 2, 1–8 (2007).

[610] Lorat, Y. et al. Beyond repair foci: DNA double-strand break repair in euchromatic and heterochromatic compartments analyzed by transmission electron microscopy. PLoS ONE 7 (2012).

[611] Chailleux, C. et al. Quantifying DNA double-strand breaks induced by site-specific endonucleases in living cells by ligation-mediated purification. Nature Protocols 9, 517–528 (2014).

[612] Karanam, K., Kafri, R., Loewer, A. & Lahav, G. Quantitative Live Cell Imaging Reveals a Gradual Shift between DNA Repair Mechanisms and a Maximal Use of HR in Mid S Phase. Molecular Cell 47, 320–329 (2012).

[613] Ingram, S. P. et al. Mechanistic modelling supports entwined rather than exclusively competitive DNA double-strand break repair pathway. Scientific Reports 9, 1–13 (2019).

[614] Mao, Z., Bozzella, M., Seluanov, A. & Gorbunova, V. DNA repair by nonhomologous end joining and homologous recombination during cell cycle in human cells. Cell Cycle 7, 2902–2906 (2008).

[615] Mito, Y., Henikoff, J. G. & Henikoff, S. Genome-scale profiling of histone H3.3 replacement patterns. Nature Genetics 37, 1090–1097 (2005).

[616] Stracker, T. H., Carson, C. T. & Weitzman, M. D. Adenovirus oncoproteins inactivate the Mre11–Rad50–NBS1 DNA repair complex. Nature 418, 348–352 (2002).

[617] Girard, P.-M., Riballo, E., Begg, A. C., Waugh, A. & Jeggo, P. A. Nbs1 promotes ATM dependent phosphorylation events including those required for G1/S arrest. Oncogene 21, 4191–4199 (2002).

[618] Lim, D.-S. et al. ATM phosphorylates p95/nbs1 in an S-phase checkpoint pathway. Nature 404, 613–617 (2000).

[619] Sun, Y., Jiang, X., Chen, S. & Price, B. D. Inhibition of histone acetyltransferase activity by anacardic acid sensitizes tumor cells to ionizing radiation. FEBS letters 580, 4353–4356 (2006).

[620] Sanulli, S. et al. Jarid2 Methylation via the PRC2 Complex Regulates H3K27me3 Deposition during Cell Differentiation. Molecular Cell 57, 769–783 (2015).

[621] Riley, T., Sontag, E., Chen, P. & Levine, A. Transcriptional control of human p53- regulated genes. Nature reviews Molecular Cell biology 9, 402–412 (2008).

[622] Berkovich, E., Monnat, R. J. & Kastan, M. B. Roles of ATM and NBS1 in chromatin structure modulation and DNA double-strand break repair. Nature Cell Biology 9, 683–690 (2007).

[623] Stracker, T. H. & Petrini, J. H. The MRE11 complex: Starting from the ends. Nature Reviews Molecular Cell Biology 12, 90–103 (2011).

[624] You, Z., Bailis, J. M., Johnson, S. A., Dilworth, S. M. & Hunter, T. Rapid activation of ATM on DNA flanking double-strand breaks. Nature Cell Biology 9, 1311–1318 (2007).

[625] Tsukuda, T., Fleming, A. B., Nickoloff, J. A. & Osley, M. A. Chromatin remodeling at a DNA double-strand break site in Saccharomyces cerevisiae. Nature 438, 379–383 (2005).

[626] Chong, S. Y. et al. H3K4 methylation at active genes mitigates transcription-replication conflicts during replication stress. Nature Communications 11, 1–16 (2020)

[627] Bayona-Feliu, A., Barroso, S., Munoz, S. & Aguilera, A. The SWI/SNF chromatin remodeling complex helps resolve R-loop-mediated transcription–replication conflicts. Nature Genetics 53 (2021).

[628] Rashi-Elkeles, S. et al. Parallel profiling of the transcriptome, cistrome, and epigenome in the cellular response to ionizing radiation. Science signaling 7, rs3–rs3 (2014).

[629] Martin, R. D., Hebert, T. E. & Tanny, J. C. Therapeutic targeting of the general RNA polymerase II transcription machinery. International Journal of Molecular Sciences 21 (2020).

[630] Varambally, S. et al. The polycomb group protein EZH2 is involved in progression of prostate cancer. Nature 419, 624–629 (2002).

[631] Kleer, C. G. et al. EZH2 is a marker of aggressive breast cancer and promotes neoplastic transformation of breast epithelial cells. PNAS 100, 11606–11611 (2003).

[632] Versteege, I. et al. Truncating mutations of hSNF5/INI1 in aggressive pediatric cancer. Nature 394, 203–206 (1998).

[633] Biegel, J. A. et al. Germ-line and acquired mutations of INI1 in atypical teratoid and rhabdoid tumors. Cancer research 59, 74–79 (1999).

[634] Wiegand, K. C. et al. ARID1A mutations in endometriosis-associated ovarian carcinomas. New England Journal of Medicine 363, 1532–1543 (2010).

[635] Lee, R. S. et al. A remarkably simple genome underlies highly malignant pediatric rhabdoid cancers. The Journal of clinical investigation 122, 2983–2988 (2012).

[636] Betz, B. L., Strobeck, M. W., Reisman, D. N., Knudsen, E. S. & Weissman, B. E. Re-expression of hSNF5/INI1/BAF47 in pediatric tumor cells leads to G 1 arrest associated with induction of p16ink4a and activation of RB. Oncogene 21, 5193–5203 (2002).

[637] Brock, A., Krause, S. & Ingber, D. E. Control of cancer formation by intrinsic genetic noise and microenvironmental cues. Nature Reviews Cancer 15, 499–509 (2015).

[638] Szilard, R. K. et al. Systematic identification of fragile sites via genome-wide location analysis of γH2AX. Nature Structural & Molecular Biology 17, 299–305 (2010).